NATIONAL ADVISORY COMMITTEE FOR AERONAUTICS

TECHNICAL NOTE 2533

EVALUATION OF HIGH-ANGLE-OF-ATTACK AERODYNAMIC-DERIVATIVE DATA AND STALL-FLUTTER PREDICTION TECHNIQUES

By Robert L. Halfman, H. C. Johnson, and S. M. Haley

Massachusetts Institute of Technology

Washington

November 1951

NATIONAL ADVISORY COMMITTEE FOR AERONAUTICS

TECHNICAL NOTE 2533

EVALUATION OF HIGH-ANGLE-OF-ATTACK AERODYNAMIC-DERIVATIVE DATA AND STALL-FLUTTER PREDICTION TECHNIQUES

By Robert L. Halfman, H. C. Johnson, and S. M. Haley

SUMMARY

The problem of stall flutter is approached in two ways. First, using the M.I.T.-NACA airfoil oscillator, the aerodynamic reactions on wings oscillating harmonically in pitch and translation in the stall range have been measured, evaluated, and correlated where possible with available published data, with the purpose of providing empirical information where no aerodynamic theory exists. The major effects of Reynolds number, airfoil shape, and reduced frequency on the aerodynamic reactions have been reaffirmed. No instances of negative damping were observed in pure translatory motion and the ranges of negative damping occurring in pure pitch had the same general trends noted by other experimenters. Data on the time-average values in the stall range of both lift and moment are presented for the first time.

Second, the results of numerous experimental observations of stall flutter have been reviewed and the various known attempts at its prediction have been examined, compared, and extended. The sharp drop in critical speed and change to a predominantly torsional oscillation usually associated with the transition from classical to stall flutter is apparently primarily but not entirely caused by the marked changes in moment due to pitch. Fairly good stall-flutter predictions have been reported only when adequate empirical data for this aerodynamic reaction happened to be available for the desired airfoil shape, Reynolds number range, and reduced-frequency range. A semiempirical method of predicting the variations of moment in pitch with airfoil shape, reduced frequency, initial angle of attack, and amplitude of oscillation has been presented.

INTRODUCTION

Stall flutter differs from classical flutter in that the flow over the airfoil is stalled during all or part of the cycle of oscillation. Although stall flutter has been observed in aircraft propellers for some time, new interest in the phenomenon has been generated by the

advent of the aircraft gas turbine where turbine-blade stall flutter is a serious problem. Even though it is known that the critical speed drops sharply from the value predicted by classical theory as portions of the flow begin to stall, no adequate prediction techniques have yet been proposed primarily because not enough is known about the behavior of the aerodynamic reactions in the oscillating partially stalled flow.

Work on stall flutter was begun at M.I.T. in the summer of 1947 when the evaluation of the low-angle-of-attack aerodynamic-derivative data was completed. The M.I.T.-NACA airfoil oscillator was modified to operate in the stall range and a large mass of aerodynamic-derivative data was accumulated which within its somewhat limited range gives a far more complete picture than has been heretofore available.

In this report an attempt has been made to evaluate these data with comparison, where possible, with other available data. The information thus obtained was used in critically examining proposed stall-flutter prediction techniques and actual stall-flutter tests.

This work was done at the Massachusetts Institute of Technology under the sponsorship and with the financial assistance of the National Advisory Committee for Aeronautics.

SYMBOLS

ω	angular frequency of forced motion
q	dynamic pressure $\left(\frac{1}{2}\rho V^2\right)$
α	pitching angle of wing, positive in direction of stall
h	vertical translation of wing at 37-percent chord, positive downward
β	angle between front and rear actuator wheels or, as defined in reference 1, angle between pitching and translatory motion
b	semichord
V	air-stream velocity
K	reduced-frequency parameter $(\omega b/V)$
θ	angle by which pitching motion leads translational motion

Description of Apparatus

Actuator and linkage.- The test-section arrangement is shown in figure 1. The mechanical features of the oscillator are shown diagrammatically in figures 2(a) and 2(b), which also briefly outline the functions of the various parts. The numbers in parentheses in the description below correspond to numbers of figures 2(a) and 2(b).

Power is supplied to the line shaft (1) by a 15-horsepower electric motor with a Ward-Leonard speed control. V-belts drive sheaves (2), which are geared to drive the crank wheels (3). These crank wheels all have variable-amplitude cranks and connecting rods which drive the vertical cross heads (4) at oscillator frequency. The phase β between the front and rear pairs of crank wheels may be varied in increments of 3.75° with the use of the angular scale (15). The position indicator (6) gives the position of the rear vertical members and the position of the other members may be found if the phase angle β between the front and rear crank-wheel pairs is known.

From the vertical cross heads the motion is carried to the cam (16) by steel bands (7). These bands are attached to the vertical cross heads by turnbuckles and to the cam by forks operating in ball bearings. A similar set of bands connects the cam to the springs (9) in the overhead structure, and the required initial band tension is attained by use of electric motors and gear trains (10). The motion of the cam is transmitted to the wing and accelerometers (17) through a four-bar linkage. The vertical bar (18) at the cam center is free to move vertically so that the cam may translate vertically, pitch, or move in any combination of the two motions.

The three airfoils used in these tests were constructed of sycamore wood and 0.007-inch magnesium-alloy sheet. The uncovered frame is shown in figure 3. Airfoil section and ordinates are given in figure 4.

Instrumentation.- The instrumentation used in these tests is that of figure 5. The amplifying equipment, the bridge balances, and the recording oscillograph are products of the Consolidated Engineering Corporation.

(1) The strain gages which measure lift, moment, drag, position, and translational and pitching accelerations are supplied with 1000-cycle carrier voltage by an oscillator manufactured by the Consolidated Engineering Corporation. Four strain-gage pairs are used to measure lift, two for drag, two for moment, and two each for pitching and translational acceleration.

(2) The equalizer panel consists of 15-ohm potentiometers in series with each strain gage (200 ohms) so that the sensitivity of each strain

gage may be varied individually; thus the strain-gage outputs may be made equal under a given load.

(3) The offset circuit utilizes resistances to unbalance the bridges by a known amount. Its purpose is to balance out the portion of the strain-gage signal due to static lift, drag, or moment, at high angles of attack. Thus the oscillating portions may be rendered on the sensitive paper of the oscillograph at a reasonable amplitude, keeping the amplifier output within the linear range.

(4) The bridge balance units consist of both a phase and resistance balance and are used to adjust the strain-gage output to zero under any tare loading.

(5) The position indicator serves to indicate reference points in the wing's cycle of motion.

(6) The attenuator boxes are used only in the lift and moment inertia circuits for balancing the inertia signal from the accelerometers against that of the wing. A better understanding of their use and operation may be gained by reading the section on calibrations.

(7) The amplifiers, as might be supposed, amplify and rectify the modulated 1000-cycle signals from the strain gages, for use in the oscillograph. The injected carrier shown feeding into the amplifiers in figure 6 is used to provide a reference signal amplitude level so that the amplifier output shows the positive or negative sense of the signal.

(8) The add circuit box serves the purpose of subtracting the inertia signal (from accelerometers) from the total (aerodynamic plus inertia) signal in lift and/or moment. The box is equipped with a switch so that the operator can control whether the signals shall pass through the add box and appear separately on the oscillograph record, or whether the subtraction described above shall take place and only the aerodynamic portion of the signal be recorded on the sensitive paper.

(9) The recording oscillograph utilizes high-natural-frequency galvanometers which deflect a beam of light onto sensitive paper for recording purposes. There are 14 channels available for use, 8 of which were used in these tests. The quantities measured together with their trace numbers are listed below:

1	Lift	9	Lift inertia
3	Drag	10	Moment inertia
5	Position	11	Lift inertia
7	Moment	12	Moment inertia

D	drag
L	lift force on airfoil
M	moment on airfoil
ϕ	phase angle between motion and reaction for sinusoidal reactions or lag angle as defined in reference 1
C	coefficient
T_r	characteristic time, defined in section, "Stall-Flutter Analysis"
K_r	reduced frequency involving characteristic time T_r
ΔC_M	variation of C_M from static curve $\left(C_{M_{actual}} - C_{M_{steady\text{-}state}}\right)$
λ	dynamic slope of moment against angle-of-attack curve
F	Theodorsen's function as defined in reference 2 (F(K))
G	Theodorsen's function as defined in reference 2 (G(K))
C(K)	Theodorsen's function as defined in reference 2 (F(K) + iG(K))
a	ratio of distance of elastic axis behind midchord point to semichord
c	chord of wing
Δh	increment of translatory motion
$\Delta\alpha$	incremental angle of attack or interval between mean angle of oscillation and steady-state stalling angle
t	time
$\delta\alpha$	interval between dynamic and steady-state stall $\left(\alpha_{stall} - \alpha_{steady\text{-}state\ stall}\right)$
j_3	torsional damping parameter as defined in reference 3
λ_c	frequency parameter used in British nomenclature $\left(\frac{\omega c}{V} = 2K\right)$
x_α	dimensionless center-of-gravity distance as defined in reference 2

I_α moment of inertia per unit length of wing about a

S_α static unbalance parameter for wing as defined in reference 2

r_α dimensionless radius of gyration of wing as defined in reference 2

C_α torsional stiffness parameter as defined in reference 2

C_h bending stiffness parameter as defined in reference 2

ω_α natural torsional frequency

ω_b natural bending frequency

$m/\pi\rho b^2$ mass ratio for wing as defined in reference 2

W work

Subscripts:

c critical

t torsion

L lift

M moment

T due to translational motion

P due to pitching motion

i initial or mean geometric position of airfoil

o amplitude of fundamental harmonic of motions or reactions (e.g., $\alpha = \alpha_o e^{i\omega t}$)

M.I.T. EXPERIMENTAL PROGRAM

The apparatus used in the over-all research (reference 4) was modified to make the apparatus useful for studies at high angles of attack. A review of the various elements of the mechanism both mechanical and electrical, and a complete outline of calibration, testing, and analysis procedures is contained in the following pages of this section.

It will be noted that lift inertia and moment inertia are each given two oscillograph channels. The reason behind this apparent duplication is that one lift inertia and one moment inertia trace will not appear on the record after subtraction from the appropriate total aerodynamic reaction signals.

Testing Procedure and Analysis of Data

Linkage setting and adjustment.- Immediately after assembly of the oscillator mechanism in the wind tunnel, careful adjustments of the linkage were made. These adjustments consisted of the following:

(1) Adjustment of amplitude of each crank to prevent any relative motion between the left and right wing supports

(2) Adjustment of turnbuckles to level all elements in the zero-amplitude position

(3) Check and adjustment of the clearances between the wing and end plates

After the linkage was adjusted, it was set to give a pure pitching motion. This was accomplished by setting the amplitudes of the cranks equal, and with 180° phase angle between the front and rear cranks. Phase angles between front and rear cranks were obtained by pinning the rear cranks in position, unmeshing the driving gears and setting the phase angle with the aid of the scale adjacent to the front crank wheel, and then remeshing the driving gears.

After the linkage was adjusted to give the desired motion, it was necessary to be able to set accurately the initial angle. A protractor incorporating a very sensitive level was used to measure the angle of the wing-support strain-gage beams with the horizontal. The angular measurements made with this device were quite accurate, being within ±0.1° of the desired value. In order to be certain that all four wing-support points were in a plane, a leveling plate was used. After the initial angle was set on the left side, the right rear element was lowered and the leveling plate was placed over the remaining three points. An adjusting screw was utilized to bring the rear element up into contact with the plate, the contact being indicated by a deflection of the needle on the dial of the amplifier attached to the moment bridge. This method permitted very accurate setting of the four supporting points so that their deviation from a plane was not greater than about 0.002 inch.

When the initial angle was set, the strain-gage beams were loosened and removed, and the wing was placed between the end plates; then the

strain-gage beams were inserted in their slots and tightened, the removable fairing plates replaced, and the mechanical apparatus was ready for tests.

Calibration.- Before any tests were actually run it was necessary to calibrate the equipment. The accelerometer circuits were provided with attenuators in the form of voltage dividers so that the accelerometer output could be varied from the full output to zero in 0.01-percent steps. Since the accelerometers were to be used to cancel the inertia signals of the wing, a device putting out the same inertia signal as the wing was indicated. The desired inertia signal was provided by the use of a "dummy" wing. The dummy was placed in the linkage in the same manner as the wing and oscillated in a desired motion. The signals from the accelerometer and the dummy wing were then added and fed into a cathode-ray oscilloscope. By varying the output of the accelerometer with the voltage divider described above it was possible to cancel out almost exactly the dummy-wing inertia signal. The best apparent setting of the voltage divider was chosen and the added signals were fed into the recording oscillograph. Records were taken at the best apparent voltage-divider setting and at several values on either side. After these oscillograph records were developed it was possible to find one in which the resultant signal was zero. The voltage-divider setting corresponding to this near perfect cancellation was then used throughout the entire series of tests.

If an indication of the average force or moment on a unit span of the wing was to be measured, it was necessary to have the sensitivities of all strain gages measuring that quantity equal. This was accomplished by applying an equal load to each supporting beam in turn, and adjusting the appropriate potentiometers in the equalizer box until the output for any one of the positions of loading was the same as for the others. This procedure was carried out for each of the lift, moment, and drag measuring elements.

Having equalized the sensitivities of the force measuring elements, it was possible to calibrate. For lift, this was accomplished by placing a wooden platform over the dummy wing and loading it with weights of known value. Moment was calibrated by hanging known weights on a bar at the center line of the rear elements, while drag calibration required a special rig of wire and pulleys so that loads could be applied in a horizontal plane.

In all these calibrations tare loads were taken into account and zero checks were made after every series of loads. A complete calibration of force measuring elements was made after every series of tests, and at all values of attenuation used during the tests.

A previous tunnel-throat survey indicates negligible variations in velocities across the test section; therefore no time was spent in making a similar survey, since conditions in general were almost identical. The tunnel calibrations were limited to a measurement of the velocity at the wing position in comparison with the velocity at the tunnel pitot-tube position.

Wind-on tests.- The first wind-on tests were conducted to obtain the static airfoil characteristics of the three wing sections. These tests were run at 95 miles per hour, and consisted of a measurement of the lift and moment on the airfoils at intervals of angle of attack of approximately 3° from the angle of zero lift up through the stall angle. The results of these tests are plotted in figures 7, 8, and 9.

It was found that three men were required to run the systematic tests: One to operate the wind tunnel and oscillator, one to operate the instrumentation, and one to take data and check the steps of the instrumentation operator. Tests were carried out through the complete oscillator frequency range on each of the three airfoils at initial angles of 0°, 6°, 10°, 12°, 14°, 18°, and 22° in pitch and translation.

The test procedure was about the same for all of the tests. With the wings installed between the end plates, and at the proper mean angle of attack, all necessary electrical adjustments were made and the tunnel was brought up to speed.

With the manometer set at 4.00 inches of alcohol the static lift force and moment signals were offset to as near zero-airspeed position as possible, and the oscillator was started and run up to the desired test frequency.

With the oscillator at test frequency the inertia and aerodynamic signals were adjusted separately to be just within the linear range of the amplifiers. The signals were then added and a record was taken.

The above procedure was repeated for each frequency, and then the tunnel power was shut off.

When the tunnel airspeed had reached zero, the offsets were all adjusted to the no-load position, and zero records were taken at all values of attenuation used in the tests.

Readings of temperature were taken for each series of tests so that necessary corrections in velocities could be made.

The procedure followed in each test is outlined again in the following check-off list:

(1) Check carrier voltage (10 volt)
(2) Balance bridges (injected carrier "off")
(3) Set injected carrier switch to "strain gages"
(4) Switch add box on "sep"
(5) Locate galvanometer zeros for lift, moment, and drag channels
(6) Put oscillator in neutral (pitch only)
(7) Start tunnel and bring up to speed
(8) Offset lift, moment, and drag to galvanometer zero positions
(9) Start and bring oscillator up to test frequency
(10) Set attenuator for maximum allowable amplitude (all traces)
(11) Set all meter switches on "galvanometer"
(12) Switch add box on "add"
(13) Take a record
(14) Repeat steps (8) through (13) for each frequency

Systematic tests.- The two types of motion considered are: (1) A pure pitching motion about the 37-percent chord with an amplitude of 6.08° and (2) pure translation with an amplitude of 0.9 inch.

The first series of tests in both pitch and translation were carried out at about 95 miles per hour and included tests at angles of 0°, 6°, 10°, 14°, and 18° with frequencies of 4, 8, 12, and 16 cycles per second for each airfoil at each angle of attack. A supplementary series of tests was devoted entirely to pure pitching motion with the threefold purpose of extending the range of K, showing trends at critical angles of attack not included in previous tests, and showing that small changes in Reynolds number would not affect the data to a large extent.

The supplementary tests were carried out at about 95 miles per hour except where noted and included (1) tests of each airfoil at each of the angles of attack listed above at frequencies of 2 and 18 cycles per second, (2) tests on each of the airfoils at mean angles of attack of 12°, 16°, and 22°, and (3) tests on the intermediate airfoil at a mean angle of attack of 14° at frequencies of 2, 4, 8, 12, 16, and 18 cycles per second, with velocities of 65, 80, 95, and 110 miles per hour.

Record analysis.- The analysis of records described below consists of a measurement of peak amplitudes and apparent phase angles and a harmonic analysis to determine net work per cycle and fundamental amplitude and phase of moment in pure pitch. The oscillograph traces utilized in this analysis are lift, moment, and position. No data on drag are presented in this report since a preliminary analysis of drag data indicated a coupling of lift and drag in such a manner that at times a considerable error in drag was introduced. It appears, however, that drag

forces are of little significance in the high-angle-of-attack flutter problem, so that this omission is relatively unimportant.

The lift and moment inertia traces were not used directly in record analysis. The presence of these traces on the record served as a continuous check on general accelerometer performance and also provided a basis for spot checks which compared the measured accelerations with calculated values.

The lift and moment traces are representations of the oscillating aerodynamic lift and moment, so that measuring the amplitude of the lift or moment trace and multiplying it by an over-all calibration factor give values of oscillatory lift or moment in pounds or inch-pounds, respectively. The coefficients of lift and moment (which are plotted in figs. 16 through 19) were calculated by use of the formulas:

$$C_L = \frac{L}{4qb(\text{span})}$$

$$C_M = \frac{M}{4qb^2(\text{span})}$$

The symbols C_L and C_M were used since they represent a magnitude without reference to wave form, whereas $\sqrt{R^2 + I^2}$ which was used in reference 4 indicates the amplitude of a sinusoid.

The phase angle ϕ is defined as the angle by which the force or moment leads the motion. This definition, however, is applicable only to a sinusoid. At large angles of attack, both the lift and moment traces tend to deviate from the pure sinusoids predicted by flutter theory. In cases where the wave form of the trace is not sinusoidal at the peak, no phase angles have been measured. In all cases, at angles of attack above 6°, caution must be exercised in the interpretation of measured phase-angle data. The plotted values of ϕ are averages of data taken from four cycles of each oscillation.

The positive directions of reactions, the peaks associated with maximum reactions, the location of peak angles of attack, and the distances measured to obtain phase angles are described in the diagram of figure 10.

The work per cycle for a pure sinusoidal motion and reaction may be determined as follows:

$$W_{pitch} = \oint M \, d\alpha = \pi \alpha_o M_o \sin \phi_M$$

$$W_{translation} = \oint L \, dh = \pi h_o L_o \sin \phi_L$$

Since in general M and L were not pure sinusoids it was desirable to resort to a graphical integration to obtain work per cycle. One cycle of each record was chosen and integrated, and occasional spot checks were made to insure that a typical cycle was chosen. The increments $\Delta\alpha$ and Δh were related to equal time increments in the manner illustrated by the table of figure 11, which also shows the graphical layout for the integration.

The axis directions of figure 10 determine the sign of the work so that a positive sign indicates work done on the wing by the air stream, and a negative sign indicates work done on the air stream by the wing.

Since work per cycle is proportional to the magnitude of the imaginary component of the fundamental harmonic of moment, a similar integration from a plot of moment against a motion 90° out of phase with the actual motion gives an area which is proportional to the real component. The ratio of work per cycle to this second area in work units is the tangent of the phase angle of the fundamental. From the equation above it can be seen that:

$$M_o = \frac{W_{pitch}}{\pi \alpha_o \sin \phi_M}$$

where M_o is the amplitude of the fundamental harmonic of the moment. Thus amplitude and phase angle of the fundamental harmonic of moment can be calculated.

The computation of the time-average values of lift and moment involves both measurements from the oscillograph records and the electrical offsets. First the distance from the mean line of the lift (or moment) trace to the zero-airspeed trace was measured. This distance was converted to a force (or moment) by a calibration factor for the particular attenuation used. The recorded value of electrical-offset in terms of force (or moment) was added to the value obtained by measurement

of distance on the oscillograph record to give the time-average value of the reaction.

ANALYSIS AND CORRELATION OF EXPERIMENTAL DATA

The experimental data discussed in the following pages of this section are the results of two different types of tests: (1) A series of flutter tests on wings of various properties held at high angles of attack in an air stream and (2) tests involving the use of mechanical apparatus which is designed to impart a particular motion to an airfoil in a wind stream.

The tests in the category of item (1) above have mostly been conducted in Europe, though two sets of American data are referenced later in this section. The data from such tests serve to describe the mechanisms producing flutter at high angles of attack in a very general way, so that forces and moments producing the oscillations cannot be directly related to the motions they produce. In order to relate reactions and motions the apparatus of item (2) above has been developed together with appropriate electrical measuring equipment.

Thus the aerodynamic reactions associated with a given motion may be accurately determined. The apparatus used in the M.I.T. tests is described under Description of Apparatus of this report and the equipment used in the British tests is described in reference 5.

Lift and moment in both pitching and translational motions are measured to obtain the M.I.T. data presented below. The British data involve only a measurement of moment in pitch or the out-of-phase component of moment in pitch.

The M.I.T. data have been taken with the value of Reynolds number near 1×10^6 while other investigators have used Reynolds numbers between 1.32×10^5 and 4×10^6 with the majority of the data from tests in a range below Reynolds numbers equal to 4×10^5.

Only very high Reynolds number data are applicable to aircraft wings, but the data taken with Reynolds number 1×10^6 and below are in the proper range for aircraft propeller and turbine blades.

M.I.T. Data

The oscillograph records from 150 tests have been analyzed and are presented in graphical form in figures 12 through 48, and in tabular form in tables I to IX.

The majority of the graphs use $K = \frac{\omega b}{V}$ as the abscissa. In most of the tests, airspeed has been held constant so that K is proportional to frequency. In cases where velocity has been varied, the velocities used are designated on the graph.

All data presented are within 5 percent of the true value. The maximum error in check calibrations is 2 percent and the instrumentation introduces an error no greater than 3 percent. These variations were allowed because of the nature of the data and the extreme amount of time and expense required to maintain greater accuracy with the equipment used in taking data. Some data in the vicinity of the stall are not reproducible to the accuracy described above because the aerodynamic situation here is somewhat akin to a state of neutral equilibrium and the condition of the flow depends on tunnel flow inconsistencies as well as on the motion of the airfoil. These data, however, represent a very small part of the total, and data from angles near the stall may be accepted as representative of the situation existing unless it is otherwise noted on the graph or tabulation.

Some data have been obtained by a direct measurement from the oscillograph records of amplitudes and phase angles. Since the reaction traces are not sinusoids in many cases the measured values lose some significance. However, the basic trends of the data are well-presented in this manner, and the method permits the analyst to cover a great deal of territory quickly.

Dimensionless coefficients of oscillatory force and moment and the phase relation of each of these with the motion have been measured directly from the oscillograph records and are plotted in figures 12 through 19. It will be noted that for low angles of attack the experimental points compare quite well with the theory. At high angles of attack, however, the traces of force and moment are no longer sinusoids, so that direct measurement on the oscillograph records gives values which represent the peak value of an arbitrary wave form and the time interval between its peak and the peak of the motion. The high-angle-of-attack values are plotted as phase angle and amplitude because the phase angles particularly have been found to be very close to the values obtained from harmonic analysis even where the trace of the reaction is far from sinusoidal. Further, both phase angles and amplitudes have been found to have the same general variation with K as the values calculated by the harmonic-analysis method which involves considerably more time and expense.

Some points in the figures mentioned above have no curves faired through them. This may indicate that the points are from low-angle-of-attack data where the reactions are essentially sinusoidal and hence should compare well with theory. Also in some instances at high angles

of attack, experimental points have fallen very near theoretical curves and have been left without curves faired through them to avoid confusion.

The plots of work per cycle (figs. 20 through 26) and the plots of phase angles and amplitudes from harmonic analysis (figs. 27 through 32) are the results of the graphical integration described in the section on record analysis.

In the plots of work per cycle, the positive-work range indicates that work is done on the wing by the air stream, while the negative-work range indicates that work is done on the air stream by the wing. It can be seen that positive work corresponds to negative damping so that in a free oscillation the amplitude would tend to increase if no other damping were present.

In the plots representing work per cycle in pure pitch the curves appear to describe a range of K in which positive work may be done. The graphs of figures 20 through 22 show the lower limit of this positive-work range and indicate that an upper limit exists by their tendency to assume a negative slope at higher values of K. The data compiled by Victory in reference 3 and discussed in the following section show a continuation of this trend at values of K higher than those plotted in figures 20 through 22.

In the plots representing work per cycle in pure translation, the curves all tend to remain in the negative-work region. At very low values of K (much lower than were obtainable with the equipment available in this program) it appears that there may be a possibility of positive work. Such a possibility is discussed by Den Hartog in reference 6 in connection with transmission line galloping. A further discussion of this possibility is contained in the section Stall-Flutter Analysis.

The graphical integration described in the section on record analysis has been used to determine the fundamental amplitude and phase angle in the trace of moment due to pitching. This type of analysis parallels the analysis of reference 7, so that it is possible to compare the trends of the two sets of data (see following section). Further, the trace of moment in pitch, while periodic, is farther from a pure sinusoid than any of the other reaction traces; and the fact that there is good agreement in the general trends of the data from the harmonic analysis and data measured directly from oscillograph records serves as an indication that the measured data (figs. 12 through 19) may be accepted as representing the trends to be expected from a harmonic analysis of the same basic data. A comparison of the phase angles of figure 12 with those of figures 27, 28, and 29 shows quite a remarkable agreement in order of magnitude and slope of the curves.

In general the coefficients of moment in pitch, plotted from the data of the harmonic analysis (fig. 30), are lower in value than the coefficients measured directly from the oscillograph records (fig. 16). This is to be expected since there are obviously higher harmonics which will contribute to the peak amplitude.

Figures 31 and 32 are respectively phase angle and amplitude of the fundamental harmonic of moment in pure pitch for various airspeeds. These tests were made on the intermediate airfoil to find if the test data were severely affected by Reynolds number at high angles of attack. A mean angle of attack of 14° was used in all tests. This is the stalling angle of the intermediate airfoil at 95 miles per hour.

Both of the above plates show some effects due to velocity changes. However, the trends of all curves are similar, and it is suspected that the primary reason for the differences is the variation of stalling angle with Reynolds number.

Figures 33 through 36 are presented to indicate the possible values of time-average lifts or moments under oscillatory conditions and to compare these with steady-state values. These coefficients could be used to calculate the total mean force or moment on the airfoils under oscillatory conditions.

Figures 33 and 34 are plots of the time-average moment coefficients. Figure 33 shows the time-average moment coefficients due to pitching. These vary considerably from the steady-state coefficients even at mean angles well below the stall. This deviation occurs on all of the curves, so that it is too consistent to be attributed to experimental error. It seems that this variation must be due to a change in center of pressure caused by stalling of the flow where local angles of attack induced by the pitching motion are high. It is of interest to note that at 18° mean angles the curves of figure 33 show that moment increases with K, while at 22° the opposite is true. The curves of figure 34 show only relatively small deviations from the steady-state curves, and in general it seems that the stalling angles are almost the same with translatory oscillations as in the steady-state case. At higher values of K, the maximum value of lift coefficient is slightly greater than the steady-state maximum value in all cases.

Figures 35 and 36 are plots of the time-average lift coefficients in both pitching and translation. The data for the blunt wing in figure 35 are somewhat incomplete since the zero records for 6° and 10° were found in error for all values of K except 0.06. However, with the data from the other two airfoils and from both motions, these data seem to indicate that time-average values of lift below the static stall may be assumed to be equal to the steady-state values without serious error. Near the steady-state stalling angle the time-average values of

lift may either exceed or be less than steady-state values for a pitching motion (fig. 35), but the lift continues near the maximum value for angles well above the steady-state stalling angle. The relation of lift coefficient to K in figure 35 at high angles of attack is interesting in comparison with the relation of moment coefficient to K in figure 33. As in figure 33, at 18° mean angle the coefficient increases with K, but at 22° mean angle, where the variation of moment coefficient with K is reversed, the variation of lift coefficient with K remains the same thus indicating that between 18° and 22° mean angles the center of pressure has shifted.

The curves of figure 36 for the blunt and sharp wings indicate that the lift in translation is somewhat higher than the steady-state lift, while the data for the intermediate wing show about the same values for each. The lift coefficient increases with K in all cases, and the maximum values of lift coefficient are higher than those in the steady-state case, although not necessarily occurring at the steady-state stalling angle.

All of the figures presented above give the results of various operations on the basic experimental data, and while they show correctly the trends and magnitudes of the quantities involved it is believed that the reader may gain a better physical feeling for the problem and a better understanding of what actually occurs during a cycle of oscillation if information such as that in figures 37 through 41 and 46 through 48 is presented him.

Figures 37 through 41 illustrate the variation of moment in pure pitch throughout a cycle of motion. The amplitude of the sinusoidal pitching motion is 6.08° in all cases and the pitching axis is at 37-percent chord.

Figure 37 illustrates the change with increasing mean angle of attack at a constant frequency. It will be noted that at 0° and 6° mean angles the moment traces a near elliptical shape quite similar to the path predicted in conventional flutter theory. The difference between the plotted figures and the elliptical path predicted by theory is due in part to the presence of hash on the oscillograph records and in part to the fact that the transcribed points were connected by straight lines rather than faired curves.

At 10° mean angle there is a definite break away from the ellipse at the maximum angle of attack, tending to reduce the negative-work area enclosed in the loop. At 14° mean angle the top portion of the loop is similar in position and curvature to the ellipse predicted by theory, but the airfoil stalls sharply near the maximum angle of attack so that the loop is enclosed by a clockwise progression of the moment, and the enclosed area is thus a measure of positive work. It is this type of

moment variation which causes negative damping at high mean angles of attack. At 18° mean angle the airfoil is always partially stalled as is indicated by the fact that the moment never reaches its steady-state value. At 22° mean angle the airfoil is almost entirely stalled throughout the cycle and the work area has again become negative. The variations in moment are probably due principally to shifts in the center of pressure. The negative moment (figs. 37(e) and 37(f)) does in fact indicate that the center of pressure has moved behind the 37° chord line. The small positive-work area near the minimum angle of attack indicates that the airfoil partially recovers from the stalled condition, and then stalls again almost immediately.

Figure 38 shows the increase in enclosed area with increasing frequency for a pure pitching oscillation about a mean angle of 6°, all other conditions being held constant. This effect is predicted by flutter theory which is a good approximation to the actual situation at this low angle of attack.

The loops described by the variation of the moment through a cycle assume various shapes depending on airfoil shape, mean angle, amplitude of motion, and K. Figure 39 illustrates a variation of the frequency through the range previously described. Since this oscillation is partially in the stall the effect is different from the low-mean-angle case described above. It is evident from an examination of these curves that the paths are composed of a part in which the moment attempts to follow the low-angle-of-attack slope of the moment curve, and another portion in which stall and recovery occur. For low frequencies the recovery is made before the minimum angle is reached, but at the highest frequency complete recovery from the stall does not occur until after the minimum angle is passed. Figure 40 shows the same general variation with frequency as figures 38 and 39, but at a different mean angle.

Figure 41 is included to show types of moment variations not shown in other plates. It can be seen that in general (or at least in the case of these three airfoils) with increasing mean angle of attack the moment through a cycle describes (1) an ellipse as predicted by theory, (2) a near ellipse except for a concavity on its upper side, (3) a figure-eight-shaped curve in which one loop indicates negative work and the other indicates positive work, (4) a loop which indicates all positive work, (5) another figure eight similar to curve (3), and (6) a loop which indicates all negative work when the airfoil is at a mean angle high enough that it never recovers from the stalled condition.

Several investigators, notably Reid in reference 8, have noted that in a pitching oscillation the stall may occur at an angle of attack considerably above the static stalling angle. The amount which the oscillatory stalling angle exceeds the static stalling angle is dependent on

a number of factors among which are K, $d\alpha/dt$, airfoil shape, and amplitude of oscillation. Figures 42, 43, and 44 are graphs showing the variation of $\delta\alpha = \alpha_{stall} - \alpha_{steady\text{-}state\ stall}$ with K for the three airfoils of the tests at various mean angles and for an amplitude of oscillation of 6.08°. Figure 45 shows plots of $\delta\alpha$ against $\dot{\alpha} = \frac{d\alpha}{dt}$ at stall for the same conditions. On all of these plots the curves are faired through the points in order of increasing frequency and the upper points at $\dot{\alpha} = 0$ are calculated on the assumption that at a sufficiently high frequency the airfoil will not stall before its maximum pitching amplitude is reached. The data required for all of the $\delta\alpha$ plots were obtained by measuring the oscillatory stalling angles from plots similar to those of figures 37 through 41.

Figures 46 through 48 illustrate the variation of lift in pure translation throughout a cycle of motion. The amplitude of the sinusoidal translatory motion is 0.9 inch in all cases.

Figure 46 illustrates the effect of increasing mean angle of attack for the airfoils in a pure translatory motion. It can be seen that the loops enclose very nearly equal areas except for the case where the airfoil is completely stalled. The change in size of these work loops for a given airfoil is dependent upon $K = \frac{\omega b}{V}$ in addition to the mean angle; hence the plots of work per cycle in translation (figs. 23 through 25) reveal a more complete picture. The more general trend in translation is an increase in negative work per cycle up to a mean angle approximately equal to the static stalling angle and then a sharp decrease in negative work per cycle for angles above the static stall.

Figure 47 illustrates the effect of increasing frequency at a constant mean angle of 10°. As in the case of pitching motion, the enclosed area increases in size with frequency. This seems to be a general tendency for airfoils in translational motion.

Figure 48 shows comparative data for the three airfoils used in the tests.

Figures 49 through 56 were chosen as typical examples of the oscillograph data analyzed and presented in this section, and where possible these plates are actually the basic data which are presented as the variation of lift or moment through a cycle of oscillation in figures 37 through 41 and 46 through 48. These figures are presented to show in a qualitative way the variation of the reactions with time and the order of magnitude of the extraneous reactions and oscillations encountered. The additional points described below will be evident after an examination of the figures by the reader.

Figure 49 through 51 are for a harmonic pitching motion. In the four pictures of figure 49 one can see the pure sine wave at 0°, a slight distortion of the sine wave at 10°, and at 18° a wave which is periodic but bears very slight similarities to a sine wave.

Figure 50 illustrates the differences in stalling characteristics and in recovery from stall for the three airfoils shown in figure 4.

The records of figure 51 show the effect of increasing frequency on the sharp-nosed airfoil of figure 4.

Figures 52 through 54 are for a harmonic translatory motion. Figure 52 shows the effect of increasing mean angle on the intermediate airfoil. Figure 53 shows differences in airfoils at a mean angle of 10° and a frequency of approximately 8 cycles per second, while figure 54 shows the effect of increasing frequency on the sharp airfoil. It will be noted that in general the differences in corresponding records for translatory motion are much less than for pitching motion.

Figure 55 shows the record obtained from the blunt airfoil at an angle very near the static stalling angle. This record is not periodic, apparently indicating a condition of partial stall all through the cycle of motion with the amount of stall not directly related to induced angle but probably more a function of tunnel flow inconsistency. Figure 56 is another record taken very near the static stalling angle. It can be seen that the wing is stalled during some cycles and unstalled during others. The records of figures 55 and 56 are indications of the poor degree of reproducibility of data at angles near the stall as mentioned earlier in this section. This situation occurs more frequently in translatory motion than in pitching motion, and its effects are more pronounced in translation. It is apparent that the solution to this problem is a tunnel with an absolutely uniform flow.

Correlation with Experimental Data from Other Sources

Other experimental data which have been gathered on airfoils oscillating at high angles of attack may be divided into two general types: (1) Critical speeds obtained in a manner similar to that used in conventional flutter tests, except that the airfoil is placed at an initially high angle of attack in the air stream and (2) tests which measure the oscillating aerodynamic moment in pure pitch in a manner similar to that used in the M.I.T. tests, but which neglect other reactions and motions. The tests under the category of item (1) above were carried out for the most part several years ago. Several investigators have contributed to these data, Studer and Kaufman whose work is summarized by Victory in reference 3, Rauscher in reference 9, and Bollay and Brown in reference 10 being the most noteworthy.

An even larger number of experiments has been made in the category of item (2) above. Victory in reference 3 describes tests in which only the out-of-phase component was measured, and Bratt and Scruton in reference 5 plot the path of moment through a cycle of oscillation much in the same manner as is done in this report.

Bratt and Wight in reference 7 have been able to measure both the in-phase and out-of-phase components of moment, thus making possible the computation of vector amplitude and phase angle of the fundamental.

One further interesting reference is available which falls into neither of the categories listed above. Reference 11 by Bratt, Wight, and Chinneck is an investigation of aerodynamic damping in pure pitch as affected by initial angle and angular amplitude of oscillation.

High-angle-of-attack flutter tests.- Rauscher and Studer were among the first experimenters to show the sharp drop in critical speed as angle of attack is increased toward the stall. Studer's investigation showed, and since then other investigators have shown, that, for low values of frequency parameter, the drop in flutter speed may be as much as 60 percent of the classical flutter speed. However it has also been shown that as frequency parameter is increased the percentage drop in flutter speed decreases so that at very high values of K the classical and stalling flutter speeds tend to approach a common value.

Studer (reference 12) was able to obtain some interesting results by varying the mass and geometrical properties of his wing. A minimum stalling flutter speed was found to occur when the elastic and gravity axes were coincident so that there was no inertia coupling. A critical speed below even this minimum was obtained by restraining the wing from translatory motion and allowing only freedom in pitch.

Studer also varied the bending torsion frequency ratio, and found that the critical speed in stalling flutter was quite insensitive to such variations. In all of the cases investigated in Europe the flutter motion was observed to be predominantly a pitching oscillation even though the same physical configuration had primarily a translatory motion in classical flutter. However, Bollay and Brown at Harvard observed a stalling flutter of a solid Duralumin propeller section in principally the first bending mode. The critical speed was 127.5 miles per hour as compared with a classical flutter speed of 900 miles per hour so that it is almost certain that the rather violent vibrations were actually stalling flutter. It is possible that the first bending mode of the blade was equivalent to a translation plus an in-phase rotation about an axis in front of or behind the blade, but there are insufficient data really to fix the mode of flutter in reference 10. Bollay and Brown differentiated between the usual stall flutter and the excitation associated with Kármán vortices. Their results showed that, since the

Kármán vortex frequency was directly proportional to velocity, moderate vibrations built up at airspeeds where vortex frequency coincided with a natural frequency of the wing. These vibrations however were much less violent than the oscillations described above and the reduced frequency for Karman vortex excitation was about three times that for stall flutter. These same experimenters made a number of tests on another wing, and their results are used as a basis for some of the computations and text in the next section.

Measurement of aerodynamic reactions.- A large part of the data in reference 3 which includes the work of Bratt and Scruton (reference 5) has been replotted against the same variables used in the presentation of M.I.T. data.

It can be seen that the M.I.T. and the British data cannot be made to compare quantitatively since there is no theoretical correction such as that described in reference 4, which can be applied to account for changed pitching-axis position. Further the airfoil shapes used in obtaining the British data are different from the airfoils described in this report, and the Reynolds numbers are widely different. Also because of the low airspeeds used in the British tests considerably higher values of the frequency parameter were obtainable, so that the two sets of test data do not cover the same range.

Figures 57 through 60 are taken from reference 3, and it is possible to obtain rather good qualitative comparisons with M.I.T. test data if $\Delta\alpha$ is defined as the angular interval between the mean angle and the steady-state stalling angle of the airfoil (positive when α_i is greater than the steady-state stall), and this parameter is used as a basis of comparison. By using data from the M.I.T. tests for the low K range and the British data for the higher K range, and the highest angle-of-attack range, figure 61 was constructed using parts of figures 20 through 22 and 57 through 60. This figure shows approximately the way in which work per cycle (or aerodynamic moment) varies with K and α. First for low angles of attack the curves of work per cycle against K remain negative and near the theoretical curves, gradually approaching zero work as $\Delta\alpha$ approached zero. Near $\Delta\alpha$ equal to zero a positive-work area appears at very low values of K. As $\Delta\alpha$ is further increased the maximum value of positive work is increased and the range of positive work is narrowed but continues to move to higher values of K.

Reference 3 has summarized the results of several investigations into the effect of Reynolds number on the out-of-phase component of aerodynamic moment. The curves and tabulated data in this summary show that for high Reynolds numbers (above 2×10^6) and moderately high values of frequency parameter (above 0.5) the effect of angle of attack on the out-of-phase component of aerodynamic moment is small. Thus in this range a pure pitching oscillation with a conventional rotational-axis position

would be damped. Bratt and Wight in reference 7 devote a considerable portion of their work to an investigation of the effects of aspect ratio, which is beyond the scope of this report. However these investigators were able to measure both components of the oscillatory aerodynamic moment, so that their data can be plotted in a manner similar to the M.I.T. data. Figure 62 is a plot of work per cycle against K. These data compare quite favorably with M.I.T. data if the basis of comparison is $\Delta\alpha$ rather than α_1.

Figure 63 is a plot of oscillatory moment coefficients and phase angles and it can be seen that these curves are quite similar to some of the data plotted from the M.I.T. tests. Theoretical curves are also plotted in figure 63 and phase angles particularly can be seen to agree quite well with theory for low angles of attack.

All of the data taken in Great Britain measures the oscillating aerodynamic moment less the still-air inertia and damping forces. In reference 7 a coefficient to account for still-air damping has been obtained experimentally, but none of the figures described above has such a correction applied. However in most cases the effect of this damping is small enough that the general trends of the data are preserved.

Effect of oscillation amplitude.- In all of the British references it has been observed that the reactions on an airfoil oscillating at high angles of attack are functions of the amplitude of the oscillation as well as Reynolds number, frequency, velocity, and initial angle of attack.

Especially in reference 7 was this particular phase of the problem investigated. This series of experiments definitely established the fact that there are amplitude effects at high initial angles of attack, but for any given set of conditions only two amplitudes of oscillation were studied so that no curves of aerodynamic reactions against oscillation amplitude can be plotted.

The authors of reference 11 attack the problem of amplitude effects in a different manner from the other experimenters. Their thesis is that for any initial angle of attack there is some magnitude of angular deflection which can cause partial stalling of the flow and thus cause negative damping of the motion. The mechanical apparatus used in this series of experiments was an airfoil restrained against translational motion and spring-mounted in pitching so that, if it were deflected and released, a pure pitching oscillation resulted. At various values of reduced frequency, tests were run in which the airfoil was deflected through larger and larger angles from a given initial angle of attack until an undamped pitching oscillation was observed on release of the airfoil. Thus a series of critical angular amplitudes was obtained, below which oscillations were damped and above which the oscillations

tended to diverge. Figure 64 is a plot of such data taken directly from reference 11. These curves show a stable range at low and at very high angles of attack and a range of instability in between. A similar effect (with a constant angular amplitude) may be observed by referring to figures 20, 21, and 22, and noting that with increasing initial angle of attack the curves move into the positive-work range and then back into the negative-work range.

STALL-FLUTTER ANALYSIS

The term "stall flutter" is usually associated with a periodic self-excited vibration of an "airfoil" with definite mass and elastic properties in a flow which is separated during part or all of the motion. The basic difference between "classical flutter" and "stall flutter" is in the character of the flow. As pointed out by Victory in reference 3, stall flutter is not likely to occur on conventional airplane wings, but it does occur on propeller blades and turbine blades and some basis for predicting stall flutter or at least some knowledge of its characteristics would be very helpful. Of course in these applications three-dimensional and cascading effects further complicate the picture.

The experimental evidence of stall flutter has been obtained for the most part under controlled laboratory conditions where the flow is two-dimensional and the airfoil is rigid and supported on springs. Even for these tests, however, no adequate method of prediction has been evolved.

This problem of prediction by analytical means can probably best be approached by examining the additional complexity introduced by the stalling of the airfoil. Basically the mass and stiffness properties of the wing are unchanged but a new variable, the initial angle of attack α_i, has been introduced into the determination of the aerodynamic derivatives. Perhaps a better form for this new variable is something like $\Delta\alpha = \alpha_i - \alpha_{stall}$ used in figures 42 through 45. Regardless of the form, however, the problem becomes extremely complex because the aerodynamic derivatives can no longer be simply superimposed as in classical-flutter theory; that is, the aerodynamic results of a pitching motion cannot be separated from that of a simultaneous translatory motion. There is the further effect that even in a pure motion the introduction of the new angle-of-attack variable automatically requires consideration of the large effects of such factors as Reynolds number and airfoil shape.

Thus an exact mathematical formulation of the problem is out of the question at present and the attack must be made along empirical lines. Unfortunately only a small amount of empirical data has been published

although a number of general characteristics of the usual stall flutter can be deduced from these tests. As the angle of attack is raised through the stall region and the flow is stalled during larger and larger parts of the cycle of vibration:

(1) The flutter speed drops severely
(2) The flutter frequency rises slowly toward the torsion frequency of the wing
(3) The motion appears to become predominantly pure torsion although the axis of rotation is not in general the elastic axis
(4) Usually the flutter speed reaches a minimum and then rises again as the flow becomes completely stalled

A study of these general characteristics has suggested the following plan of attack which is based on proceeding from the comparatively firm ground of classical flutter into the realm of stalled flows.

(1) Attempt to take initial angle of attack into account by modifying the existing classical theory by whatever means suggest themselves through experience or intuition. Preferably these analyses should automatically reduce to the classical case at low initial angles of attack.

(2) Determine which general kinds of modification produce the trends which have been observed in actual cases of stall flutter.

(3) Attempt to correlate these findings with existing aerodynamic-derivative data in the hope of discovering which aerodynamic terms play a dominant part in stall flutter.

(4) Try to predict the possible variations of these critical terms using airfoil data ordinarily available.

This plan of course is aimed at the kind of stall flutter in which the angle of attack does not exceed the steady-state stall angle by more than 8° or 10°.

Den Hartog's Simplification

Den Hartog (reference 6) shows that one type of transmission line galloping is actually a stall flutter where the angle of attack of the ice-coated cable is of the order of 90°. For an analysis of this motion it would of course be foolish to try to modify classical aerodynamic terms rather than make an attempt at estimating the aerodynamic derivatives in the completely stalled flow. Since the frequency of the galloping is only about 1 cycle per second ($K \approx 0.01$), Den Hartog, as a first attempt, works only with an assumed static or steady-state lift curve. Considering

the changes in angle of attack to be induced by the vertical motion, he shows that the motion is negatively damped on the negative-slope portion of the lift curve. Although an excellent qualitative discussion, it is suggested that if quantitative answers to this problem are desired the rotation of the transmission line cannot be overlooked. It seems certain that, with the very low torsional stiffness of the long span of cable, the combined effect of the mass unbalance caused by the ice formation and the aerodynamic moment about the cable axis will produce changes in angle of attack of the same order of magnitude as those induced by the vertical motion.

Victory's Use of Experimental Data

Turning to the more usual type of stall flutter, Victory in reference 3 follows the first three steps of the outlined plan of attack to show the dominant effect of the torsional damping parameter. This parameter j_3 is equivalent to

$$\frac{\pi}{4}\left[\frac{1}{2}\left(\frac{1}{2}-a\right)-\left(\frac{1}{4}-a^2\right)F-\left(\frac{1}{2}+a\right)\frac{G}{K}\right]$$

in the usual expression for aerodynamic moment in the vortex-sheet theory:

$$M=-4\pi qb^2\left(\left[\frac{aK^2}{2}-\left(\frac{1}{2}+a\right)iKC\right]\frac{h}{b}+\left\{\frac{1}{2}\left[iK\left(\frac{1}{2}-a\right)-K^2\left(\frac{1}{8}+a^2\right)\right]-\left(\frac{1}{2}+a\right)\left[1\times iK\left(\frac{1}{2}-a\right)C\right]\right\}\alpha\right)$$

It had long been suspected by the British that the reduction in flutter speed near stalling angles of attack was caused by a reduction of aerodynamic torsional damping. Thus Victory decided to try modifying the classical theory by varying only the parameter j_3.

Fortunately experimental measurements of j_3 had been made at the National Physical Laboratories for an airfoil which was very similar to one used by Studer (reference 12) for actual stall-flutter tests under almost identical conditions. In each case the symmetrical airfoil had a reference axis at one-half chord and was tested through about the same Reynolds number and frequency-parameter ranges. Thus, by this happy circumstance, it was possible to substitute measured values of j_3 into

the modified classical theory and then check the results against comparable stall-flutter tests. Inasmuch as the agreement between calculated and experimental flutter speeds is very good, an examination of the procedure is probably well worth while.

The series of tests by Studer for which calculations were made had a common value of torsional frequency and six different bending frequencies so that the range of frequency ratio ω_α/ω_b was from 1.06 to 2.12. Flutter calculations were made for these conditions for values of j_3 ranging from 0 to 1.0 so that plots of flutter speed, frequency, and frequency parameter $\lambda_c = 2K$ against j_3 could be constructed. These plots have been reproduced as figure 65. A curve of the classical variation of j_3 with λ_c has been superimposed on figure 65(b) to show the amount of variation of torsional damping required at any value of the frequency parameter to produce flutter. The intersection of this curve with each of the other lines indicates the value of j_3 corresponding to the classical-flutter solution for each frequency ratio. These values of j_3 then determine the flutter speeds and frequencies as marked by circles in figure 65(a).

In order to obtain the semiempirical stall-flutter points, Victory plotted the six theoretical curves of λ_c against j_3 on the same sheet as the N.P.L. (j_3,λ_c) curves, where they cut most of the experimental curves at least once. At these points of intersection the correct experimental correspondence exists between j_3 and λ_c for the particular angle of attack at which the experimental curve was plotted. The flutter speeds corresponding to these values of j_3 were then obtained from figure 65(a). The agreement between these calculated and Studer's experimental flutter speeds is quite good, especially for the larger frequency ratios where the flutter speed does not vary so sharply with j_3. As mentioned by Victory the calculated flutter speeds have their sharp drop at a slightly lower angle of attack than the experimental speeds largely because the static stalling angle of Studer's wing is about 2.5° higher than the N.P.L. wing. If the speeds had been plotted against $\Delta\alpha = \alpha_i - \alpha_{stall}$ rather than α_i, this difference would disappear.

Thus it appears that the decrease, although not necessarily the disappearance, of torsional damping is an important, almost predominant, factor in the stall flutter of this particular wing.

In an attempt to extend these findings to another range of parameters, some theoretical points similar to those of figure 65 have been calculated for wing II tested by Bollay and Brown (reference 10) and used by Mendelson (reference 1) in his analytical approach. The results of these calculations appear in table X along with results stemming from Mendelson's analysis.

Mendelson's Modification of Classical Theory

A somewhat different approach to the stall-flutter problem was employed by Mendelson in reference 1. Following to some extent the plan of attack outlined earlier in this section, the classical theory was modified in the stall range to take into account a suspected aerodynamic hysteresis or lag. As stated by Mendelson, "The assumption was made that the absolute magnitude of the oscillatory aerodynamic forces and moments are the same at the stall as at zero angle of attack but that the vector magnitudes of these forces and moments are changed, this change being caused by the lag of aerodynamic damping and restoring forces behind the velocities and displacements at stall, thus giving rise to a hysteresis effect." Denoting this lag by the angle ϕ, the classical expressions for lift and moment become:

$$\frac{L}{4qb} = -\pi\left(-\frac{K^2}{2} - KG + iKFe^{-i\phi}\right)\frac{h_o}{b}e^{i\omega t} - \pi\left\{\frac{aK^2}{2} - K\left(\frac{1}{2} - a\right)G + Fe^{-i\phi} + i\left[\frac{K}{2} + G + K\left(\frac{1}{2} - a\right)F\right]e^{-i\phi}\right\}\alpha_o e^{i(\omega t-\beta)}$$

$$\frac{M}{4qb^2} = -\pi\left[\frac{aK^2}{2} + K\left(\frac{1}{2} + a\right)G - iK\left(\frac{1}{2} + a\right)Fe^{-i\phi}\right]\frac{h_o}{b}e^{i\omega t} - \cdot\ \pi\left\{-\frac{K^2}{2}\left(\frac{1}{8} + a^2\right) + K\left(\frac{1}{4} - a^2\right)G - \left(\frac{1}{2} + a\right)Fe^{-i\phi} + i\left[-\left(\frac{1}{2} + a\right)G - K\left(\frac{1}{4} - a^2\right)F + \frac{K}{2}\left(\frac{1}{2} - a\right)\right]e^{-i\phi}\right\}\alpha_o e^{i(\omega t-\beta)}$$

Substituting these expressions in the usual bending-torsion flutter relations

$$-m\omega^2 h_o e^{i\omega t} - S_\alpha \omega^2 \alpha_o e^{i(\omega t-\beta)} + C_h h_o e^{i\omega t} - L = 0$$

$$-I_\alpha \omega^2 \alpha_o e^{i(\omega t-\beta)} - S_\alpha \omega^2 h_o e^{i\omega t} + C_\alpha \alpha_o e^{i(\omega t-\beta)} - M = 0$$

expanding the determinant of the coefficients of h_o and $\alpha_o e^{-i\beta}$, and separating into a real and an imaginary equation, there result two quadratics in $(\omega_\alpha/\omega)^2$ with coefficients involving K and ϕ. These may be written:

$$\left(\frac{\omega_\alpha}{\omega}\right)^2 = F_1(K,\phi) = F_2(K,\phi)$$

If the properties of a given wing are substituted in F_1 and F_2, the equation can be solved for K for a given value of ϕ by finding the intersections of F_1 and F_2 plotted against K.

This was done by Mendelson for the wing used by Bollay and Brown (reference 10). For zero aerodynamic lag, that is, for $\phi = 0^\circ$, the solution gives the classical flutter speed of 79 miles per hour. For increasing values of ϕ the flutter speed drops almost linearly to about 30 miles per hour at a ϕ of 55°. Encouraged by this result Mendelson proceeded to relate this change in ϕ to the steady-state lift curve.

A closer examination of his answer, however, would have produced disquieting results. The drop in flutter speed is also accompanied by a decrease in flutter frequency which is contrary to the Bollay and Brown tests, to the usual experimental results, and to Victory's predictions. It also appears that the assumed values of aerodynamic lag ϕ are, especially for moment due to pitch, opposite in sign to the experimentally observed behavior in forced motion discussed in the next section. For the assumed change in vector but not absolute magnitudes, the only way for Mendelson's ϕ to follow the trends indicated experimentally is to take on negative values, that is, values less than 360°.

This second observation indicates that perhaps Mendelson was looking for the equality between F_1 and F_2 for the wrong range of ϕ. To check this observation a calculation was made at a reduced frequency of 0.30 which corresponds to a ϕ of 35° on Mendelson's curve. As can be seen in figure 66, another intersection exists for this K at $\phi = 351^\circ$ which yields a higher flutter frequency but lower flutter speed than for the classical case. The frequency is somewhat higher than might be expected as shown in table X but the trend is correct.

Since observed stall-flutter oscillations are usually described as predominantly pure pitching motions a check was made of amplitude ratio and phasing between the motions for the classical case and for $\phi = 23^\circ$, 35°, and 351°. A ϕ of 23° corresponds to a calculated flutter speed equal to the experimental speed measured at an initial angle of attack of 11.2°. Values of ϕ of 35° and 351° correspond to a calculated

flutter K very nearly the same as the experimental K for the same test. The results as shown in table X indicate that for all three values of ϕ the motion is predominantly pitch although about quite different axes. For $\beta = 10.7^{\circ}$ ($\phi = 35^{\circ}$) the effective axis of rotation is about half a semichord ahead of the elastic axis; for $\beta = 172.4^{\circ}$ ($\phi = 351^{\circ}$) the effective axis is about the same distance behind the elastic axis. It is unfortunate that Bollay and Brown did not record either phasing or effective axis of rotation.

A basic difference between Mendelson's and Victory's approaches is the number of terms in the classical expressions which are modified in the stall range. Victory modifies only one critical term, the torsional damping. Mendelson applies his factor to a majority of the aerodynamic terms. In order to compare the results of the two procedures calculations were made at a reduced frequency of 0.3 for the Bollay and Brown wing using Victory's modification. In addition calculations were made at the same reduced frequency applying Mendelson's "corrected" factor ϕ only to moment in pitch. The results, as shown in table X, show that for this case the additional modifications imposed by Mendelson had a very small effect, although none of the answers check very well with the experimental values.

This latter discrepancy may indicate that another aerodynamic term should be modified in an as yet untried manner although it is possible that small errors in wing properties may be greatly magnified in the calculations because the frequency ratio is quite near unity. To investigate which aerodynamic terms play an important part in the critical balance at flutter, vector plots have been constructed to illustrate some of the solutions. As shown in figure 67 the plots are referred to a unit α vector with separate vectors for lift and moment due to pitch about the elastic axis and for lift and moment due to translation. Lift and moment are plotted in such a way that the components of the moment vectors perpendicular to α are a measure of the work per cycle in pitch and the components of the lift measured perpendicular to h multiplied by the amplitude ratio $h/b\alpha_0$ are a measure of the work per cycle in translation.

It appears that in the cases corresponding to stall flutter the energy balance is governed by the torsional damping, the lift due to pitch, the phasing between the lift due to pitch and the translational motion, and the amplitude ratio. Thus the aerodynamic reactions resulting from the translation are very small but the work per cycle associated with translation combined with lift due to pitch is a very important part of the energy balance. On this basis a more complete evaluation of the available data on lift due to pitch seems to be desirable in order to determine what other modification of the classical theory is appropriate. Variation of torsional damping is important, perhaps predominant, but is not the complete answer to stall-flutter prediction.

Haley's Prediction of Aerodynamic Moment

Apparently, then, it is possible to predict to some extent the trends of stall flutter for a particular configuration if experimental oscillatory data, especially for moment in pitch, are available. The data, however, must be for the correct airfoil shape, Reynolds number range, and reduced, frequency range.

These data, of course, are hardly ever available and are very expensive to obtain experimentally. Thus a very necessary step in an adequate prediction technique concerns the deduction of this information from steady-state data normally available. These available data should contain insofar as possible the effects of airfoil shape and Reynolds number.

Mendelson (reference 1) attempted to correlate his phase lag ϕ with the changes in slope of the curve of steady-state lift against angle of attack. This type of correlation may be a fair first approximation for relating a correction to the theory to the characteristics of the airfoil section but it makes no allowance for the variation in ϕ with reduced frequency which definitely does occur.

Haley[1] attempts in the case of moment in pitch to use the curve of steady-state moment against angle of attack to predict the actual variation of moment in the stall range including the effects of reduced frequency and amplitude of oscillation. Actually all of his work was done for one airspeed but, as will be shown, the method can be generalized quite easily. Some intelligent guessing and experience is needed to get reasonable and useful results by this method but the end result could quite possibly be a satisfactory set of curves of torsional damping against reduced frequency for a useful range of angles of attack.

Since the original paper is not generally available, a detailed and somewhat improved development is presented here.

If at a given airspeed and instantaneous angle of attack the actual value of moment coefficient (or moment) differs from the steady-state value by an amount ΔC_M, a possible assumption is that the rate of return of C_M to the steady-state value is proportional to ΔC_M. This can be written simply:

$$\frac{dC_M}{dt} = -\frac{\Delta C_M}{T_r} \tag{1}$$

where T_r can be thought of as a characteristic time. Equations of this form describe many simple physical systems whose response to a

[1]Unpublished M.I.T. Master's thesis by H. C. Johnson and S. M. Haley, "Analysis of the Aerodynamic Reactions on Airfoils Oscillated in the Stall Range," June 1949.

step function is a simple exponential governed by the characteristic time or time constant T_r.

As might be expected, however, this equation is a little too simple to describe the variation of moment.

In comparing the predictions of this equation with the known behavior of moment during oscillations at angles of attack below the stall, it was found that T_r is different for different frequencies of oscillation and that the very simple definition of ΔC_M is not adequate. An arrangement similar to the static and dynamic load-line concept in electronics was found to be necessary for handling oscillations at various initial angles and frequencies. Thus ΔC_M is now redefined (fig. 68) as

$$\Delta C_M = C_M - \left(C_{M_i} + \lambda\alpha\right) \tag{2}$$

where C_{M_i} is the value of C_M given by the steady-state characteristic for the initial angle of attack α_i, λ is the "dynamic" slope of moment against angle of attack, and α is the instantaneous angle of attack referred to α_i and is usually written $\alpha = \alpha_o e^{i\omega t}$. Using the new definition of ΔC_M together with the basic differential equation

$$\frac{dC_M}{dt} = -\frac{\Delta C_M}{T_r} \tag{1}$$

the following equations are obtained:

$$\frac{d(\Delta C_M)}{dt} + \frac{\Delta C_M}{T_r} = -\lambda \frac{d\alpha}{dt}$$

$$\frac{d}{dt}\left(C_M - C_{M_i}\right) + \frac{1}{T_r}\left(C_M - C_{M_i}\right) = \frac{\lambda}{T_r}\alpha$$

Assuming in each case a constant frequency oscillation $\alpha = \alpha_o e^{i\omega t}$,

$$\Delta C_M = -\frac{\lambda\alpha_o\omega T_r}{1 + (\omega T_r)^2}(\omega T_r + i)e^{i\omega t} \tag{3}$$

$$C_M = C_{M_i} + \frac{\lambda \alpha_o}{1 + (\omega T_r)^2}(1 - i\omega T_r)e^{i\omega t} \tag{4}$$

The classical expression for moment due to pitch is (reference 2):

$$C_M = C_{M_i} + \frac{\pi}{2}\alpha_o e^{i\omega t}\left\{\left[2\left(\frac{1}{2} + a\right)F - 2\left(\frac{1}{4} - a^2\right)KG + \left(\frac{1}{8} + a^2\right)K^2\right] + i\left[2\left(\frac{1}{2} + a\right)G + 2\left(\frac{1}{4} - a^2\right)KF - \left(\frac{1}{2} - a\right)K\right]\right\}$$

Equating the two expressions for C_M,

$$\omega T_r = -\frac{2\left(\frac{1}{2} + a\right)G + 2\left(\frac{1}{4} - a^2\right)KF - \left(\frac{1}{2} - a\right)K}{2\left(\frac{1}{2} + a\right)F - 2\left(\frac{1}{4} - a^2\right)KG + \left(\frac{1}{8} + a^2\right)K^2} \tag{5}$$

$$\lambda = \frac{\pi}{2}\left[2\left(\frac{1}{2} + a\right)F - 2\left(\frac{1}{4} - a^2\right)KG + \left(\frac{1}{8} + a^2\right)K^2\right]\left[1 + (\omega T_r)^2\right] \tag{6}$$

Thus it appears that the simple assumed differential equation is adequate for unstalled flow if ωT_r and λ are determined for a given reduced frequency from the above relations.

The fact that the product ωT_r is the important parameter rather than T_r alone suggests that a better formulation is possible. The product ωT_r can be considered as a frequency ratio which compares the frequency of the motion to a frequency which is characteristic of the aerodynamic moment at the given airspeed. By suitable juggling it can also be written that

$$\omega T_r = \frac{\omega b}{V}\frac{V T_r}{b} = \frac{K}{K_r}$$

Thus there is a characteristic quantity K_r which includes both T_r and its associated velocity in such a fashion that K_r is a function only of reduced frequency K since equation (5) becomes

$$K_r = K\left[-\frac{2\left(\frac{1}{2}+a\right)F - 2\left(\frac{1}{4}-a^2\right)KG + \left(\frac{1}{8}+a^2\right)K^2}{2\left(\frac{1}{2}+a\right)G + 2\left(\frac{1}{4}-a^2\right)KF - \left(\frac{1}{2}-a\right)K}\right] \tag{7}$$

The basic equation (1) becomes:

$$\frac{dC_M}{d(\omega t)} = \frac{dC_M}{2\pi d\left(\frac{t}{T}\right)} = \frac{\frac{-1}{K}}{K_r}\Delta C_M \tag{8}$$

where

$$T = \frac{2\pi}{\omega}$$

which shows that the rate of change of C_M based on a time scale related to the motion is proportional to ΔC_M where the factor of proportionality depends only on the reduced frequency K. Equation (4) becomes:

$$C_M = C_{M_i} + \frac{1 - i\left(\frac{K}{K_r}\right)}{1 + \left(\frac{K}{K_r}\right)^2}\lambda\alpha_o e^{i\omega t} \tag{9}$$

which corresponds to an elliptical contour on the plane of moment against angle of attack. The center of the ellipse is at $\left(C_{M_i},\ \alpha_i\right)$; the line joining the center with $C_{M_{max}}$ and $C_{M_{min}}$ is of slope λ; and both the eccentricity of the ellipse and the slope λ depend only on the reduced frequency K.

Proceeding now to oscillations which are partly or altogether in the stall region, certain observations can be made from the experimental results which can be a guide in extending the analytical technique.

The variation of the moment with angle of attack apparently can assume quite a variety of shapes as shown in figures 69 and 37 through 41 but certain general characteristics can be observed. For oscillation into and out of the stall region:

(1) The unstalled portion of the moment variation is essentially a part of the ellipse easily determined from the equations based on the dynamic slope λ.

(2) In the stalled portion, the moment at any angle of attack appears to tend toward the steady-state value of moment at the angle in a manner very similar to that below the stall. Usually these stalled steady-state values can be approximated by a straight line with a decidedly negative slope.

(3) The actual stall occurs at an angle of attack above the steady-state stall angle but usually below the peak angle of attack of the oscillation. (See figs. 42 through 45.) The recovery begins approximately at the steady-state stall angle.

For oscillations which are entirely above the stall such as the curve on the right side of figure 69, the moment variation is approximately elliptical and appears to be related to its steady-state slope in a manner similar to the relation below the stall.

Following these observations, it is possible to make some assumptions which enable an attempt at prediction of the moment variation.

(1) For the unstalled portion of the cycle use the appropriate part of the ellipse given by equation (9)

(2) Assume that the same basic equation

$$\frac{dC_M}{d(\omega t)} = -\frac{\Delta C_M}{K/K_r} \tag{8}$$

holds in the stalled portion of the cycle

(3) Assume that $K_r = \frac{b}{VT_r}$ has the same value at all points of the cycle

(4) Replace the steady-state variation of moment against angle of attack with a line of slope λ in the unstalled range and one or more straight lines in the stalled range

The assumed constancy of K_r can be checked either by direct measurement of slope on the experimental records of from the value of work per cycle obtained by graphical integration. An accurate measure of the slope, while subject to large uncertainties, gives a direct measure of K_r at any point in the cycle, whereas the value obtained from work gives a sort of average for a cycle. Numerous measurements of both types have been made and the results plotted in figure 70 against the theoretical variation computed for the correct value of a. The comparison reveals the encouraging indication that K_r for stalled flow is certainly the same order of magnitude as for unstalled flow. It should be remembered however that these measurements all come from data obtained at one velocity so that the results are somewhat limited in scope.

A number of moment variations were computed using these basic assumptions by a computer who was familiar with the general shapes obtained experimentally but did not have prior access to the particular experimental plots corresponding to his predictions. In some cases it was assumed that the angle at which stall occurred was the peak angle reached; in others, stall angles were interpolated from the experimental curves of figures 42 through 45. To make reasonable transitions at stall and recovery from stall from the ellipse associated with one straight-line section of the moment curve to the ellipse associated with the other, step-by-step integration was used. The results are plotted in figures 71 through 73 and can be compared with the corresponding experimental curves included in figures 37 through 41. A tabular summary of the results appears in table XI.

The predictions are reasonable approximations of the actual variations especially in some very important respects. The work per cycle and over-all amplitude are in good agreement with the experimental values for all the cases tried which included a considerable variation in frequency and airfoil shape. The phase angle, however, is in poor agreement unless a good estimate is made of the stalling angle.

Thus it appears that a reasonably reliable plot of work per cycle or damping coefficient j_3 against reduced frequency could be constructed for various initial angles of attack and amplitudes of oscillation provided the pertinent steady-state moment data are available. At present, of course, the accuracy of such predictions is known to be reasonable only in the general Reynolds number and reduced-frequency ranges for which the above calculations were carried out.

As stated earlier in this section, it may also be desirable to be able to predict the variation in the stall range of lift caused by pitching. Although no such attempt has been made, a procedure similar to that used above may be possible.

If it is assumed, just as for moment, that

$$\frac{dC_L}{dt} = -\frac{\Delta C_L}{T_L}$$

and

$$\Delta C_L = C_L - \left(C_{L_i} + \lambda_L \alpha\right)$$

the expression for C_L at low initial angles of attack becomes:

$$C_L = C_{L_i} + \frac{\lambda_L \alpha_o}{1 + \left(\omega T_L\right)^2}\left(1 - i\omega T_L\right)e^{i\omega t}$$

The classical expression for lift due to pitch is (reference 2):

$$C_L = C_{L_i} + \frac{\pi}{2}\alpha_o e^{i\omega t}\left\{\left[-aK^2 - 2F + 2\left(\frac{1}{2} - a\right)KG\right] - i\left[K + 2G + 2\left(\frac{1}{2} - a\right)KF\right]\right\}$$

Comparison of the two expressions produces the relations

$$\omega T_L = -\frac{K + 2G + 2\left(\frac{1}{2} - a\right)KF}{aK^2 + 2F - 2\left(\frac{1}{2} - a\right)KG}$$

$$\lambda_L = -\frac{\pi}{2}\left[aK^2 + 2F - 2\left(\frac{1}{2} - a\right)KG\right]\left[1 + \left(\omega T_L\right)^2\right]$$

which are similar to equations (5) and (6). Of course, the product ωT_L can be replaced by a reduced-frequency ratio of the form K/K_L so that K_L and λ_L are functions only of the reduced frequency.

Thus lift due to pitch for low initial angles of attack can be described in a manner very similar to that used previously for moment. Whether a similar procedure can be used at and above the stall is not yet known.

CONCLUSIONS

The aerodynamic reactions on a wing oscillating sinusoidally at or near the stall vary in a periodic but definitely nonsinusoidal manner. The form of the periodic variations, which is usually evaluated in terms of its fundamental components, depends on the mean angle of attack, the frequency parameter, the airfoil shape, the amplitude of oscillation, the Reynolds number, and, in the case of a pitching motion, on the location of the rotational axis. This large number of important variables increases the difficulty of predicting, or even measuring, the aerodynamic reactions far beyond the known complexity of the classical case at zero mean angle of attack.

Most of the measurements to date have been confined to observations of the aerodynamic moment resulting from a sinusoidal pitching oscillation, although the M.I.T. data presented in this report are a valuable source of information on the behavior of lift as well as moment in both pitching and translational oscillations. Representative results from the various sources of data have been reproduced in graphical form in this report but because of the large number of significant parameters involved only a few general conclusions can be drawn.

It appears that the variation of torsional damping with mean angle of attack, which can be rather precipitous in the general reduced-frequency range of 0.1 to 0.6 for Reynolds numbers of the order of 10^6 and less, becomes quite small for comparatively large values of reduced frequency and Reynolds number. This is particularly significant in the light of the demonstrated importance in stall flutter of variations in torsional damping. Airfoil shape affects primarily the suddenness and type of flow breakaway under dynamic stalling conditions and, of course, together with Reynolds number determines the range of angles of attack in which stalling will occur. This last observation illustrates the inadequacy for this type of work of referring angle of attack to the zero-lift condition. A more useful and meaningful reference is the angle of stall on the steady-state lift curve at the test Reynolds number for the airfoil in question. The effects on torsional damping of amplitude of oscillation and of rotational-axis position, while fairly pronounced in some instances, are for the most part quite thoroughly obscured and distorted by the variations of the other parameters.

No instances of negative damping have been observed in the case of pure translation although it appears that negative damping may possibly occur for values of the reduced frequency of about 0.05 or less. Inasmuch as stall flutter is ordinarily predominantly a torsional motion and the aerodynamic reactions associated with the rotational component are of a much greater magnitude than those associated with the translational part of the motion, it is likely that further measurements for pure translation will produce no useful results.

No serious attempt has apparently been made to predict the aerodynamic reactions under dynamic stalling conditions except for moment in pure pitch as has been proposed by Haley earlier in this report. This rather promising technique which requires only the appropriate steady-state lift and moment curves includes to some extent in its prediction the effect of all of the important parameters in what appear to be their critical ranges. Extension of this technique to the prediction of lift in pitch appears possible.

Considerable data on time-average values of lift and moment are available for the first time in this report and should prove useful in estimation of average or mean deflections of an airfoil such as a propeller blade for which a stall-flutter prediction is being attempted.

The observation and prediction of stall flutter itself have led to several interesting conclusions. As mentioned above most cases of stall flutter have exhibited a predominantly torsional motion with critical speeds much lower than predicted or observed at zero mean angle of attack. This difference in critical speeds usually reaches a maximum for mean angle not far from the steady-state stall angle and becomes less and less pronounced as the reduced frequency becomes large. Stall flutter should be differentiated from the forced excitation near a natural frequency which is often associated with the shedding of the well-known Kármán vortex trail. Stall flutter involves the interaction of airfoil motion and aerodynamic reactions whereas the Kármán vortices are observed behind even stationary objects.

The prediction of stall flutter has been approached by attempting to modify adequately the usual classical theory and has been moderately successful in a limited range. All of the results so far obtained indicate the major importance of changes in torsional damping and when adequate experimental information on this parameter was introduced into the calculations the predicted stall-flutter speeds approximated the experimental values quite closely. However it also seems evident that even though stall flutter is predominantly torsional in character it cannot be reduced to a single-degree-of-freedom problem. The motion appears to be torsional only because rotation and translation of the reference axis are either almost exactly in phase or exactly out of phase. In the several cases examined closely the critical condition involved a balance between the damping in the translational motion and the pitching motion, both referred to the elastic axis. The lift arising from the pitching motion collaborates with what seems like quite a small amplitude translational motion to produce a large amount of negative

damping. Thus although the stall-flutter motion appears to be quite elementary, that appearance merely hides the basic complexity of the energy balance.

Massachusetts Institute of Technology
Cambridge, Mass., October 15, 1949

REFERENCES

1. Mendelson, Alexander: Effect of Aerodynamic Hysteresis on Critical Flutter Speed at Stall. NACA RM E8B04, 1948.

2. Theodorsen, Theodore: General Theory of Aerodynamic Instability and the Mechanism of Flutter. NACA Rep. 496, 1935.

3. Victory, Mary: Flutter at High Incidence. R. & M. No. 2048, British A.R.C., Jan. 1943.

4. Halfman, Robert L.: Experimental Aerodynamic Derivatives of a Sinusoidally Oscillating Airfoil in Two-Dimensional Flow. NACA TN 2465, 1951.

5. Bratt, J. B., and Scruton, C.: Measurements of Pitching Moment Derivatives for an Aerofoil Oscillating about the Half-Chord Axis. R. & M. No. 1921, British A.R.C., Nov. 1938.

6. Den Hartog, J. P.: Mechanical Vibrations. Second ed., McGraw-Hill Book Co., Inc., 1940.

7. Bratt, J. B., and Wight, K. C.: The Effect of Mean Incidence, Amplitude of Oscillation, Profile and Aspect Ratio on Pitching Moment Derivatives. R. & M. No. 2064, British A.R.C., June 4, 1945.

8. Reid, Elliott G.: Experiments on the Lift of Airfoils in Non-Uniform Motion. Stanford Univ. Rep., July 23, 1942.

9. Rauscher, Manfred: Model Experiments on Flutter at the Massachusetts Institute of Technology. Jour. Aero. Sci., vol. 3, no. 5, March 1936, pp. 171-172.

10. Bollay, William, and Brown, Charles D.: Some Experimental Results on Wing Flutter. Jour. Aero. Sci., vol. 8, no. 8, June 1941, pp. 313-318.

11. Bratt, J. B., Wight, K. C., and Chinneck, A.: Free Oscillations of an Aerofoil about the Half-Chord Axis at High Incidences, and Pitching Moment Derivatives for Decaying Oscillations. R. & M. No. 2214, British A.R.C., Sept. 1940.

12. Studer, H. L.: Experimentelle Untersuchungen über Flügelschwingungen. Mitt. aus dem Institut fur Aerod., Eidgenössische Tech. H. S., Zürich, No. 4/5, 1936.

TABLE I

EXPERIMENTAL VALUES OF MAGNITUDES AND PHASE ANGLES FOR BLUNT WING IN PURE PITCH AND PURE TRANSLATION

[Velocity, 95 mph; elastic axis at 37-percent chord; semichord, 0.484 ft; pitch amplitude, 6.08°; translation amplitude, 0.9 in.]

α_i (deg)	Pure pitch					Pure translation				
	K	C_{LP}	ϕ_{LP}	C_{MP}	ϕ_{MP}	K	C_{LT}	ϕ_{LT}	C_{MT}	ϕ_{MT}
0	0.093	0.219	178	0.056	344	0.092	0.038	288	0.007	69
	.168	.207	182	.055	337	.169	.061	274	.010	56
	.242	.182	192	.053	324	.249	.093	275	.016	52
	.334	.188	214	.064	346	.336	.126	282	.023	52
6	.056	.226	180	.055	0	.094	.069	260	.007	127
	.093	.221	182	.056	352	.169	.103	257	.010	78
	.170	.218	181	.050	328	.254	.119	245	.014	54
	.253	.217	187	.047	319	.338	.181	239	.022	69
	.314	.217	190	.054	330					
10	.056	.186	175	.057	31	.090	.036	293	.008	109
	.093	.192	183	.034	29	.167	.059	279	.013	73
	.172	.192	193	.040	335	.253	.086	271	.019	63
	.251	.193	209	.033	322	.335	.121	251	.026	73
	.349	.199	225	.036	325					
12	.057	.211	179	.080	18					
	.092	.253	202	.079	5					
	.168	.274	228	.066	3					
	.248	.258	198	.054	0					
	.323	.226	186	.049	346					
14	.077	.263	188	.109	82	.089	Nonperiodic			
	.090	.351	193	.140	71	.170	.161		.037	187
	.166	.392	240	.127	41	.260	.197		.039	159
	.250	.392	206	.139	24	.343	.208		.049	
	.331	.332		.106	356					
						.089	Nonperiodic			
				Stalled		.170	.090	286	.022	135
						.260	.113	277	.016	114
						.343	.124	267	.023	104
16	.050	.251	268	.110	99					
	.159	.375	213	.147	59					
	.241	.352	199	.166	30					
	.325	.347	202	.139	14					
18	.099	.295		.060	114	.090	Nonperiodic			
	.171	.338		.072	83	.168	.050		.015	291
	.257	.353		.065	54	.257	.089		.025	225
	.338	.316		.088	19	.340	.156		.037	217
22	.055	.117	225	.024	176					
	.090	.126	226	.070	175					
	.167	.211	208	.060	180					
	.248	.227	206	.068	163					
	.337	.307	223	.108	139					

TABLE II

EXPERIMENTAL VALUES OF MAGNITUDES AND PHASE ANGLES FOR INTERMEDIATE WING IN PURE PITCH AND PURE TRANSLATION

[Velocity 95 mph; elastic axis at 37-percent chord; semichord, 0.484 ft; pitch amplitude, 6.08°; translation amplitude, 0.9 in.]

α_1 (deg)	Pure pitch					Pure translation				
	K	C_{LP}	ϕ_{LP}	C_{MP}	ϕ_{MP}	K	C_{LT}	ϕ_{LT}	C_{MT}	ϕ_{MT}
0	0.094	0.271	178	0.0680	335	0.090	0.0388	281	0.0085	80
	.168	.240	185	.0670	339	.166	.0568	277	.0133	71
	.246	.235	188	.0665	327	.272	.0820	232	.0268	62
	.339	.229	198	.0670	320	.327	.1000	250	.0227	67
6	.055	.229	180	.0545	351	.095	.0945	258	.0087	78
	.094	.229	182	.0670	340	.171	.0990	246	.0122	68
	.171	.215	185	.0700	341	.253	.1240	242	.0199	66
	.253	.209	183	.0670	322	.327	.1570	233	.0288	70
	.339	.215	183	.0775	336					
10	.053	.189	175	.0292	35	.088	.0380	281	.0075	129
	.094	.217	184	.0305	32	.166	.0674	268	.0114	97
	.164	.217	180	.0462	343	.252	.0890	266	.0180	64
	.253	.219	201	.0502	333	.319	.1070	260	.0232	63
	.318	.212	189	.0593	319					
12	.055	.211	178	.0704	59					
	.091	.219	199	.0656	45					
	.156	.234	206	.0522	32					
	.247	.237	204	.0375	31					
	.314	.216	194	.0445	13					
14	.096	.288		.0467	65	.090	.0497	334	.0099	158
	.172	.332		.0452	41	.165	.1014	307	.0170	138
	.251	.335		.0396	338	.250	.1264	283	.0182	128
	.340	.267		.0343	329	.336	.1405	261	.0223	113
18	.095	.304		.0620	111	.091	Nonperiodic			
	.179	.368		.0775	87	.170	.0787		.0225	271
	.252	.346		.0633	41	.248	.1230		.0294	251
	.332	.310		.0734	342	.319	.1811		.0457	218
22	.055	.150	247	.045	180					
	.091	.196	218	.048	162					
	.168	.244	166	.077	208					
	.259	.278	157	.093	200					
	.335	.323	212	.108	157					

TABLE III

EXPERIMENTAL VALUES OF MAGNITUDES AND PHASE ANGLES FOR SHARP WING IN PURE PITCH AND PURE TRANSLATION

[Velocity 95 mph; elastic axis at 37-percent chord; semichord, 0.484 ft; pitch amplitude, 6.08°; translation amplitude, 0.9 in.]

α_1 (deg)	Pure pitch					Pure translation				
	K	C_{LP}	ϕ_{LP}	C_{MP}	ϕ_{MP}	K	C_{LT}	ϕ_{LT}	C_{MT}	ϕ_{MT}
0	0.095	0.249	182	0.054	351	0.089	0.035	196	0.0077	84
	.169	.234	188	.057	340	.165	.056	261	.0119	69
	.264	.234	187	.061	329	.246	.083	259	.0167	52
	.337	.224	195	.078	328	.344	.118	271	.0219	59
6	.054	.228	176	.038	22	.092	.070	270	.0061	112
	.098	.219	181	.044	10	.168	.097	254	.0065	76
	.171	.210	185	.051	351	.254	.110	251	.0107	73
	.254	.213	199	.068	334	.346	.162	243	.0170	53
8	.057	.219	184	.0476	52					
	.091	.234	180	.0287	37					
	.168	.255	214	.0615	14					
	.248	.255	206	.0663	0					
	.327	.278	202	.0655	350					
10	.056	.184	178	.0447	79	.0895	.038		.0073	139
	.093	.235	188	.0708	58	.175	.105		.0258	119
	.168	.304		.0723	38	.260	.145		.0378	102
	.251	.304		.0686	18	.332	.186		.0464	83
	.336	.306		.0940	0					
	.362	.296		.150	6					
12	.058	.179	182	.0609	90					
	.091	.242	189	.0738	79					
	.166	.330		.1025	59					
	.240	.322		.1092	30					
	.363	.292		.0844	30					
14	.095	.282		.0546	97	.091		Nonperiodic		
	.174	.390		.0587	83	.168	.140		.0638	214
	.252	.374		.0529	52	.256	.236		.0954	152
	.338	.325		.0538	32	.335	.289		.1190	129
18	.095	.243		.0448	156	.090	.030		.0095	267
	.170	.354		.0577	112	.168	.069		.0110	286
	.252	.336		.0670	80	.252	.117		.0123	272
	.349	.309		.0816	52	.331	.128		.0303	230
22	.058	.105	237	.025	190					
	.093	.126	226	.030	199					
	.170	.180	218	.047	183					
	.257	.234	212	.064	201					
	.337	.314	212	.108	183					

TABLE IV

EXPERIMENTAL TIME-AVERAGE VALUES[1] OF MAGNITUDES FOR PURE PITCH AND PURE TRANSLATION

[Velocity, 95 mph; elastic axis at 37.0-percent chord; semichord, 0.484 ft; pitch amplitude, 6.08°; translation amplitude, 0.9 in.]

α_i (deg)	Blunt wing						Intermediate wing						Sharp wing					
	Pure pitch			Pure translation			Pure pitch			Pure translation			Pure pitch			Pure translation		
	K	C_{LP}	C_{MP}	K	C_{LT}	C_{MT}	K	C_{LP}	C_{MP}	K	C_{LT}	C_{MT}	K	C_{LP}	C_{MP}	K	C_{LT}	C_{MT}
0	0.093	0.085	-0.026	0.092	-0.043	0.002	0.094	-0.023	0.002	0.090	-0.048	-0.004	0.095	0.013	0.008	0.089	-0.041	0
	.168	.078	-.016	.169	-.051	.002	.168	-.019	.002	.166	-.048	-.004	.169	.005	.007	.165	-.041	0
	.242	.081	-.016	.249	-.051	0	.246	-.015	0	.272	-.047	-.004	.264	.005	.004	.246	-.046	0
	.334	-.035	-.003	.336	-.067	-.001	.339	-.020	-.004	.327	-.060	-.006	.337	.015	0	.344	-.049	0
6	.056	-.258	.072				.055	-.285	.069				.054	-.468	.168			
	.093	-.478	.084	.094	-.264	.086	.094	-.279	.063	.095	-.296	.060	.098	-.258	.042	.092	-.292	.077
	.170	-.492	.075	.169	-.275	.090	.171	-.296	.058	.171	-.280	.058	.171	-.272	.043	.168	-.285	.078
	.253	-.495	.073	.254	-.251	.092	.253	-.284	.058	.253	-.294	.063	.254	-.270	.045	.254	-.286	.079
	.314	-.506	.069	.338	-.287	.093	.339	-.276	.050	.327	-.292	.065	.358	-.266	.065	.346	-.283	.088
10	.056	-.422	.090				.055	-.445	.093				.056	-.392	.074			
	.093	-.506	.081	.090	-.476	.117	.094	-.465	.176	.088	-.447	.106	.093	-.438	.039	.090	-.451	.109
	.172	-.578	.063	.167	-.475	.115	.164	-.472	.144	.166	-.470	.108	.168	-.455	.044	.173	-.438	.108
	.251	-.577	.065	.253	-.471	.115	.253	-.472	.147	.252	-.452	.105	.251	-.440	.066	.260	-.428	.098
	.349	-.576	.062	.335	-.472	.115	.318	-.461	.149	.319	-.458	.103	.336	-.426	.085	.332	-.438	.090
													.362	-.405	.133			
12	.057	-.472	.076				.055	-.541	.058				.058	-.445	.057			
	.092	-.451	.076				.091	-.540	.082				.091	-.459	.052			
	.168	-.437	.089				.156	-.516	.088				.166	-.472	.048			
	.248	-.462	.108				.247	-.511	.100				.240	-.492	.055			
	.323	-.499	.119				.314	-.523	.094				.363	-.491	.043			
14	.057	-.590	.087															
	.090	-.577	.174	.089	Nonperiodic		.096	-.516	.073	.090	-.608	.139	.095	-.493	.021	.091	Nonperiodic	
	.166	-.570	.191	.170	-.606	.123	.172	-.512	.072	.165	-.614	.134	.174	-.499	.024	.168	-.475	.033
	.250	-.555	.208	.260	-.614	.135	.251	-.481	.065	.250	-.681	.139	.252	-.536	.039	.256	-.539	.041
	.331	-.539	.229	.343	-.593	.140	.340	-.508	.106	.336	-.598	.137	.338	-.503	.026	.335	-.570	.043
				.089	Nonperiodic													
			Stalled	.170	-.499	.066												
				.260	-.527	.071												
				.343	-.492	.073												
18	.099	-.511	.028	.090	Nonperiodic		.095	-.544	.018	.091	Nonperiodic		.093	-.452	.022	.090	-.346	.001
	.171	-.536	.037	.168	-.366	.003	.179	-.536	.020	.170	-.419	.003	.170	-.522	.024	.168	-.361	-.002
	.257	-.553	.050	.257	-.358	.004	.252	-.573	.026	.248	-.455	-.007	.252	-.577	.025	.252	-.380	-.002
	.338	-.559	.057	.340	-.405	.002	.332	-.562	.043	.319	-.489	-.008	.349	-.577	.025	.331	-.469	-.002
22	.055	-.488	.013				.056	-.506	-.002				.058	-.457	-.018			
	.090	-.410	.002				.091	-.495	-.016				.093	-.433	-.018			
	.168	-.442	-.013				.168	-.528	-.047				.170	-.473	-.029			
	.248	-.465	-.028				.260	-.538	-.081				.257	-.497	-.053			
	.338	-.520	-.043				.336	-.572	-.093				.337	-.586	-.088			

[1]Values were cross-plotted to obtain the data at constant K's presented in figures 32 through 36.

TABLE V

NET WORK PER CYCLE IN PURE PITCH AND PURE TRANSLATION

[Velocity, 95 mph; elastic axis at 37-percent chord; semichord, 0.484 ft; translation amplitude, 0.9 in.; pitch amplitude, 6.08°]

α_1 (deg)	Pure pitch						Pure translation					
	Blunt wing		Intermediate wing		Sharp wing		Blunt wing		Intermediate wing		Sharp wing	
	K	Net work (in.-lb)	K	Net work (in.-lb)	K	Net work (in.-lb)	K	Net work (in.-lb)	K	Net work (in.-lb)	K	Net work (in.-lb)
0	0.093	-1.33	0.094	-1.85	0.095	-1.20	0.092	-3.88	0.090	-4.18	0.089	-3.92
	.168	-2.43	.168	-2.40	.169	-2.24	.169	-7.44	.166	-6.80	.165	-6.58
	.242	-2.54	.246	-3.06	.264	-2.66	.249	-10.99	.272	-9.35	.246	-9.35
	.334	-3.48	.339	-3.98	.337	-3.52	.336	-13.62	.327	-11.10	.344	-12.53
6	.056	-.74	.055	-.83	.054	-.35						
	.093	-1.62	.094	-1.82	.098	-.73	.094	-8.28	.095	-8.94	.092	-8.50
	.170	-2.42	.171	-2.81	.171	-1.66	.169	-11.51	.171	-11.15	.168	-10.80
	.253	-2.95	.253	-3.27	.254	-2.43	.254	-14.01	.253	-15.00	.254	-12.50
	.314	-3.20	.339	-4.00	.358	-3.55	.338	-17.20	.327	-16.47	.346	-16.50
8					.057	0						
					.091	.33						
					.168	.99						
					.249	.17						
					.327	-.66						
10	.056	1.42	.053	.08	.056	0						
	.093	-.54	.094	-.86	.093	.12	.090	-4.09	.088	-4.35	.090	-2.15
	.172	-1.49	.164	-1.99	.168	1.22	.167	-6.37	.166	-7.94	.173	-7.93
	.251	-1.75	.253	-2.72	.251	1.67	.253	-10.80	.252	-10.44	.260	-16.50
	.349	-2.50	.318	-4.30	.336	1.33	.335	-11.46	.319	-12.18	.332	-21.50
					.362	1.08						
12	.057	1.95	.055	1.94	.058	0						
	.092	2.76	.091	2.60	.091	1.06						
	.168	2.67	.156	2.35	.166	2.26						
	.248	.89	.247	.59	.240	3.88						
	.323	-.49	.314	-.41	.363	2.76						
14	.077	1.58										
	.090	2.58	.096	2.08	.095	-.40		.089	Nonperiodic	.090	-3.19	.091	Nonperiodic
	.166	5.00	.172	3.28	.174	1.20		.170	-12.62	.165	-9.35	.168	-2.10
	.250	5.36	.251	4.00	.252	2.66		.260	-21.50	.250	-14.50	.256	-24.00
	.331	4.55	.340	-.50	.338	3.87		.343	-25.75	.336	-19.00	.335	-28.60
								.089	Nonperiodic				
							Stalled	.170	-9.00				
								.260	-14.51				
								.343	-16.43				
16	.050	2.15											
	.159	4.78											
	.241	5.81											
	.325	5.93											
18	.099	.59	.095	1.42	.095	-1.65		.090	Nonperiodic	.091	Nonperiodic	.090	-.37
	.171	3.68	.179	2.76	.170	.39		.168	-2.88	.170	-3.60	.168	-2.52
	.257	4.27	.252	5.08	.252	2.29		.257	-5.63	.248	-9.00	.252	-7.00
	.338	8.05	.332	9.48	.349	4.80		.340	-12.89	.319	-19.30	.331	-12.20
22	.055	-.92	.055	-.193	.058	-1.18							
	.090	-1.43	.091	-2.09	.093	-1.69							
	.167	-1.83	.168	-2.00	.170	-2.36							
	.248	-2.14	.259	-1.35	.257	-3.16							
	.337	-2.85	.335	-1.57	.337	-3.85							

TABLE VI

RESULTS OF HARMONIC ANALYSIS FOR AIRFOILS IN PURE PITCH

[Velocity, 95 mph; elastic axis at 37-percent chord; semichord, 0.484 ft; pitch amplitude, 6.08°]

α_1 (deg)	Blunt wing						Intermediate wing						Sharp wing					
	K	M_I	M_R (in.-lb)	$\sqrt{M_I^2 + M_R^2}$	$C_{M\alpha}$	$\phi_{M\alpha}$ (deg)	K	M_I	M_R (in.-lb)	$\sqrt{M_I^2 + M_R^2}$	$C_{M\alpha}$	$\phi_{M\alpha}$ (deg)	K	M_I	M_R (in.-lb)	$\sqrt{M_I^2 + M_R^2}$	$C_{M\alpha}$	$\phi_{M\alpha}$ (deg)
8													0.057	0	3.0	3.0	0.0119	0
													.091	1.0	1.7	2.0	.0079	30
													.168	3.0	4.4	5.4	.0216	33
													.249	.5	8.6	8.8	.0348	3
													.347	1.9	9.4	9.8	.0393	343
10	0.056	4.3	1.4	4.6	0.0179	88	0.053	0.3	3.9	4.0	0.0157	4	.056	0	-5.2	5.2	.0206	180
	.093	-1.6	7.3	7.5	.0297	348	.094	-2.6	4.9	5.6	.0222	332	.093	.4	-5.0	5.1	.0199	172
	.172	-6.3	8.2	10.3	.0408	322	.164	-6.1	7.2	9.5	.0373	320	.168	3.7	-1.5	4.0	.0159	112
	.251						.253	-8.3	7.1	11.7	.0468	308	.251	5.1	3.8	6.6	.0259	55
	.349	-10.6	7.1	12.8	.0506	304	.318	-13.1	6.0	14.6	.0577	294	.336	4.1	12.0	12.8	.0507	18
12	.057	6.0	-4.0	7.2	.0284	124	.055	6.0	-5.6	8.2	.0325	134	.058	0	-11.0	11.0	.0432	180
	.092	8.5	-.8	8.5	.0335	96	.091	8.0	-6.7	8.5	.0335	111	.091	3.2	-10.2	11.0	.0432	163
	.168	8.2	7.0	9.4	.0371	50	.156	7.2	4.8	8.4	.0329	59	.166	6.7	-6.8	9.8	.0385	135
	.248	2.9	12.4	12.7	.0502	13	.247	1.8	9.0	9.4	.0369	11	.240	11.8	-3.6	12.5	.0493	107
	.323	-1.5	11.2	11.2	.0442	352	.314	-1.2	11.7	12.0	.0471	354	.363	8.3	6.8	9.7	.0382	61
14	.089	5.2	-8.8	10.5	.0424	149	.096	6.2	-9.7	11.6	.0468	149	.084	0	-16.2	16.2	.0653	180
	.170	9.6	-3.7	10.6	.0428	111	.172	9.8	-2.9	10.8	.0436	106	.159	6.7	-16.2	17.5	.0705	158
	.250	7.5	5.1	9.3	.0375	56	.251	11.7	4.3	14.2	.0573	62	.239	12.3	-10.2	16.0	.0645	130
							.340	1.4	12.3	12.8	.0516	7	.314	25.0	-1.5	25.1	.1012	93
	.077	6.0	-11.3	12.7	.0513	152							.350	23.6	5.9	24.2	.0975	76
	.090	7.8	-10.6	12.8	.0516	133	.054	6.0	-14.2	15.5	.0625	157						
	.166	15.1	-2.1	15.3	.0617	98	.090	9.1	-9.4	13.3	.0536	137	.095	-1.2	-13.3	13.7	.0552	185
	.250	16.2	7.9	18.0	.0726	64	.166	15.1	-5.6	16.1	.0650	110	.174	3.6	-12.8	13.7	.0552	164
	.331	10.8	15.7	18.8	.0759	44	.250	12.3	4.9	13.2	.0533	68	.252	8.0	-6.3	10.7	.0431	127
	.090	8.2	-11.4	14.0	.0565	144	.327	13.7	13.3	19.1	.0770	46	.338	11.8	2.4	13.2	.0538	73
	.097	10.2	-8.9	13.6	.0549	131	.380	6.4	18.2	19.2	.0775	19						
	.163	16.2	-3.2	16.1	.0650	101												
	.248	14.1	5.3	15.0	.0605	69												
	.894	12.7	11.3	16.9	.0682	48												
16	.050	6.5	-14.8	16.6	.0670	157												
	.159	14.3	-10.5	16.3	.0660	126												
	.241	17.5	-.5	17.4	.0702	92												
	.345	17.8	10.5	20.5	.0827	60												
18	.099	1.8	-14.7	15.5	.0625	173	.056	4.1	-21.1	21.4	.0864	170	.095	-5.0	-11.4	12.5	.0505	204
	.171	11.0	-13.0	17.8	.0719	140	.093	4.3	-14.4	15.8	.0638	164	.170	1.8	-16.6	16.7	.0673	176
	.257	13.4	-4.5	15.4	.0621	108	.179	8.3	-13.5	16.7	.0674	122	.252	7.3	-11.4	13.5	.0545	147
	.338	18.2	4.0	19.7	.0795	78	.252	15.2	-3.5	18.6	.0751	101	.349	7.1	-5.0	8.7	.0351	125
							.332	28.3	5.1	31.5	.1272	71						
	.057	5.9	-17.6	18.5	.0746	162												
	.095	7.6	-19.4	20.7	.0835	159												
20	.055	-8.8	-4.0	4.8	.0194	214	.055	-2.7	-6.0	6.6	.0266	207	.058	-3.6	-3.0	4.7	.0189	230
	.090	-4.5	-5.0	6.7	.0271	228	.091	-6.4	-6.8	9.2	.0372	223	.093	-5.0	-4.3	6.6	.0266	230
	.167	-5.5	-8.5	10.1	.0409	213	.168	-6.0	-11.1	12.6	.0508	208	.170	-7.0	-6.6	9.7	.0392	227
	.248	-6.4	-8.2	10.3	.0417	219	.259	-4.0	-13.5	14.1	.0569	197	.257	-9.4	-10.4	14.0	.0565	222
	.337	-8.5	-9.9	13.1	.0530	221	.335	-4.7	-14.5	15.2	.0614	198	.337	-11.5	-13.9	18.0	.0725	220

TABLE VII

RESULTS OF HARMONIC ANALYSIS FOR INTERMEDIATE WING

IN PURE PITCH AT VARIOUS AIRSPEEDS

[α_i, 14°; elastic axis at 37-percent chord; semichord, 0.484 ft; pitch amplitude, 6.08°]

Velocity (mph)	K	W_R (in.-lb)	M_I (in.-lb)	M_R (in.-lb)	$\sqrt{M_I^2 + M_R^2}$ (in.-lb)	C_{MP}	ϕ_{MP} (deg)
65	0.079	1.70	5.0	-5.6	7.5	0.0302	138
	.133	2.24	6.7	-4.7	8.2	.0331	125
	.244	3.02	9.1	.9	9.1	.0367	85
	.366	2.09	6.3	6.8	9.3	.0375	43
	.484	-.35	-.1	9.5	9.6	.0387	354
	.550	-.82	-.3	7.1	7.5	.0302	341
80	.064	2.25	6.8	-11.1	13.0	.0525	149
	.107	3.14	9.4	-9.4	13.3	.0536	135
	.202	4.26	12.8	-3.4	13.2	.0532	105
	.298	3.76	11.3	4.3	12.5	.0505	69
	.391	2.78	8.4	11.3	14.0	.0565	36
	.455	2.62	7.9	13.3	15.4	.0621	31
95	.054	2.02	6.0	-14.2	15.5	.0625	157
	.090	3.04	9.1	-9.4	13.3	.0536	137
	.166	5.01	15.1	-5.6	16.1	.0650	110
	.250	4.11	12.3	4.9	13.2	.0533	68
	.327	4.58	13.7	13.3	19.1	.0770	46
	.380	2.14	6.4	18.2	19.2	.0775	19
100	.048	.82	2.4	-17.5	17.7	.0714	172
	.079	1.88	5.6	-17.5	18.5	.0745	162
	.148	4.68	13.9	-12.3	18.6	.0750	131
	.216	5.90	17.5	-3.4	17.8	.0717	101
	.289	4.75	14.1	9.3	17.0	.0685	57
	.328	3.61	10.7	18.2	21.1	.0850	31

TABLE VIII

THEORETICAL VALUES OF AMPLITUDES, PHASE ANGLES, AND NET WORK PER CYCLE FOR PURE PITCH AND PURE TRANSLATION

[Pure translation h, 0.9 in.; pure pitch, 6.08°]

C_{MT}	C_{LT}	ϕ_{MT}	ϕ_{LT}	Net work Cycle (in.-lb)	K	C_{MP}	C_{LP}	ϕ_{MP}	ϕ_{LP}	Net work Cycle (in.-lb)
0	0	90	270	0	0	0.0805	0.335	360	180	0
.00117	.00486	86.87	267.48	-.584	.01	.0793	.330	356.70	177.90	-.378
.00441	.0182	81.54	264.10	-2.18	.04	.0760	.313	350.78	175.83	-.995
.00639	.0264	78.90	262.80	-3.14	.06	.0743	.302	347.66	175.42	-1.180
.00828	.0339	76.41	262.04	-4.03	.08	.0728	.293	344.94	175.50	-1.581
.01009	.0409	74.78	261.64	-4.86	.10	.0717	.284	342.52	176.00	-1.790
.01189	.0477	73.08	261.52	-5.67	.12	.0710	.2965	340.30	176.76	-1.990
.01511	.0600	70.22	261.96	-7.15	.16	.0700	.2625	336.37	178.81	-2.295
.01838	.0714	67.80	263.05	-8.53	.20	.0699	.2520	332.93	181.68	-2.62
.0216	.0820	65.65	264.56	-9.82	.24	.0705	.2445	329.87	184.83	-2.92
.0262	.0975	62.80	267.48	-11.72	.30	.0722	.2365	325.88	190.00	-3.34
.0294	.1072	61.03	269.66	-12.90	.34	.0738	.2335	323.56	193.57	-3.61
.0342	.1220	58.58	273.21	-14.70	.40	.0772	.2320	320.55	198.97	-4.08

TABLE IX

GEOMETRICAL ANGLE OF ATTACK AND ANGULAR VELOCITY OF AIRFOIL AT STALL IN A PURE PITCHING MOTION

α_1 (deg)	Blunt wing; steady-state $\alpha_{stall} = 15^\circ$				Intermediate wing; steady-state $\alpha_{stall} = 14^\circ$				Sharp wing; steady-state $\alpha_{stall} = 11^\circ$			
	K	$\Delta\alpha_{stall}$ above α_1 (deg)	$\delta\alpha$	$\dot{\alpha}_{stall}$ (radians/sec)	K	$\Delta\alpha_{stall}$ above α_1 (deg)	α_1	$\dot{\alpha}_{stall}$ (radians/sec)	K	$\Delta\alpha_{stall}$ above α_1 (deg)	α_1	$\dot{\alpha}_{stall}$ (radians/sec)
6	0.056	No stall			0.055	No stall			0.054	5.56	0.56	0.62
	.093	---do---			.094	---do---			.098	5.90	.90	.54
	.170	---do---			.171	---do---			.171	No stall		
	.253	---do---			.253	---do---			.254	---do---		
	.314	---do---			.339	---do---			.358	---do---		
10	.056	5.15	0.15	0.87	.055	4.92	0.92	0.95	.056	1.14	.14	1.66
	.093	5.25	.25	1.36	.094	5.12	1.12	1.48	.093	3.20	2.20	2.40
	.172	No stall			.164	No stall			.168	4.75	3.75	3.09
	.251	---do---			.253	---do---			.251	5.70	4.70	2.34
	.349	---do---			.318	---do---			.336	No stall		
									.362	No stall		
12	.057	5.70	2.70	.53	.055	3.08	1.08	1.42	.058	0	1.00	1.75
	.092	5.97	2.97	.28	.091	4.24	2.24	1.94	.091	1.17	2.17	2.69
	.184	5.99	2.99	.32	.156	5.08	3.08	2.49	.167	3.14	4.14	4.28
	.247	6.00	3.00	0	.247	5.16	3.16	3.78	.240	5.22	6.22	3.56
	.323	No stall			.314	5.85	3.85	2.10	.362	5.19	6.19	5.50
14	.057	.84	-.16	1.70								
	.090	1.95	.95	2.56	.096	2.54	2.54	2.62	.095	-.68	2.32	2.84
	.166	4.53	3.53	3.28	.172	4.52	4.52	3.40	.174	.78	3.78	5.20
	.250	5.48	4.59	3.06	.251	No stall			.252	3.68	6.68	6.00
	.331	No stall			.340	No stall			.338	5.11	8.11	5.33
18	.099	-2.49	.51	2.72	.095	-2.15	1.85	2.68	.095	-5.49	1.51	1.16
	.171	.71	3.71	5.12	.179	.31	4.31	5.39	.170	-2.16	4.84	4.80
	.257	3.57	6.57	6.23	.252	4.53	8.53	4.98	.252	1.02	8.02	7.53
	.338	5.66	8.66	3.35	.332	No stall			.349	3.72	10.72	8.25

TABLE X

FLUTTER CONDITIONS FOR BOLLAY AND BROWN, WING II

[Wing properties: a = -0.29; b = 3.375 in.; x_α = 0.228; r_α = 0.5 (assumed); $m/\pi\rho b^2$ = 161.2; ω_α = 87.2 radians/sec; ω_b = 80.3 radians/sec; ω_α/ω_b = 1.085]

	ϕ (deg)	V_c (mph)	K	ω_c (radians/sec)	β (deg)	h_o/b	J_3
Experimental:							
$\alpha_i = -1.36^\circ$	-----	78	0.19	77.2	-----	-----	-----
$\alpha_i = 11.2^\circ$	-----	57	.30	82.8	-----	-----	-----
Calculated:							
Classical	0	78.5	.20	81.8	125	0.159	0.371
Mendelson	23	57	.245	72.8	18.6	.402	-----
Mendelson	35	45.6	.30	71.4	10.7	.579	-----
Mendelson ("corrected")	351	64	.30	100	172	.384	-----
ϕ applied to moment in pitch only	333	63.7	.30	99.4	-----	-----	-----
Victory's modification	-----	67	.30	105	-----	-----	.027

TABLE XI

RESULTS FROM HALEY'S EMPIRICAL THEORY

	Wing				
	Sharp	Sharp	Blunt	Blunt	Intermediate
α_1, deg	12	12	10	10	14
ω, cycles per second	7.64	16.66	4.25	7.90	7.90
Stall at α max	Yes	No	Yes	Yes	No
W, experimental, in.-lb	4.52	5.85	-1.07	-2.98	6.56
W, analytical, in.-lb	4.48	6.44	-0.74	-0.79	7.39
ϕ, experimental, deg	135.0	60.8	347.6	322.0	106.0
ϕ, analytical, deg	41.2	80.8	352.7	352.0	125.8
Amplitude, experimental, in.-lb	19.4	19.4	15.0	20.6	21.6
Amplitude, analytical, in.-lb	20.2	19.4	17.5	17.1	27.7

Figure 1.- Test-section arrangement viewed from upstream.

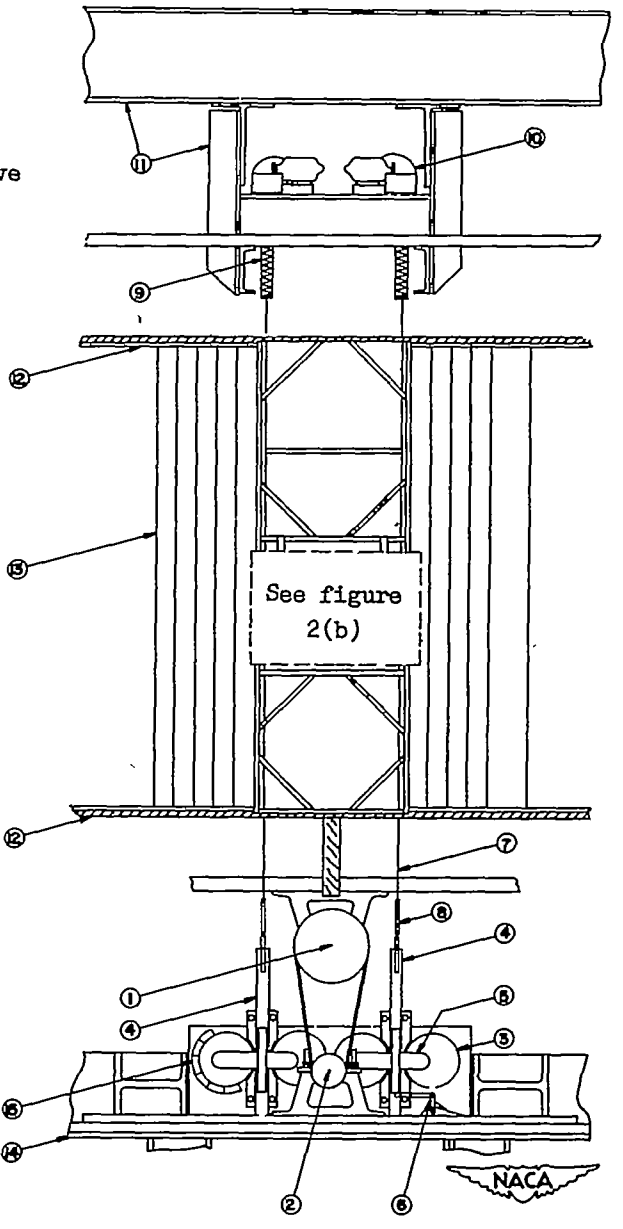

(1) Line shaft and driving V-belt sheave
(2) Driven sheave and driving gears
(3) Crank wheels
(4) Vertical crossheads
(5) Connecting rods
(6) Position indicator
(7) Steel driving bands
(8) Turnbuckles
(9) Adjusting spring for providing tension in bands
(10) Electric motor and gear train used for adjusting spring tension
(11) Upper supporting structure
(12) Wind-tunnel top and bottom
(13) Leading- and trailing-edge fairing strips for end plates
(14) Lower supporting structure
(15) Phase-setting protractor

(a) Oscillator mechanism.

Figure 2.- Diagrammatic drawing of test setup.

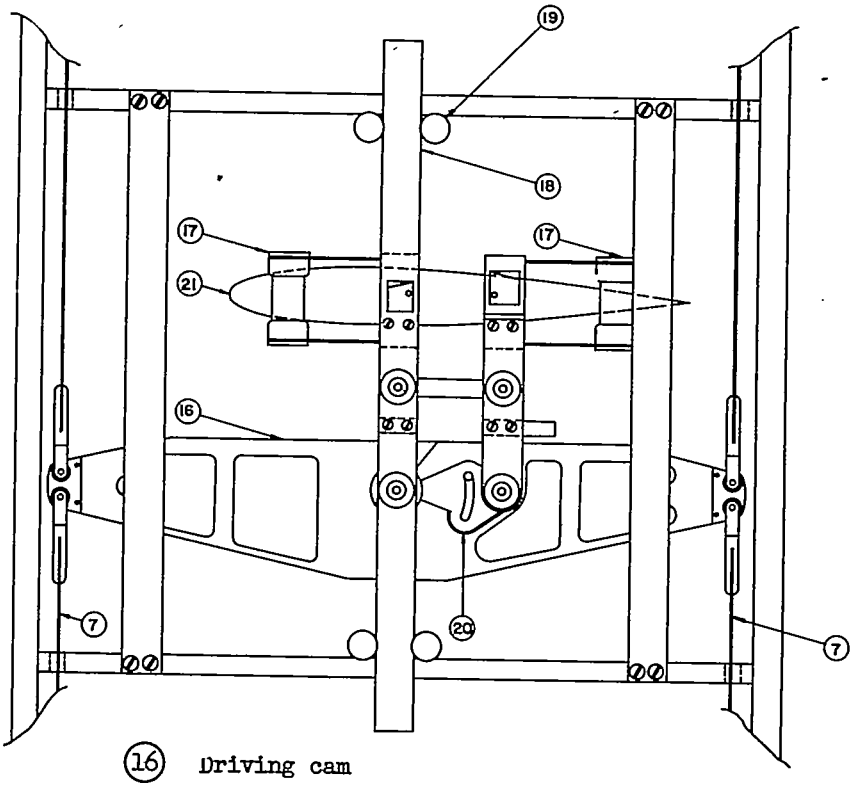

(16) Driving cam

(17) Selectively damped accelerometers

(18) Vertical guiding bar

(19) Guide bearings

(20) Initial-angle adjusting link

(21) Airfoil

(b) Model and supporting mechanism.

Figure 2.- Concluded.

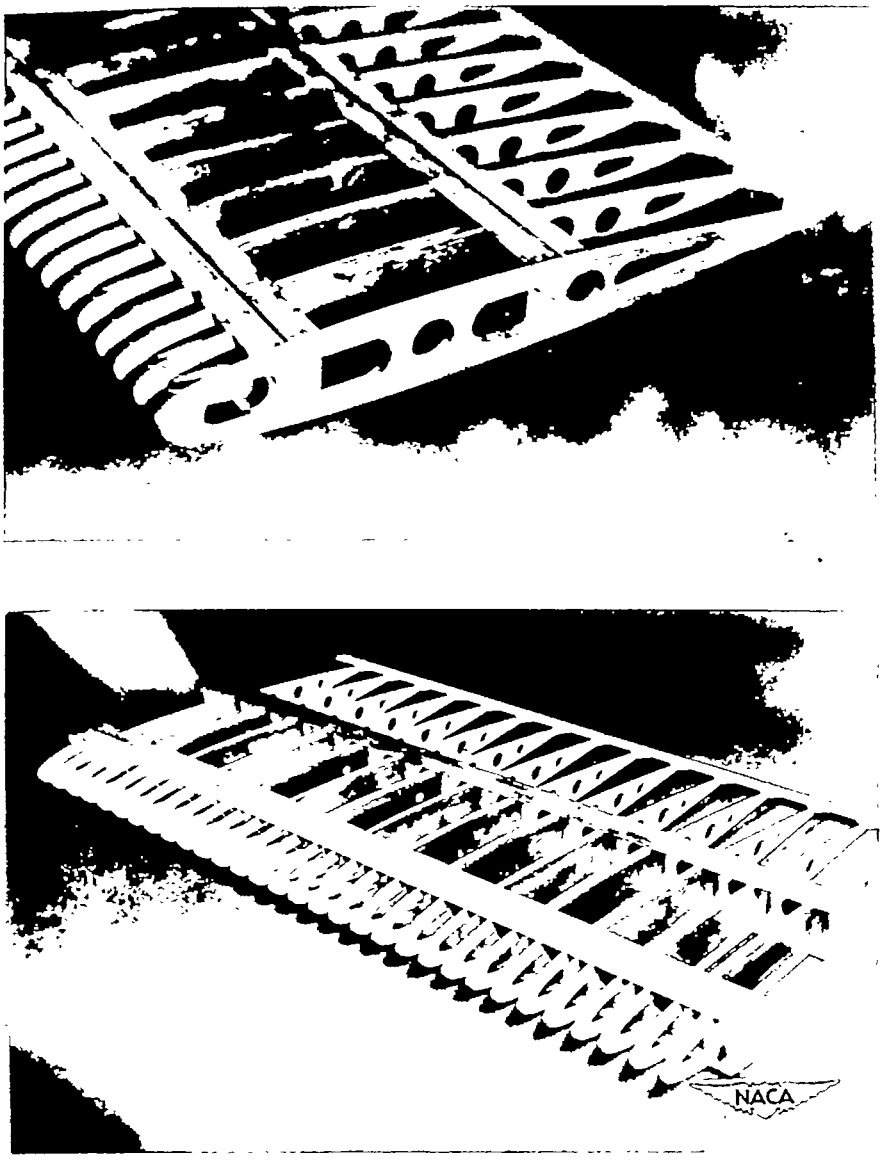

Figure 3.- Internal wing structure.

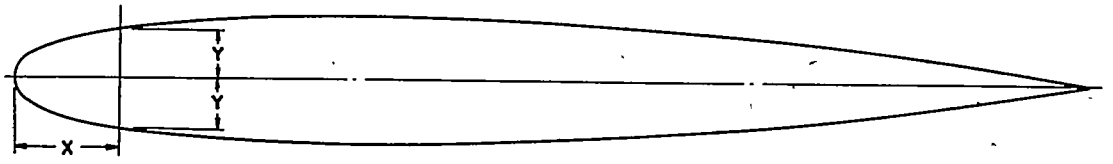

(a) Blunt wing.

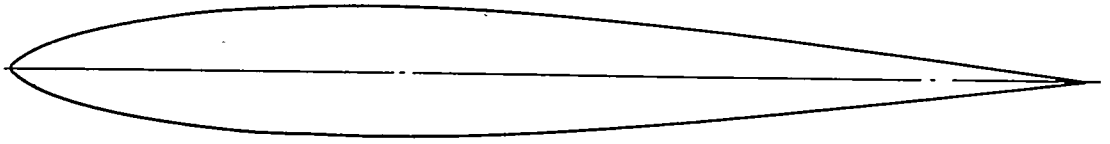

(b) Sharp wing.

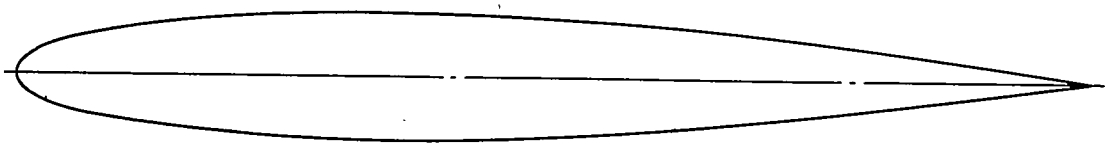

(c) Intermediate wing.

X/c	Y_1/c	Y_2/c	Y_3/c
0	0	0	0
.001	.0076	.0026	------
.005	.0148	.0072	.0109
.010	.0195	.0111	.0154
.020	.0256	.0168	.0215
.040	.0339	.0253	.0299
.060	.0392	.0318	.0358
.080	.0434	.0369	.0405
.100	.0467	.0413	.0443
.200	.0564	.0548	.0556
.300	.0597	.0596	.0596
.3330	.0599	.0599	.0599
.400	.0592	.0588	.0590
.500	.0554	.0542	.0550
.600	.0494	.0462	.0481
.700	.0412	.0367	.0390
.800	.0306	.0252	.0278
.900	.0179	.0129	.0147
1.000	0	0	0

Figure 4.- Airfoil section and ordinates.

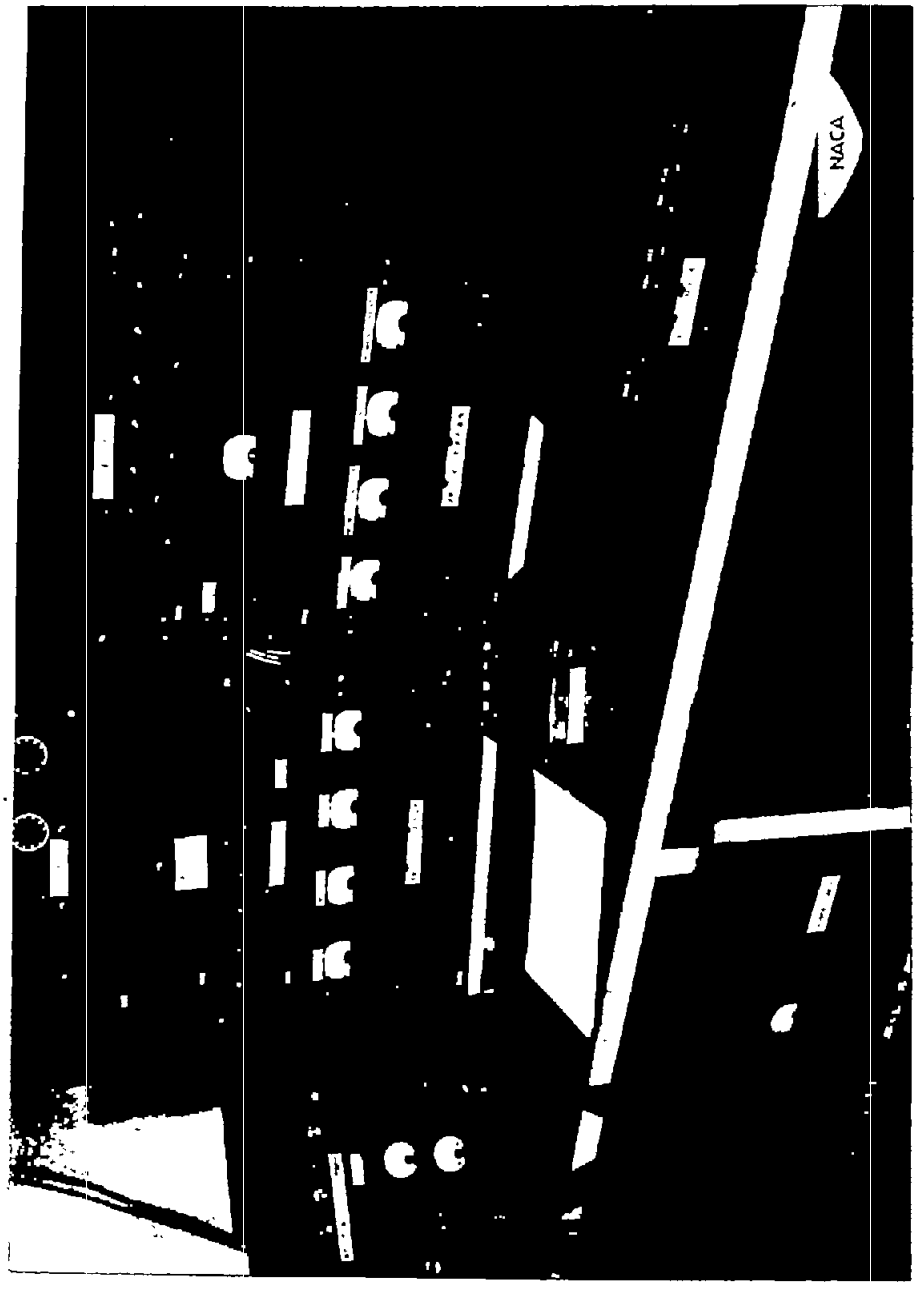

Figure 5.- Arrangement of instrumentation.

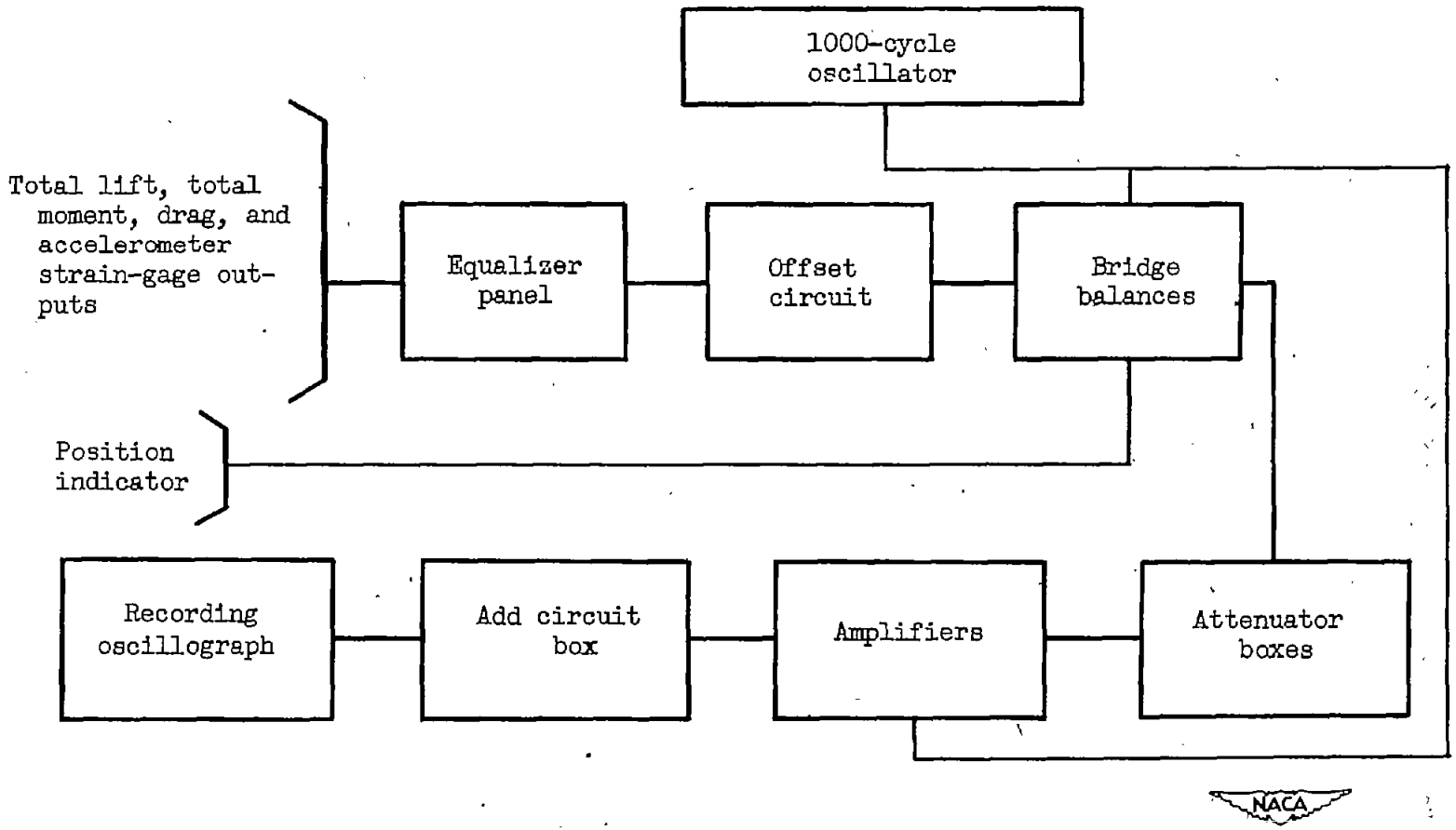

Figure 6.- Block diagram of instrumentation.

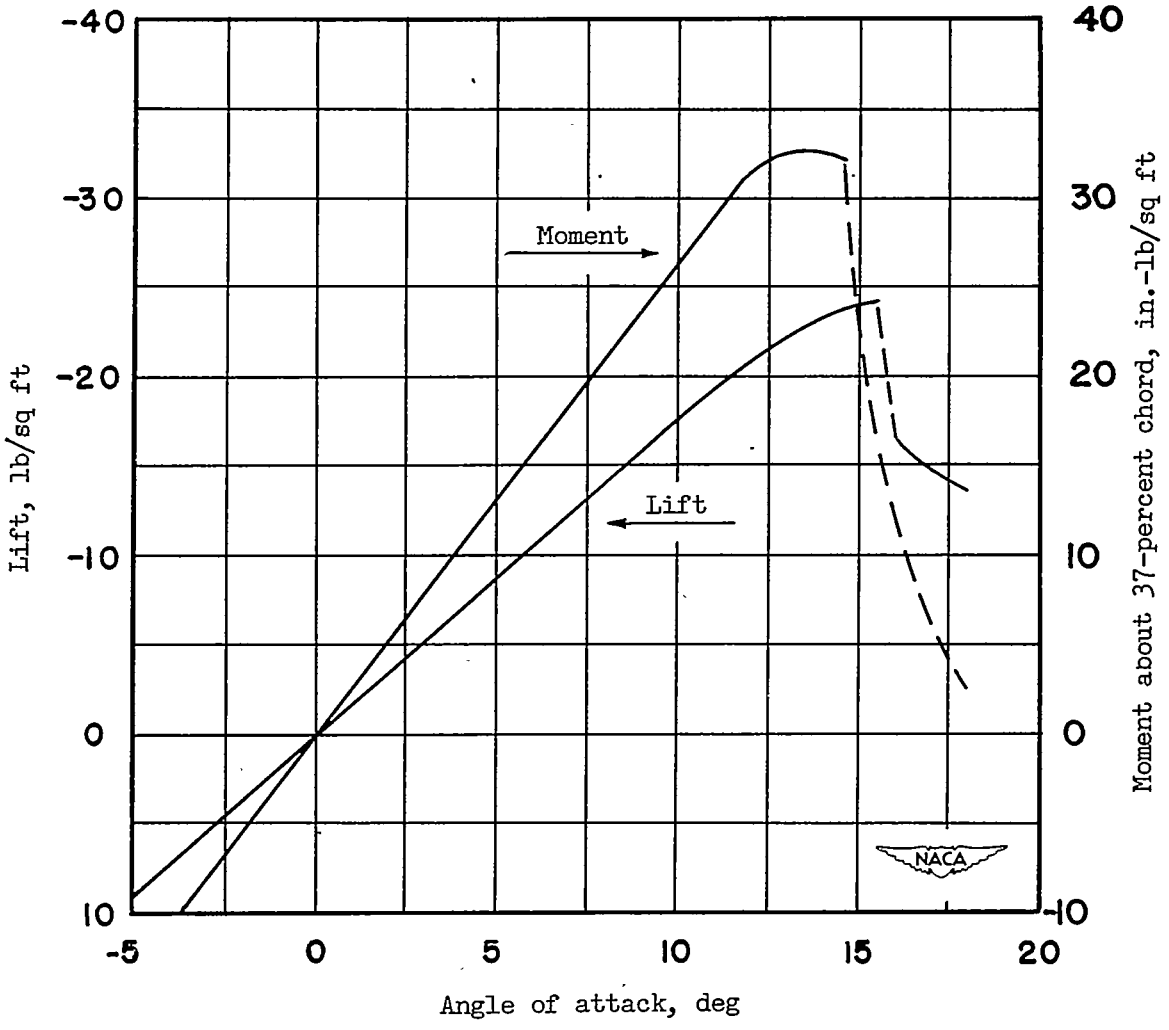

Figure 7.- Static airfoil characteristics. Blunt airfoil.

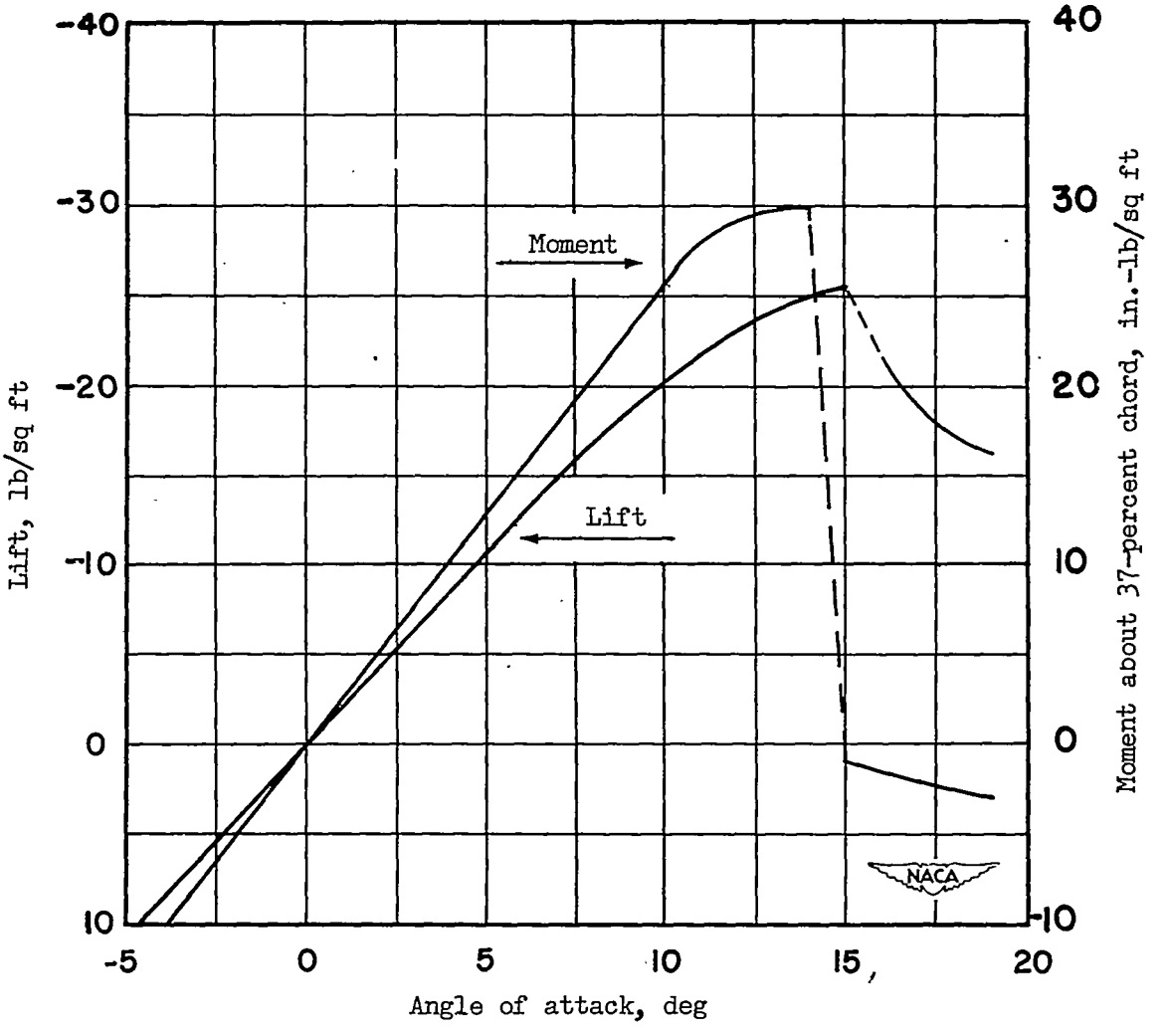

Figure 8.- Static airfoil characteristics. Intermediate airfoil.

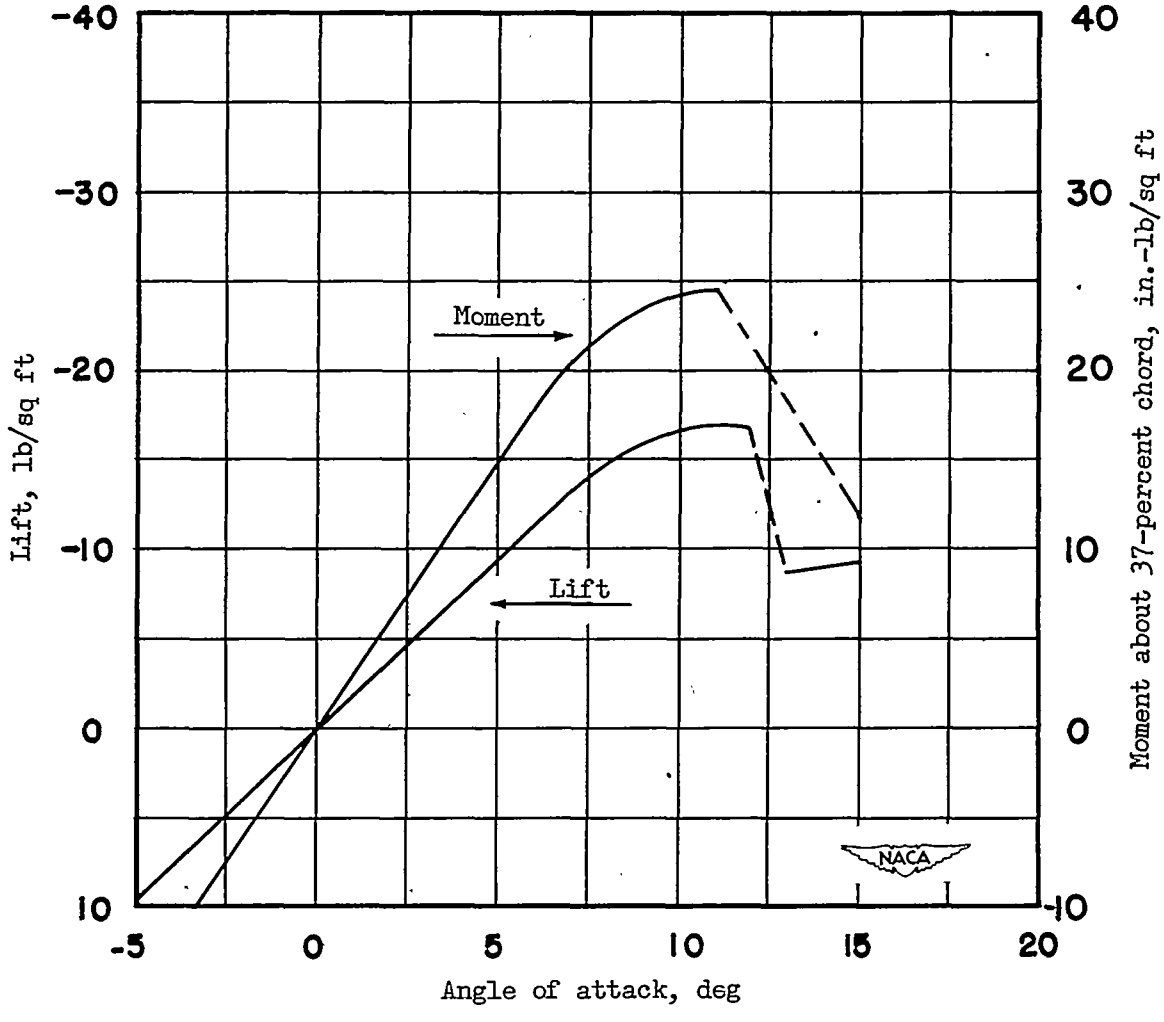

Figure 9.- Static airfoil characteristics. Sharp airfoil.

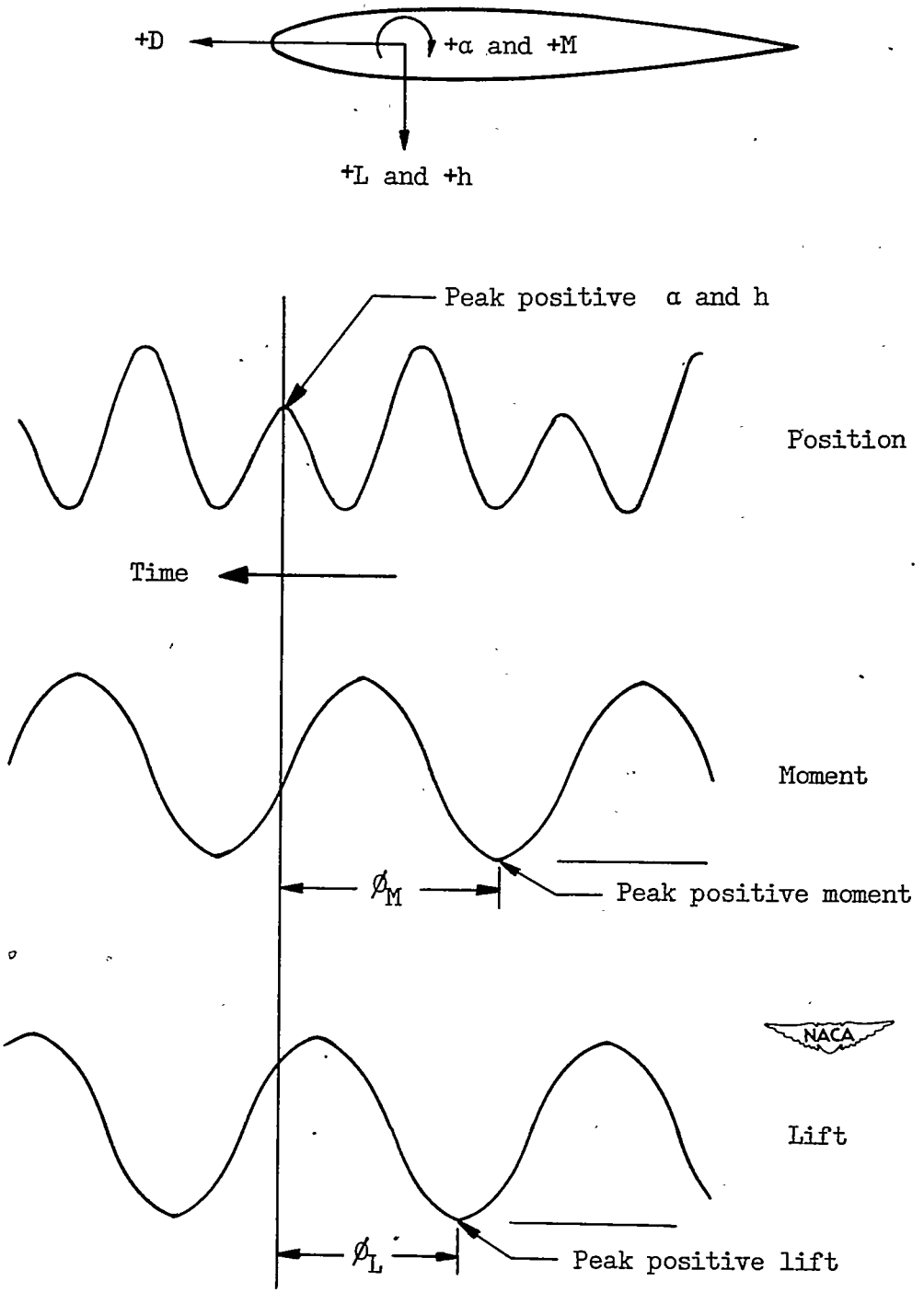

Figure 10.- Sketch of typical oscillograph record showing distances measured.

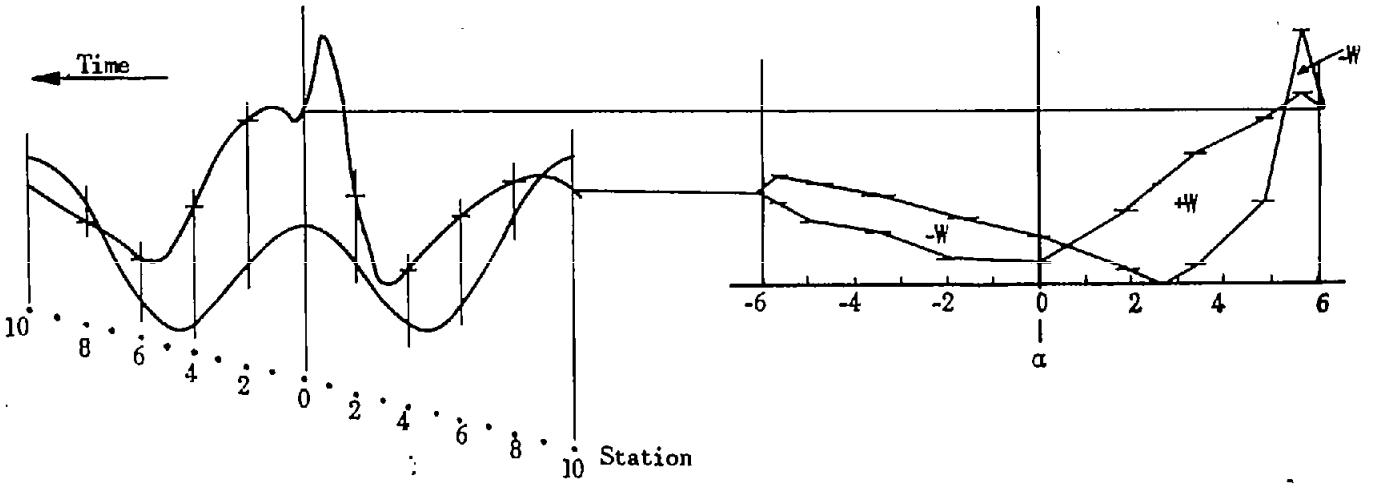

Station	Crank angle, θ (deg)	Angle of pitch, α (α = 6.08 sin θ) (deg)	↓ -Δα or Δh	Vertical position, h (h = 0.95 sin θ) (in.)
0	90	6.08		0.900
1	108	5.79		.856
2	126	4.92		.728
3	144	3.58		.530
4	162	1.87		.278
5	180	0		0
6	198	-1.87		-.278
7	216	-3.58		-.530
8	234	-4.92		-.728
9	252	-5.79		-.856
10	270	-6.08	↑ +Δα or Δh	-.900

Figure 11.- Method of graphical integration of work per cycle.

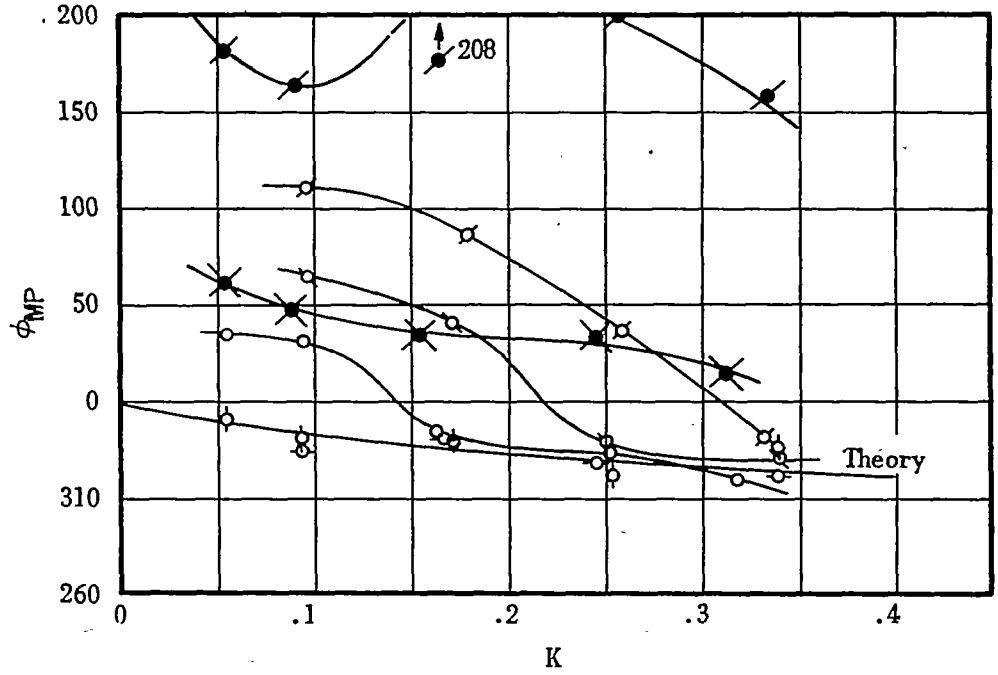

(a) Intermediate wing.

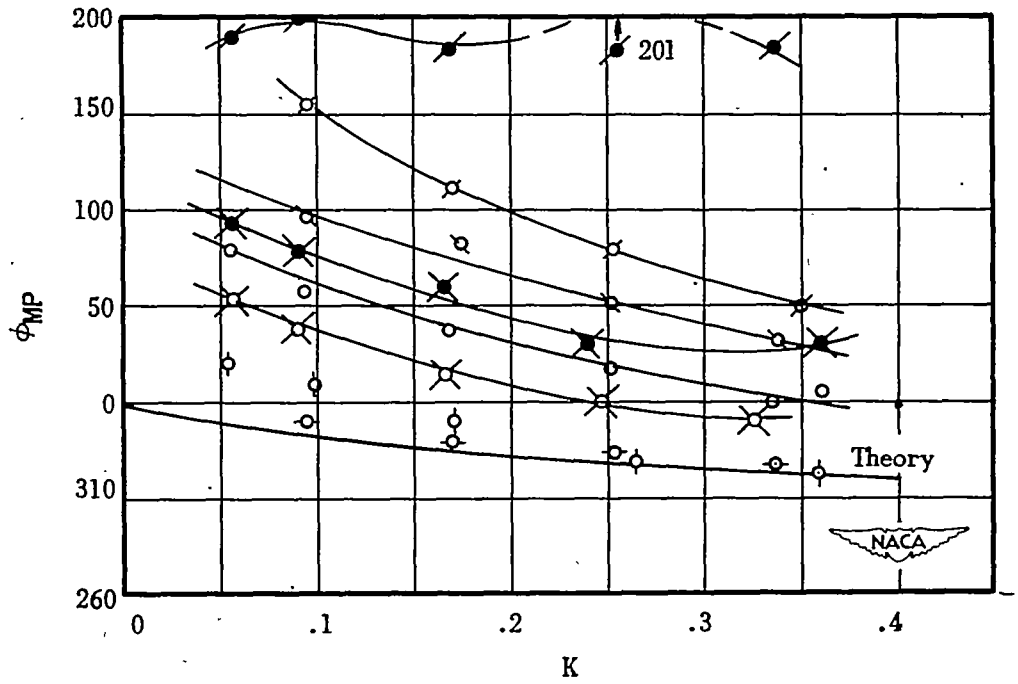

(b) Sharp wing.

Figure 12.- Moment phase angle in pure pitch.

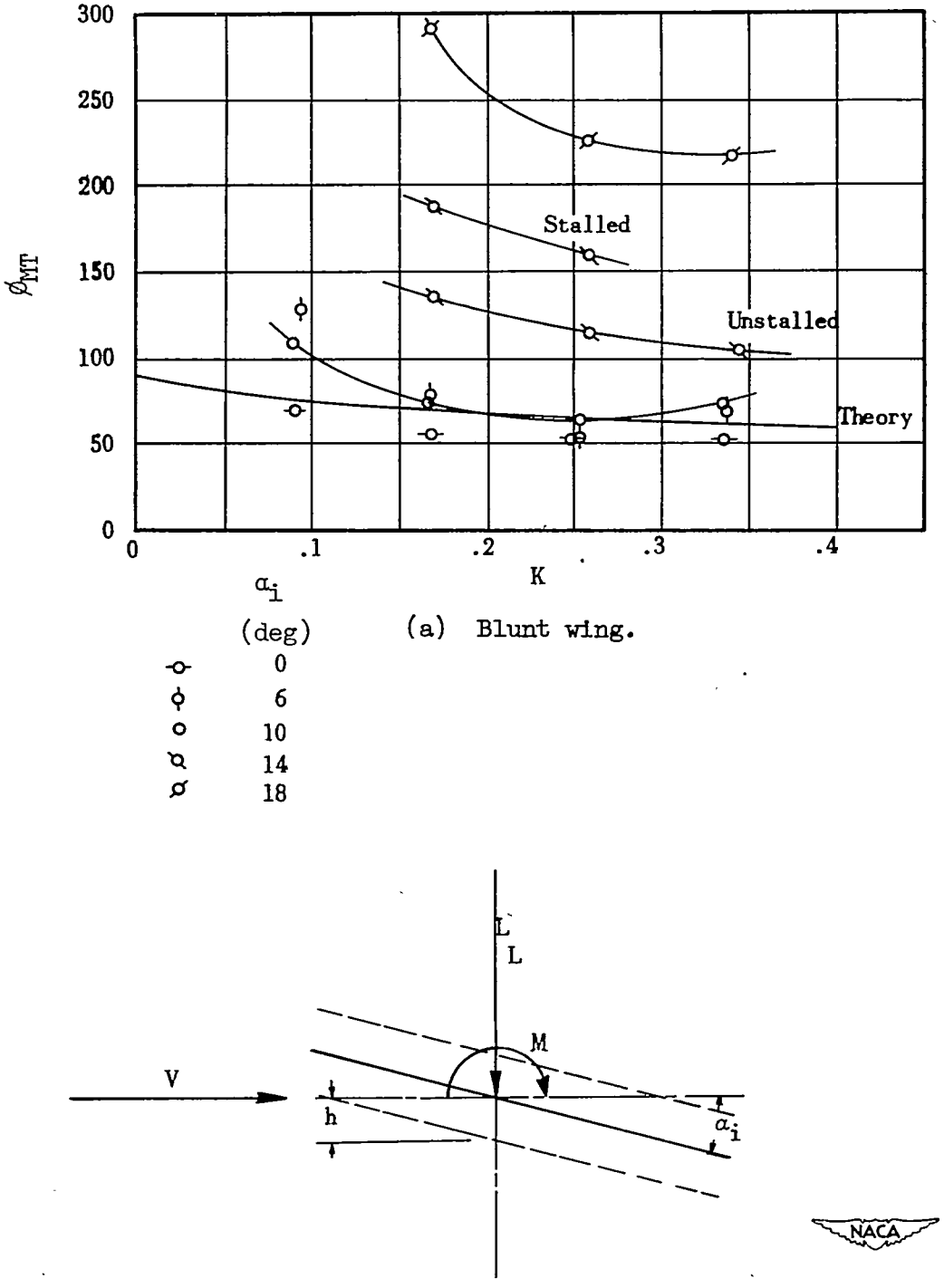

Figure 13.- Moment phase angle in pure translation.

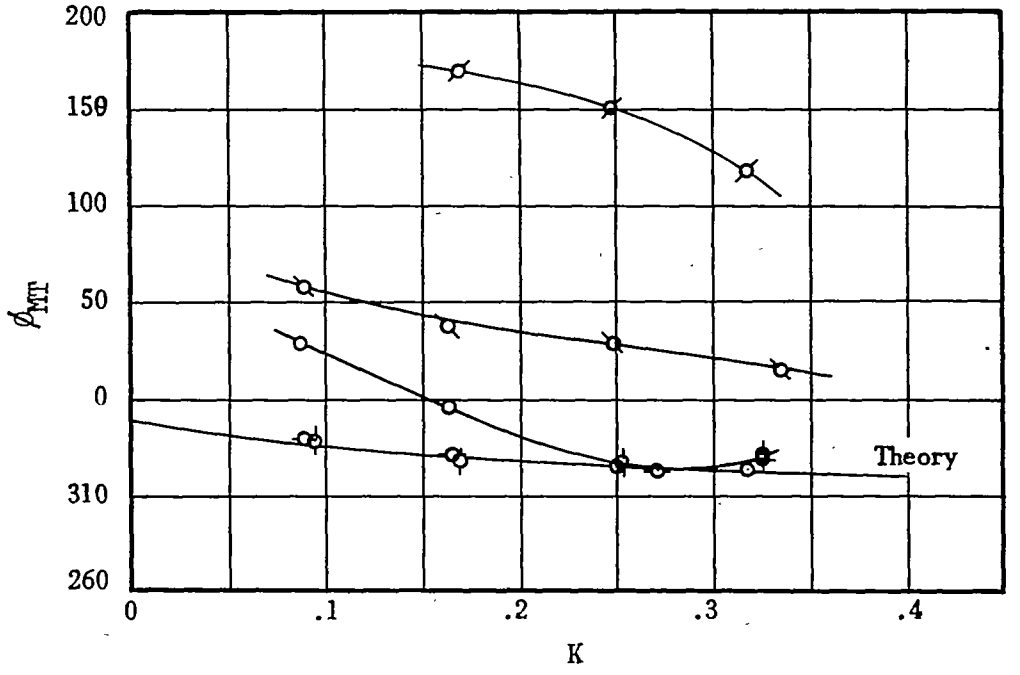

(b) Intermediate wing.

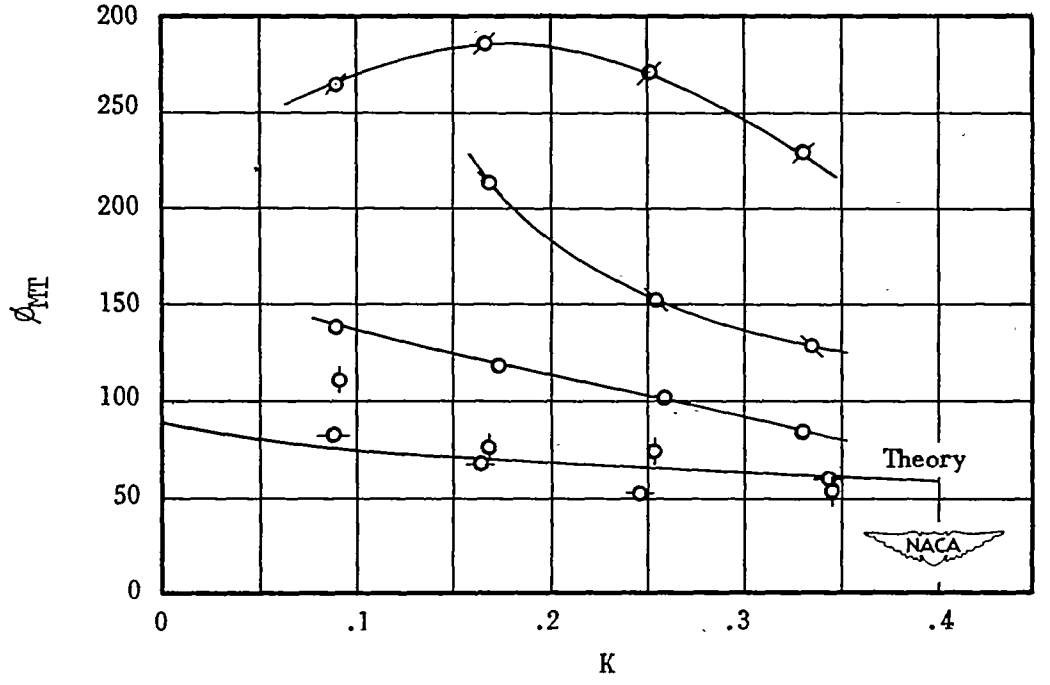

(c) Sharp wing.

Figure 13.- Concluded.

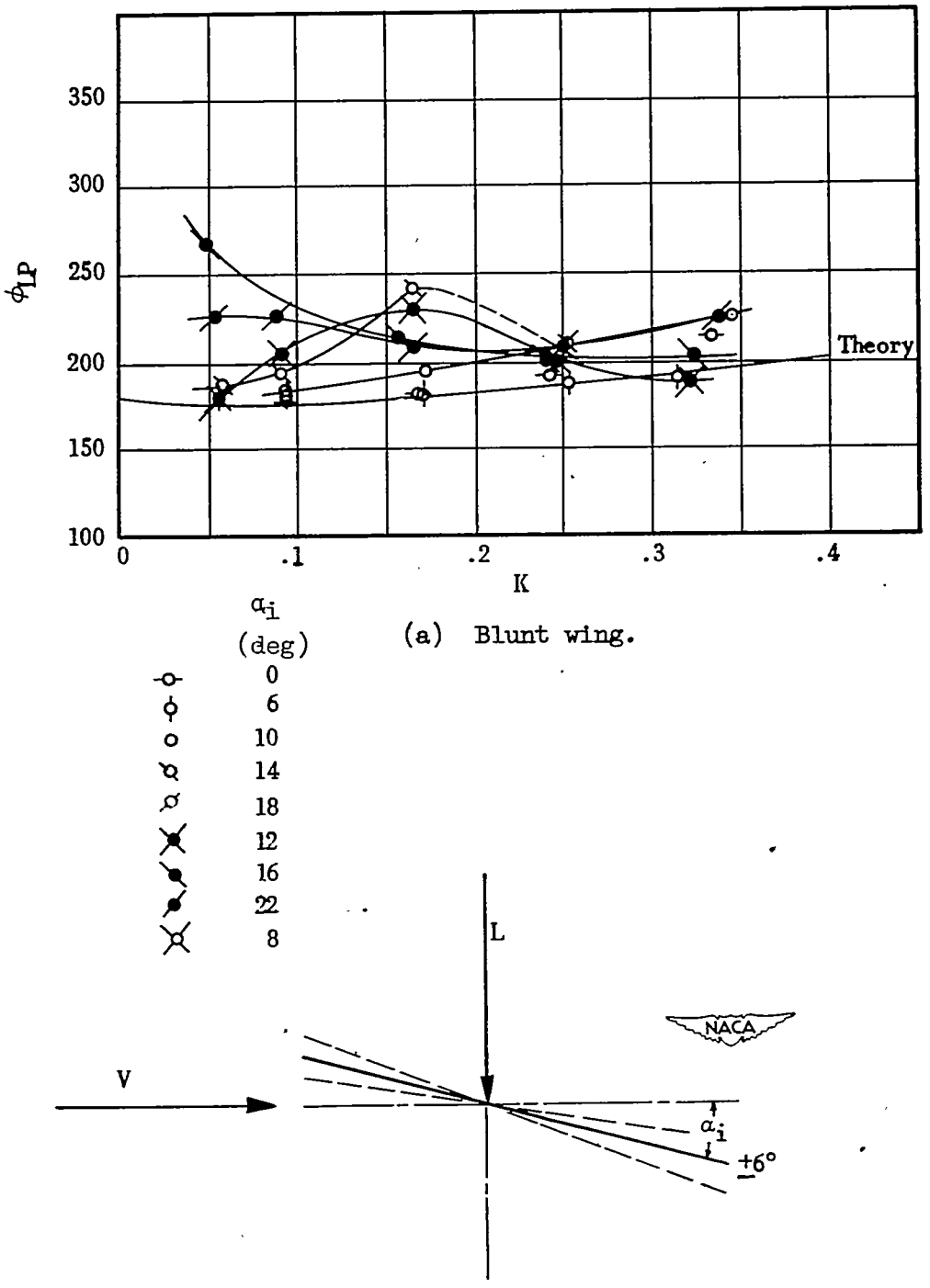

Figure 14.- Lift phase angle in pure pitch.

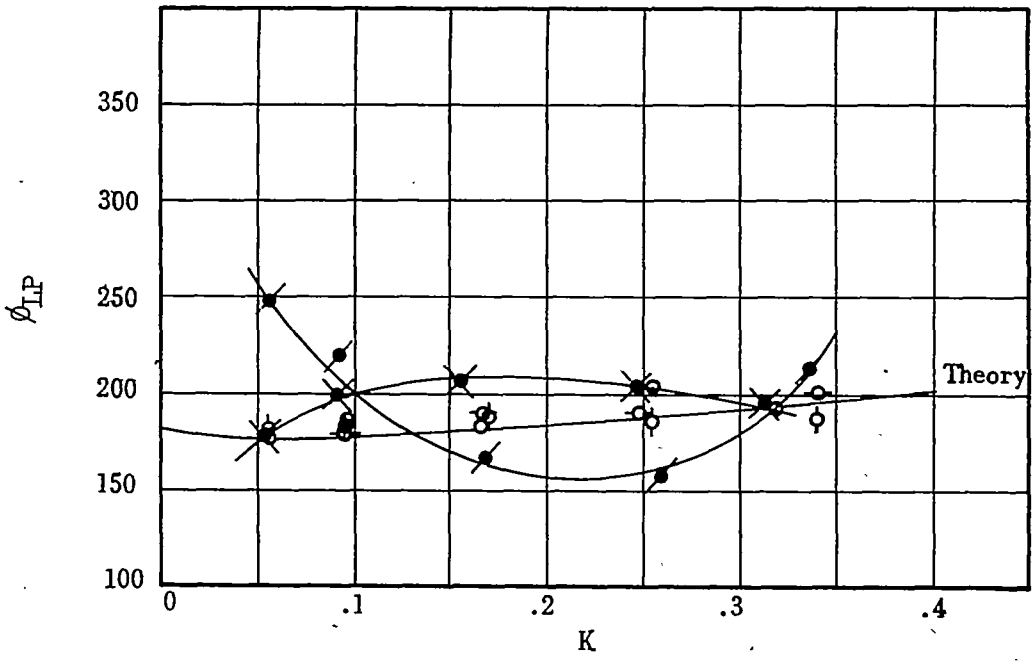

(b) Intermediate wing.

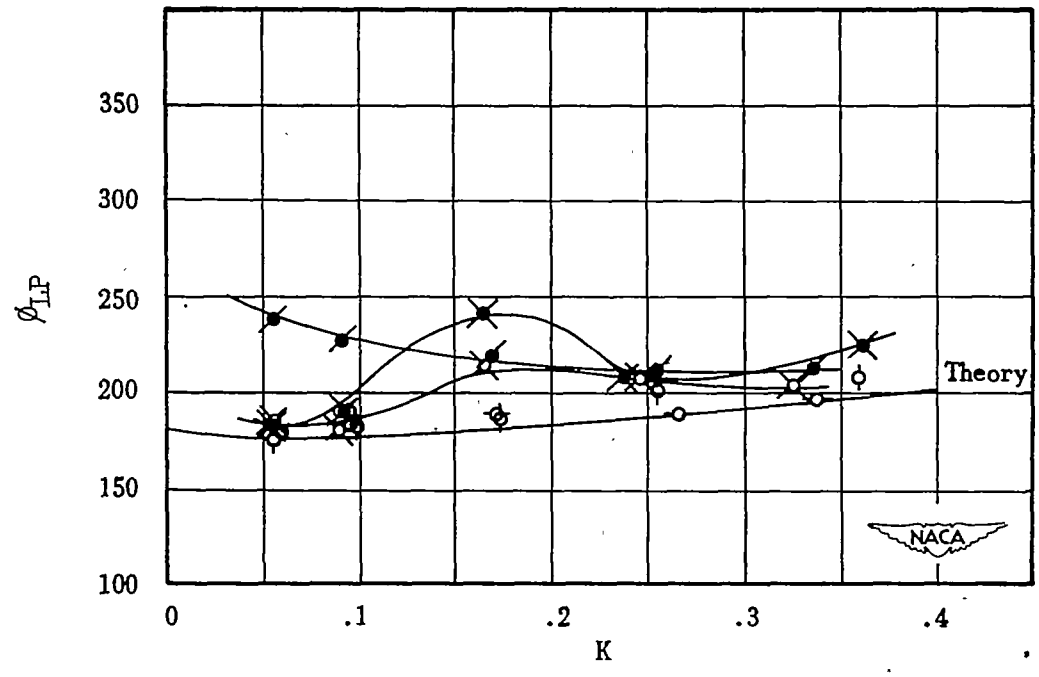

(c) Sharp wing.

Figure 14.- Concluded.

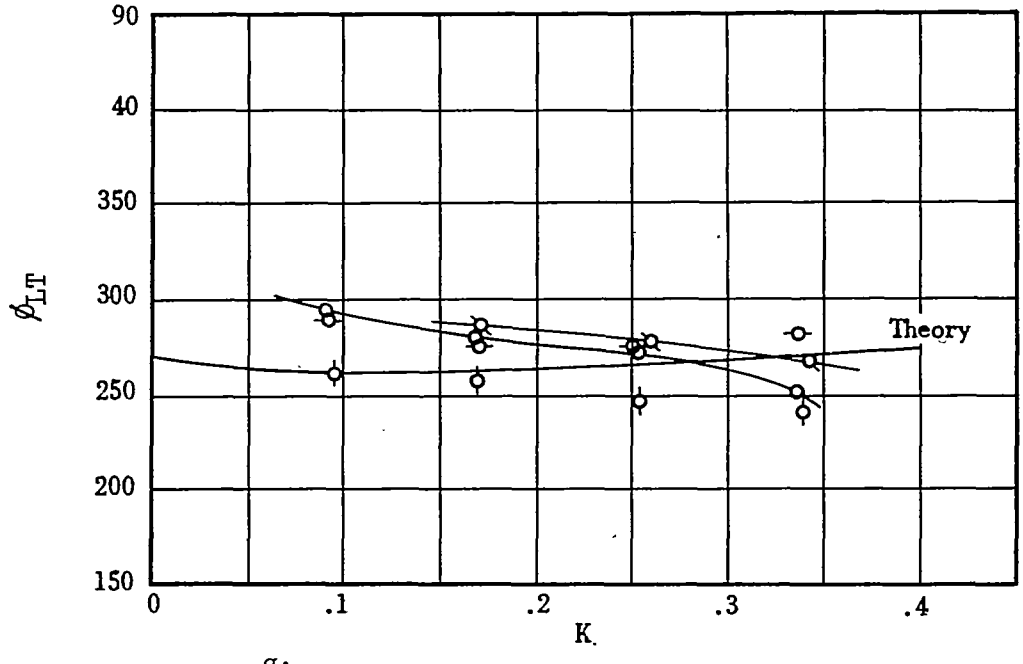

α_i (deg)
0
6
10
14
18

(a) Blunt wing.

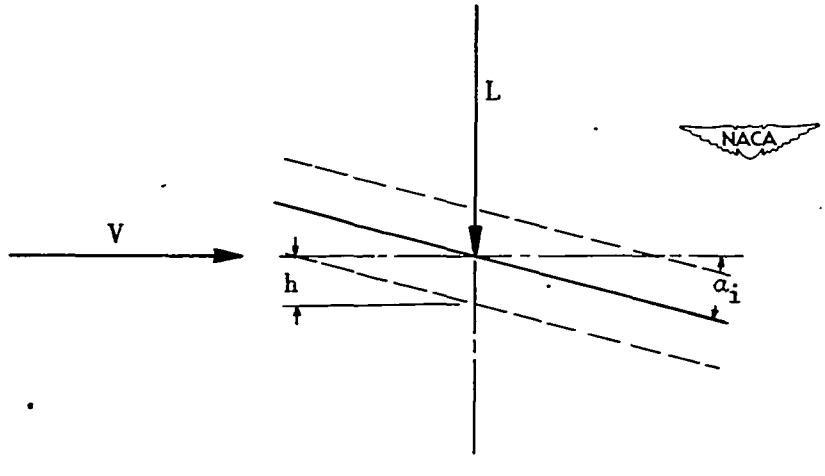

Figure 15.- Lift phase angle in pure translation.

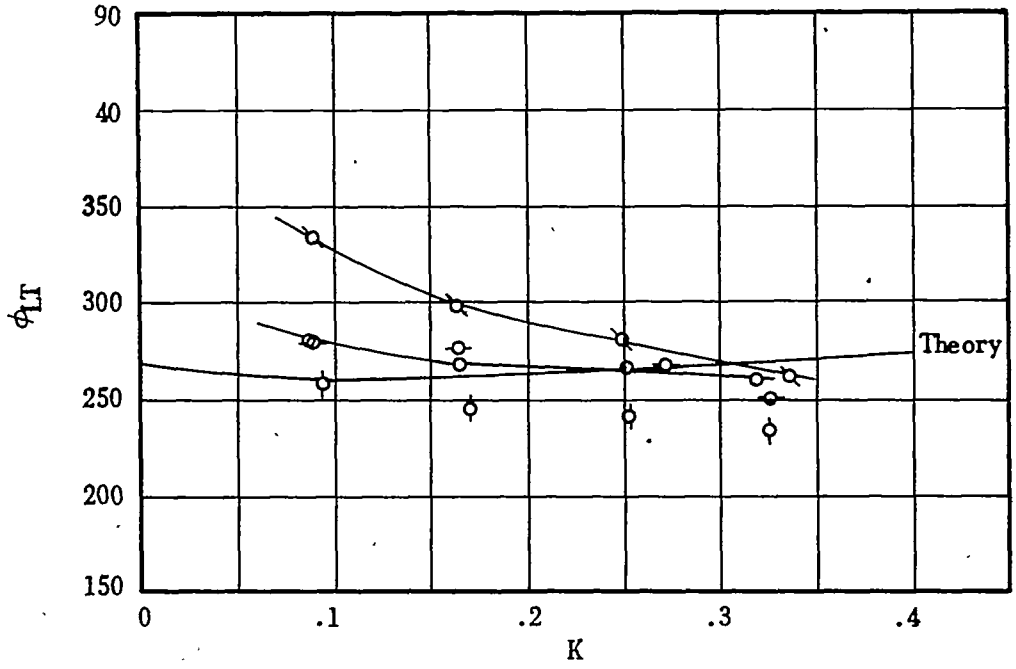

(b) Intermediate wing.

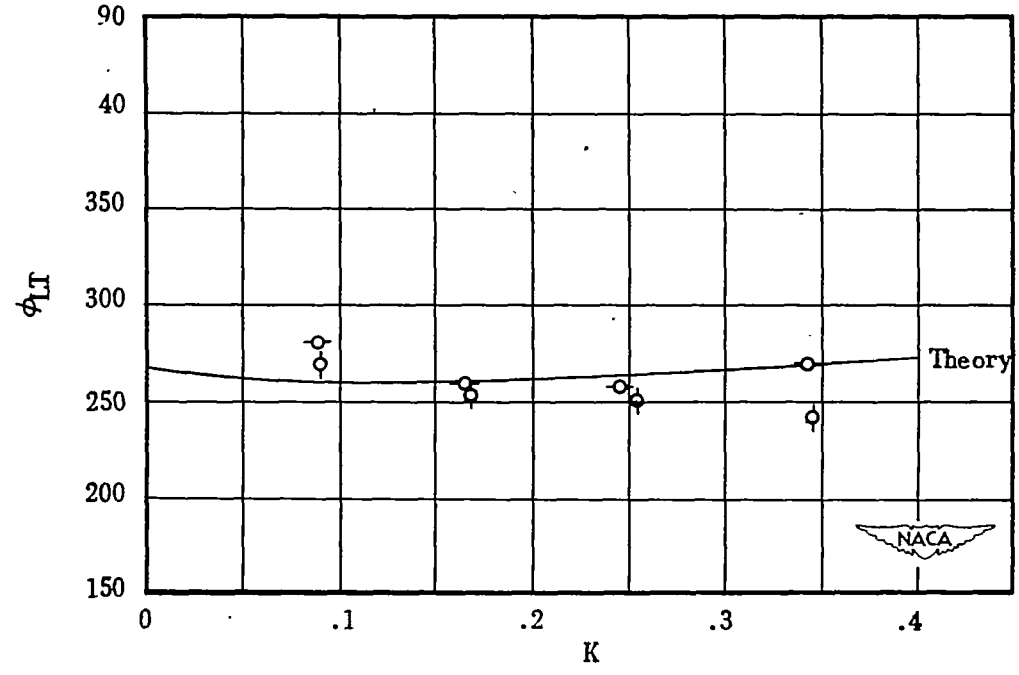

(c) Sharp wing.

Figure 15.- Concluded.

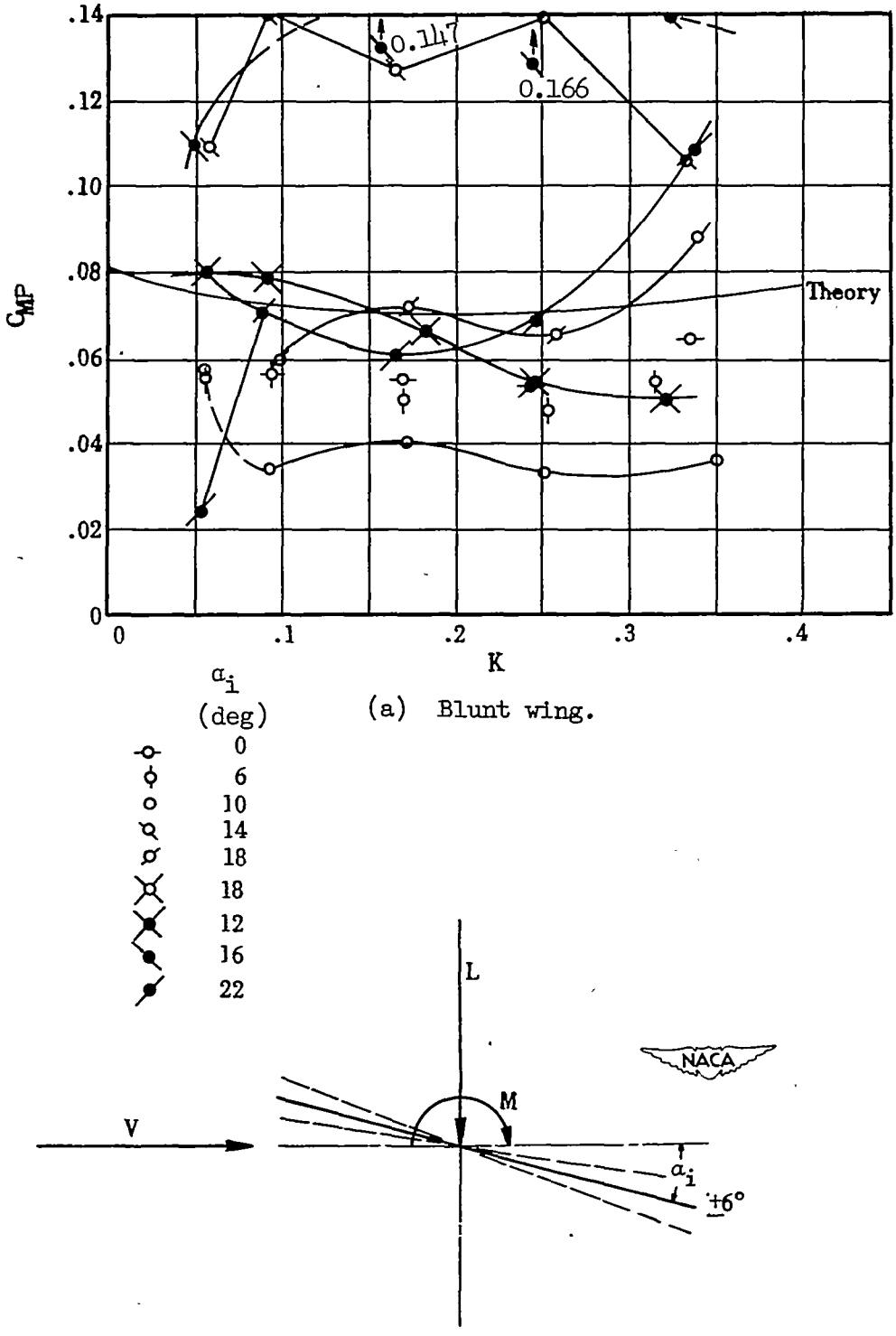

(a) Blunt wing.

Figure 16.- Moment amplitude in pure pitch.

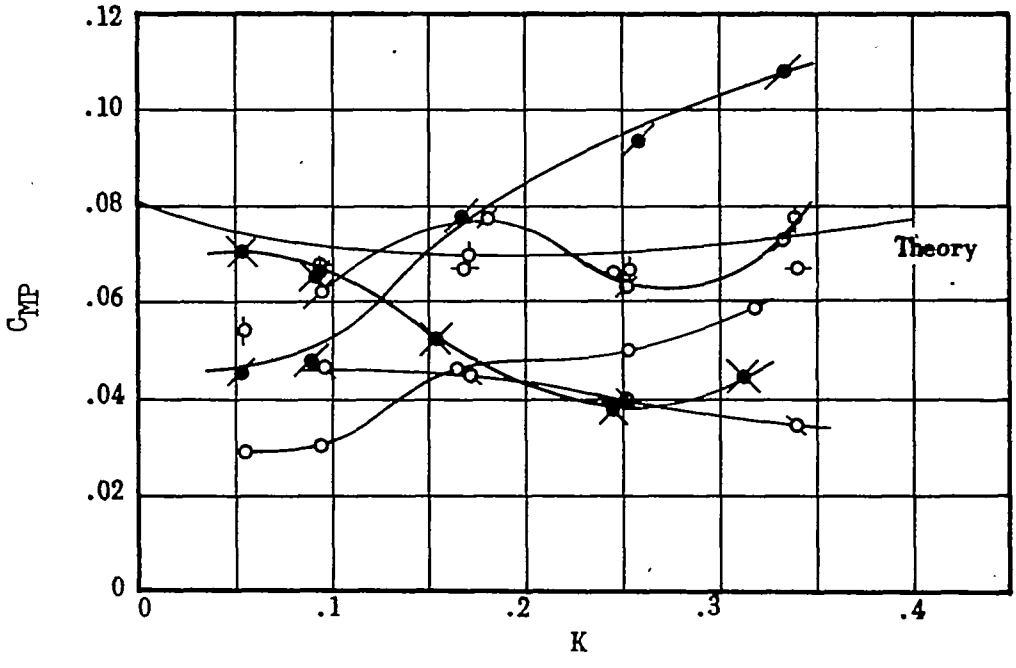

(b) Intermediate wing.

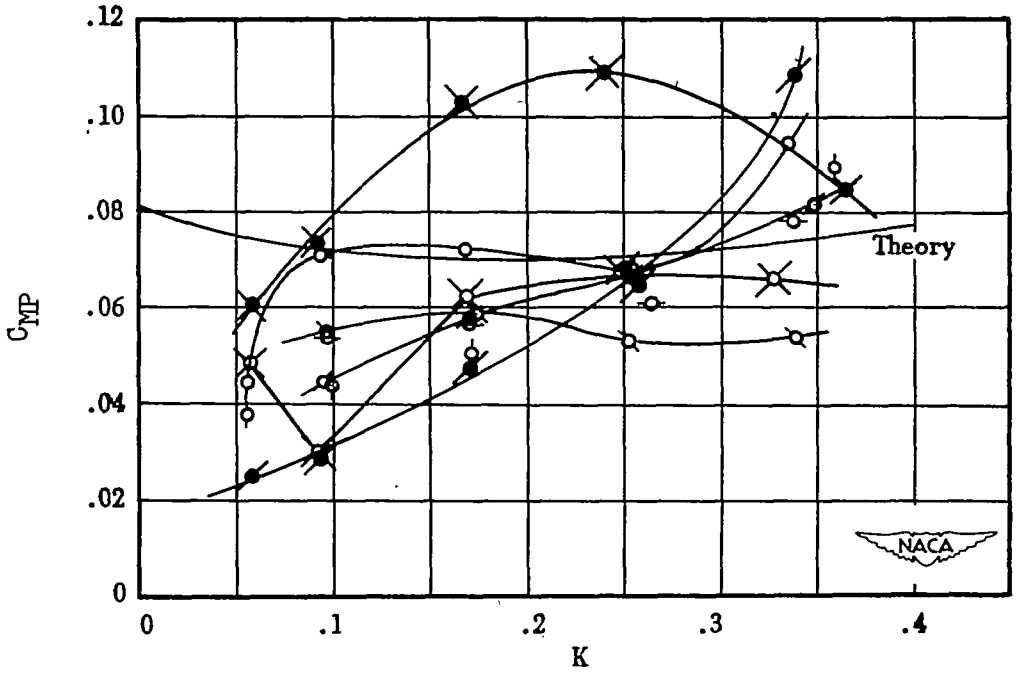

(c) Sharp wing.

Figure 16.- Concluded.

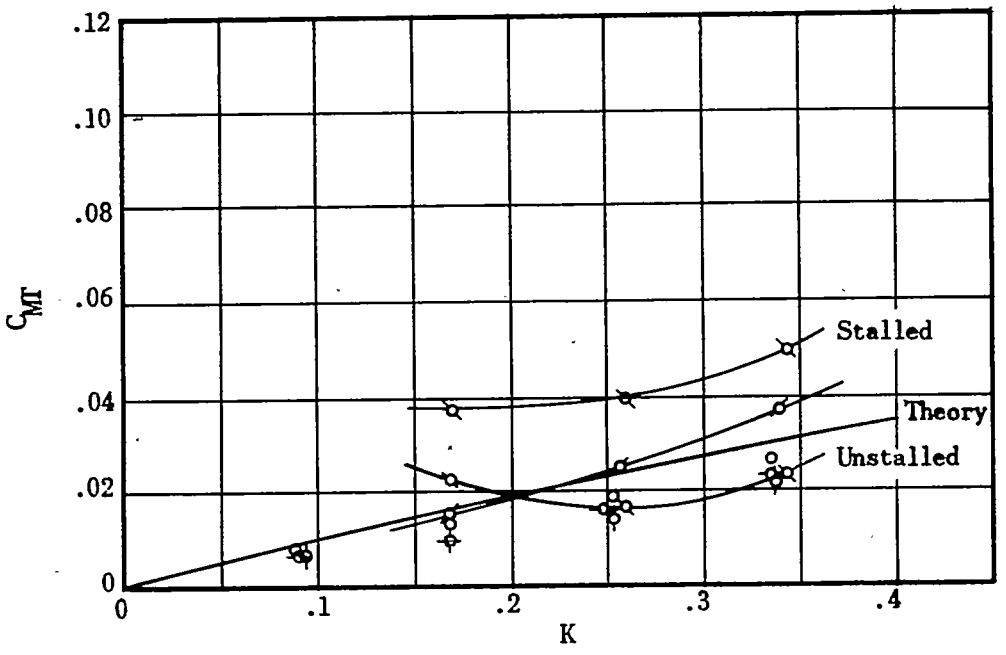

α_i (deg)
0
6
10
14
18

(a) Blunt wing.

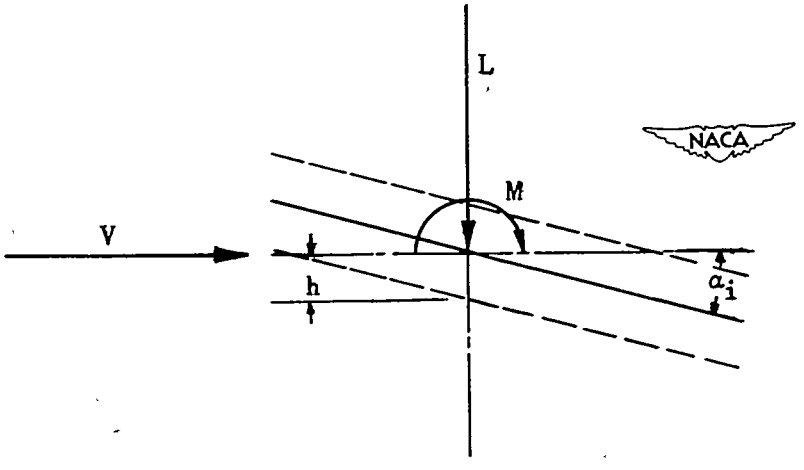

Figure 17.- Moment amplitude in pure translation.

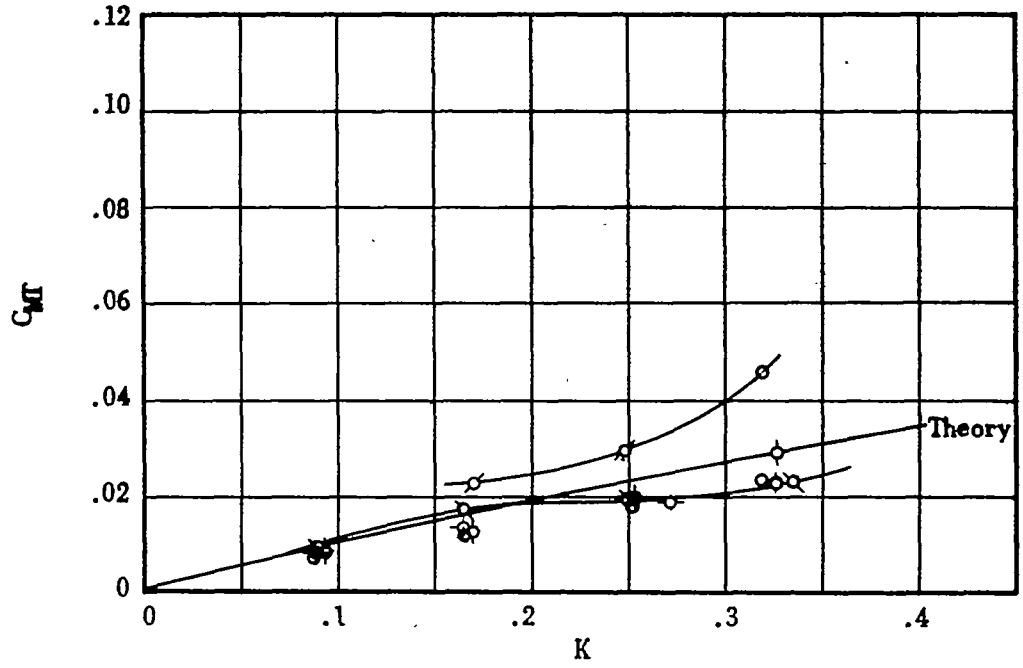

(b) Intermediate wing.

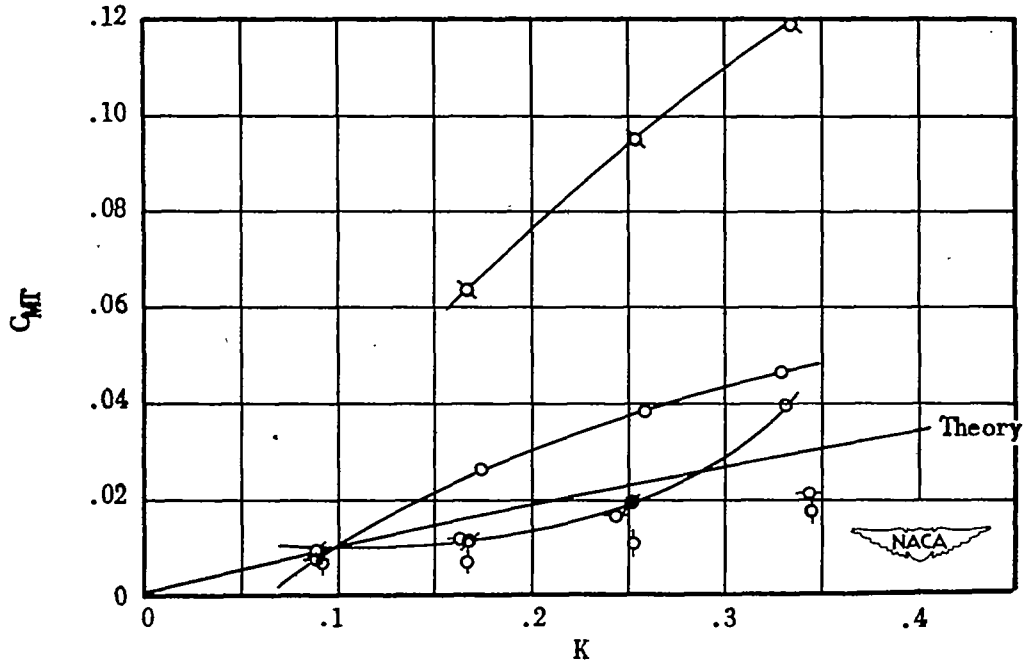

(c) Sharp wing.

Figure 17.- Concluded.

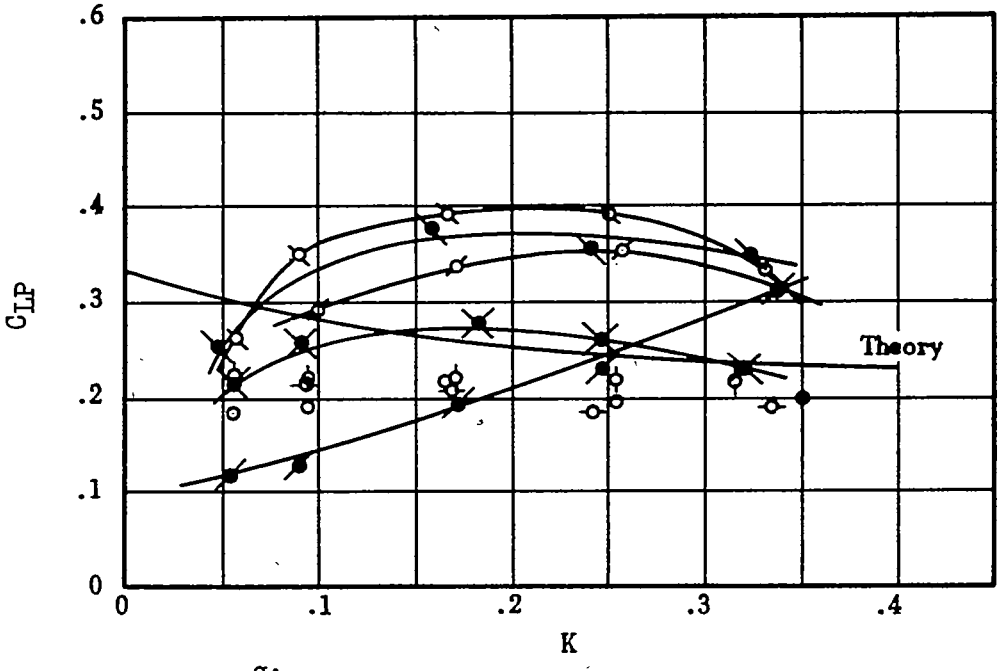

(a) Blunt wing.

α_i (deg)
0
6
10
14
18
8
12
16
22

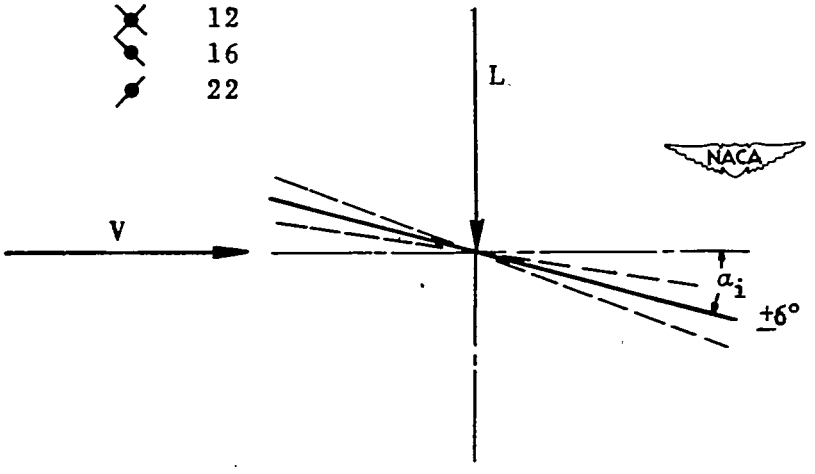

Figure 18.- Lift amplitude in pure pitch.

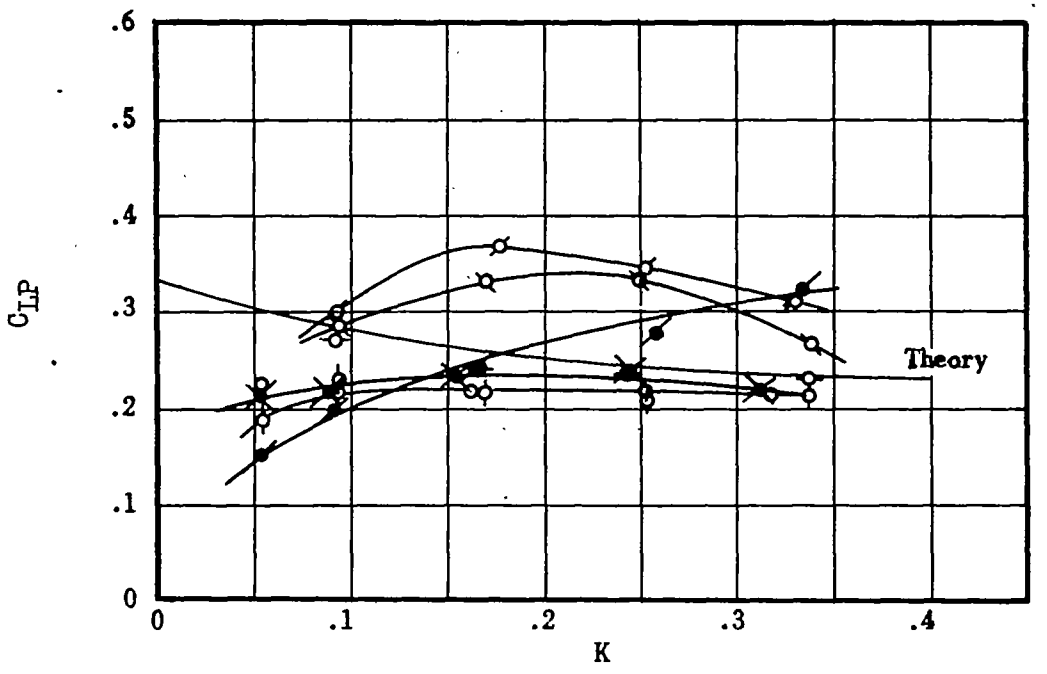

(b) Intermediate wing.

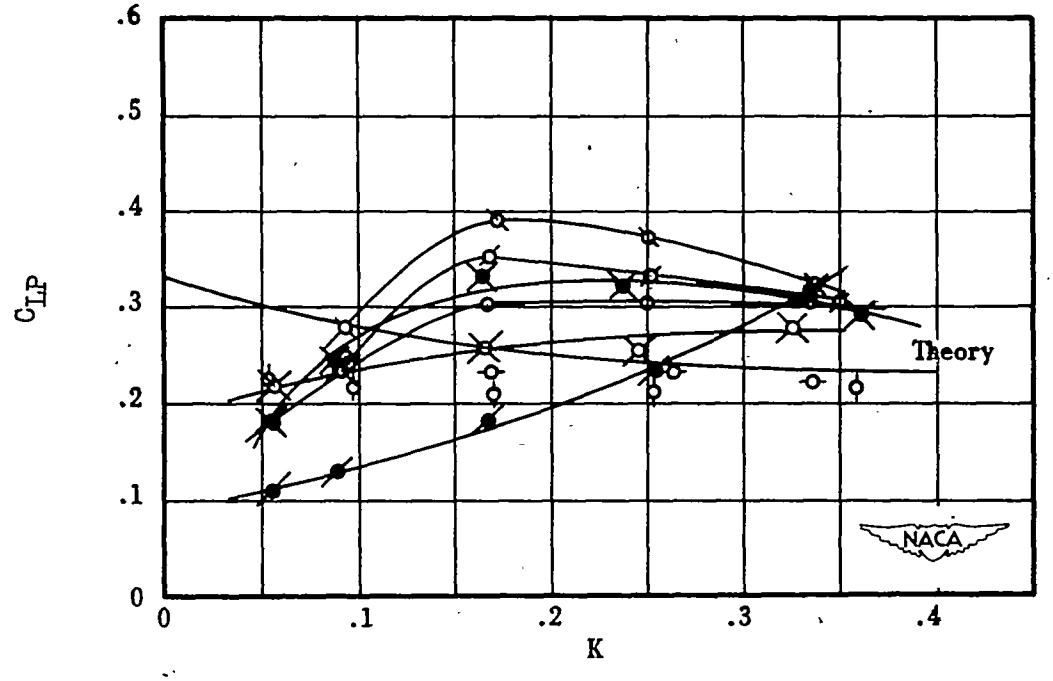

(c) Sharp wing.

Figure 18.- Concluded.

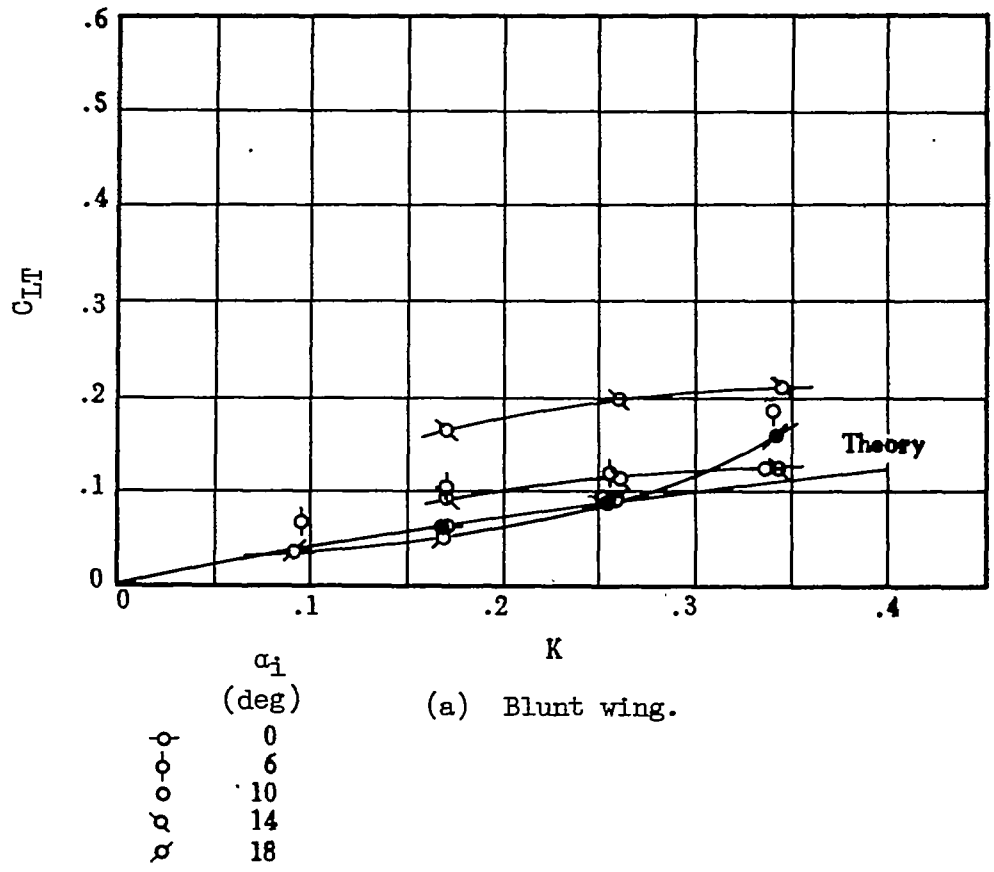

(a) Blunt wing.

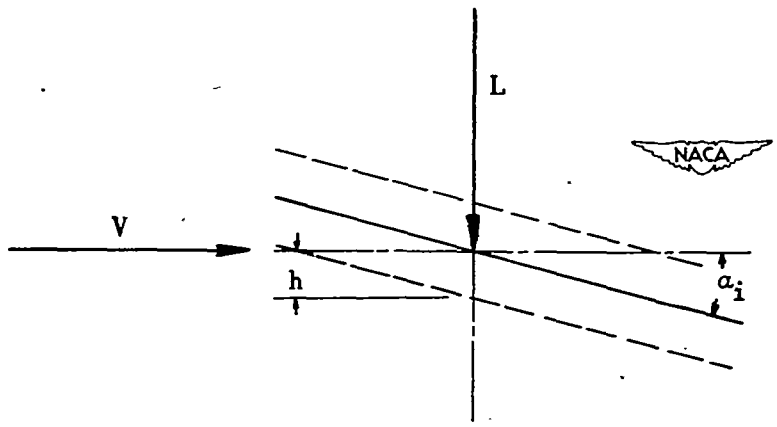

Figure 19.- Lift amplitude in pure translation.

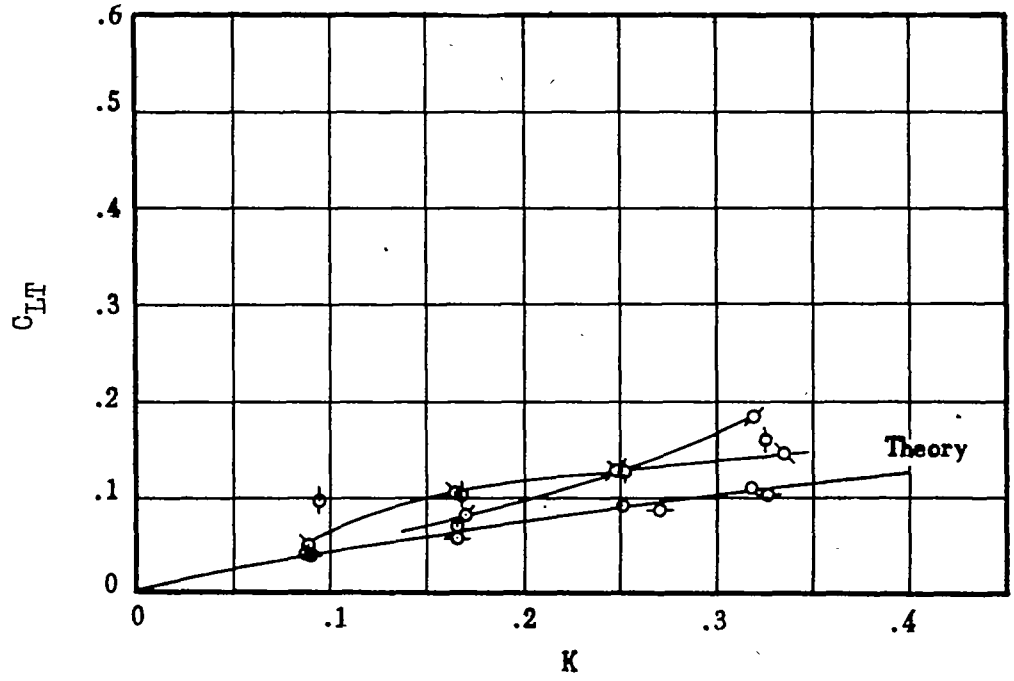

(b) Intermediate wing.

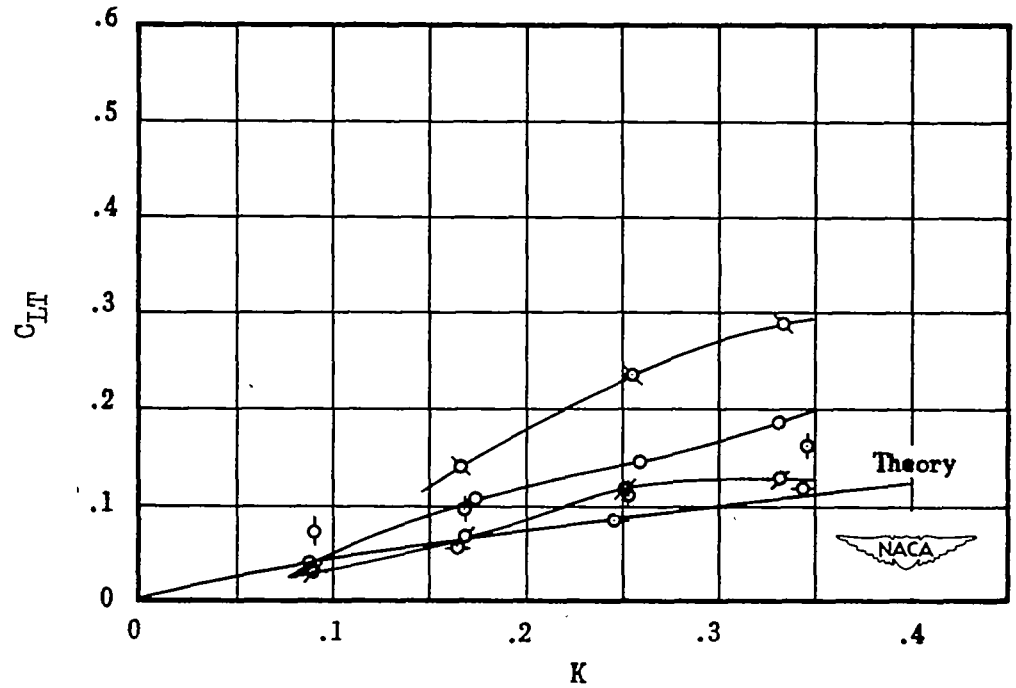

(c) Sharp wing.

Figure 19.- Concluded.

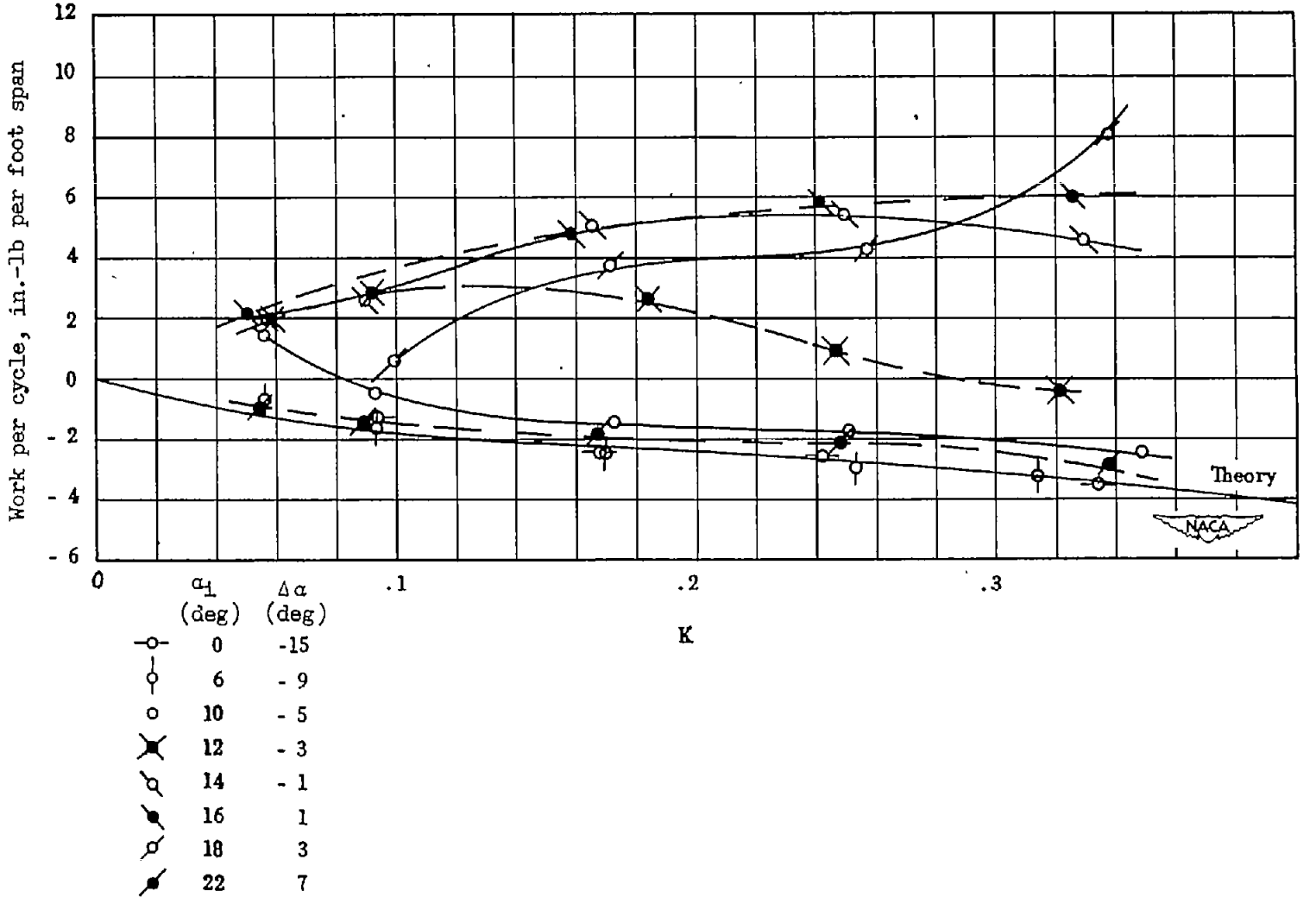

Figure 20.- Work per cycle in pure pitch. Blunt wing.
V = 95 miles per hour.

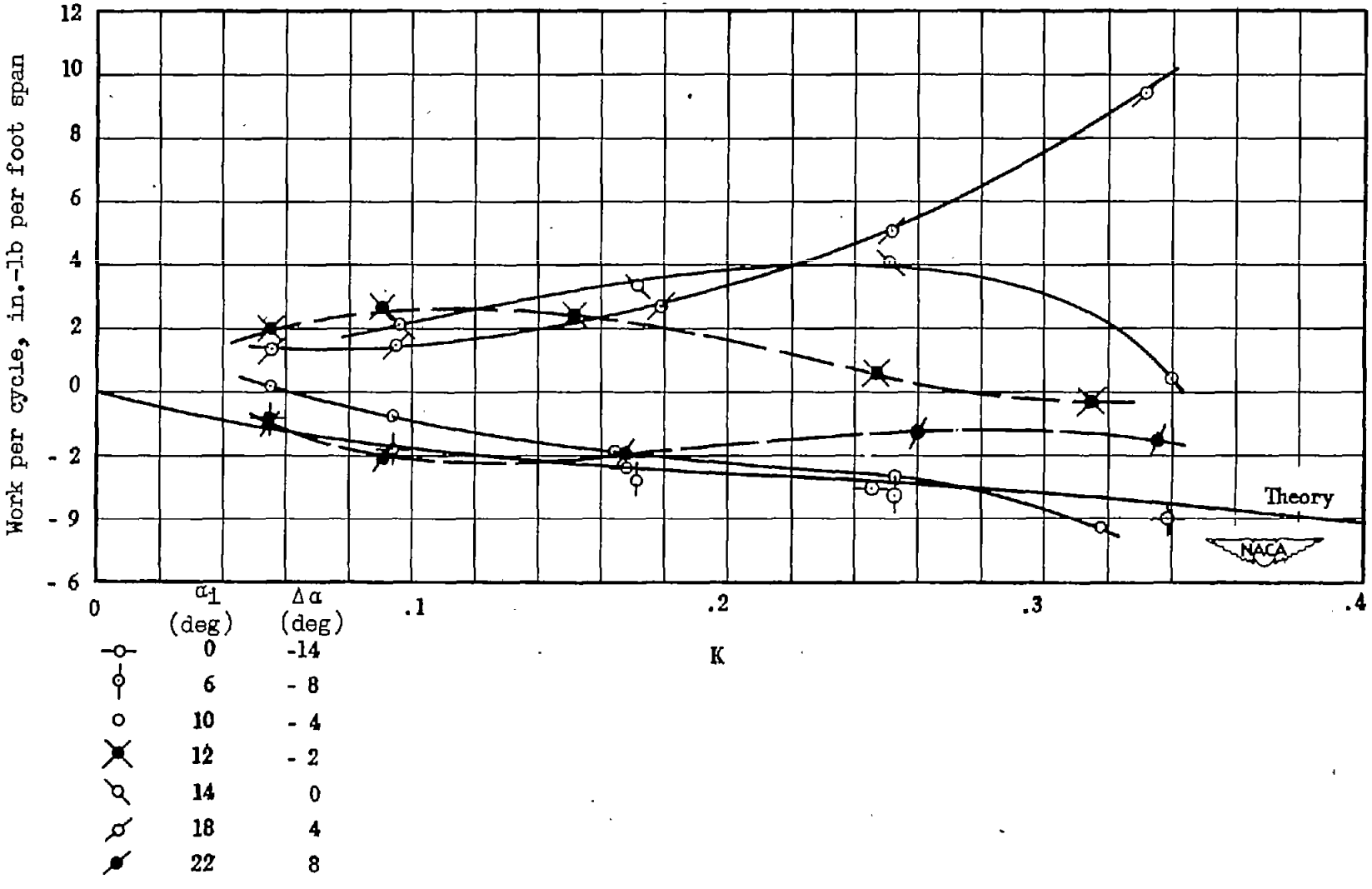

Figure 21.- Work per cycle in pure pitch. Intermediate wing.
V = 95 miles per hour.

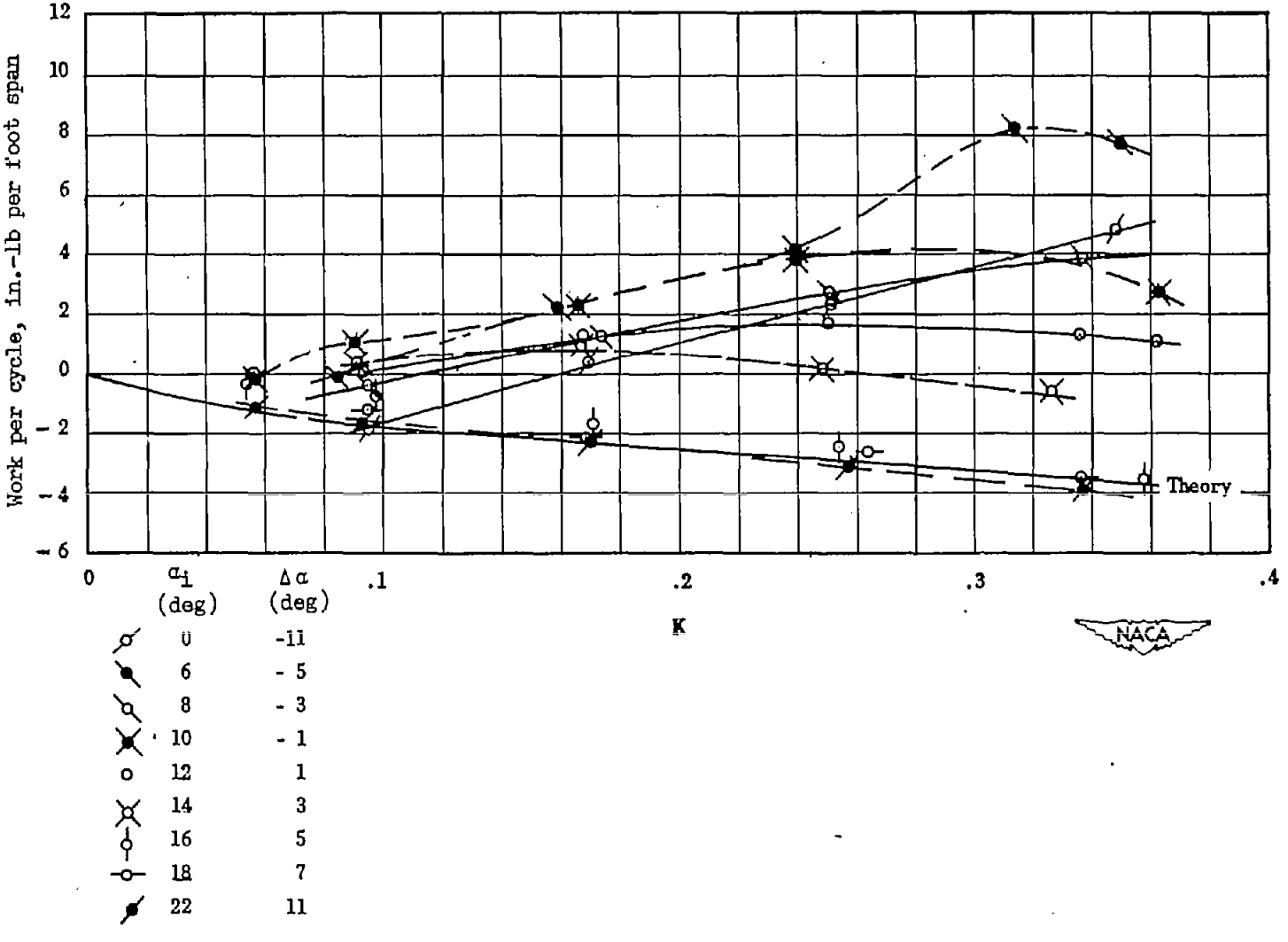

Figure 22.- Work per cycle in pure pitch. Sharp wing.
V = 95 miles per hour.

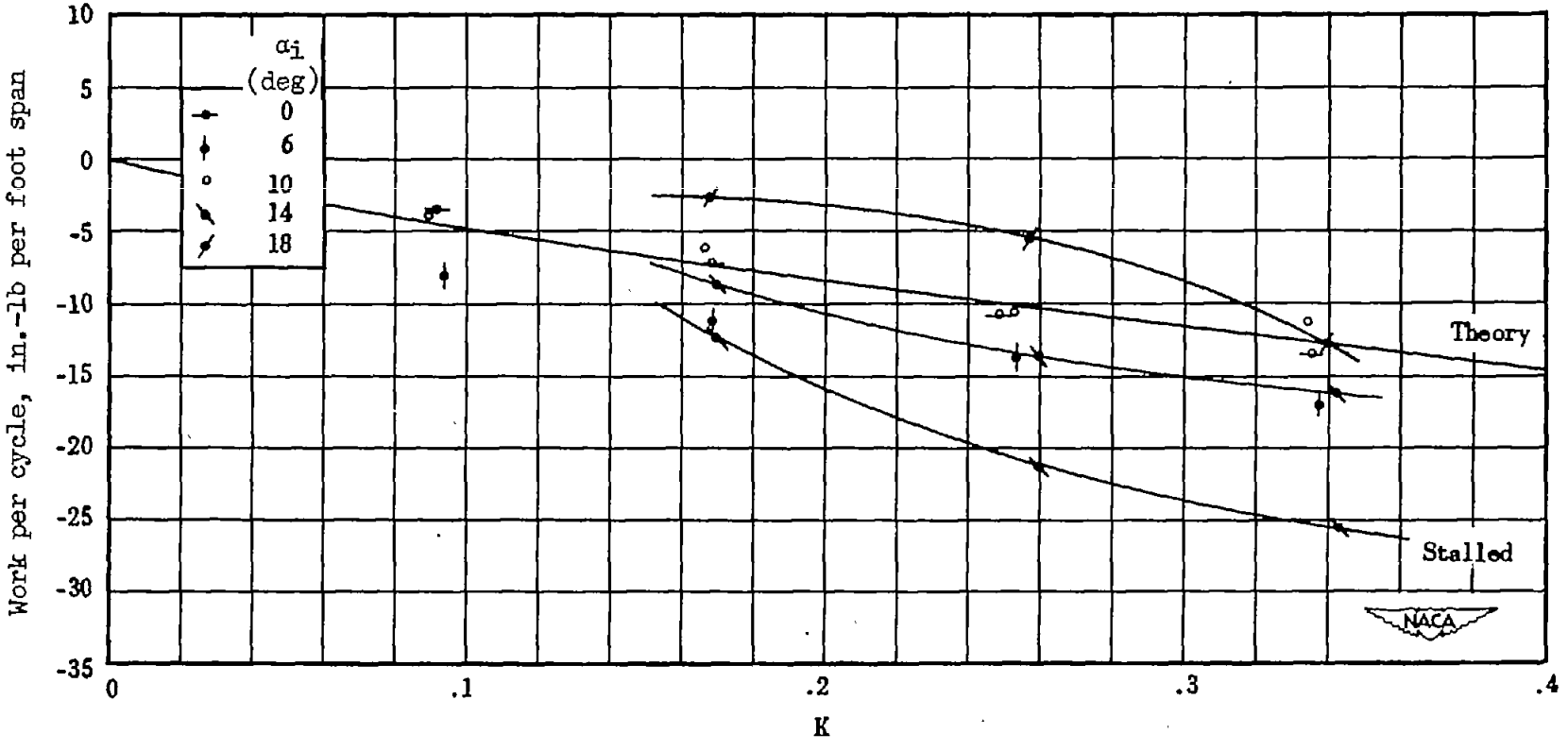

Figure 23.- Work per cycle in pure translation. Blunt wing.

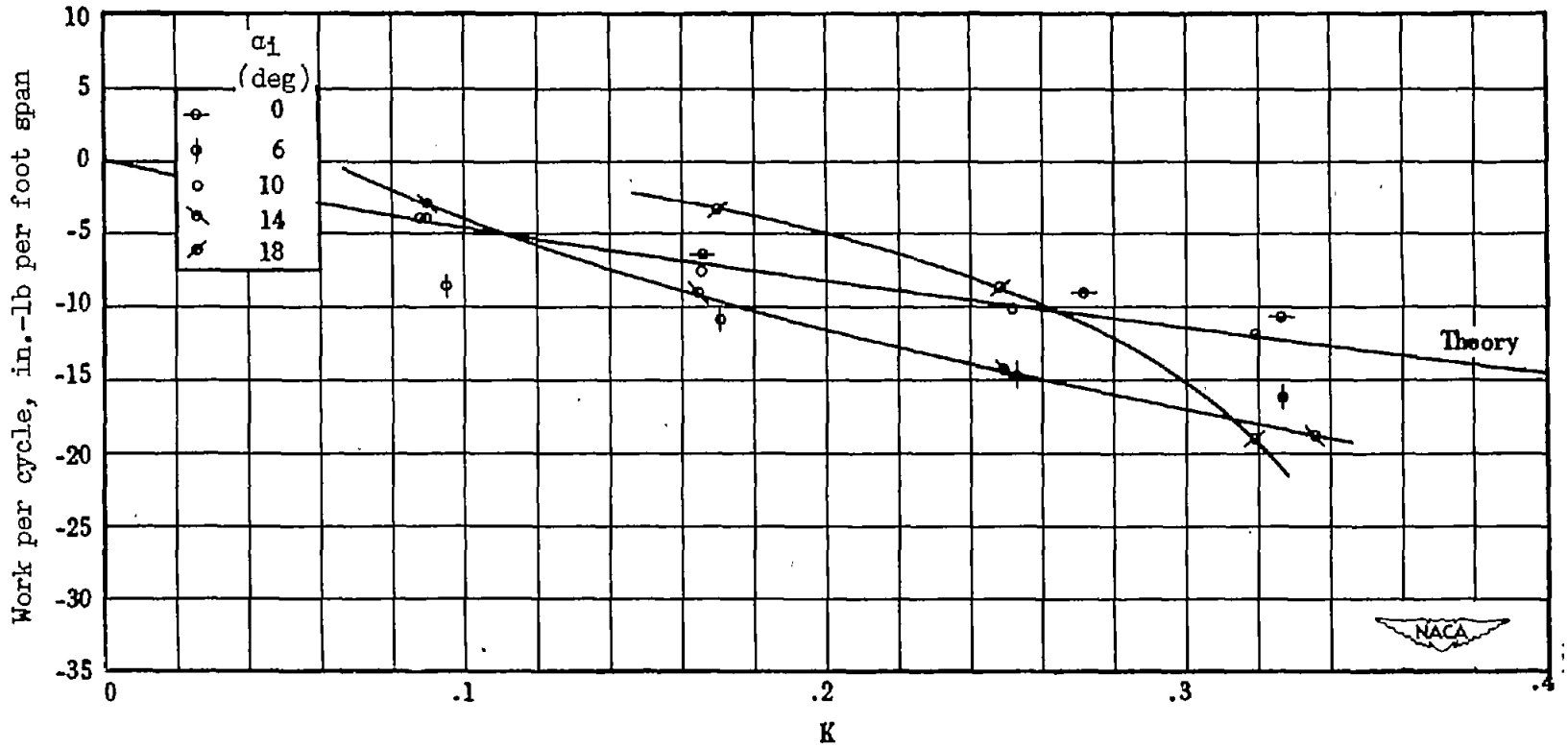

Figure 24.- Work per cycle in pure translation. Intermediate wing.

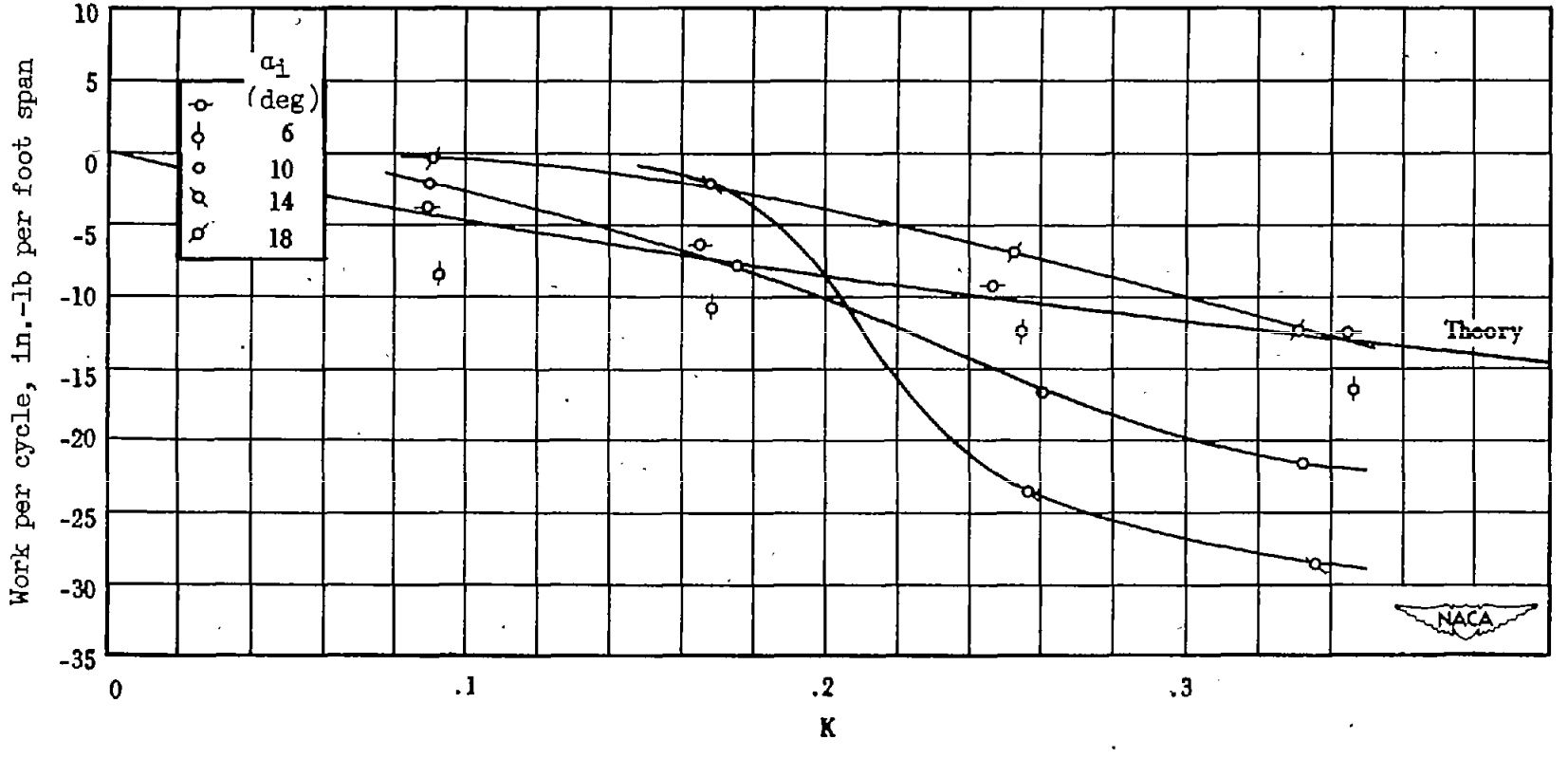

Figure 25.- Work per cycle in pure translation. Sharp wing.

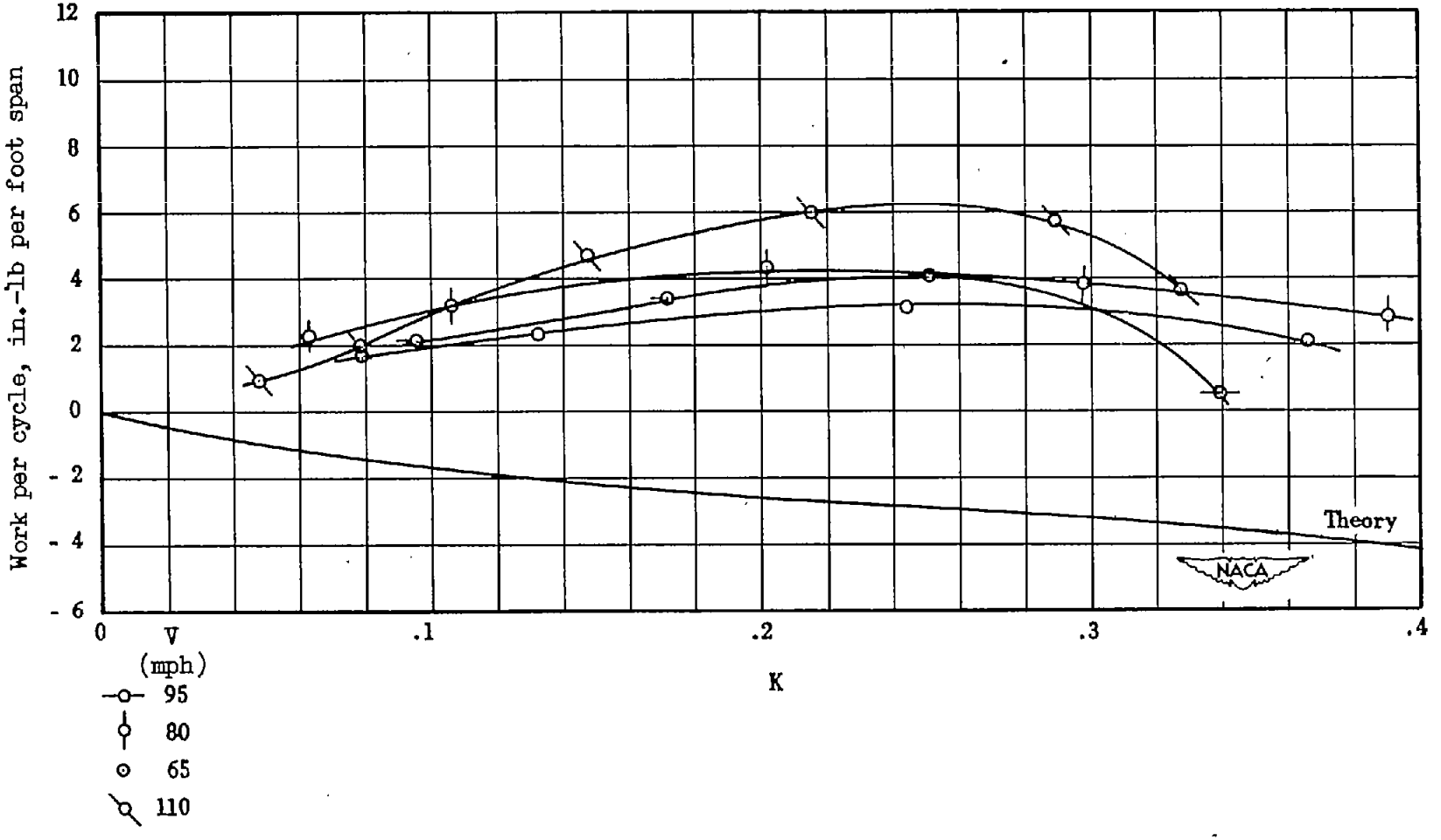

Figure 26.- Work per cycle in pure pitch. Intermediate wing.
$\alpha_i = 14^\circ$; $\Delta\alpha = 0^\circ$.

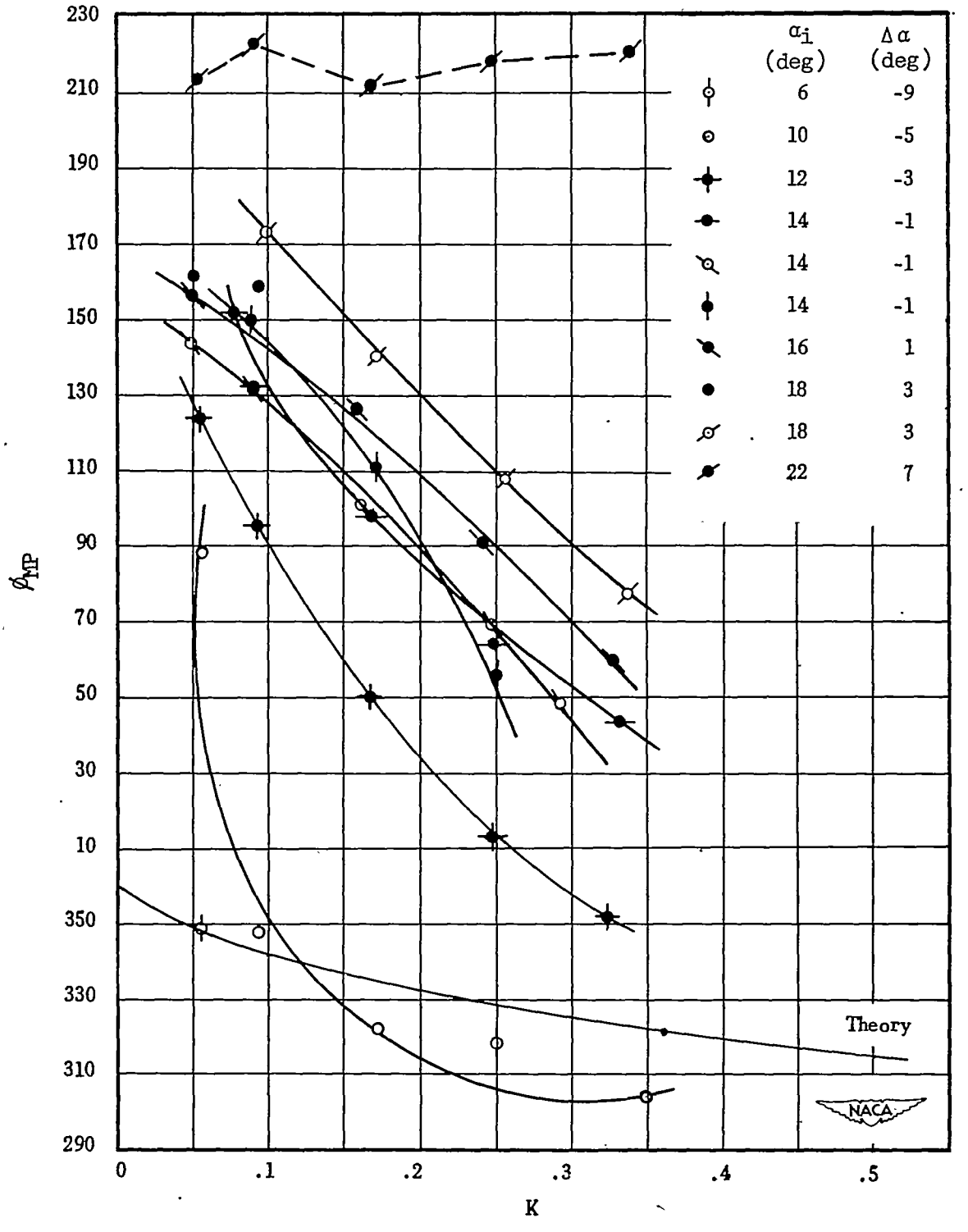

Figure 27.- Moment phase angle in pure pitch from harmonic analysis. Blunt wing.

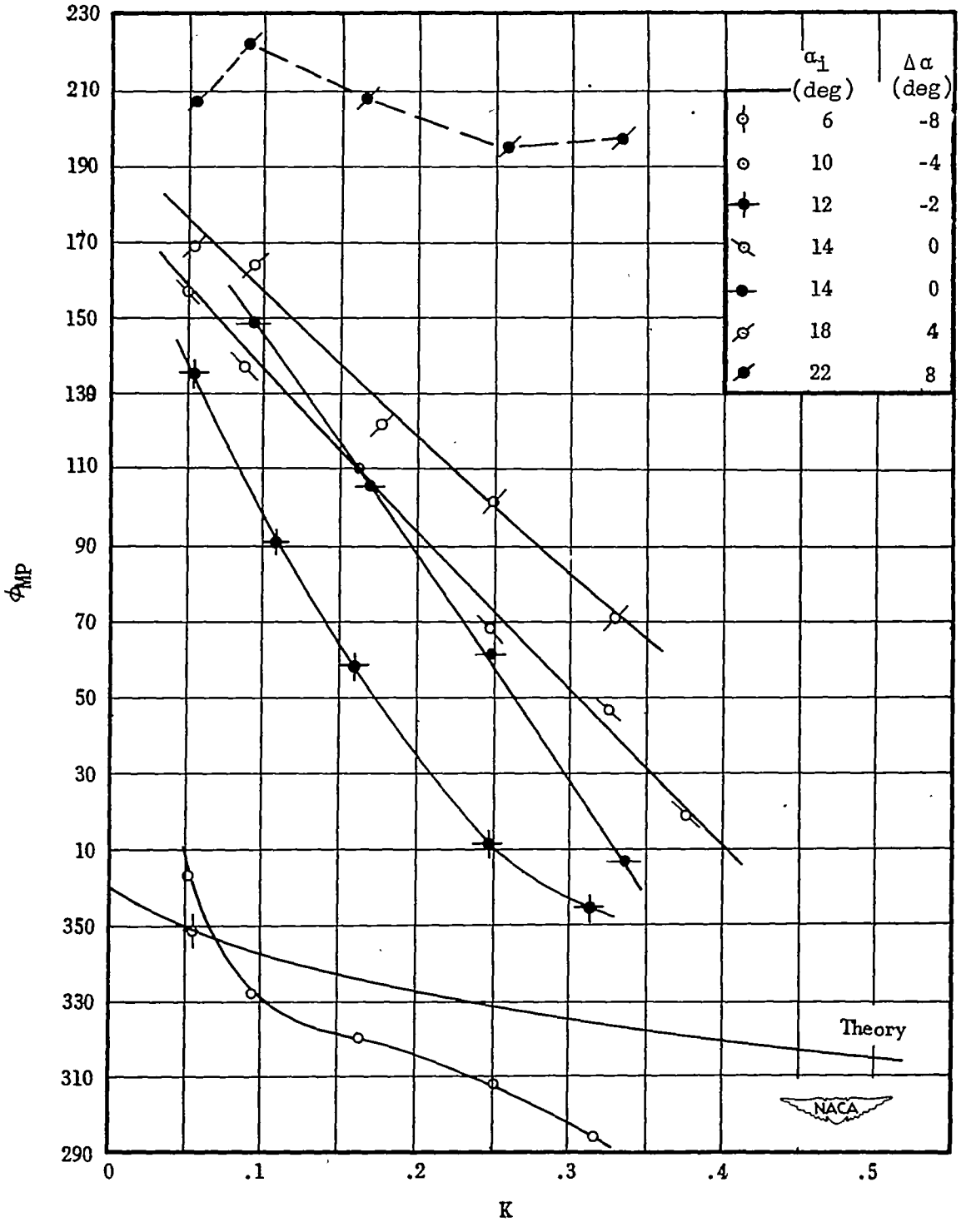

Figure 28.- Moment phase angle in pure pitch from harmonic analysis. Intermediate wing.

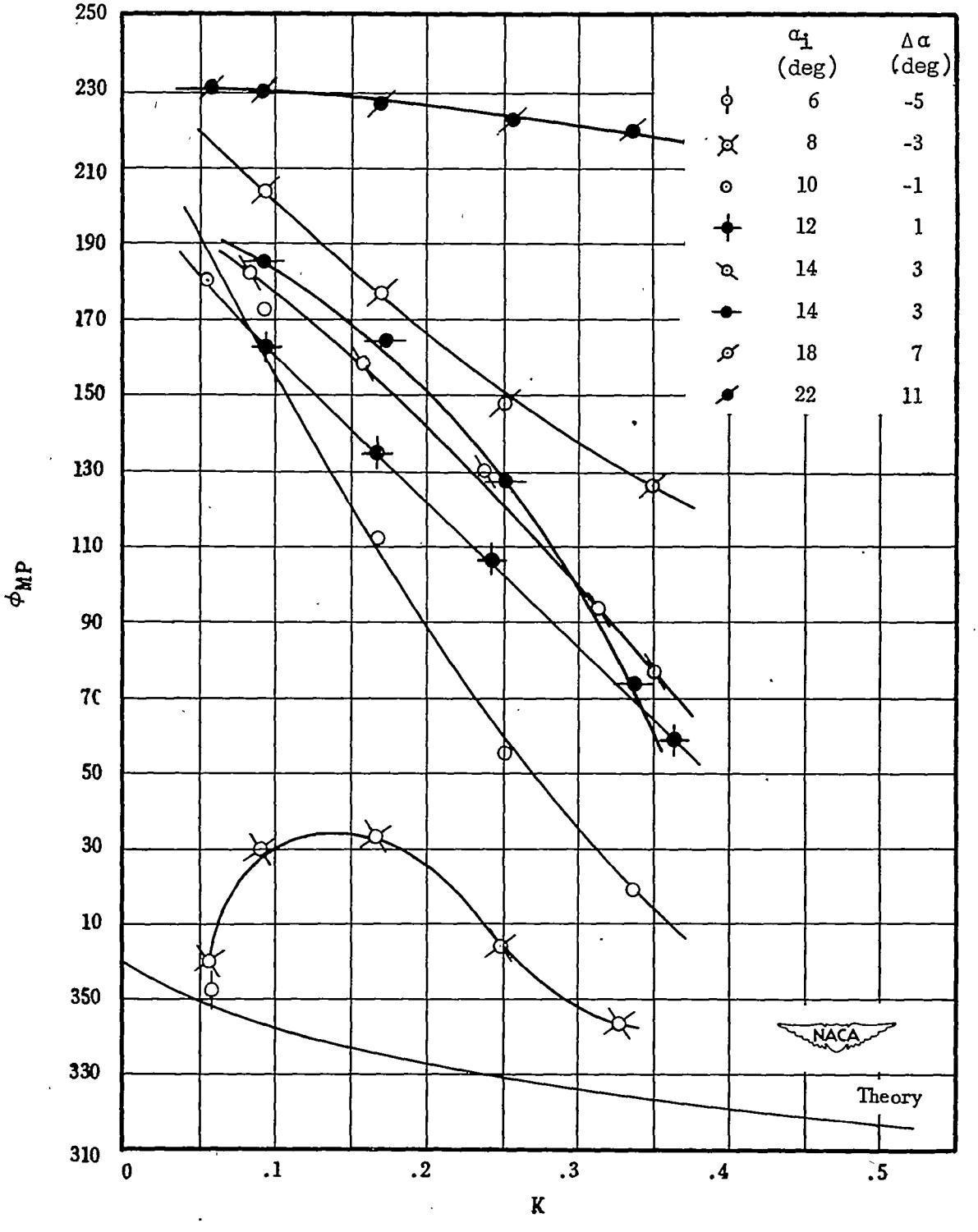

Figure 29.- Moment phase angle in pure pitch from harmonic analysis. Sharp wing.

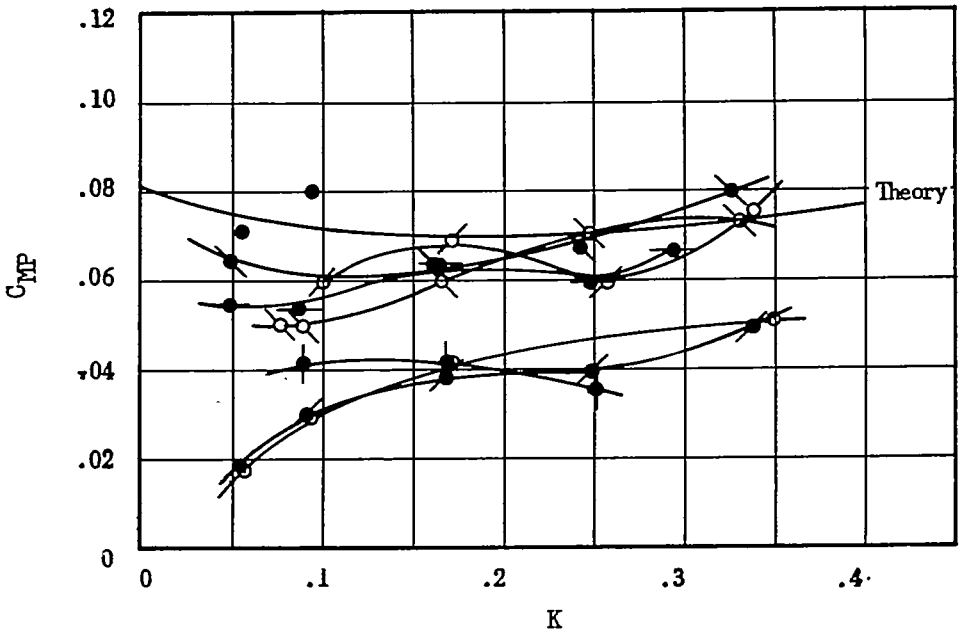

(a) Blunt wing.

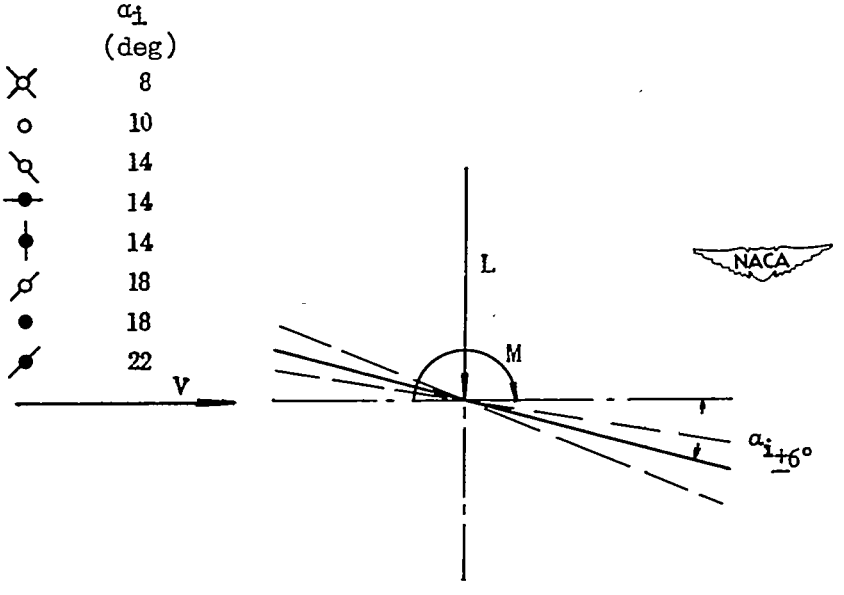

Figure 30.- Moment amplitude in pure pitch from harmonic analysis.

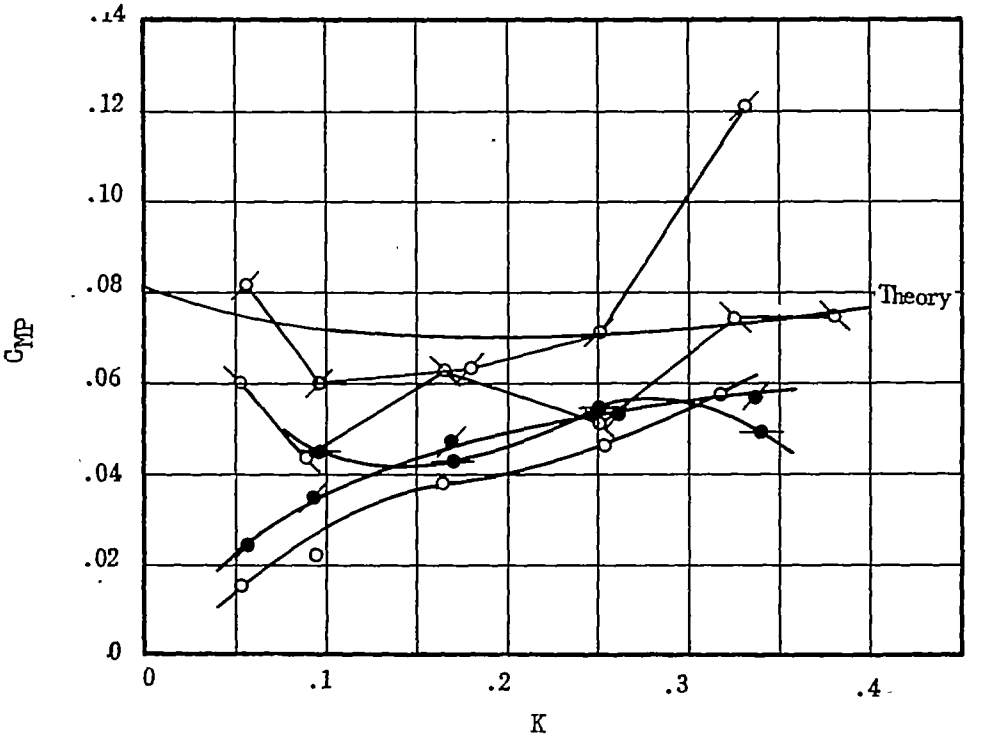

(b) Intermediate wing.

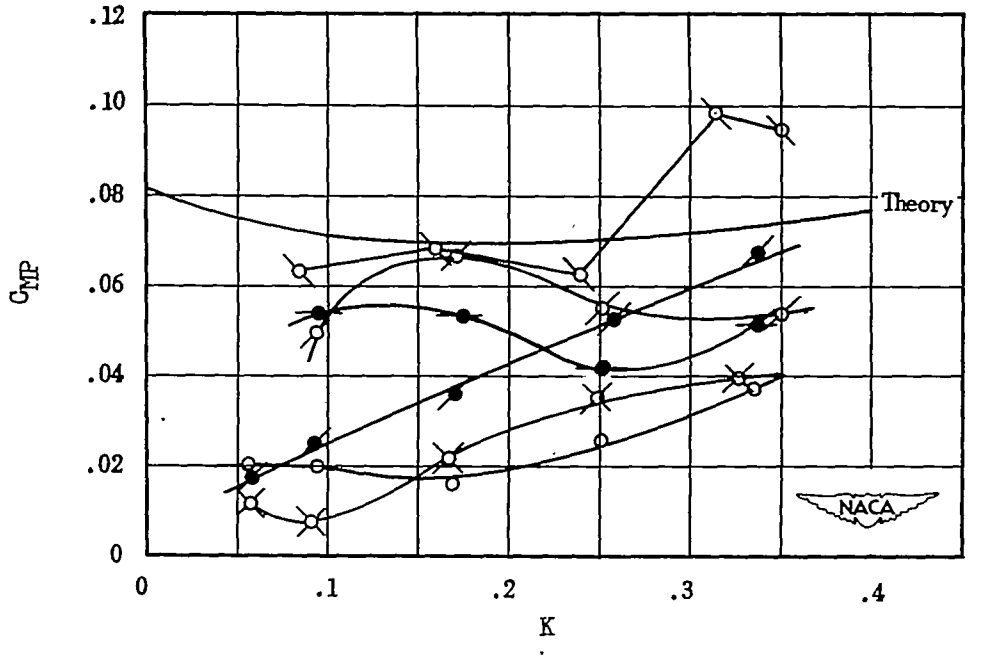

(c) Sharp wing.

Figure 30.- Concluded.

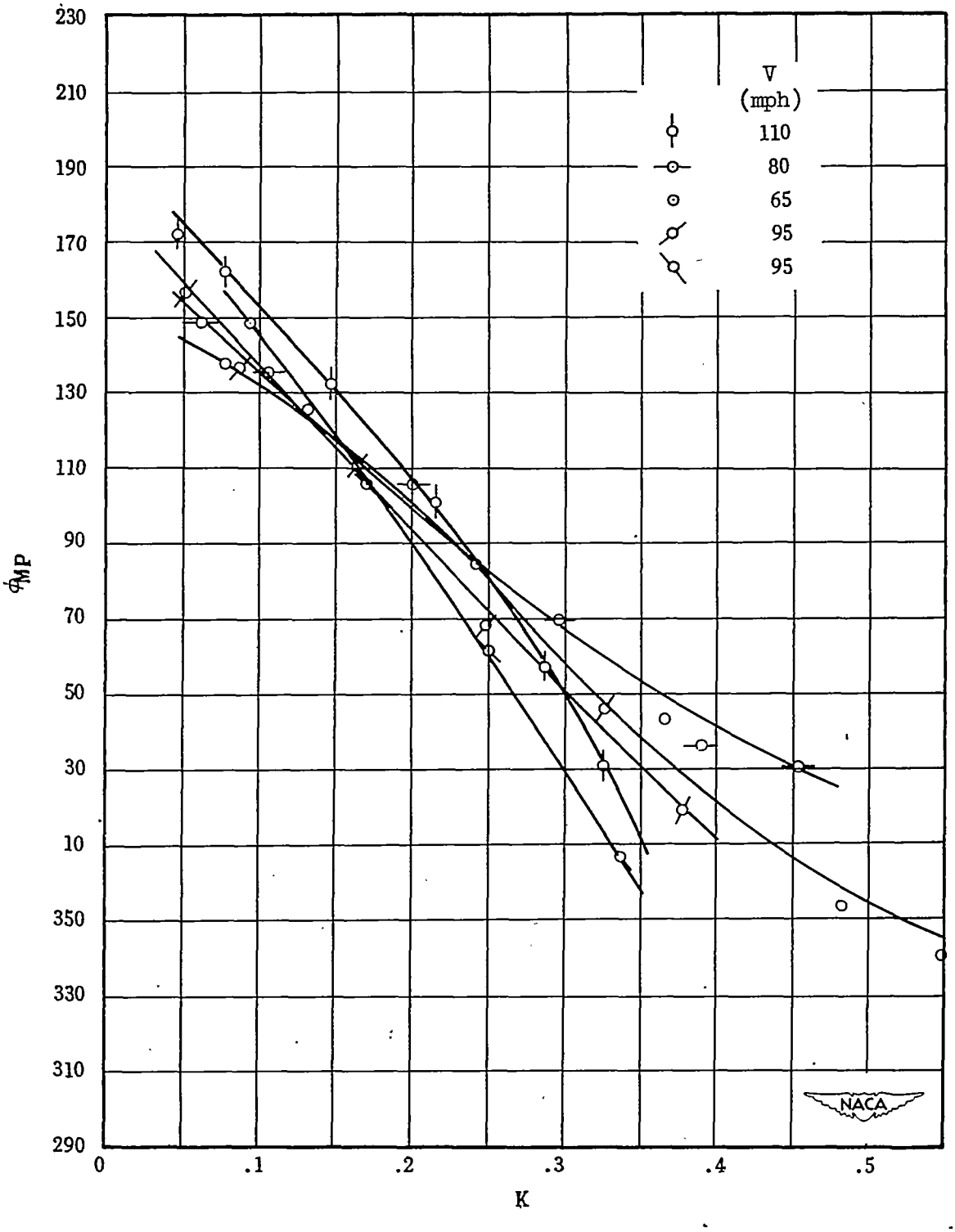

Figure 31.- Moment phase angle in pure pitch from harmonic analysis. Intermediate wing. $\alpha_i = 14^\circ$; $\Delta\alpha = 0^\circ$.

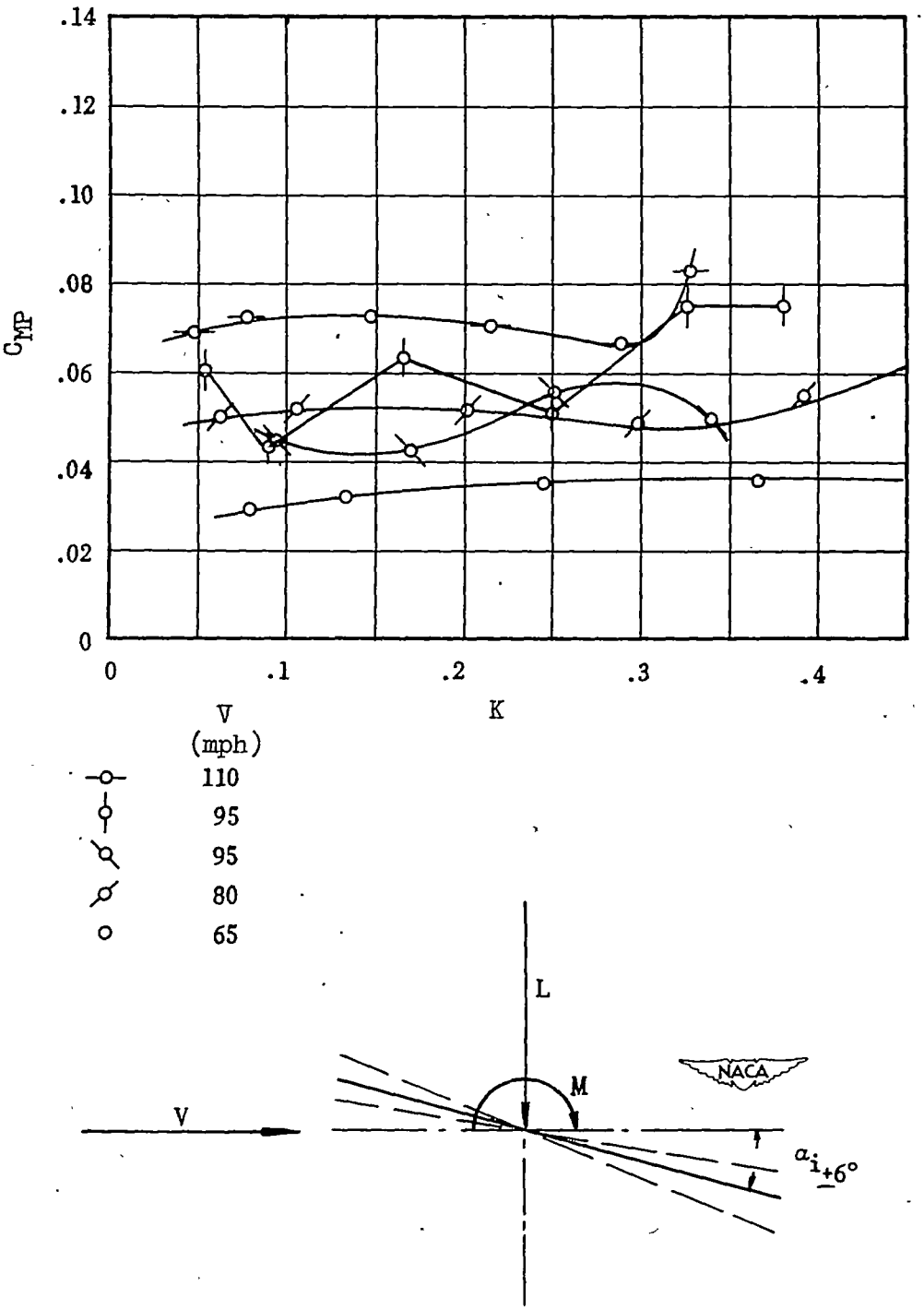

Figure 32.- Moment amplitude in pure pitch from harmonic analysis. Intermediate wing. $\alpha_i = 14^\circ$; $\Delta\alpha = 0^\circ$.

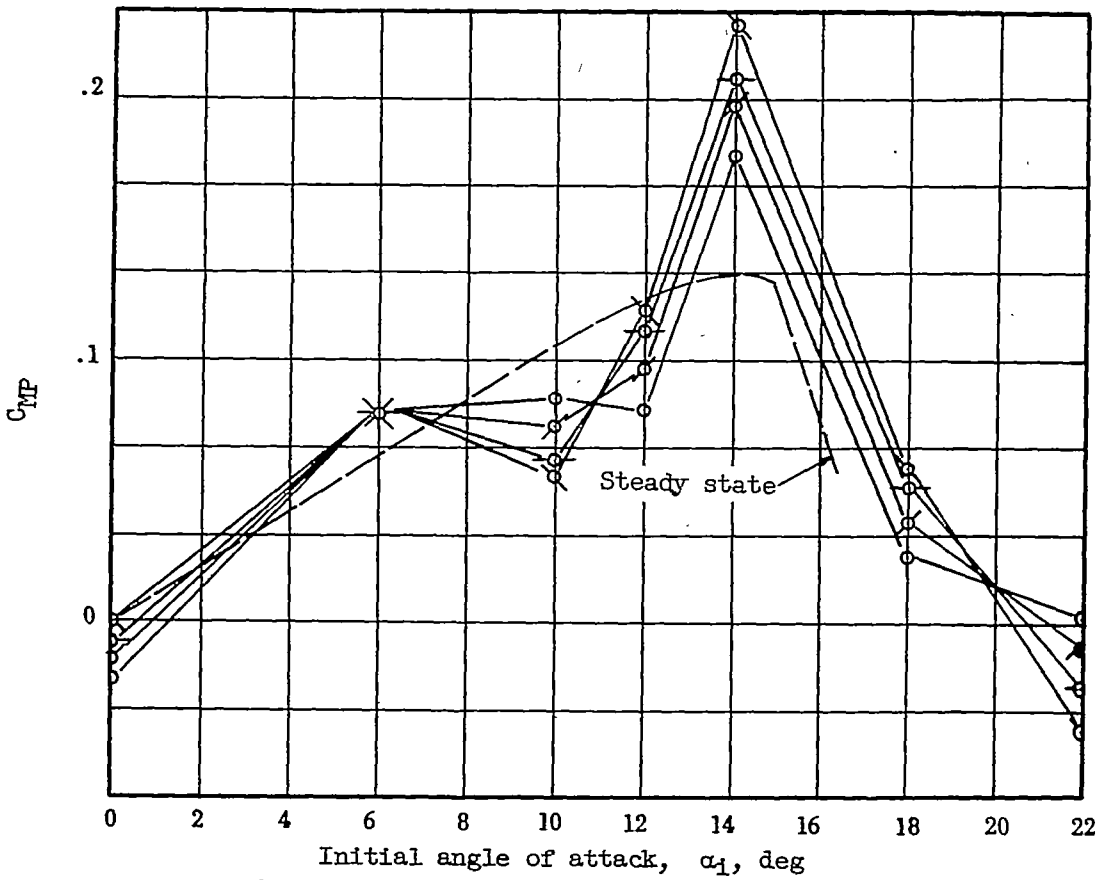

K
0.1
.2
.3
.35

(a) Blunt wing.

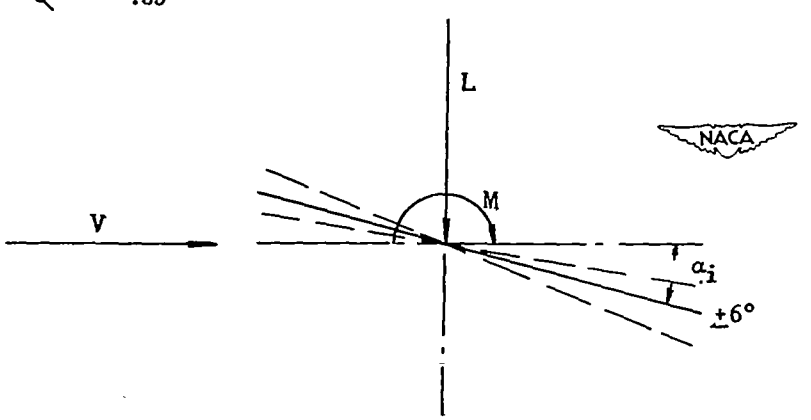

Figure 33.- Time-average value of moment in pure pitch.

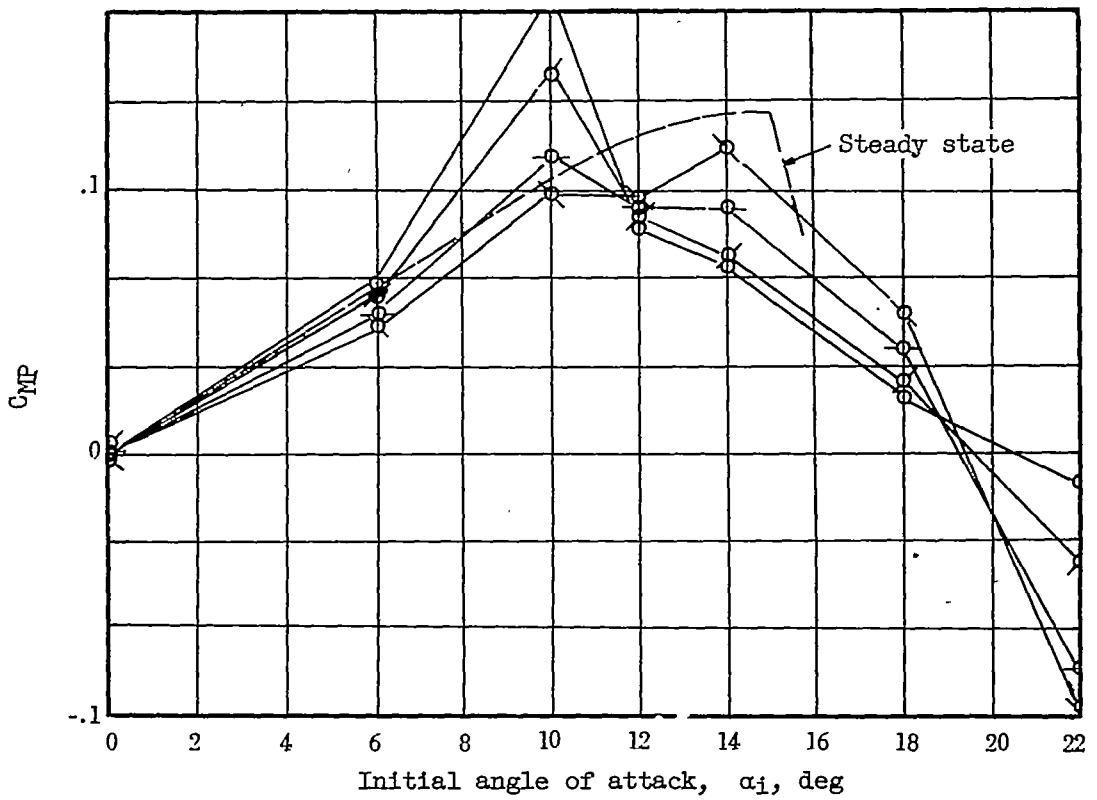

(b) Intermediate wing.

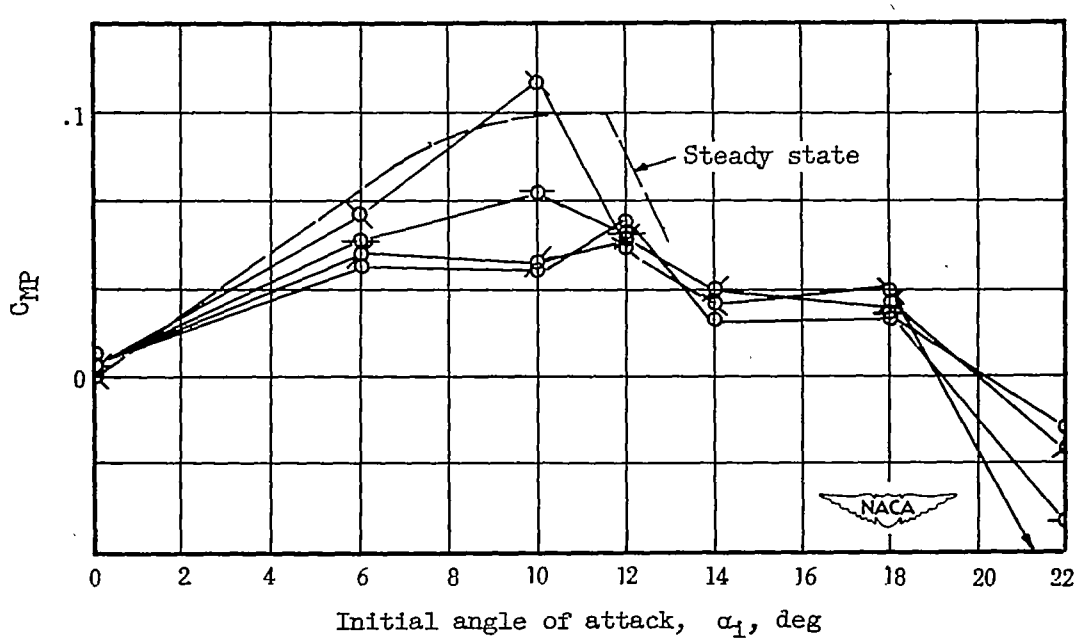

(c) Sharp wing.

Figure 33.- Concluded.

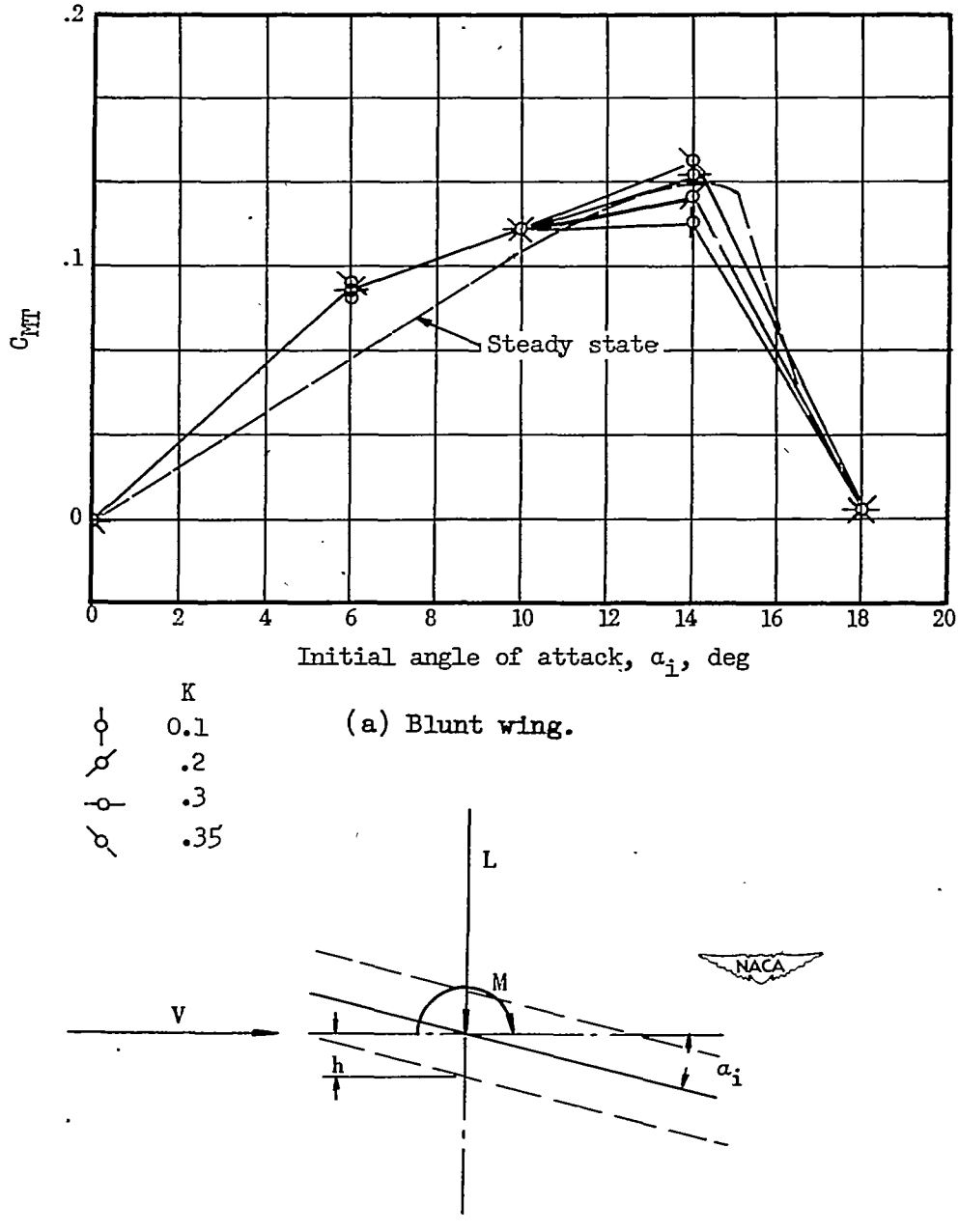

Figure 34.- Time-average value of moment in pure translation.

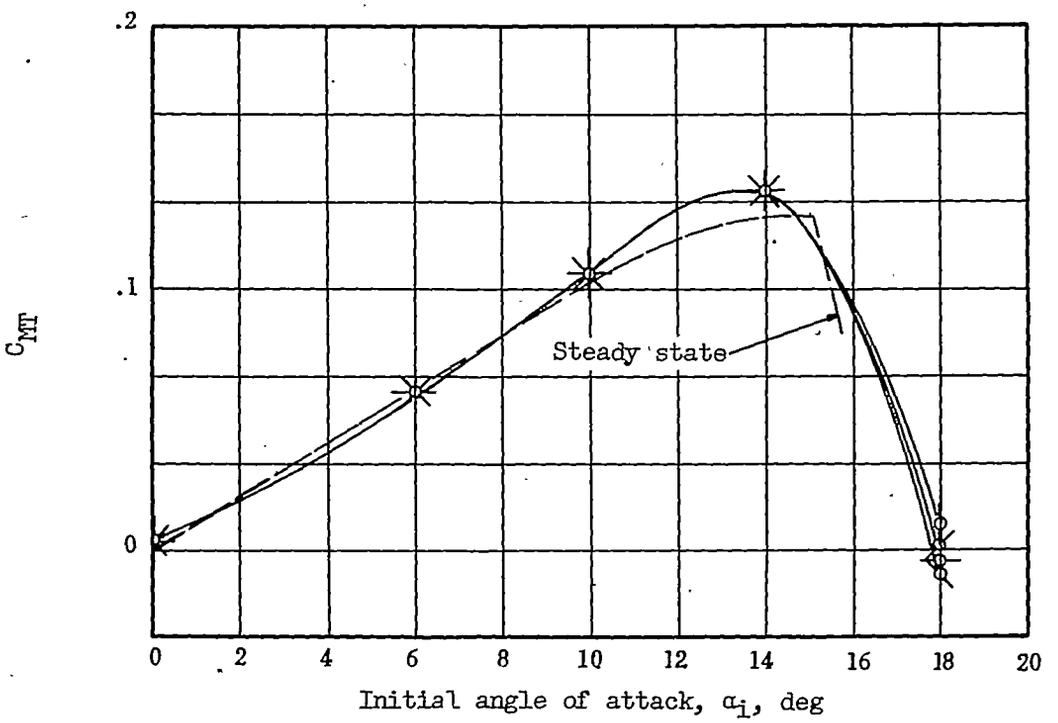

(b) Intermediate wing.

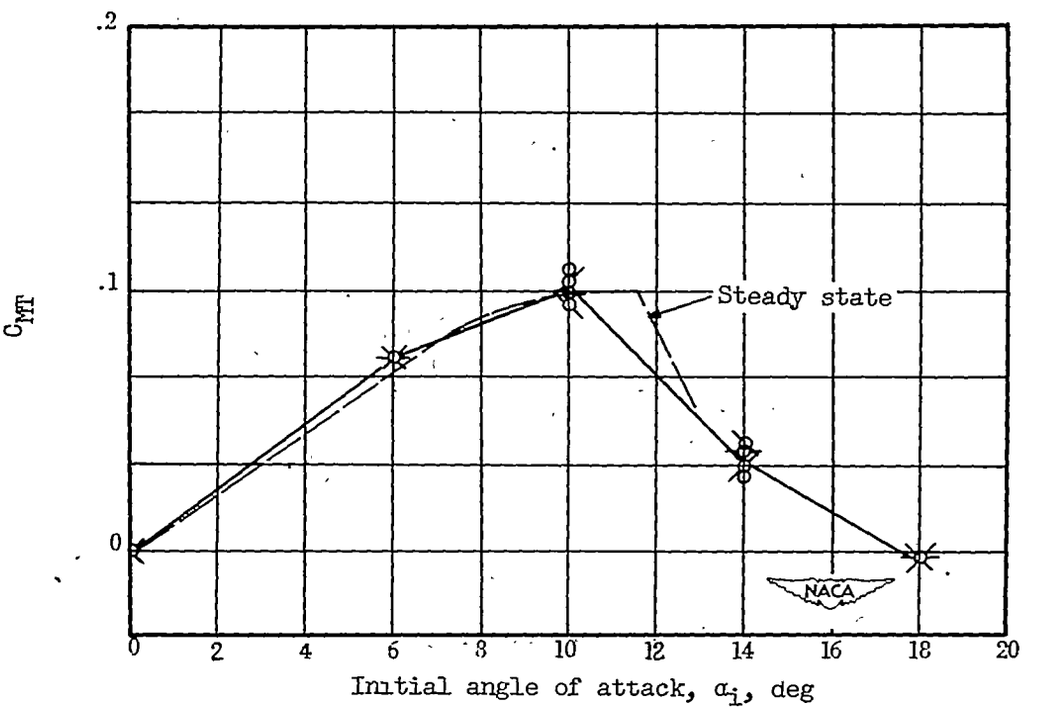

(c) Sharp wing.

Figure 34.- Concluded.

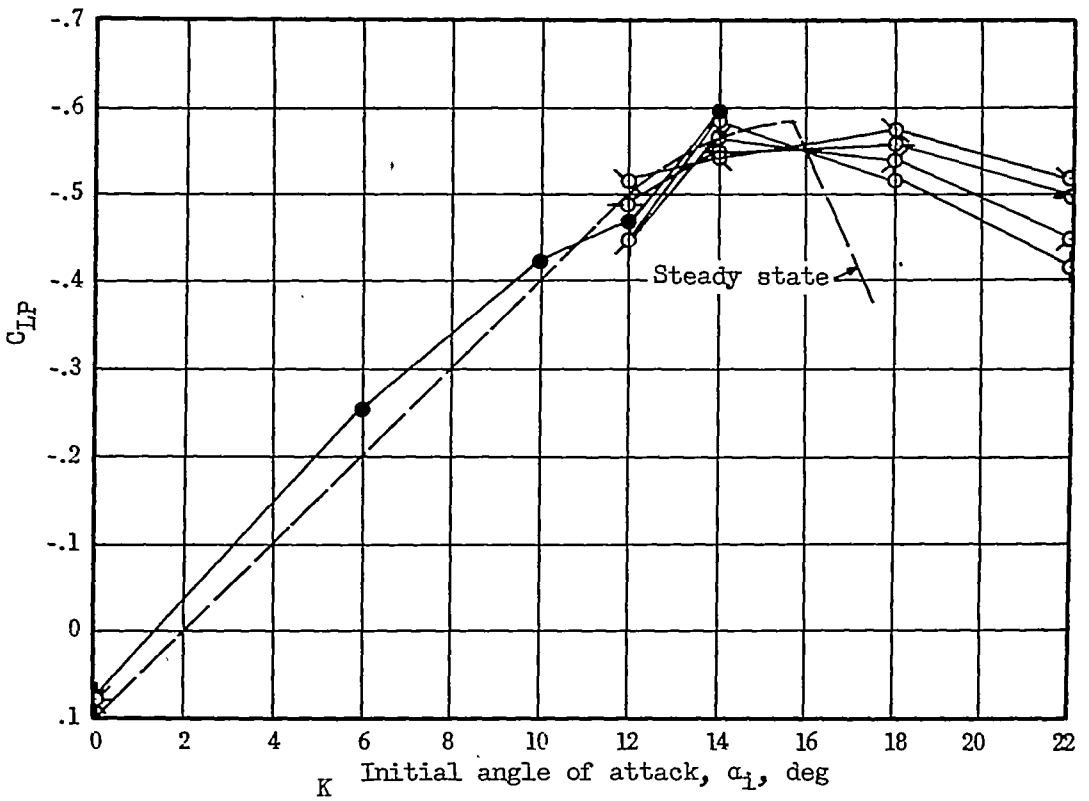

(a) Blunt wing.

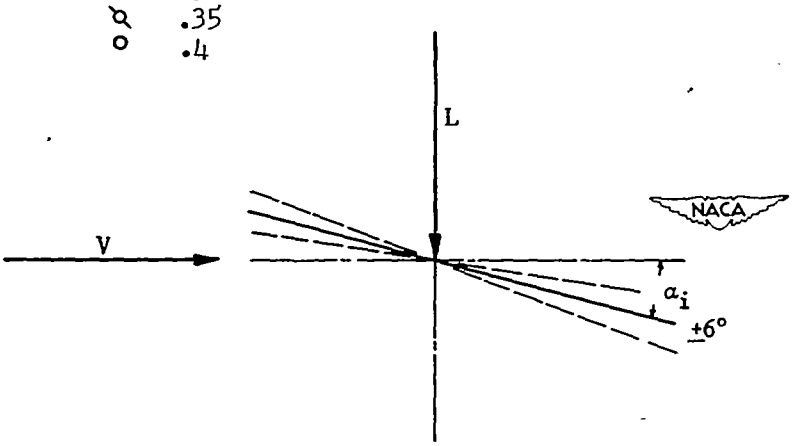

Figure 35.- Time-average value of lift in pure pitch.

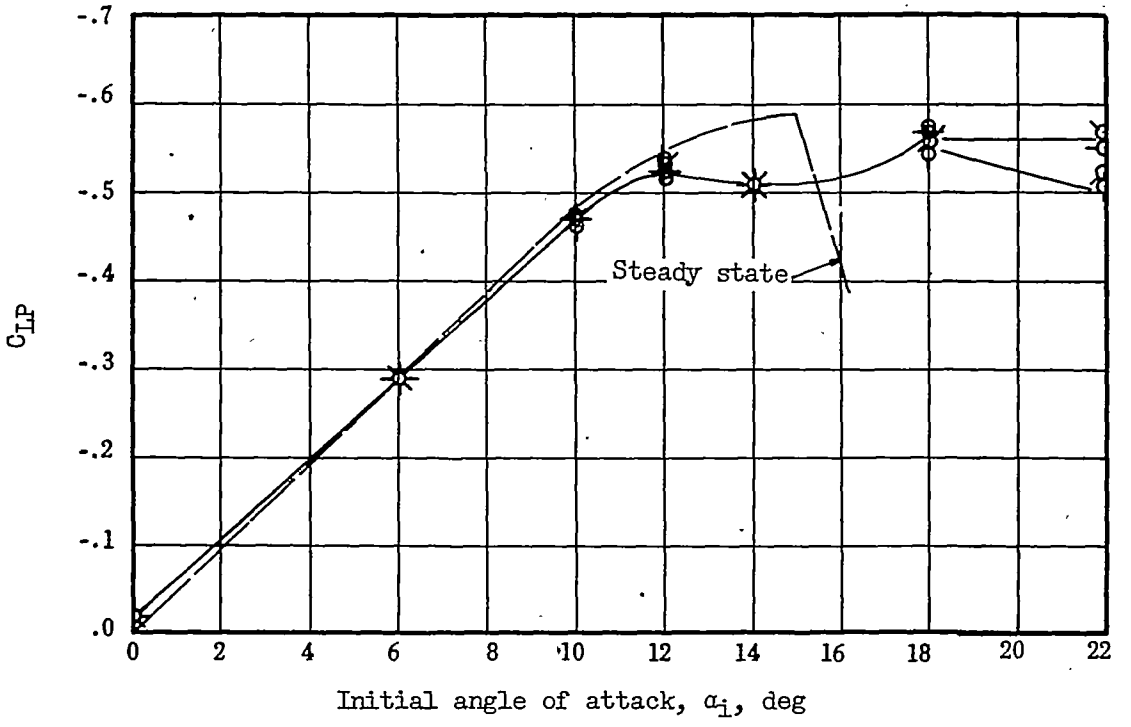

(b) Intermediate wing.

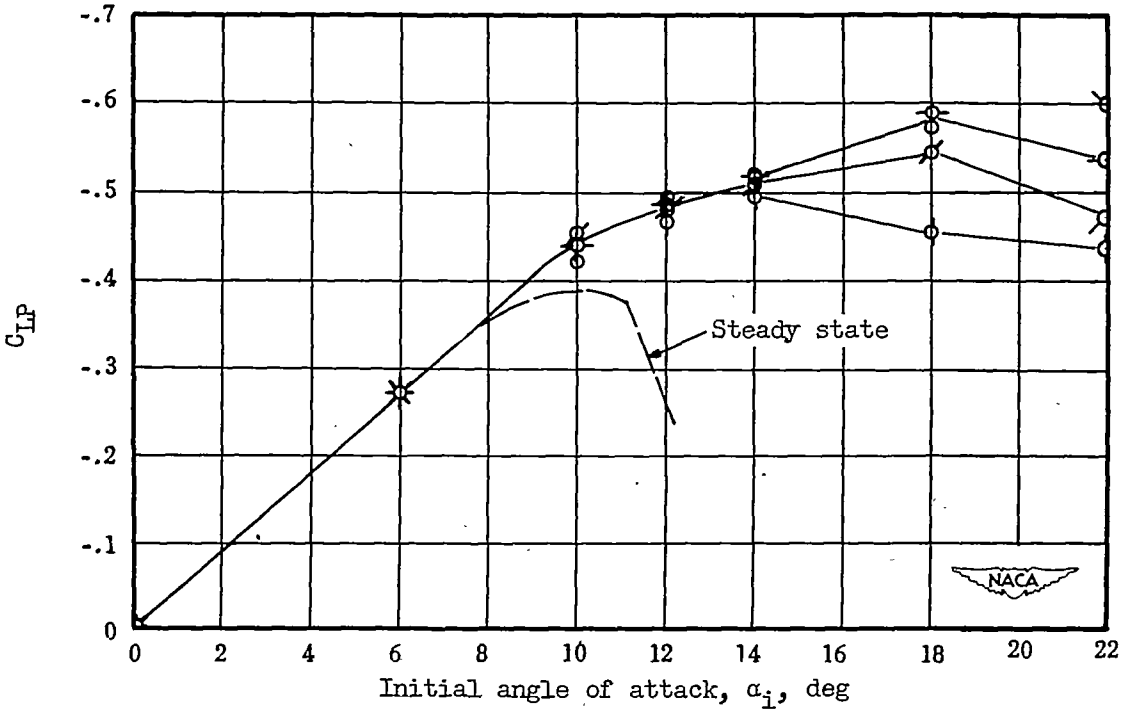

(c) Sharp wing.

Figure 35.- Concluded.

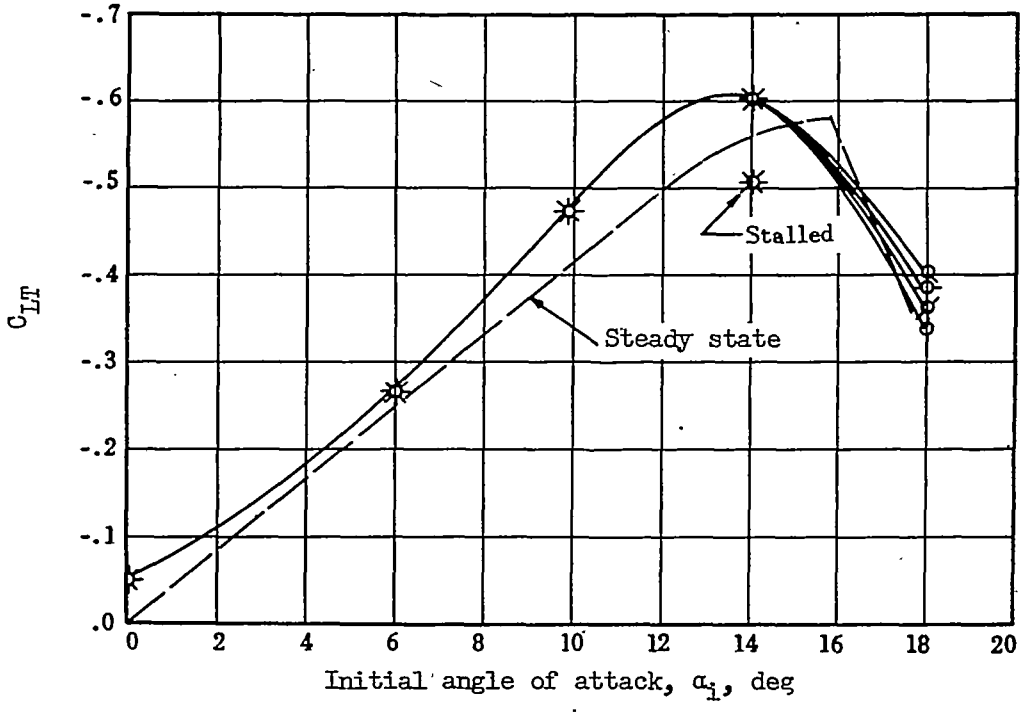

(a) Blunt wing.

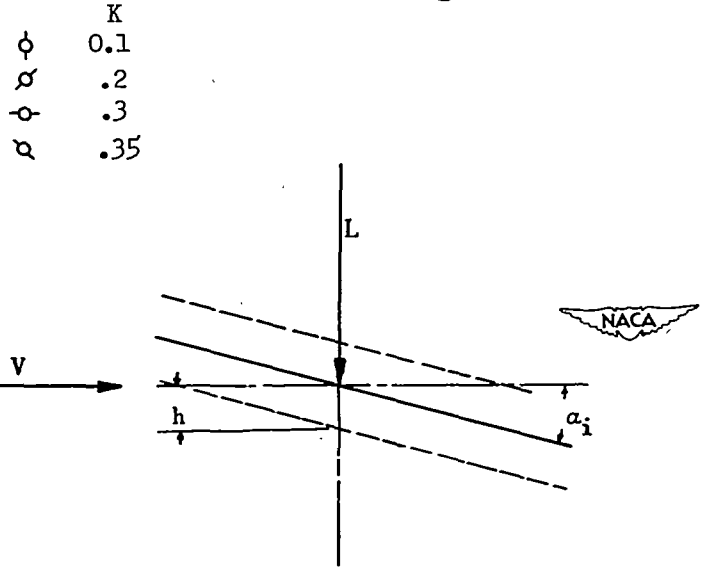

Figure 36.- Time-average value of lift in pure translation.

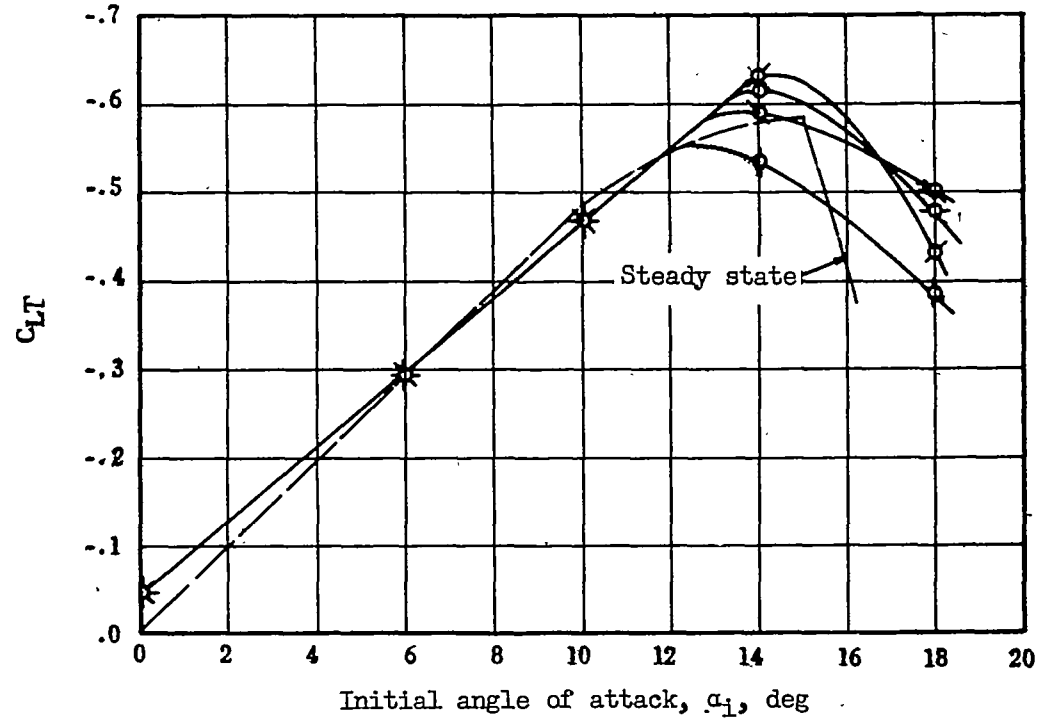

(b) Intermediate wing.

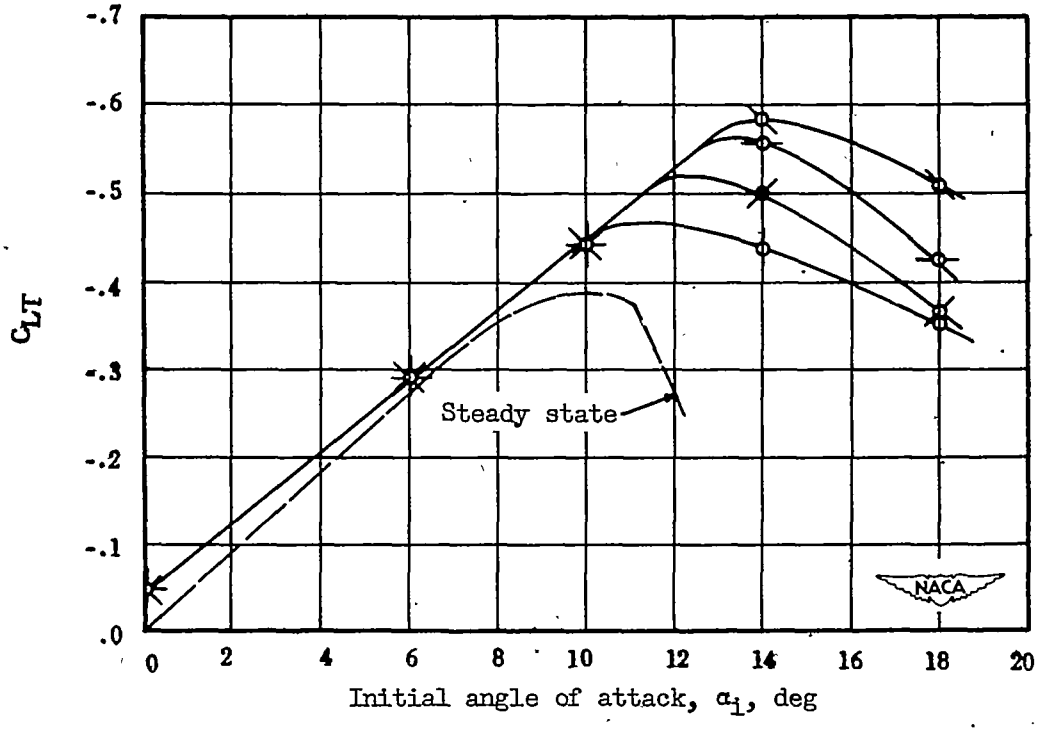

(c) Sharp wing.

Figure 36.- Concluded.

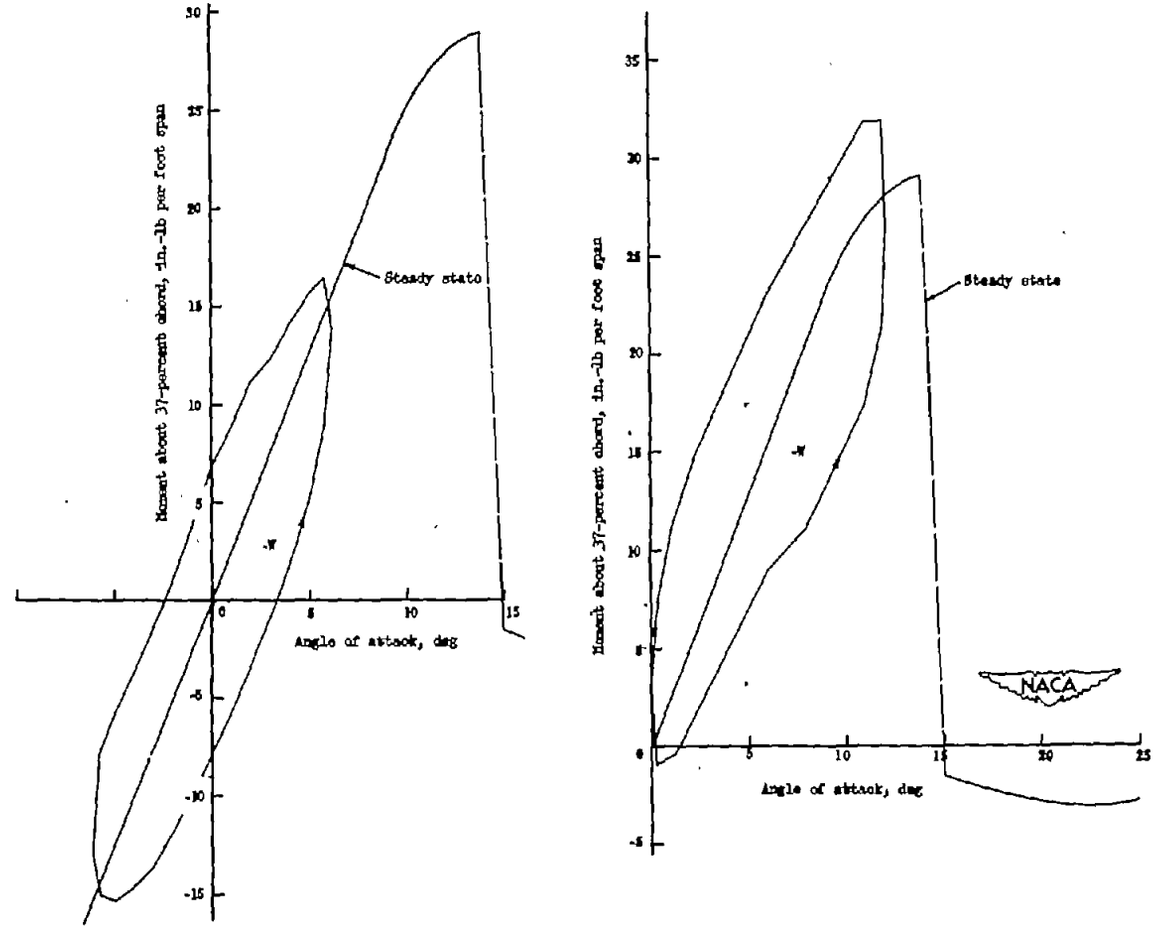

(a) $\alpha_1 = 0^\circ$; $\Delta\alpha = -14^\circ$; $\omega = 7.7$ cycles per second.

(b) $\alpha_1 = 6^\circ$; $\Delta\alpha = -8^\circ$; $\omega = 7.84$ cycles per second.

Figure 37.- Experimental hysteresis loops from moment in pure pitch. Intermediate wing.

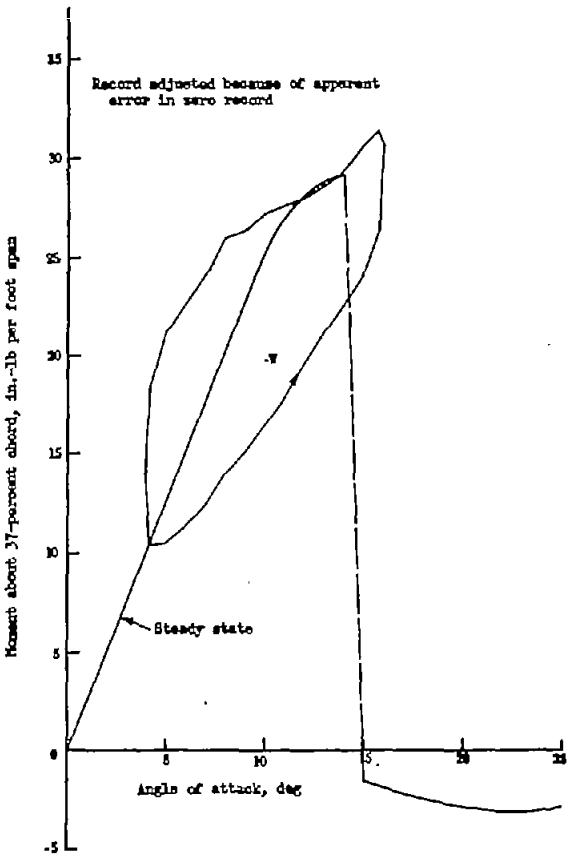

(c) $\alpha_1 = 10^\circ$; $\Delta\alpha = -4^\circ$;
$\omega = 7.5$ cycles per second.

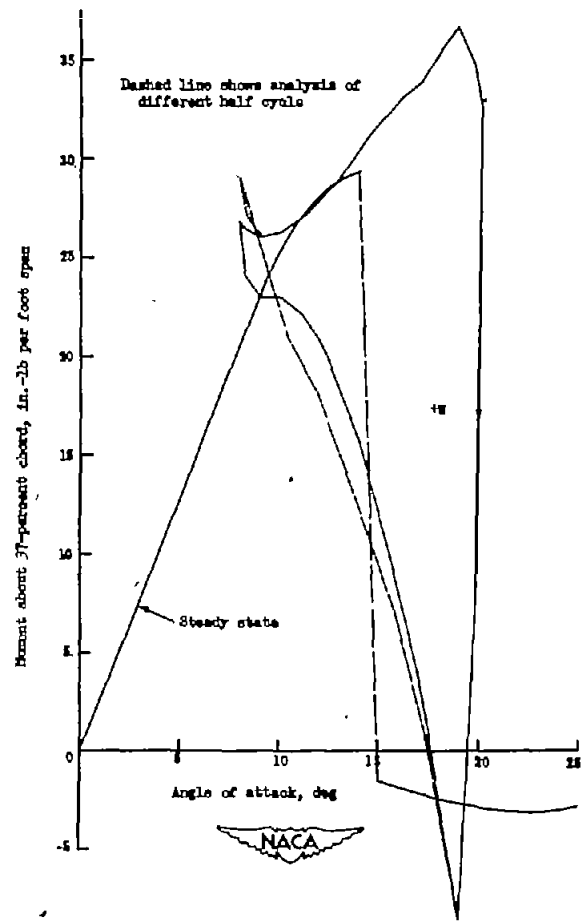

(d) $\alpha_1 = 14^\circ$; $\Delta\alpha = 0^\circ$;
$\omega = 7.9$ cycles per second.

Figure 37.- Continued.

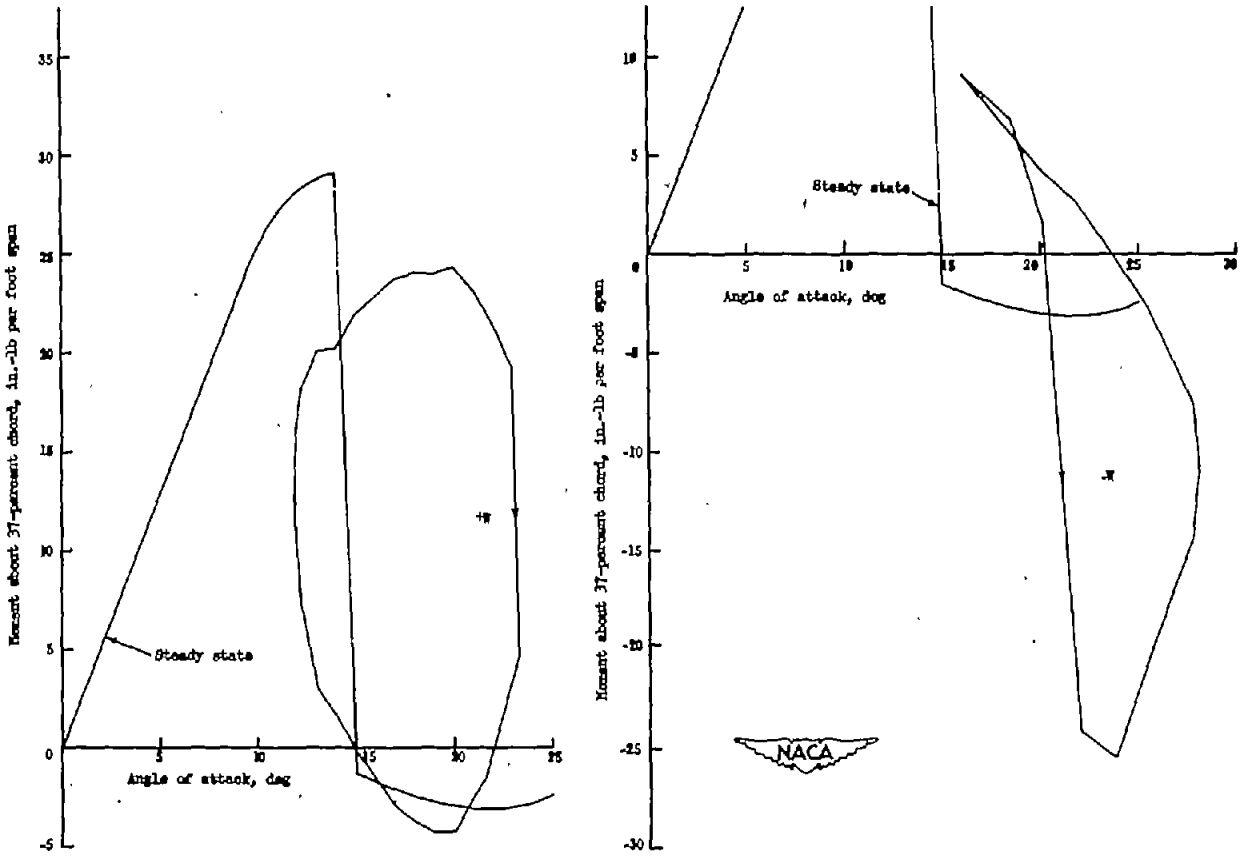

(e) $\alpha_1 = 18^\circ$; $\Delta\alpha = 4^\circ$; $\omega = 8.2$ cycles per second.

(f) $\alpha_1 = 22^\circ$; $\Delta\alpha = 8^\circ$; $\omega = 7.71$ cycles per second.

Figure 37.- Concluded.

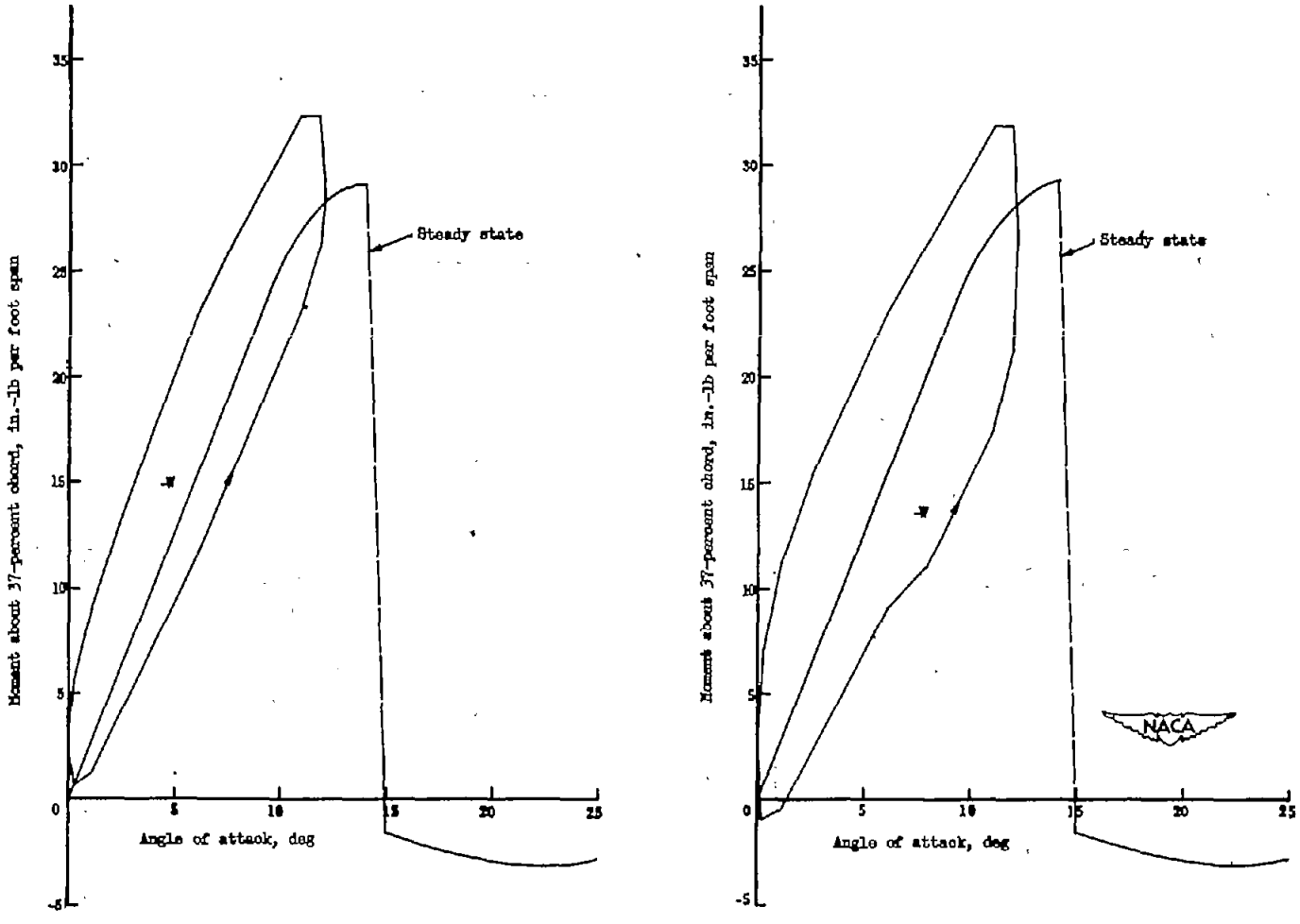

(a) $\omega = 4.33$ cycles per second. (b) $\omega = 7.84$ cycles per second.

Figure 38.- Experimental hysteresis loops from moment in pure pitch. Intermediate wing. $\alpha_1 = 6^\circ$; $\Delta\alpha = -8^\circ$.

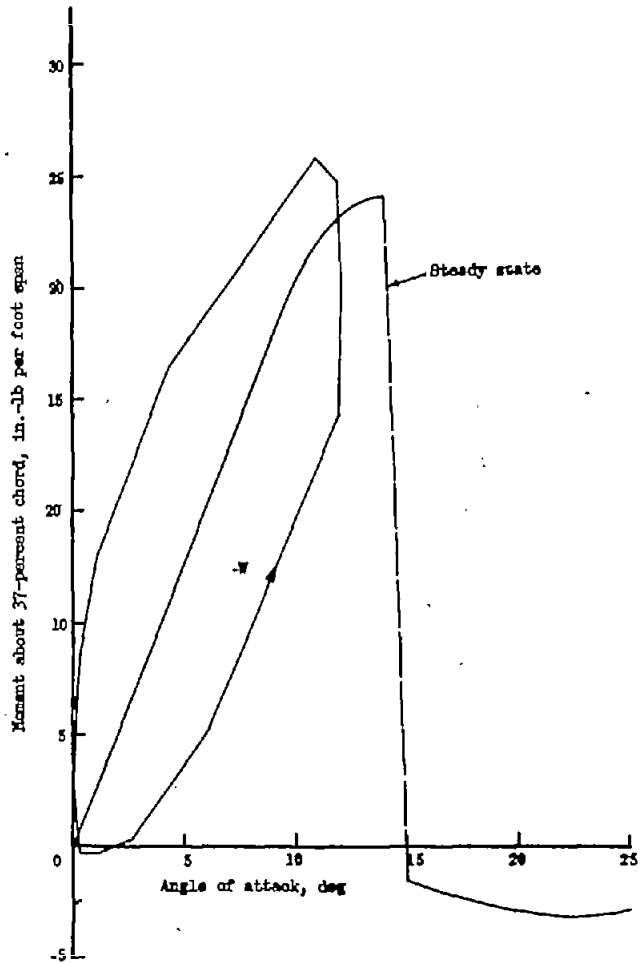

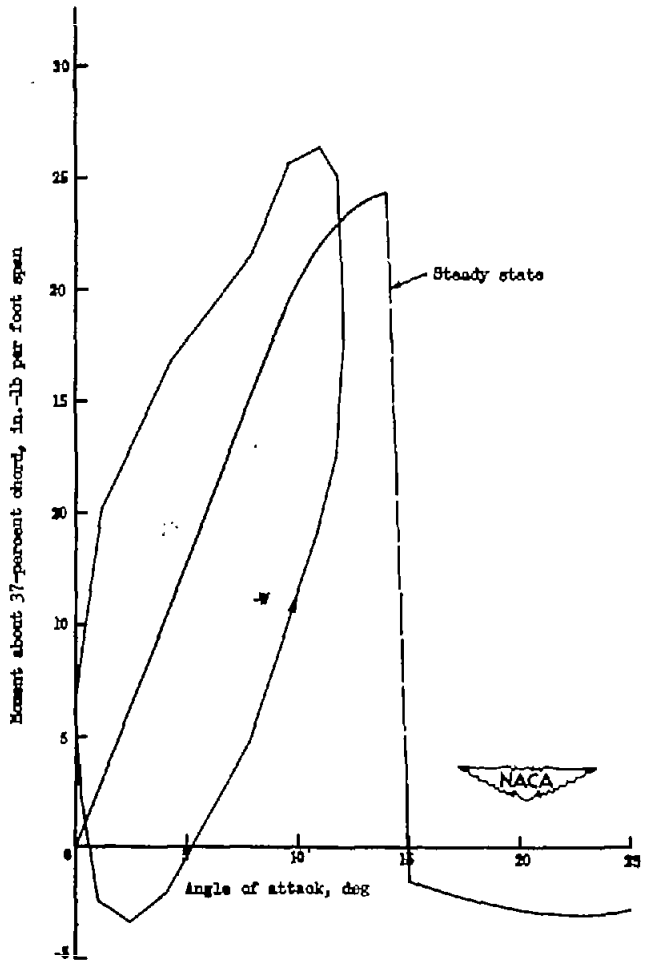

(c) ω = 11.62 cycles per second. (d) ω = 15.58 cycles per second.

Figure 38.- Concluded.

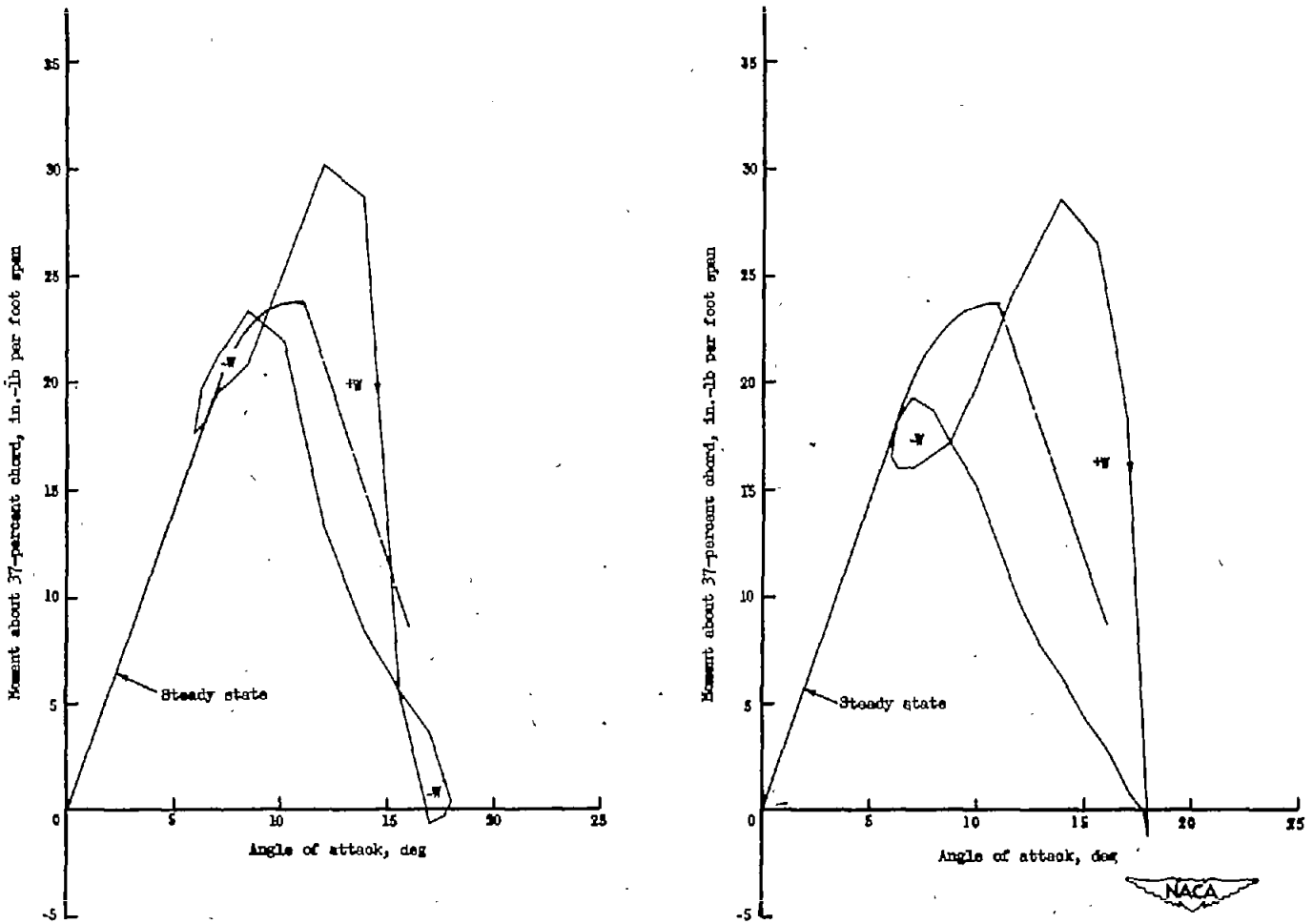

(a) $\omega = 4.18$ cycles per second. (b) $\omega = 7.64$ cycles per second.

Figure 39.- Experimental hysteresis loops from moment in pure pitch. Sharp wing. $\alpha_1 = 12^\circ$; $\Delta\alpha = 1^\circ$.

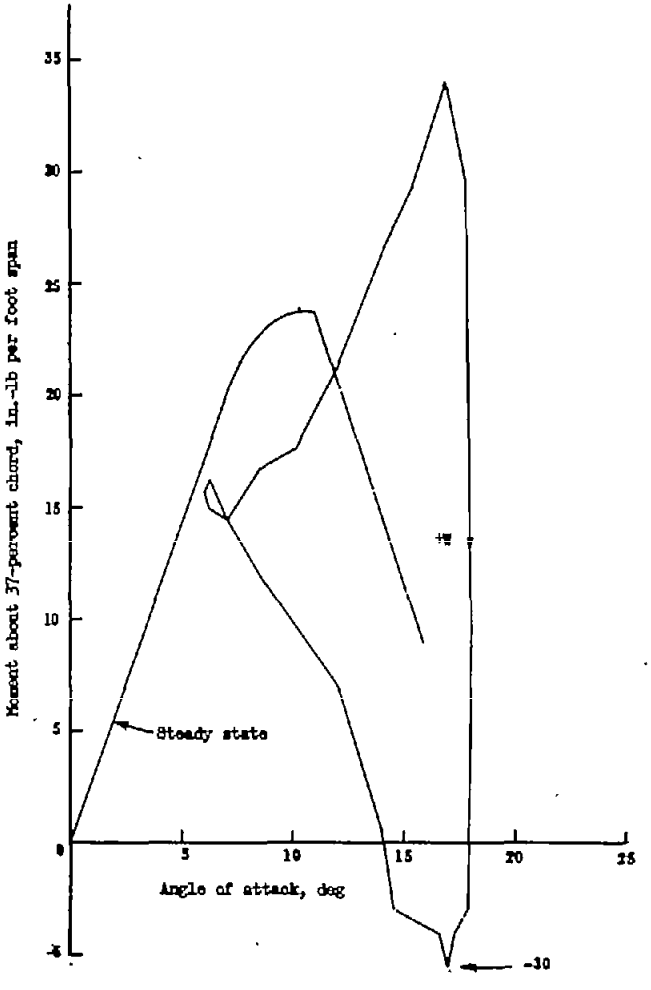

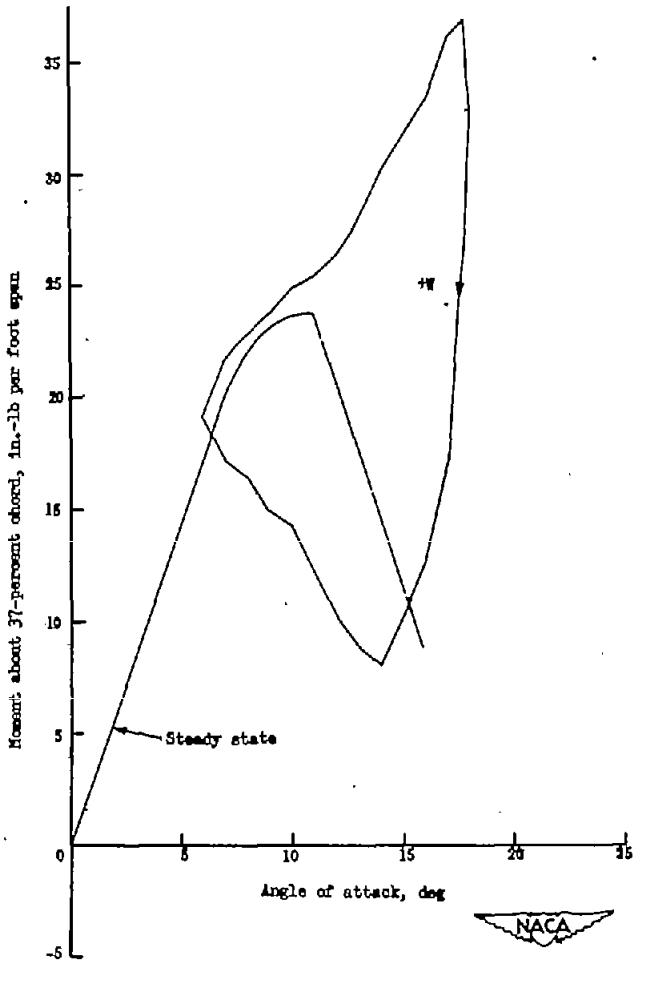

(c) $\omega = 11.0$ cycles per second. (d) $\omega = 16.7$ cycles per second.

Figure 39.- Concluded.

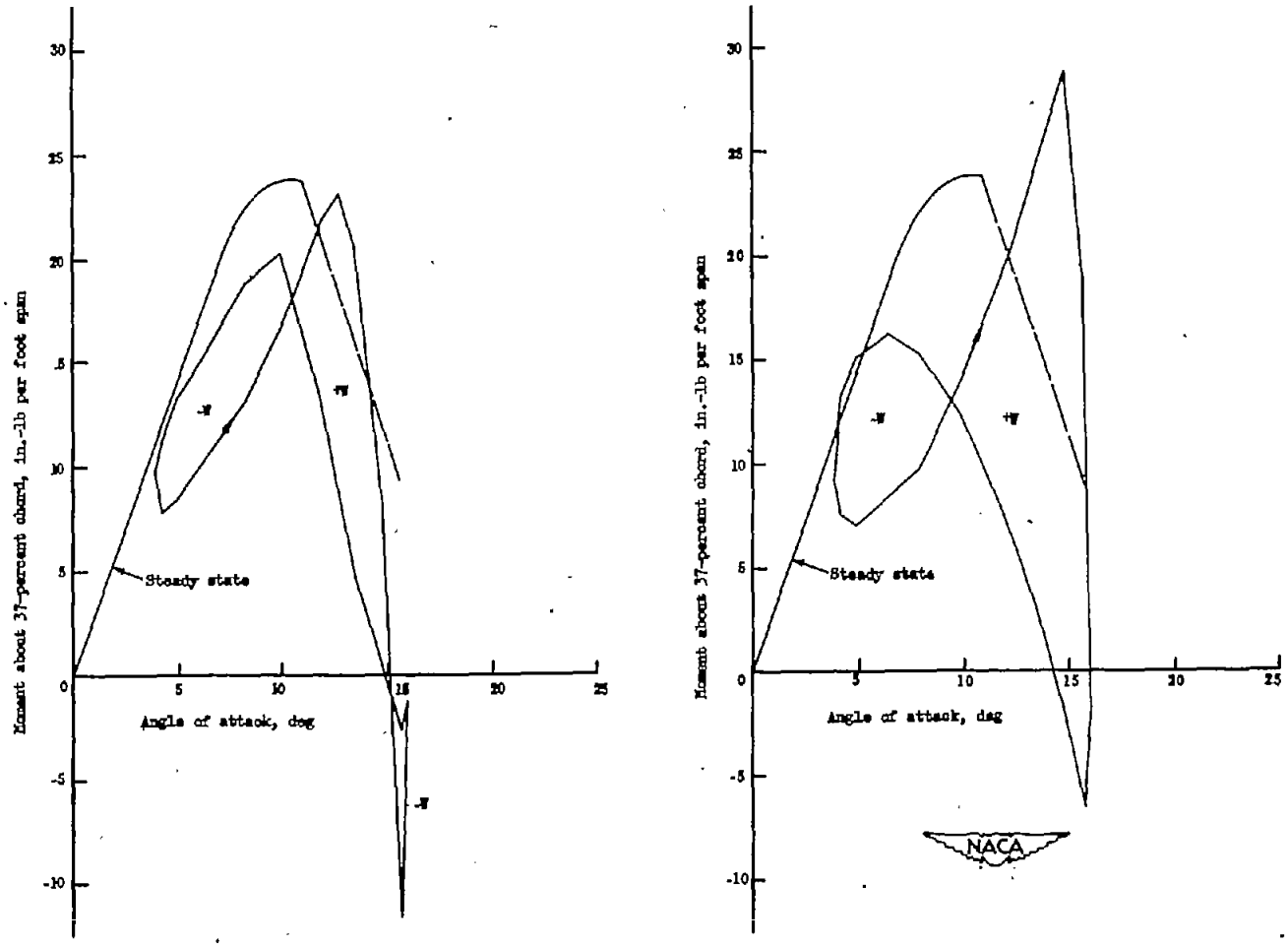

(a) $\omega = 4.27$ cycles per second. (b) $\omega = 7.72$ cycles per second.

Figure 40.- Experimental hysteresis loops from moment in pure pitch. Sharp wing. $\alpha_1 = 10^\circ$; $\Delta\alpha = -1^\circ$.

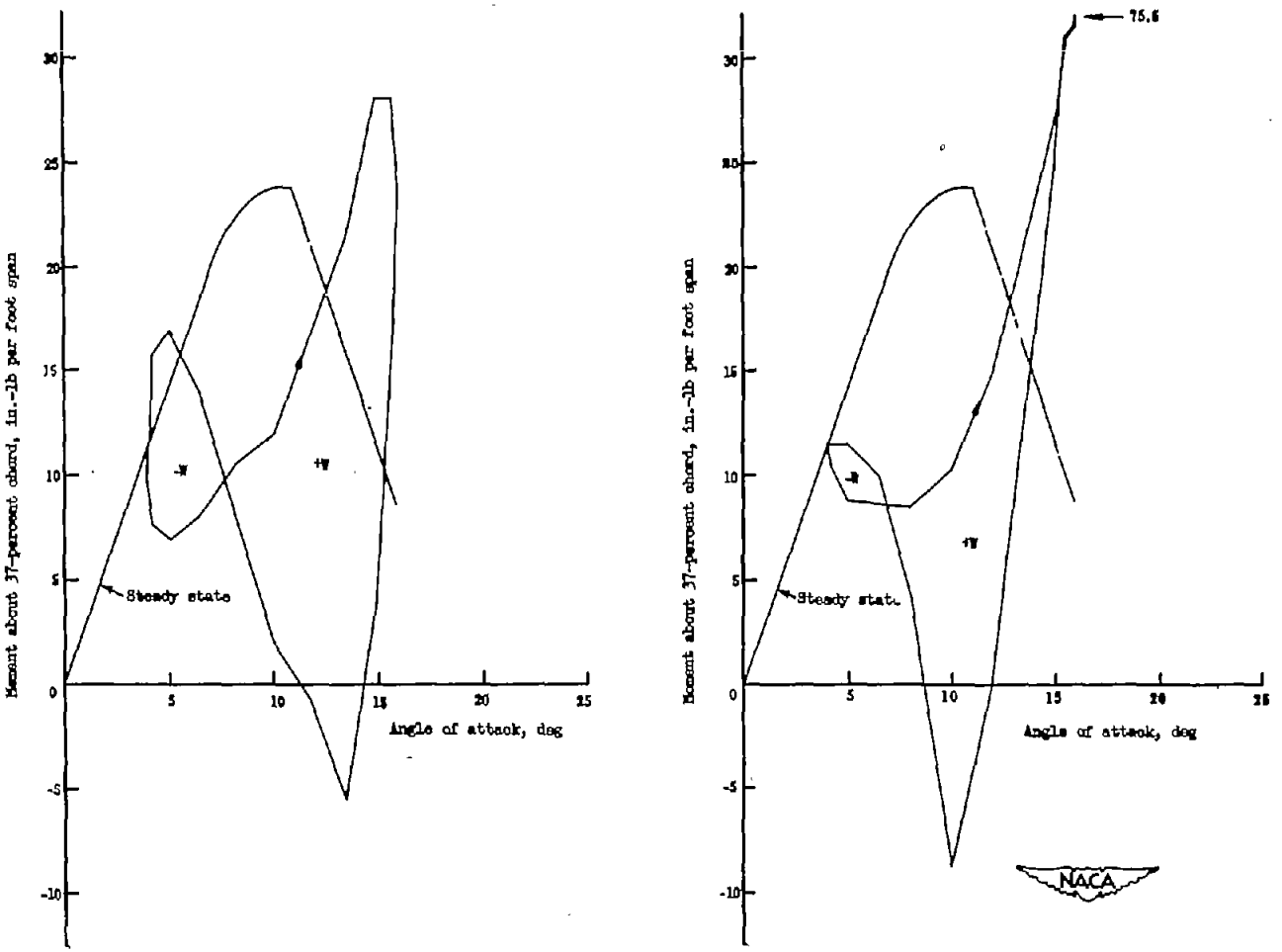

(c) ω = 11.5 cycles per second. (d) ω = 15.42 cycles per second.

Figure 40.- Concluded.

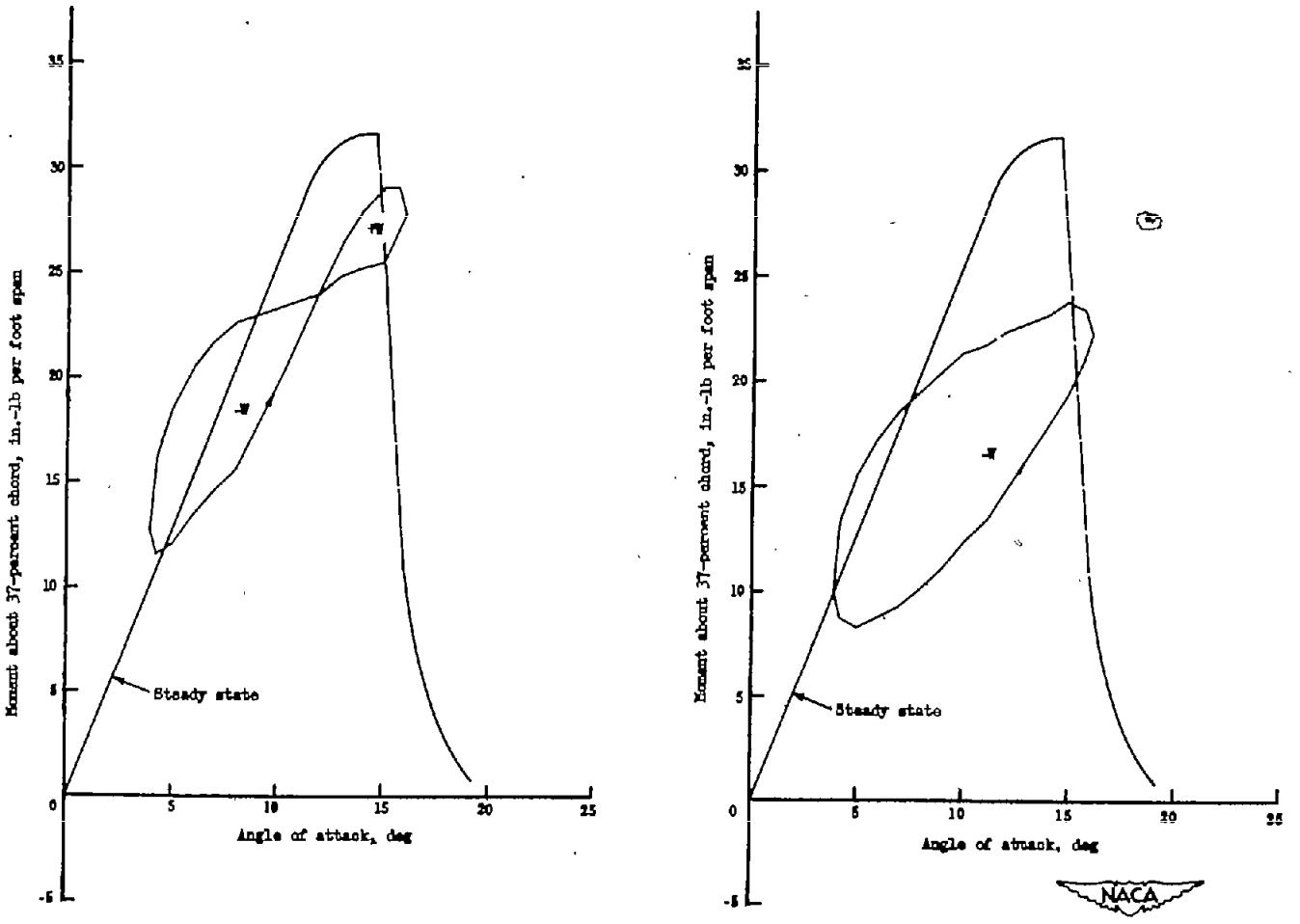

(a) $\alpha_1 = 10^\circ$; $\Delta\alpha = -5^\circ$; $\omega = 4.25$ cycles per second.

(b) $\alpha_1 = 10^\circ$; $\Delta\alpha = -5^\circ$; $\omega = 7.9$ cycles per second.

Figure 41.- Experimental hysteresis loops from moment in pure pitch. Blunt wing.

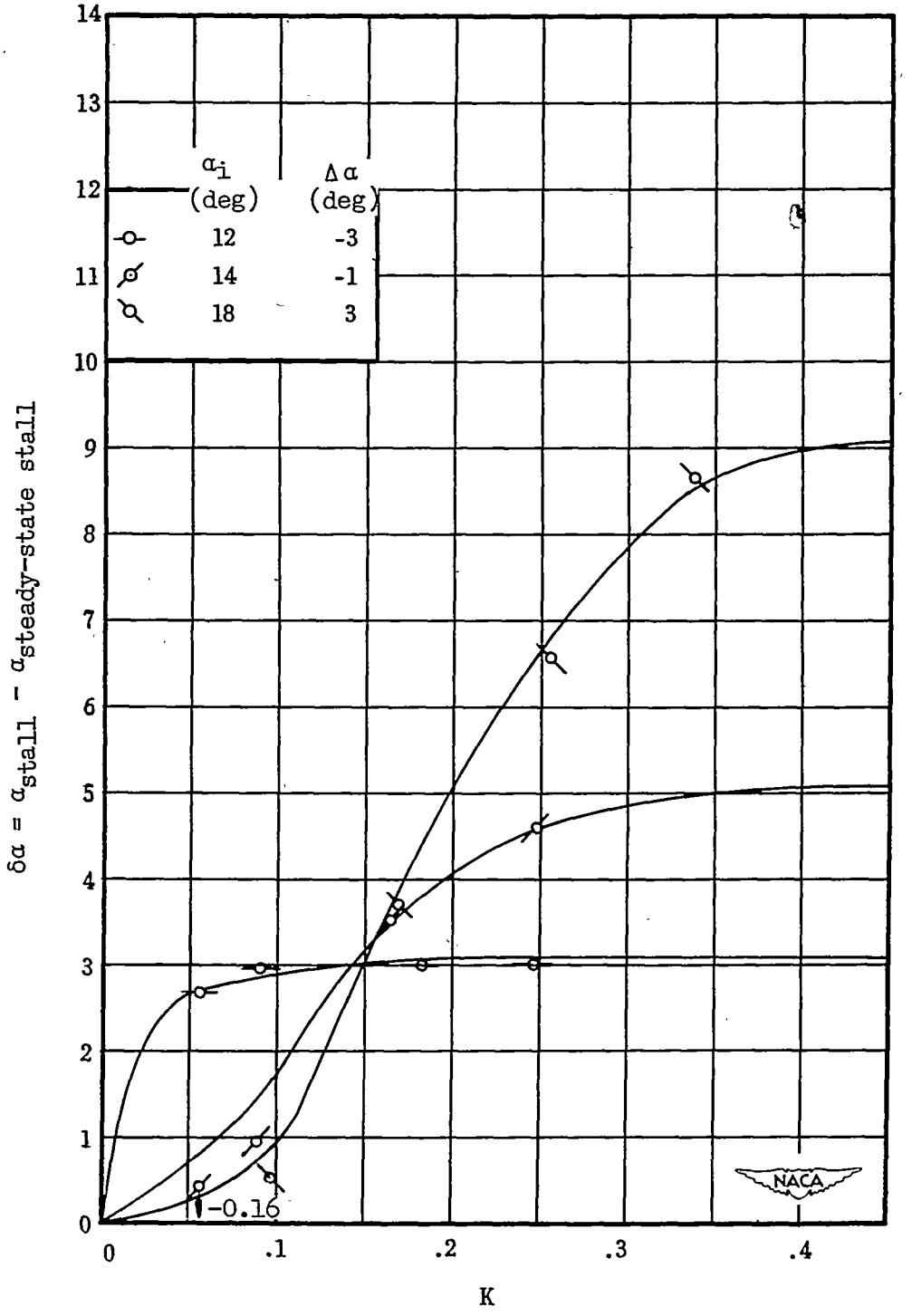

Figure 42.- Oscillatory stalling angle as a function of K. Blunt wing.

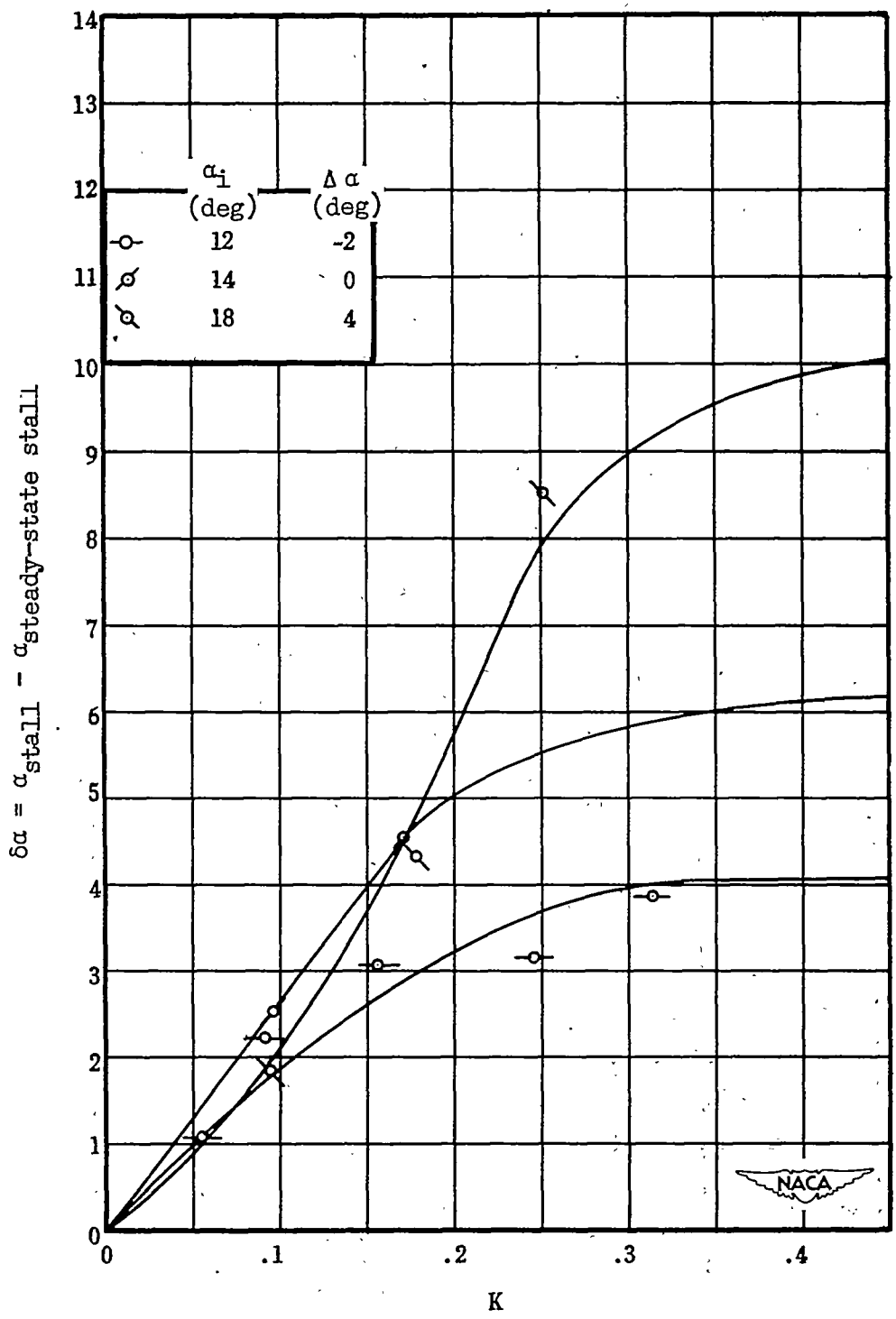

Figure 43.- Oscillatory stalling angle as a function of K. Intermediate wing.

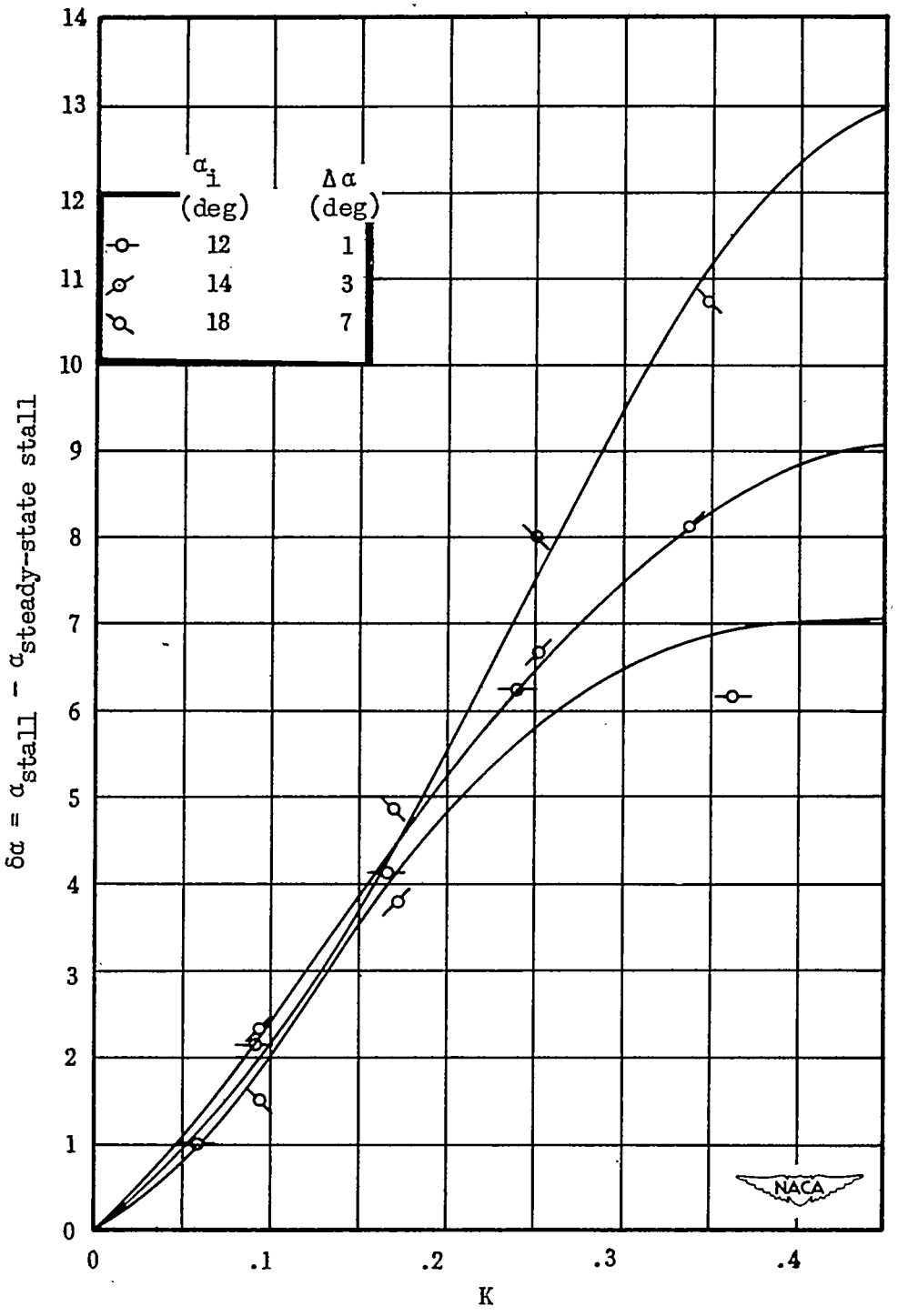

Figure 44.- Oscillatory stalling angle as a function of K. Sharp wing.

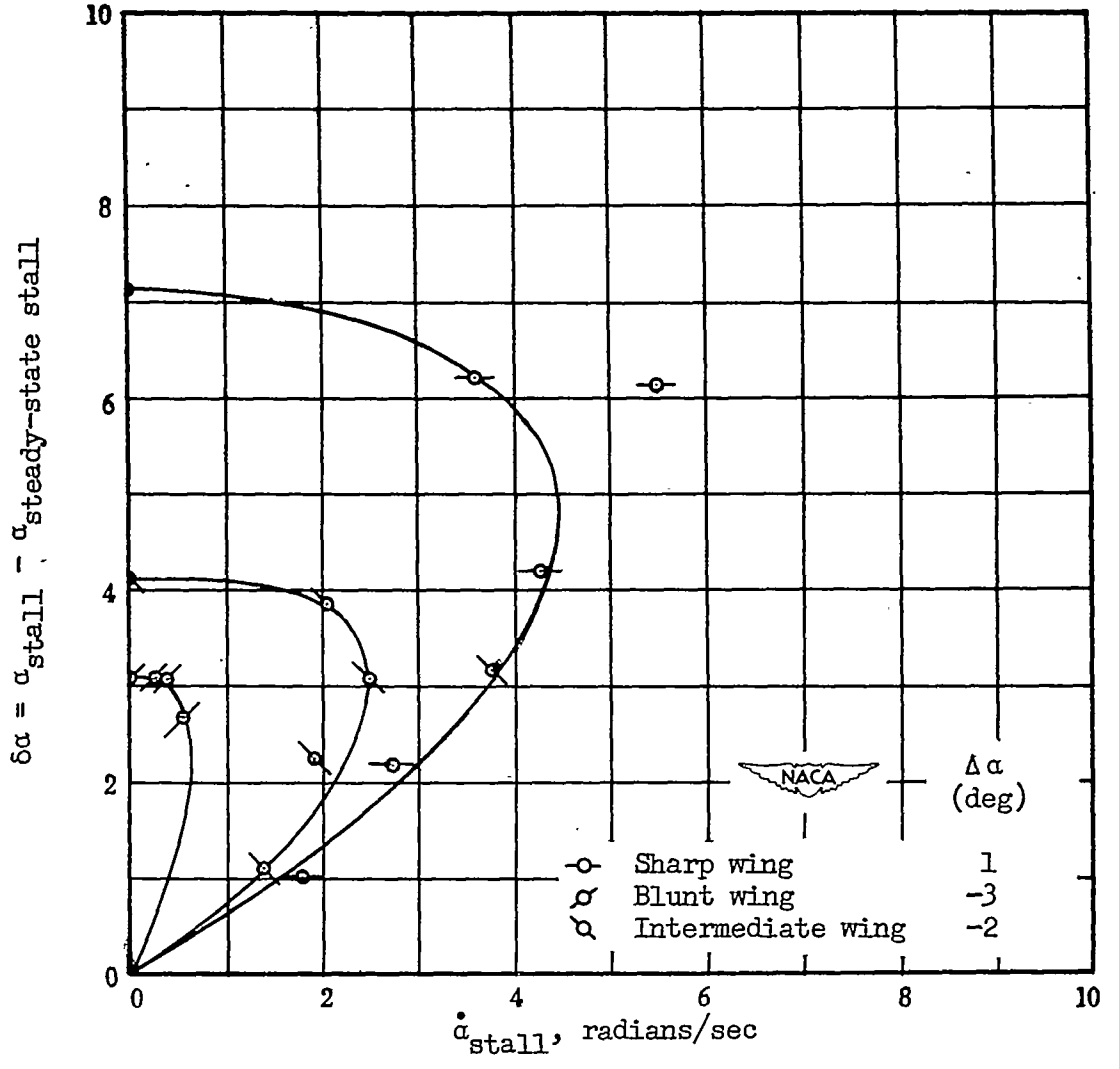

(a) $\alpha_1 = 12^\circ$.

Figure 45.- Oscillatory stalling angle as a function of angular velocity.

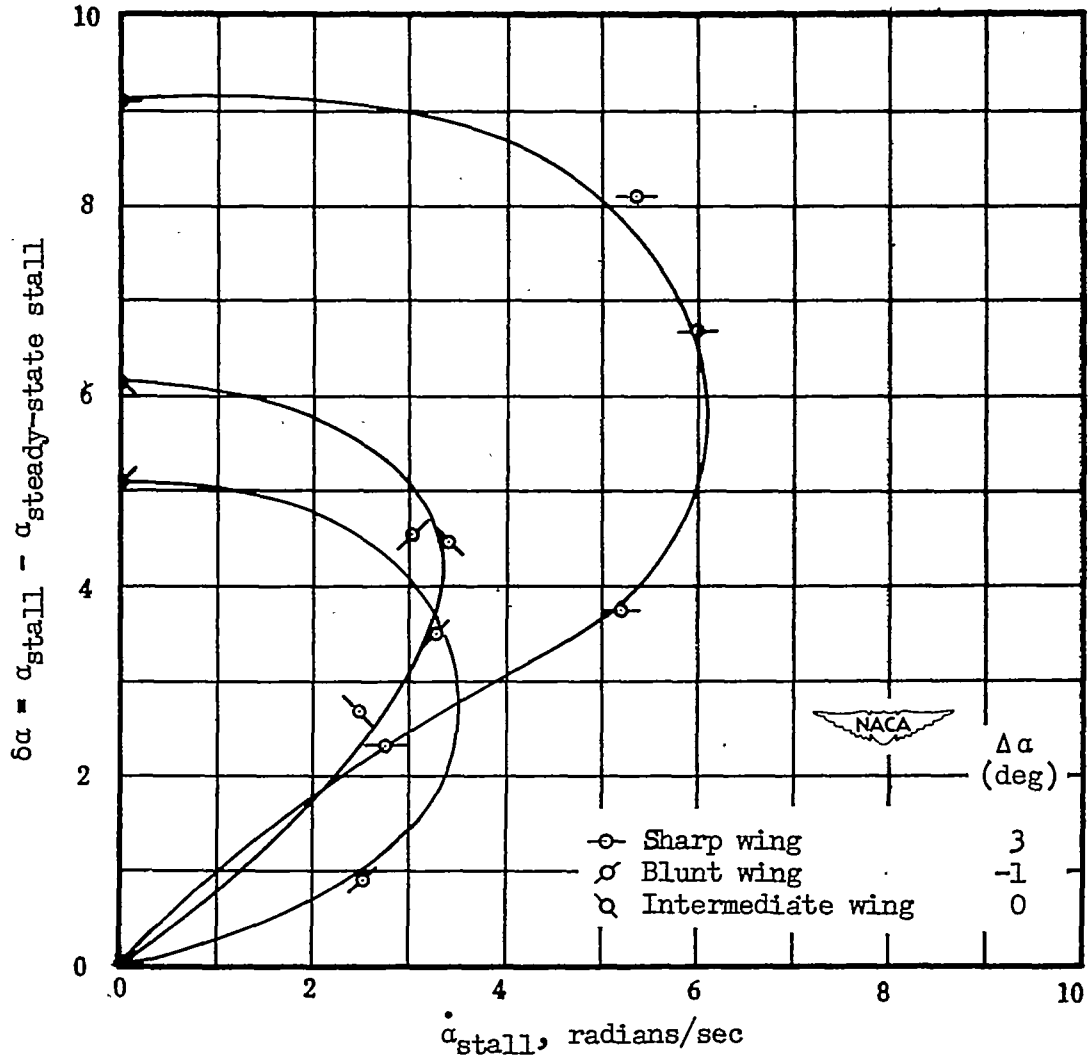

(b) $\alpha_1 = 14^\circ$.

Figure 45.- Continued.

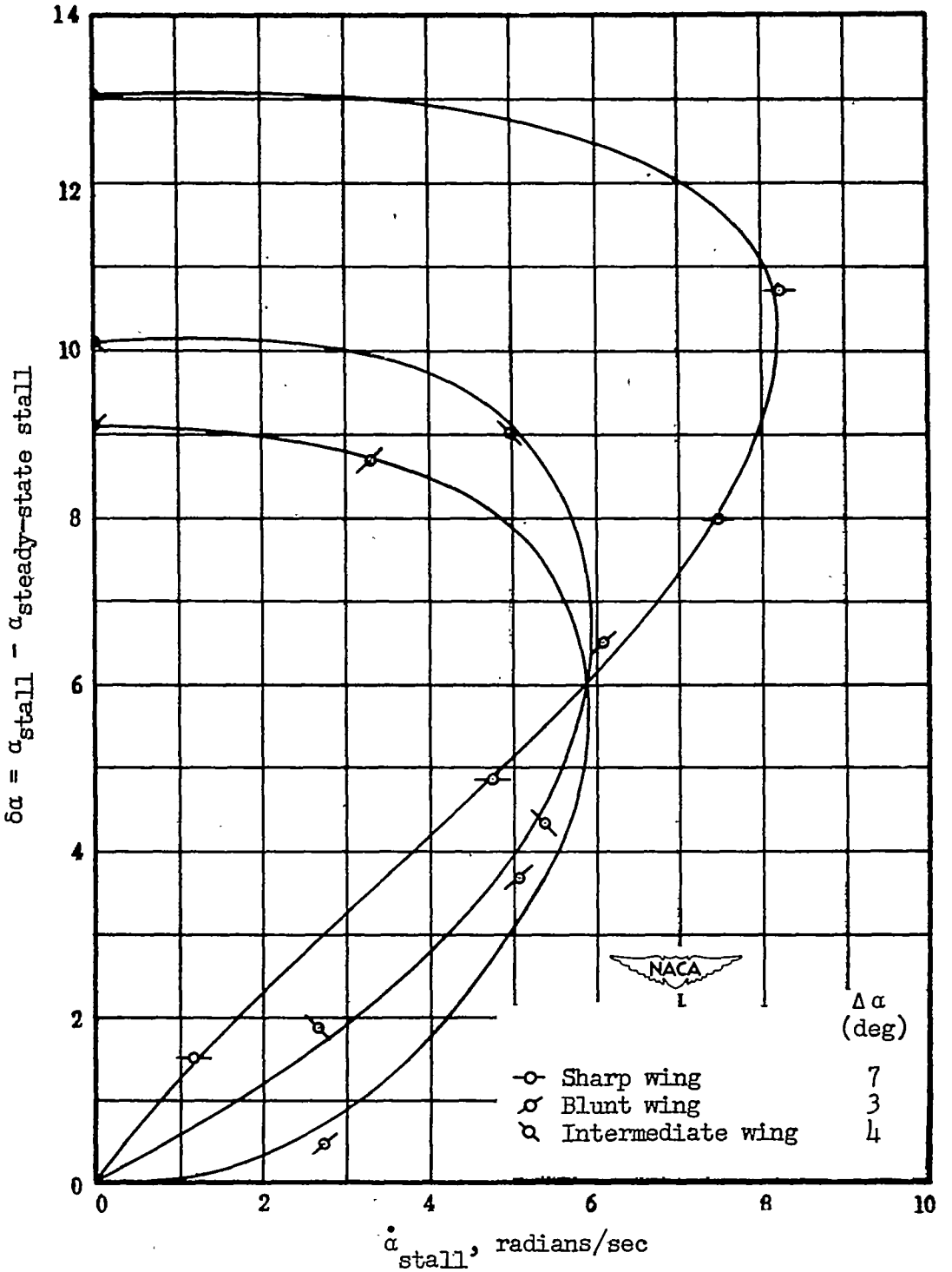

(c) $\alpha_1 = 18^\circ$.

Figure 45.- Concluded.

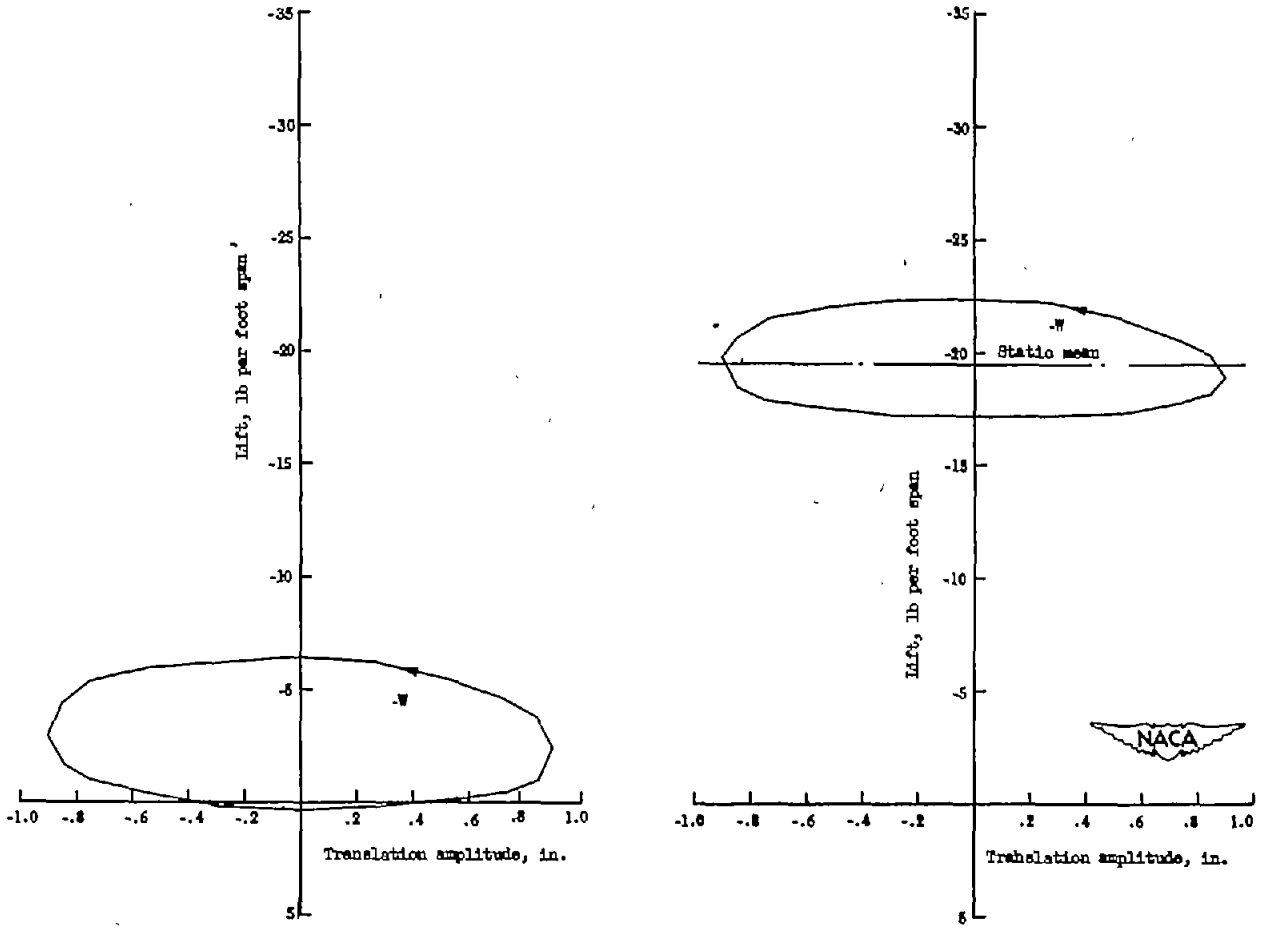

(a) $\alpha_1 = 0^\circ$; $\Delta\alpha = -14^\circ$; $\omega = 7.69$ cycles per second.

(b) $\alpha_1 = 10^\circ$; $\Delta\alpha = -4^\circ$; $\omega = 7.63$ cycles per second.

Figure 46.- Experimental hysteresis loops from lift in pure translation. Intermediate wing.

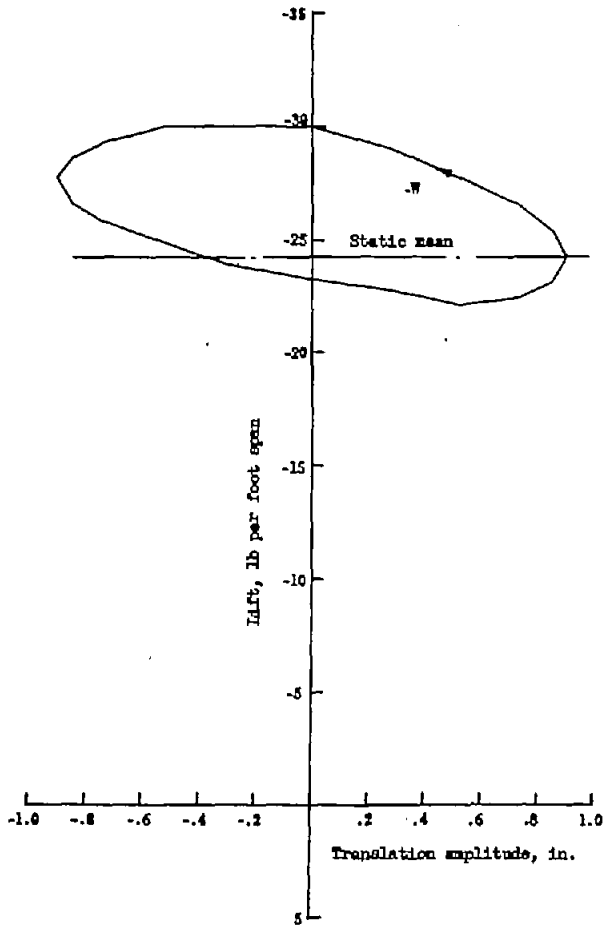

(c) $\alpha_1 = 14^\circ$; $\Delta\alpha = 0^\circ$;
$\omega = 7.58$ cycles per second.

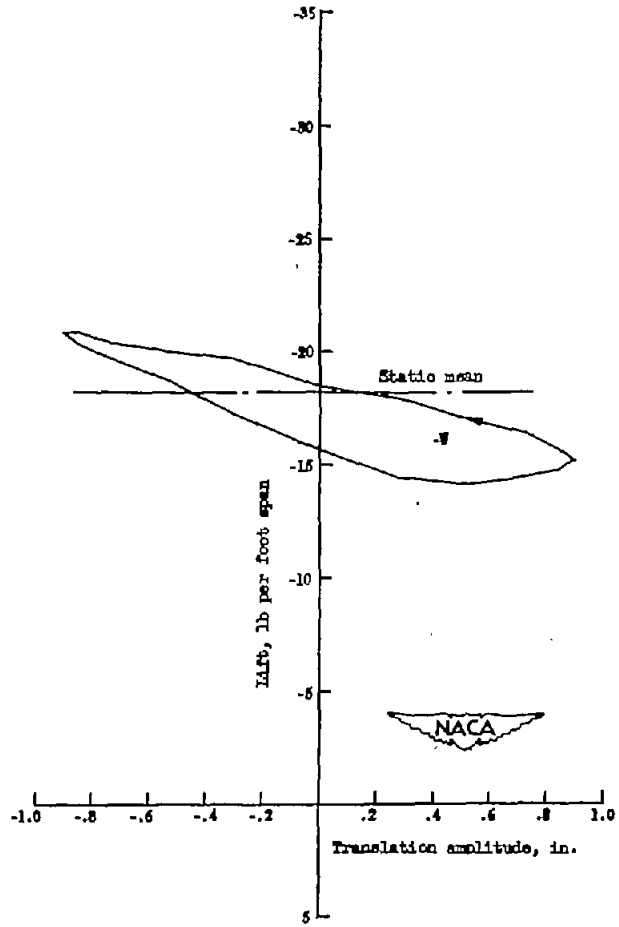

(d) $\alpha_1 = 18^\circ$; $\Delta\alpha = 4^\circ$;
$\omega = 7.77$ cycles per second.

Figure 46.- Concluded.

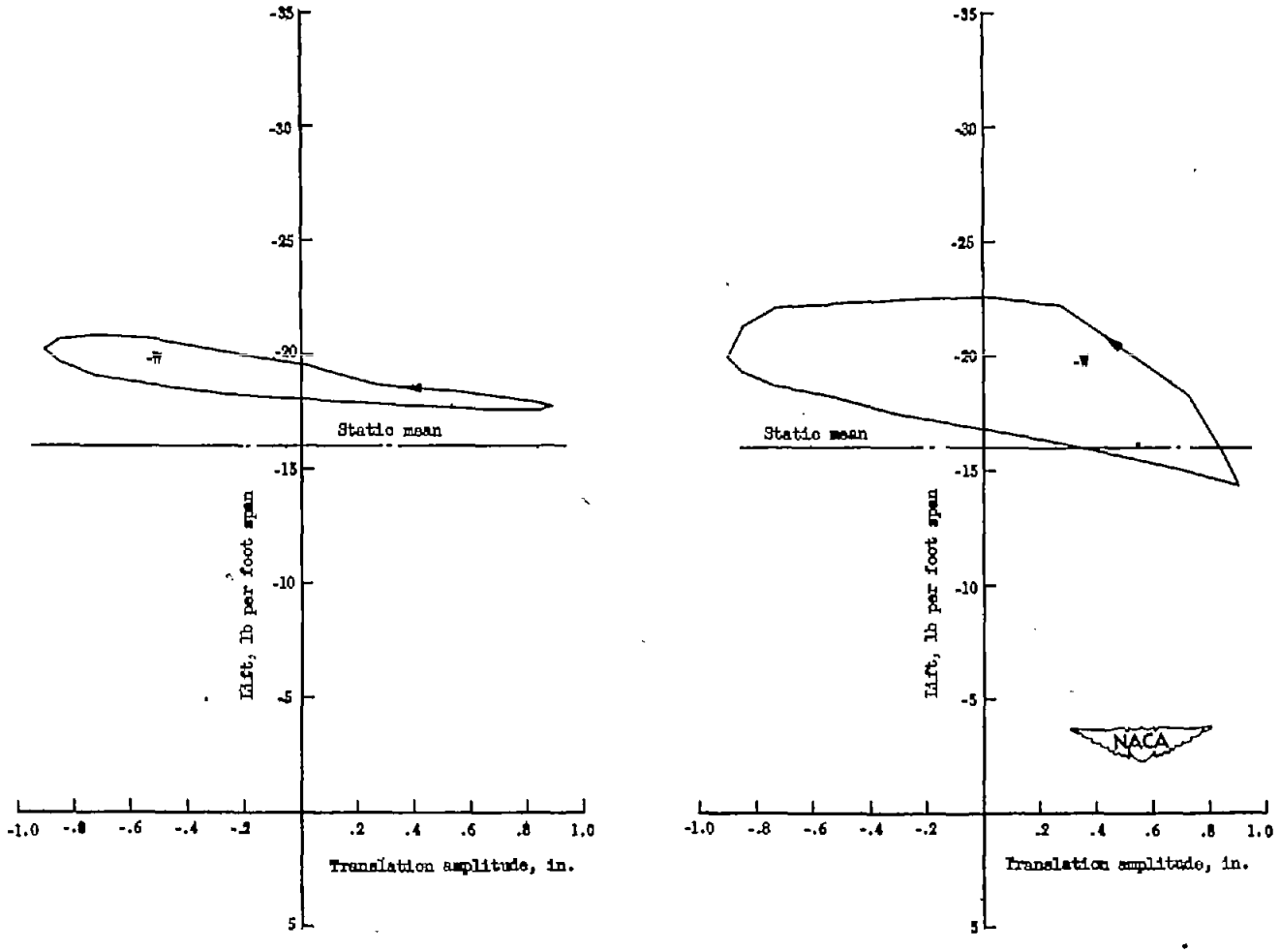

(a) $\omega = 4.11$ cycles per second. (b) $\omega = 8.00$ cycles per second.

Figure 47.- Experimental hysteresis loops from lift in pure translation. Sharp wing. $\alpha_i = 10^\circ$; $\Delta\alpha = -1^\circ$.

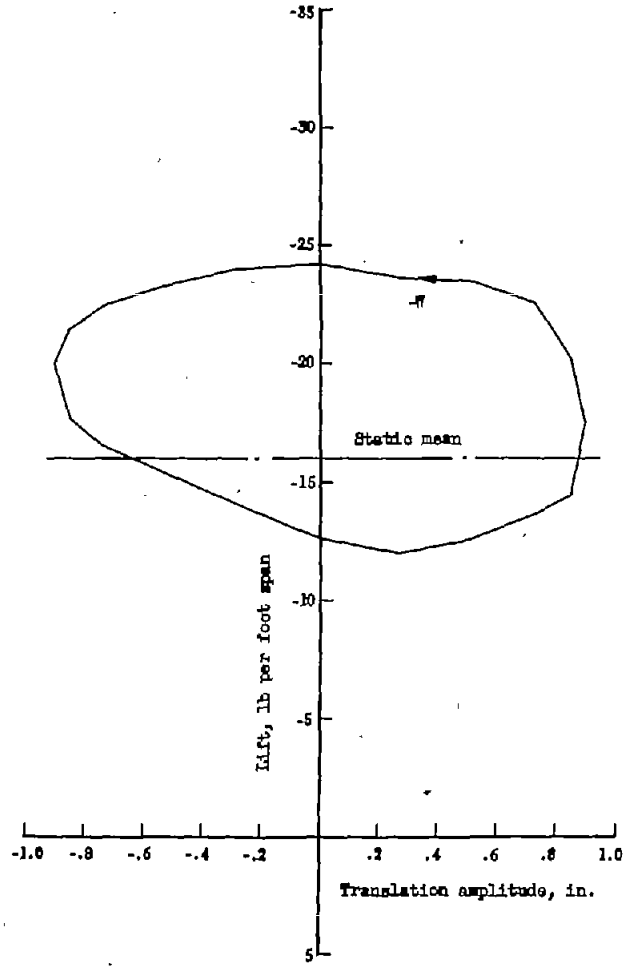

(c) ω = 11.9 cycles per second.

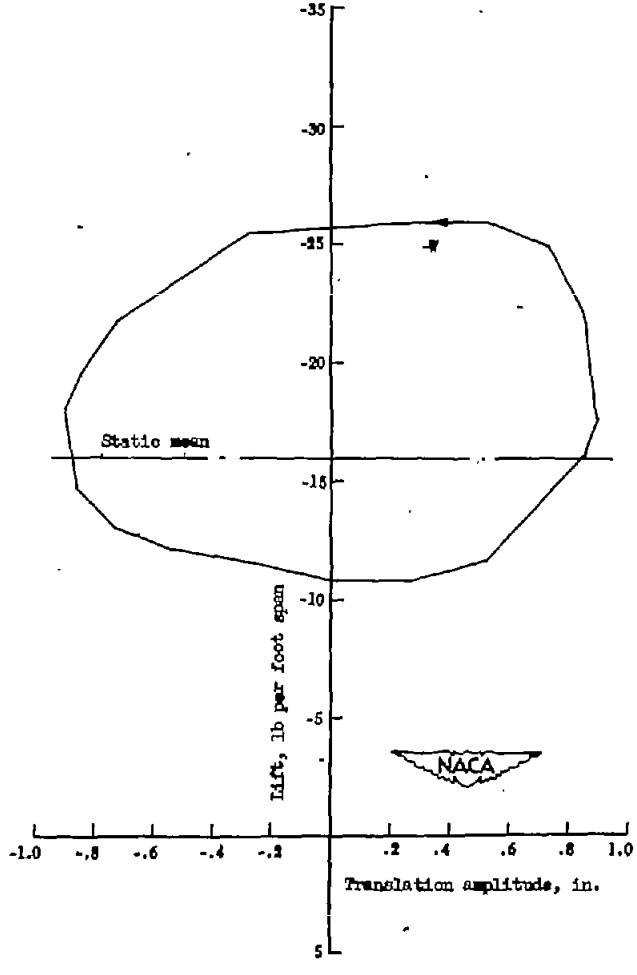

(d) ω = 15.23 cycles per second.

Figure 47.- Concluded.

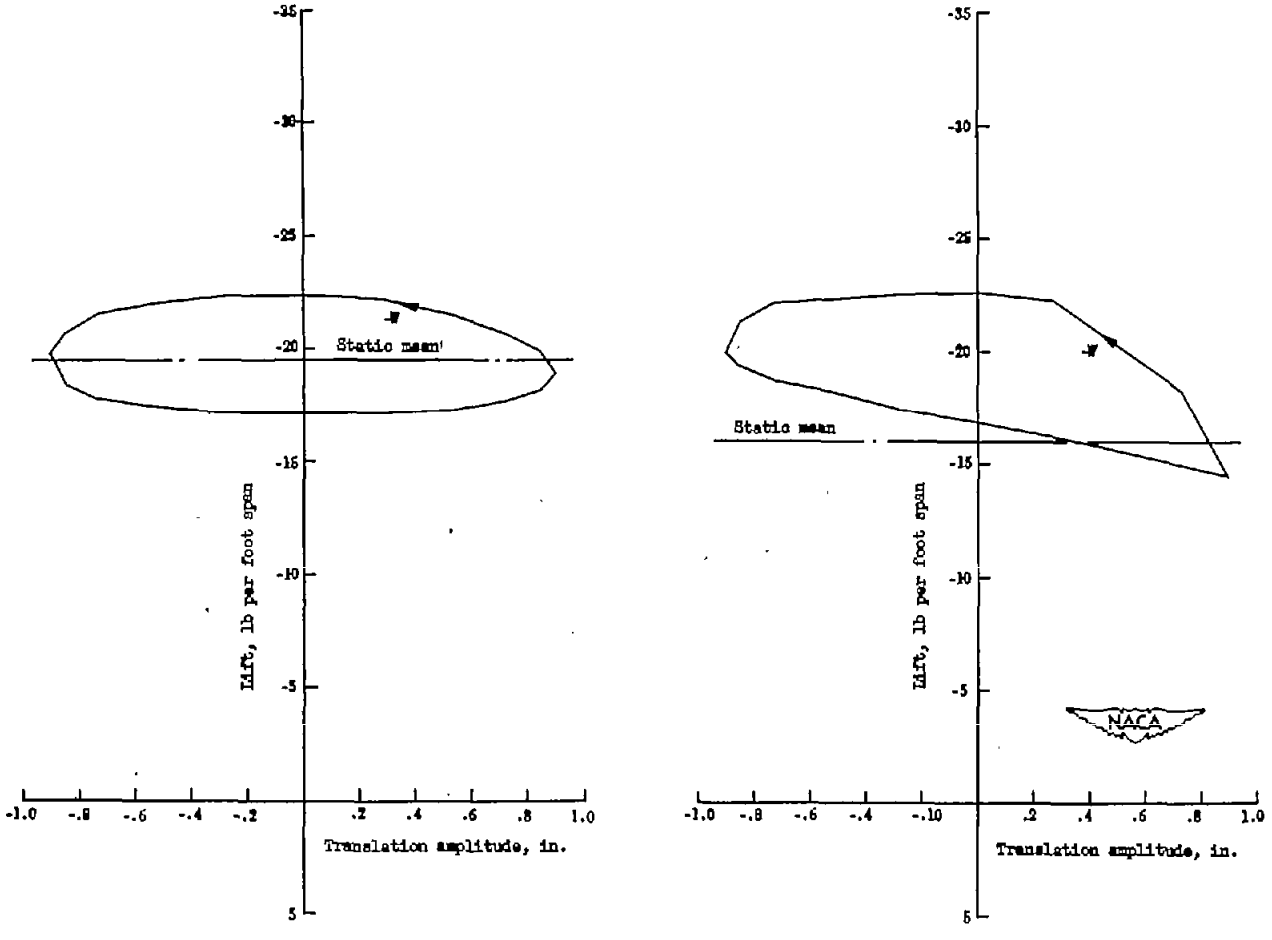

(a) Intermediate wing. $\alpha_1 = 10^\circ$; $\Delta\alpha = -4^\circ$; $\omega = 7.63$ cycles per second.

(b) Sharp wing. $\alpha_1 = 10^\circ$; $\Delta\alpha = -1^\circ$; $\omega = 8.00$ cycles per second.

Figure 48.- Experimental hysteresis loops from lift in pure translation.

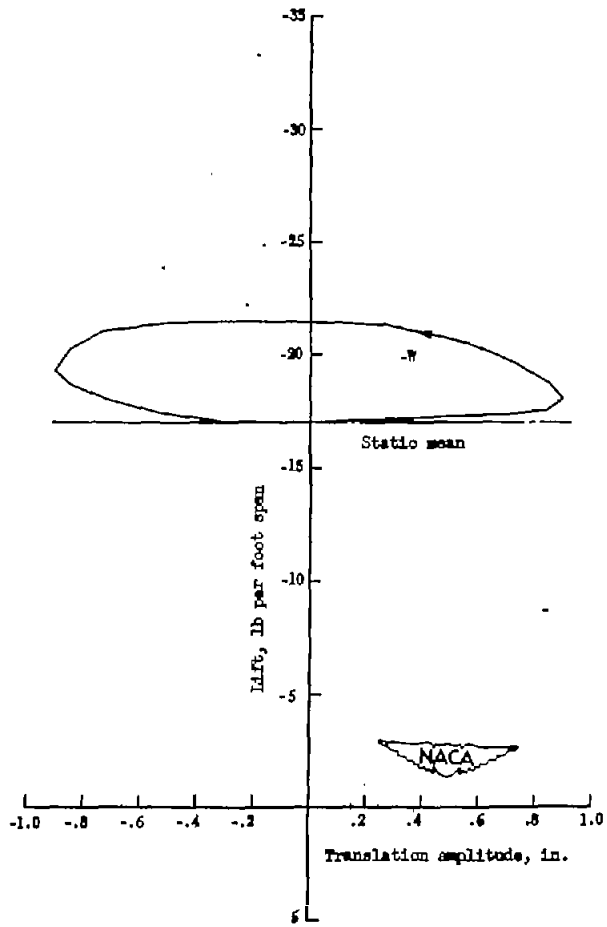

(c) Blunt wing. $\alpha_1 = 10^\circ$; $\Delta\alpha = -5^\circ$; $\omega = 7.67$ cycles per second.

Figure 48.- Concluded.

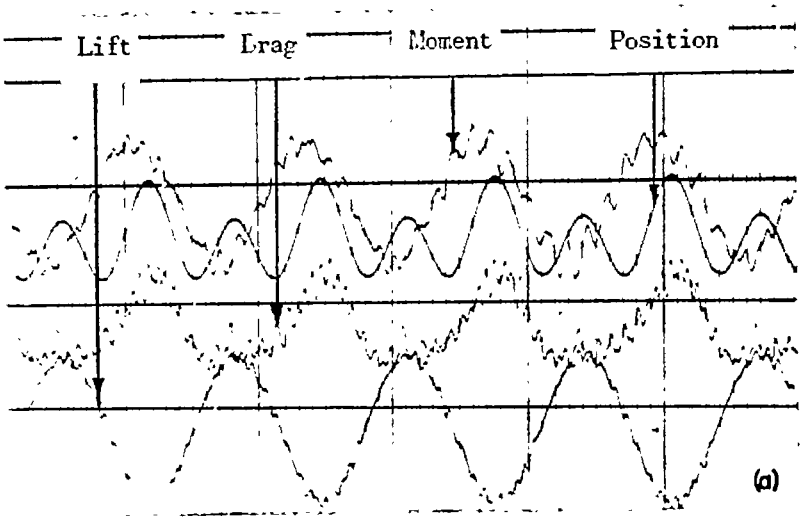

(a) $\alpha = 0^{\circ}$; $\omega = 7.7$ cycles per second. Lift attenuation, 1-5; moment attenuation, 1-7; drag attenuation, 1-1.5.

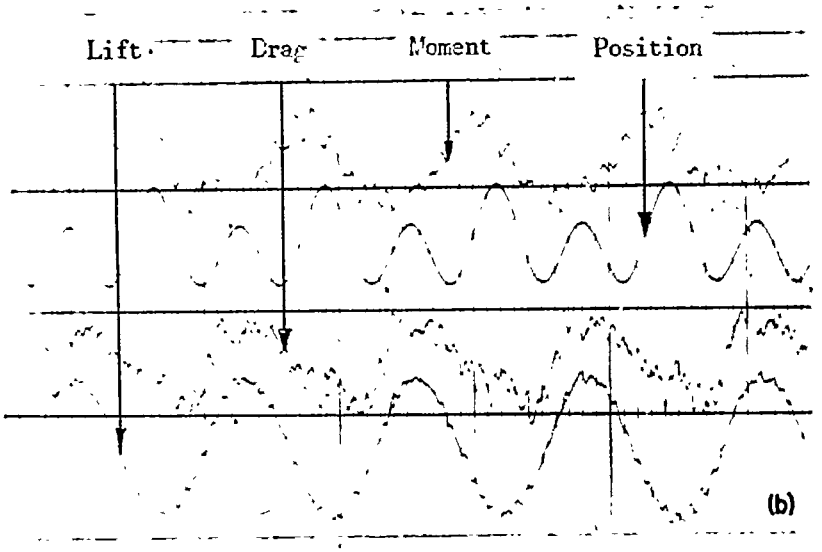

(b) $\alpha = 10^{\circ}$; $\omega = 7.5$ cycles per second. Lift attenuation, 1-5; moment attenuation, 1-7; drag attenuation, 1-1.5.

Figure 49.- Effect of mean angle of attack. Intermediate wing. Pure pitch.

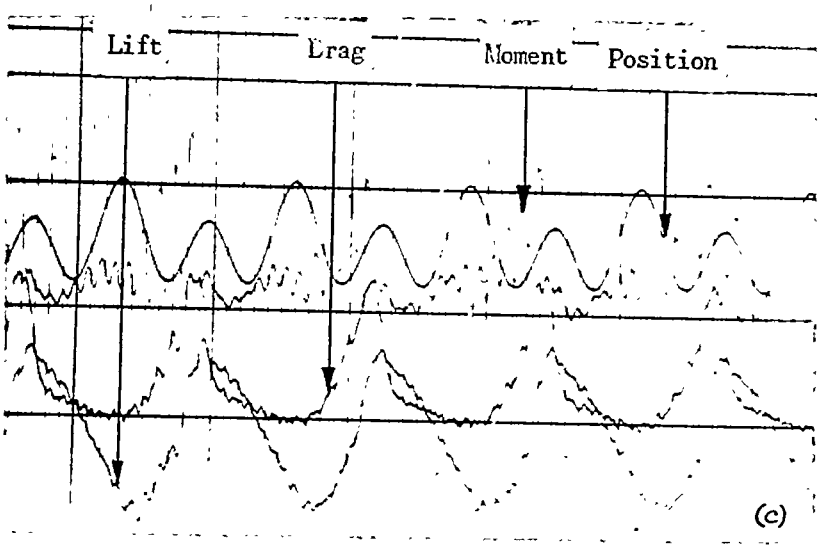

(c) $\alpha = 14^{\circ}$; $\omega = 7.90$ cycles per second. Lift attenuation, 1-7; moment attenuation, 10-1; drag attenuation, 1-7.

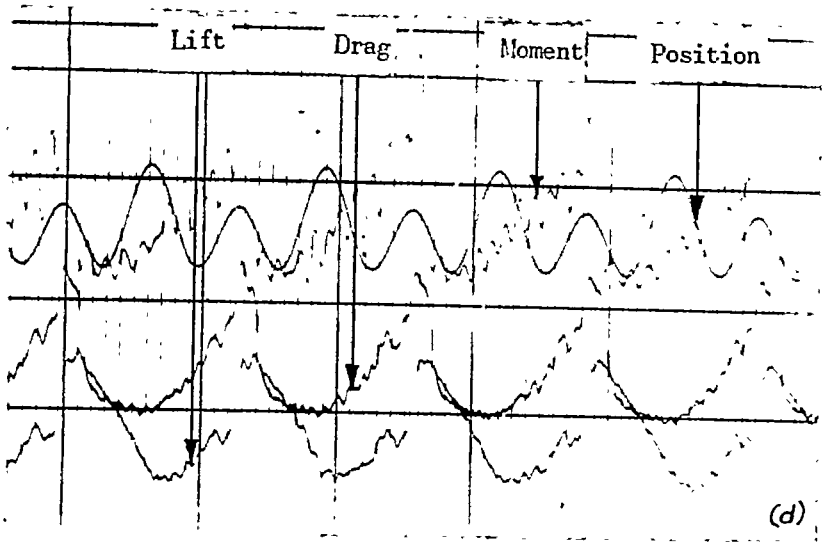

(d) $\alpha = 18^{\circ}$; $\omega = 8.2$ cycles per second. Lift attenuation, 1-10; moment attenuation, 10-1; drag attenuation, 1-10.

Figure 49.- Concluded.

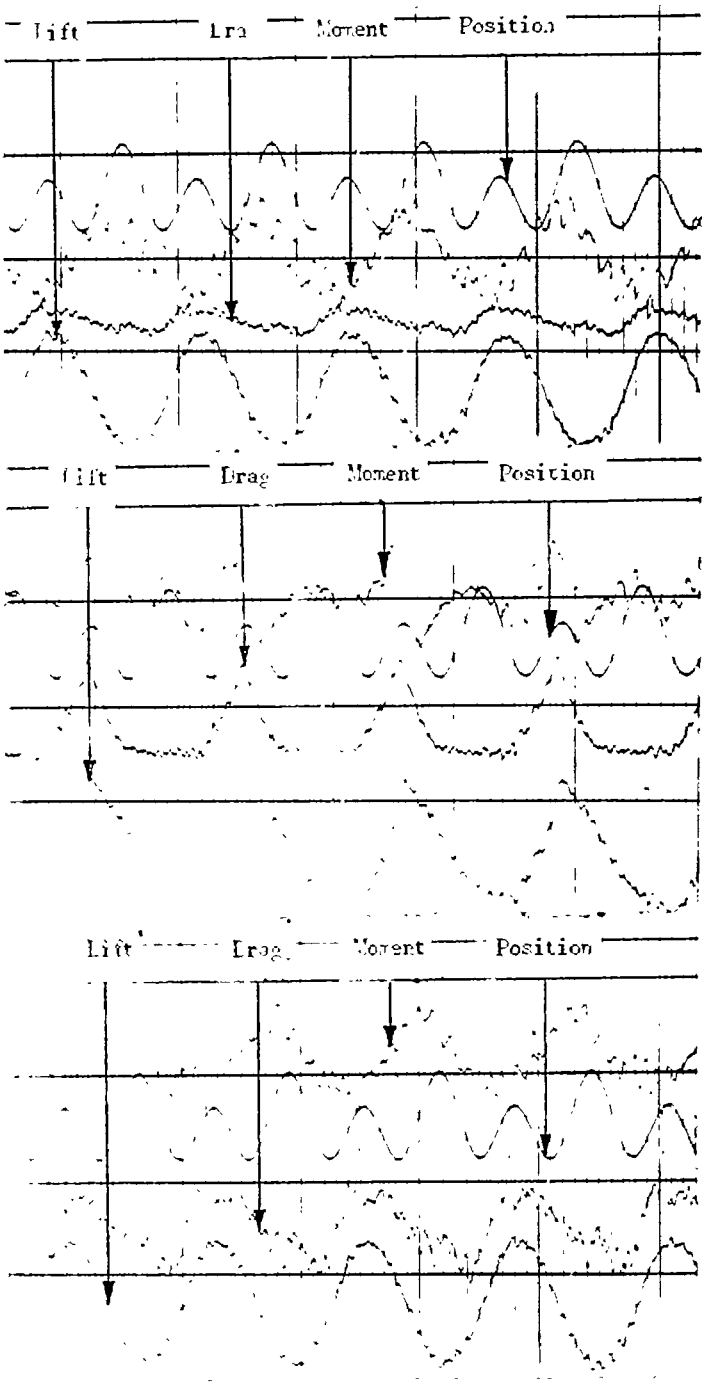

(a) Blunt wing.
$\alpha = 10^{\circ}$;
$\omega = 7.9$ cycles per second.
Lift attenuation, 1-5;
moment attenuation, 1-5;
drag attenuation, 1-5.

(b) Sharp wing.
$\alpha = 10^{\circ}$;
$\omega = 7.7$ cycles per second.
Lift attenuation, 1-7;
moment attenuation, 1-10;
drag attenuation, 1-7.

(c) Intermediate wing.
$\alpha = 10^{\circ}$;
$\omega = 7.5$ cycles per second.
Lift attenuation, 1-5;
moment attenuation, 1-7;
drag attenuation, 1-1.5.

Figure 50.- Effect of airfoil shape. Pure pitch.

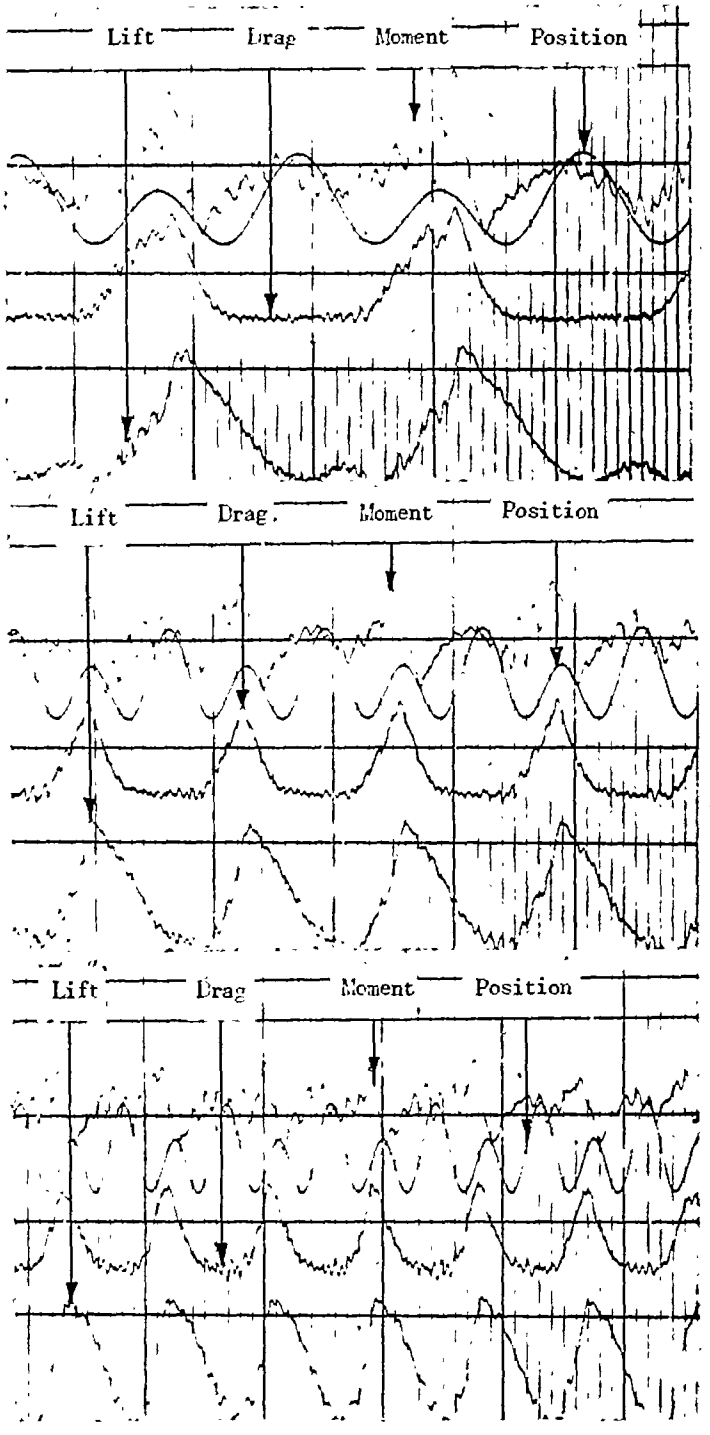

(a) $\alpha = 10^{\circ}$;
$\omega = 4.27$ cycles per second.
Lift attenuation, 1-5;
moment attenuation, 1-7;
drag attenuation, 1-5.

(b) $\alpha = 10^{\circ}$;
$\omega = 7.72$ cycles per second.
Lift attenuation, 1-7;
moment attenuation, 1-10;
drag attenuation, 1-7.

(c) $\alpha = 10^{\circ}$;
$\omega = 11.5$ cycles per second.
Lift attenuation, 1-7;
moment attenuation, 10-1.5;
drag attenuation, 1-7.

Figure 51.- Effect of frequency of oscillation. Sharp wing. Pure pitch.

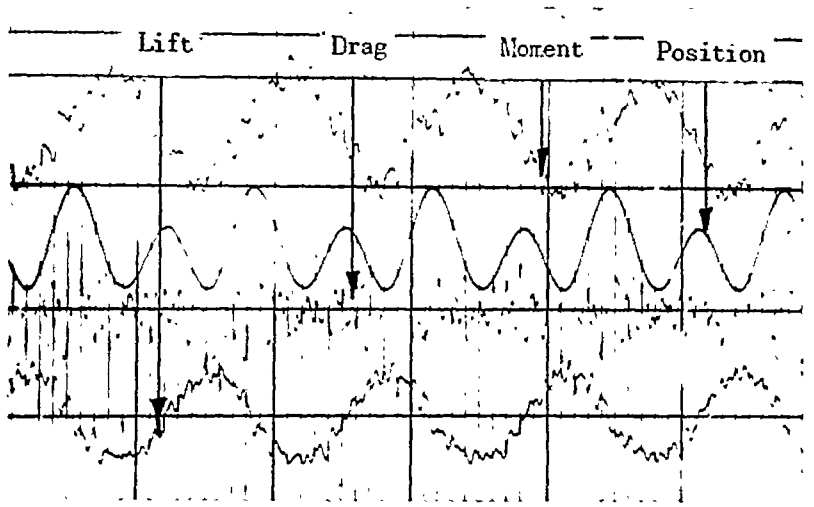

(a) $\alpha = 0^{\circ}$; $\omega = 7.69$ cycles per second. Lift attenuation, 1-3; moment attenuation, 1-1.5; drag attenuation, 1-1.

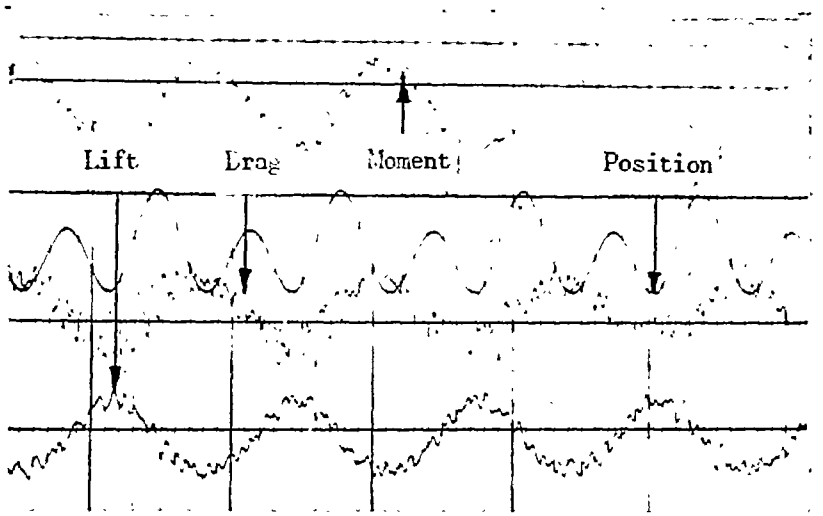

(b) $\alpha = 10^{\circ}$; $\omega = 7.62$ cycles per second. Lift attenuation, 1-3; moment attenuation, 1-2; drag attenuation, 1-1.

Figure 52.- Effect of mean angle of attack. Intermediate wing. Pure translation.

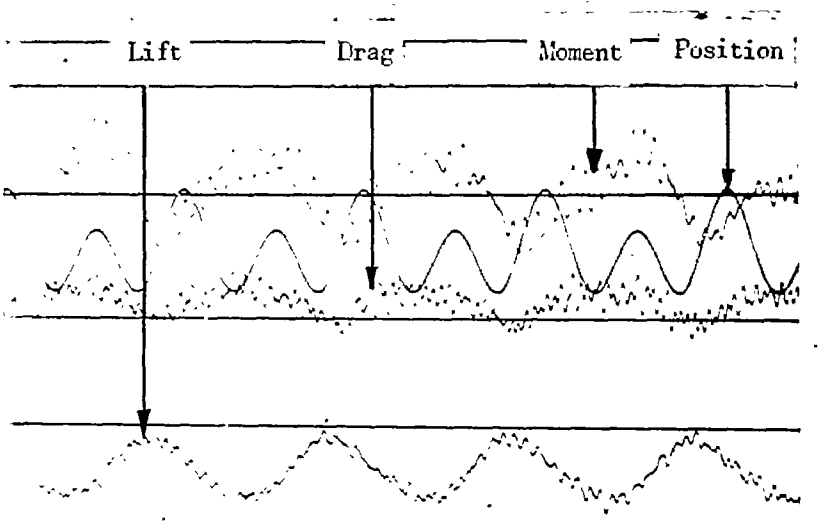

(c) $\alpha = 14^{\circ}$; $\omega = 7.58$ cycles per second. Lift attenuation, 1-5; moment attenuation, 1-3; drag attenuation, 1-2.

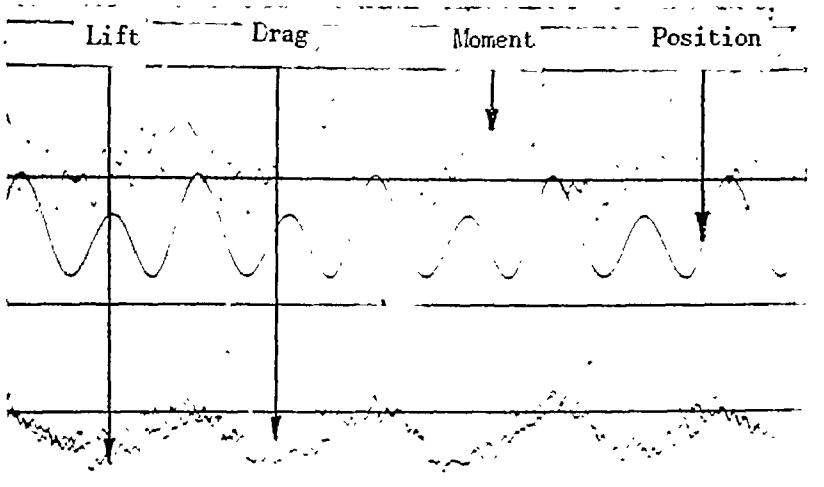

(d) $\alpha = 14^{\circ}$; $\omega = 7.77$ cycles per second. Lift attenuation, 1-5; moment attenuation, 1-5; drag attenuation, 1-5.

Figure 52.- Concluded.

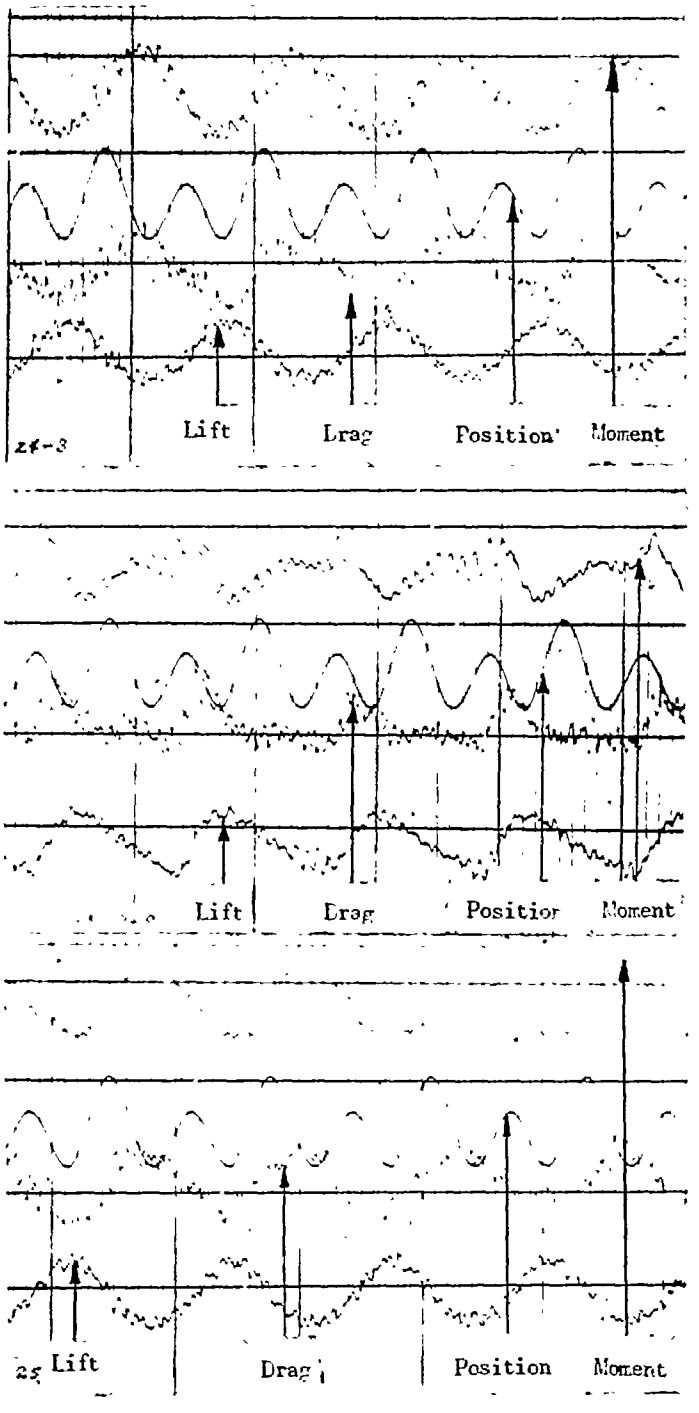

(a) Blunt wing.
$\alpha = 10^{\circ}$;
$\omega = 7.67$ cycles per second.
Lift attenuation, 1-3;
moment attenuation, 1-2;
drag attenuation, 1-1.

(b) Sharp wing.
$\alpha = 10^{\circ}$;
$\omega = 8.00$ cycles per second.
Lift attenuation, 1-5;
moment attenuation, 1-5;
drag attenuation, 1-2.

(c) Intermediate wing.
$\alpha = 10^{\circ}$;
$\omega = 7.62$ cycles per second.
Lift attenuation, 1-3;
moment attenuation, 1-2;
drag attenuation, 1-1.

Figure 53.- Effect of airfoil shape. Pure translation.

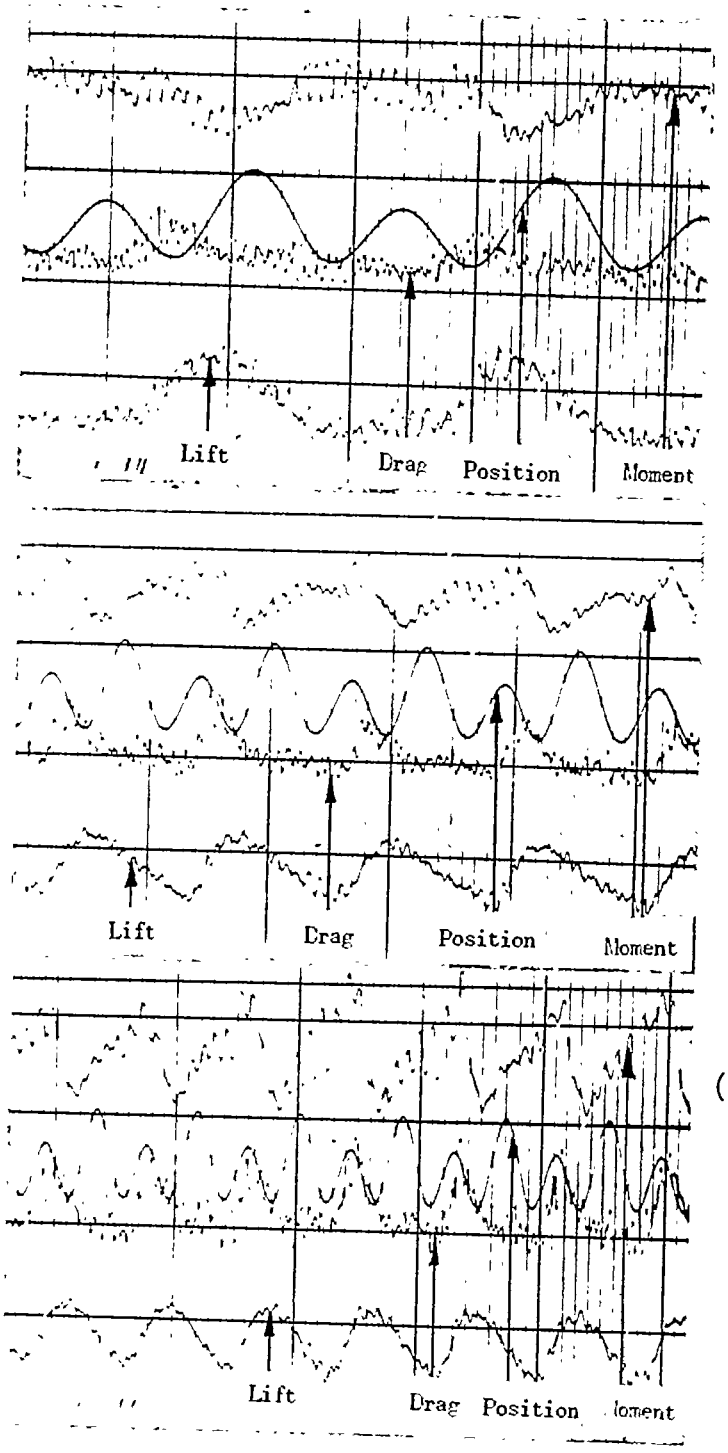

(a) $\alpha = 10^{\circ}$;
$\omega = 4.11$ cycles per second.
Lift attenuation, 1-1.5;
moment attenuation, 1-2;
drag attenuation, 1-1.

(b) $\alpha = 10^{\circ}$;
$\omega = 8.00$ cycles per second.
Lift attenuation, 1-5;
moment attenuation, 1-5;
drag attenuation, 1-2.

(c) $\alpha = 10^{\circ}$;
$\omega = 11.9$ cycles per second.
Lift attenuation, 1-7;
moment attenuation, 1-5;
drag attenuation, 1-2.

Figure 54.- Effect of frequency of oscillation. Sharp wing. Pure translation.

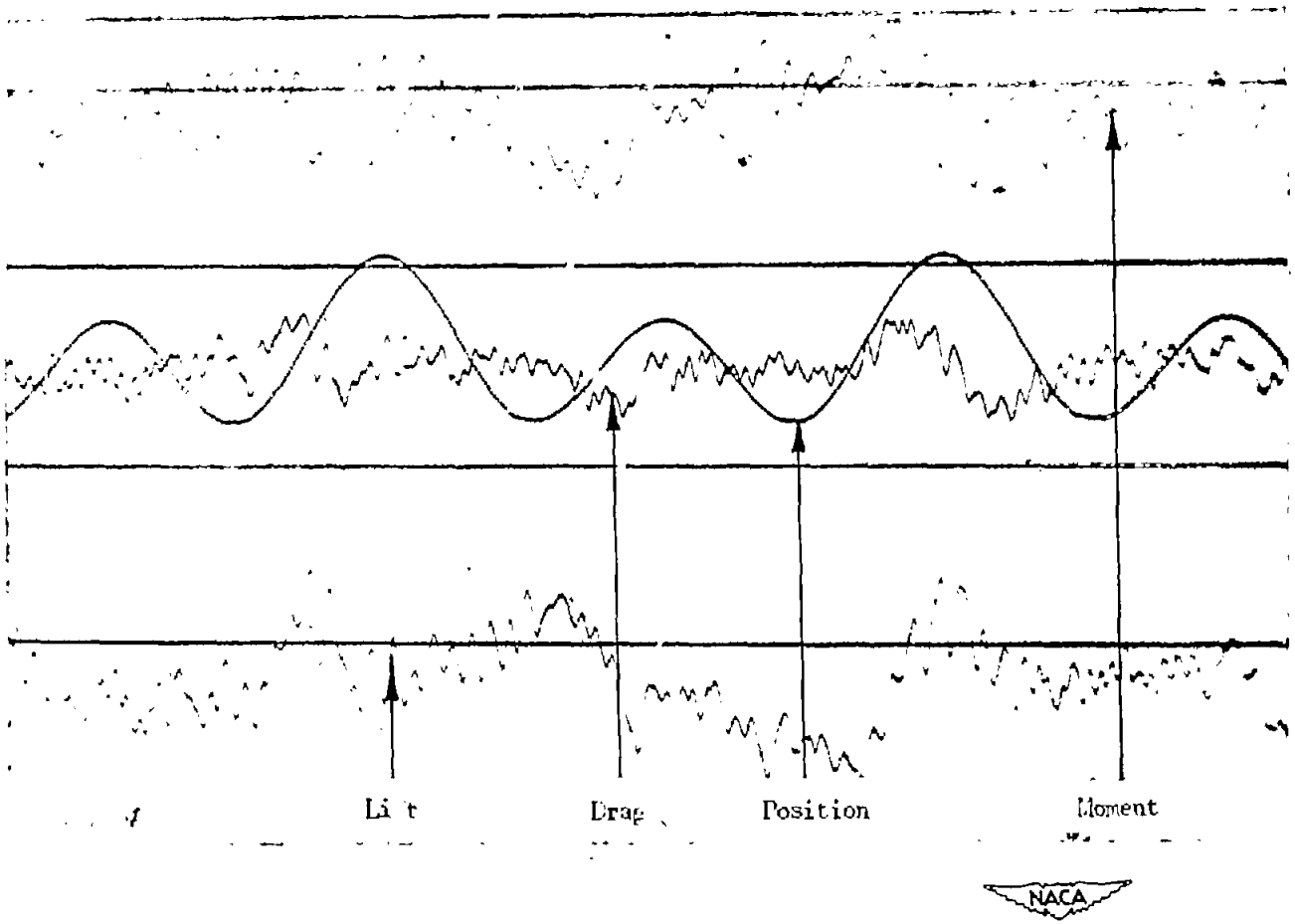

Figure 55.- Record taken near static stalling angle showing nonperiodic reactions. Pure translation. Blunt wing. $\alpha = 14^{\circ}$; $\omega = 4.06$ cycles per second. Lift attenuation, 1-3; moment attenuation, 1-7; drag attenuation, 1-3.

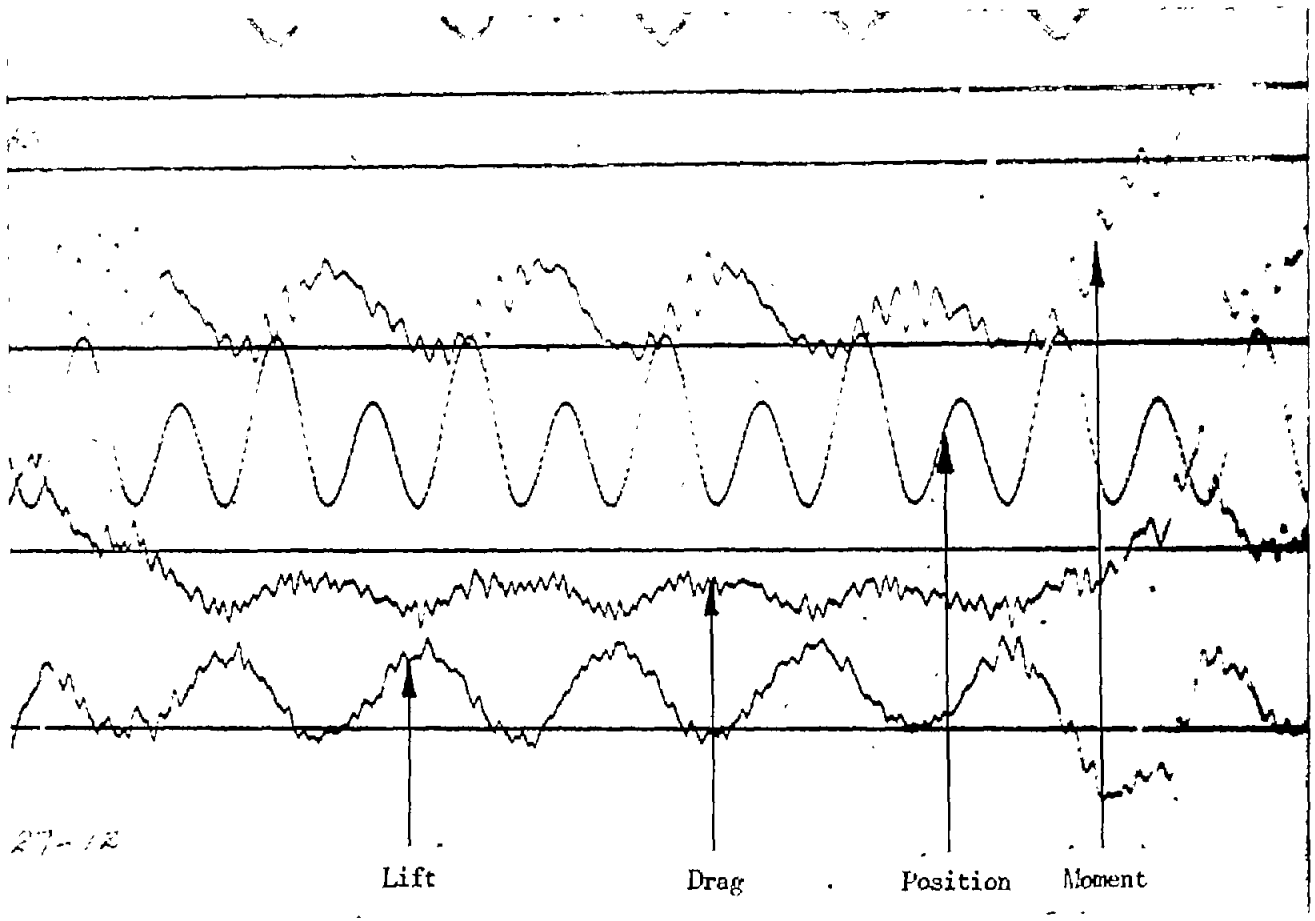

Figure 56.- Record taken near static stalling angle showing an erratic transition from stalled to unstalled flow. Pure translation. Blunt wing. $\alpha = 14^{\circ}$; $\omega = 11.9$ cycles per second. Lift attenuation, 1-7; moment attenuation, 1-7; drag attenuation, 1-5.

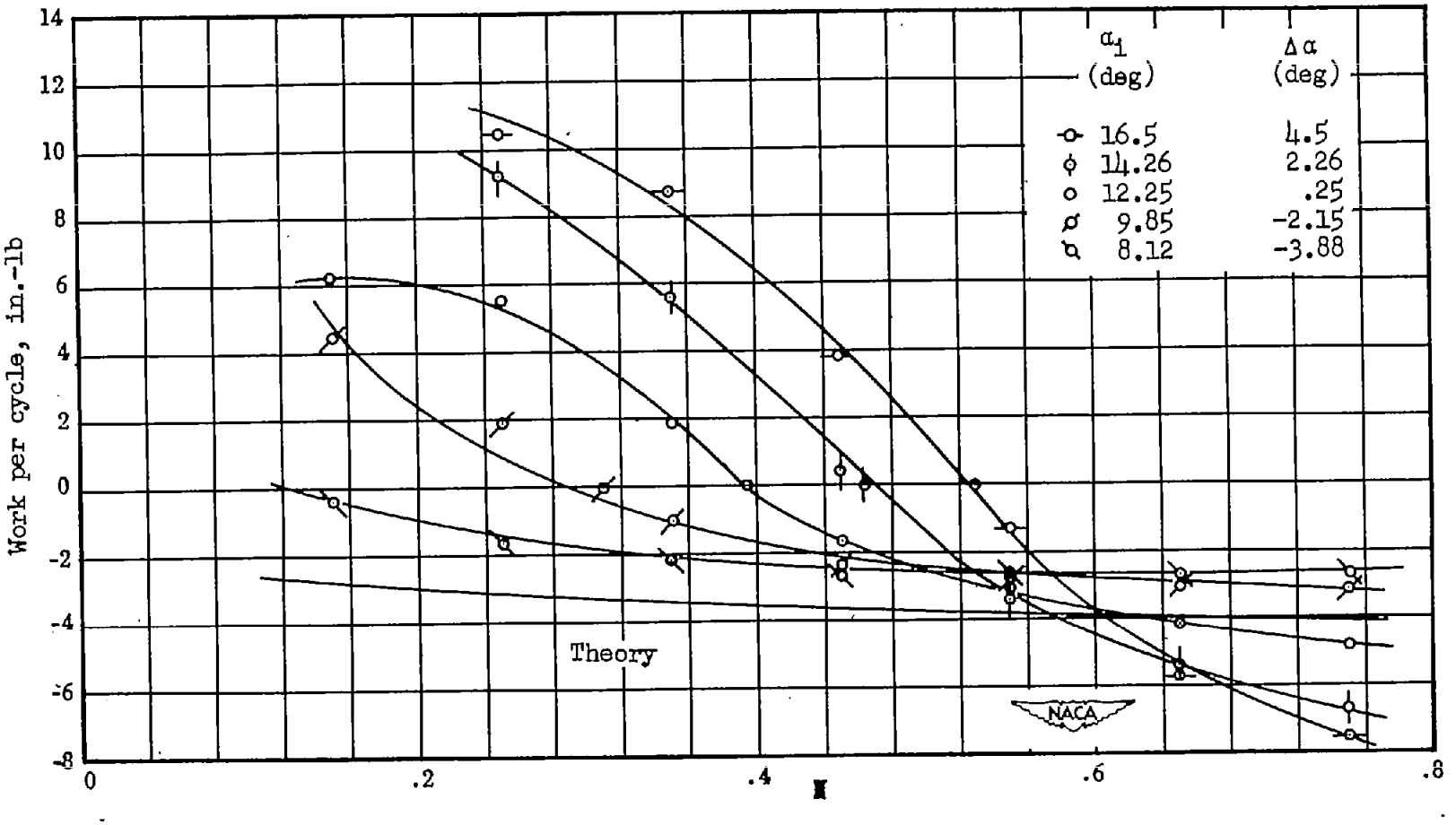

Figure 57.- Work per cycle in pure pitch. Reference 3, figure 2. $\alpha_{\text{steady-state stall}} = 12^{\circ}$; elastic axis at 50-percent chord; Reynolds number = 1.42×10^5.

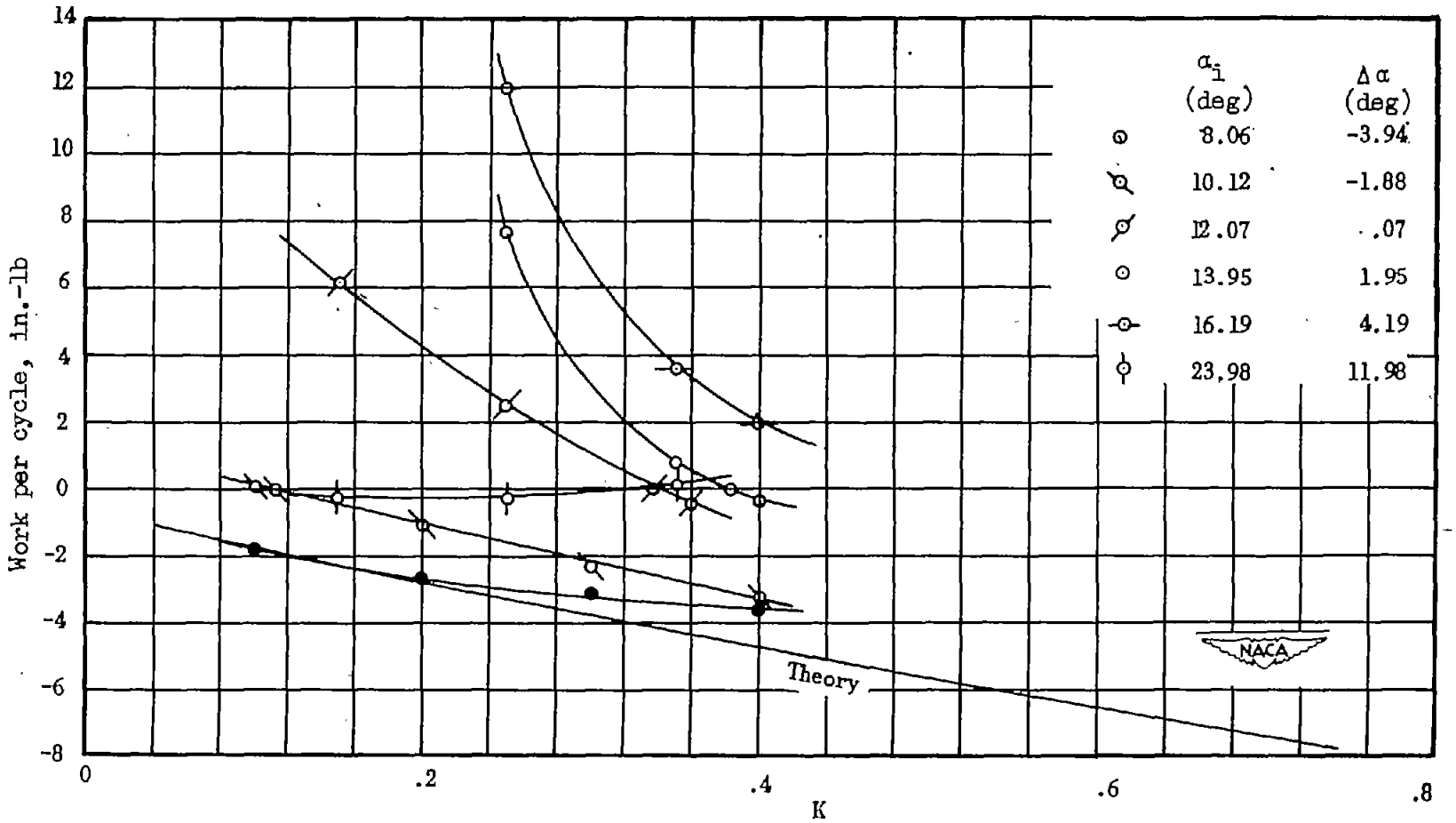

(a) Reynolds number = 2.83×10^5; elastic axis at 33-percent chord.

Figure 58.- Work per cycle in pure pitch. Reference 3, figure 4.
$\alpha_{\text{steady-state stall}} = 12^\circ$.

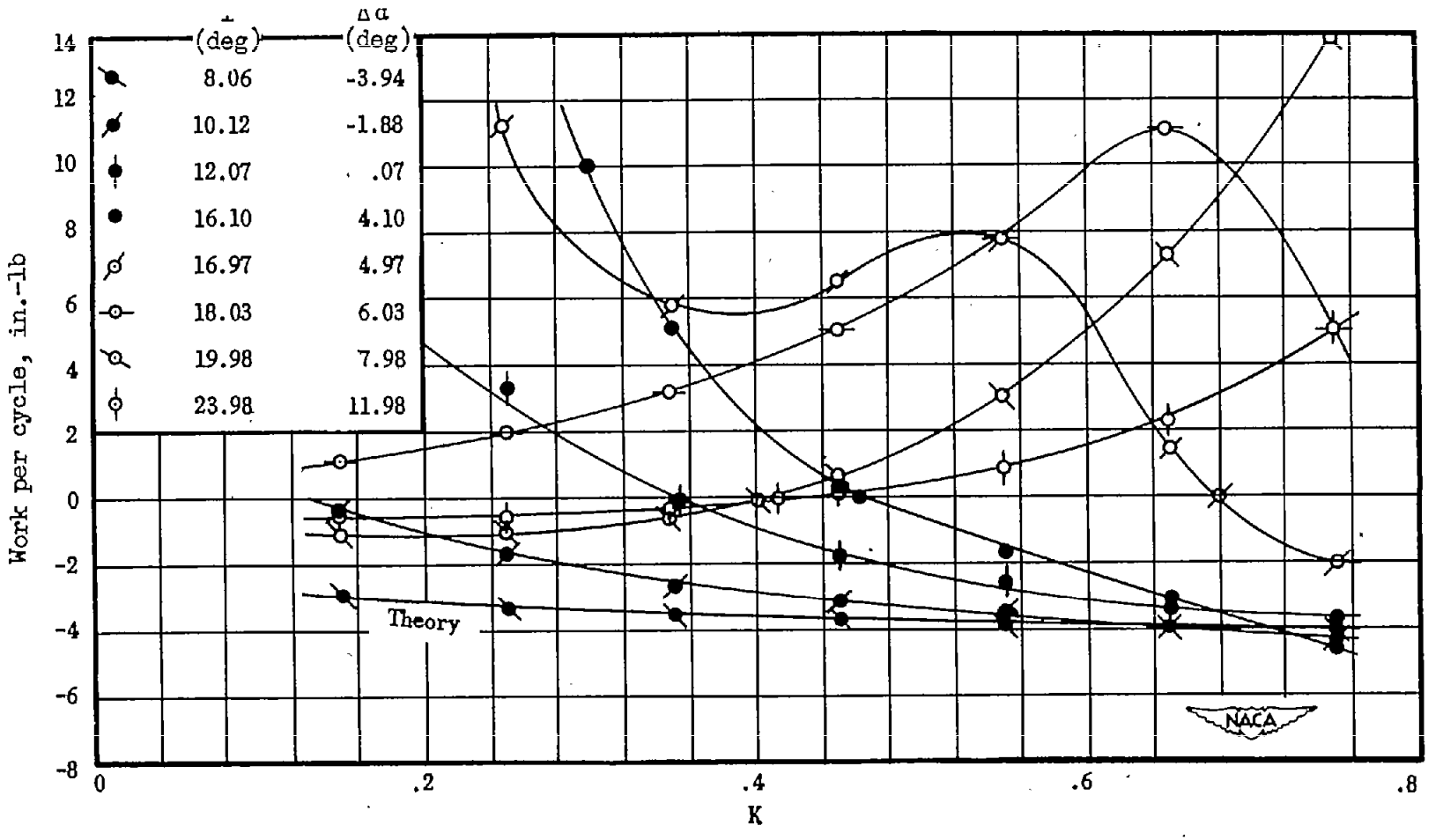

(b) Reynolds number = 1.42×10^5; elastic axis at 50-percent chord.

Figure 58.- Continued.

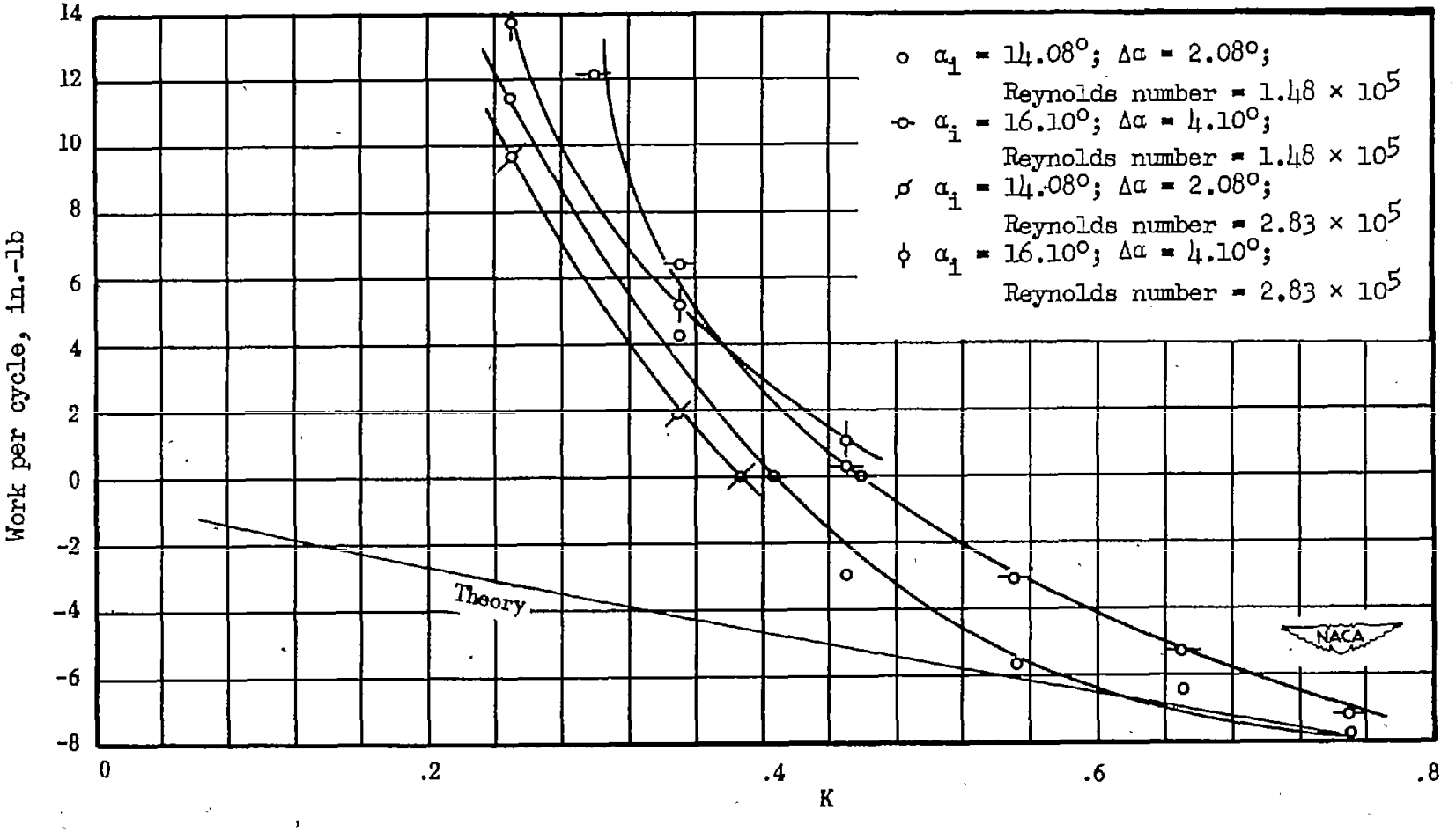

(c) Elastic axis at 33-percent chord. Various Reynolds numbers.

Figure 58.- Concluded.

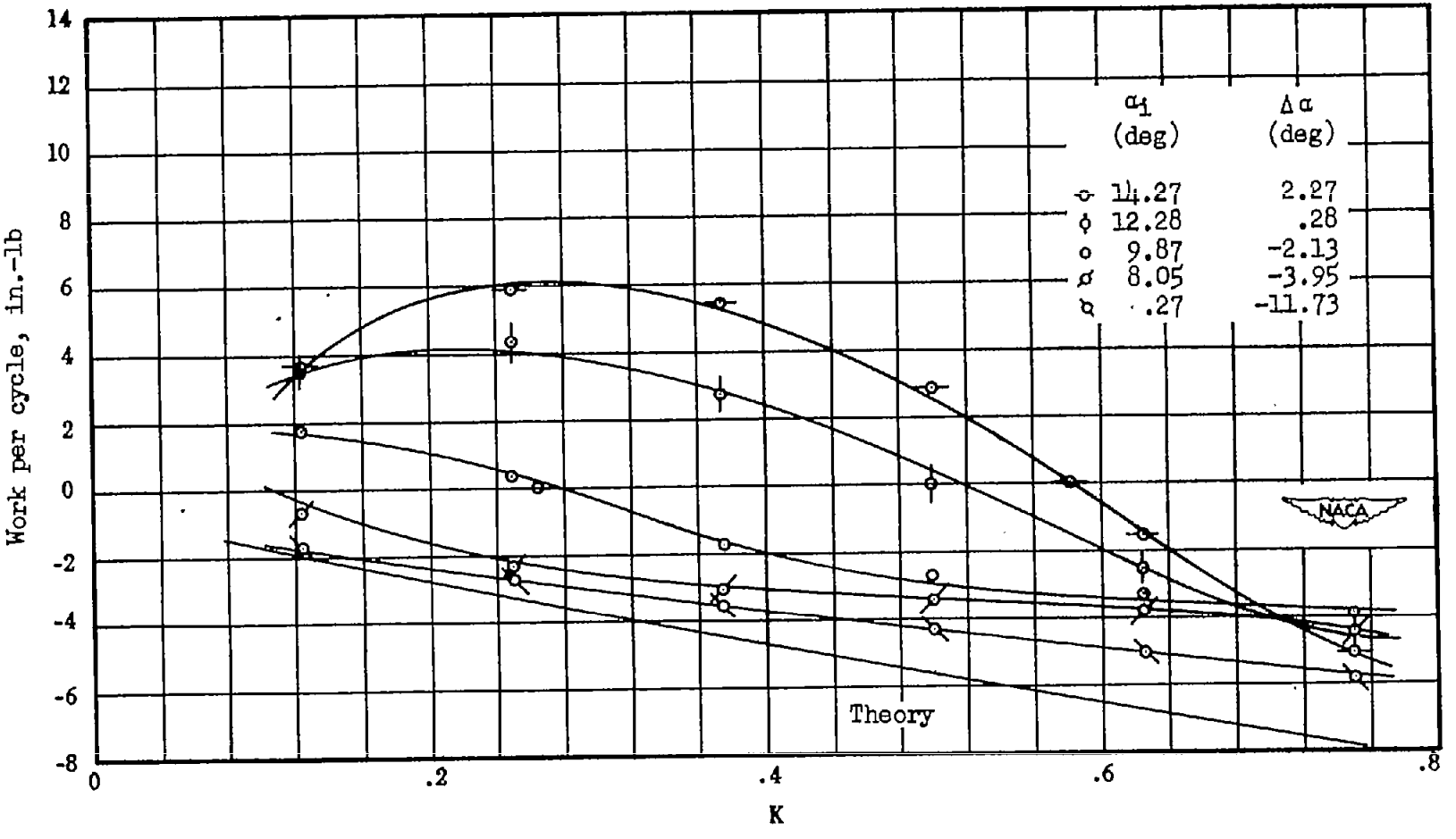

Figure 59.- Work per cycle in pure pitch. Reference 3, figure 15.
$\alpha_{steady\text{-}state\ stall} = 12^{\circ}$; elastic axis at 33-percent chord;
Reynolds number = 1.42×10^5.

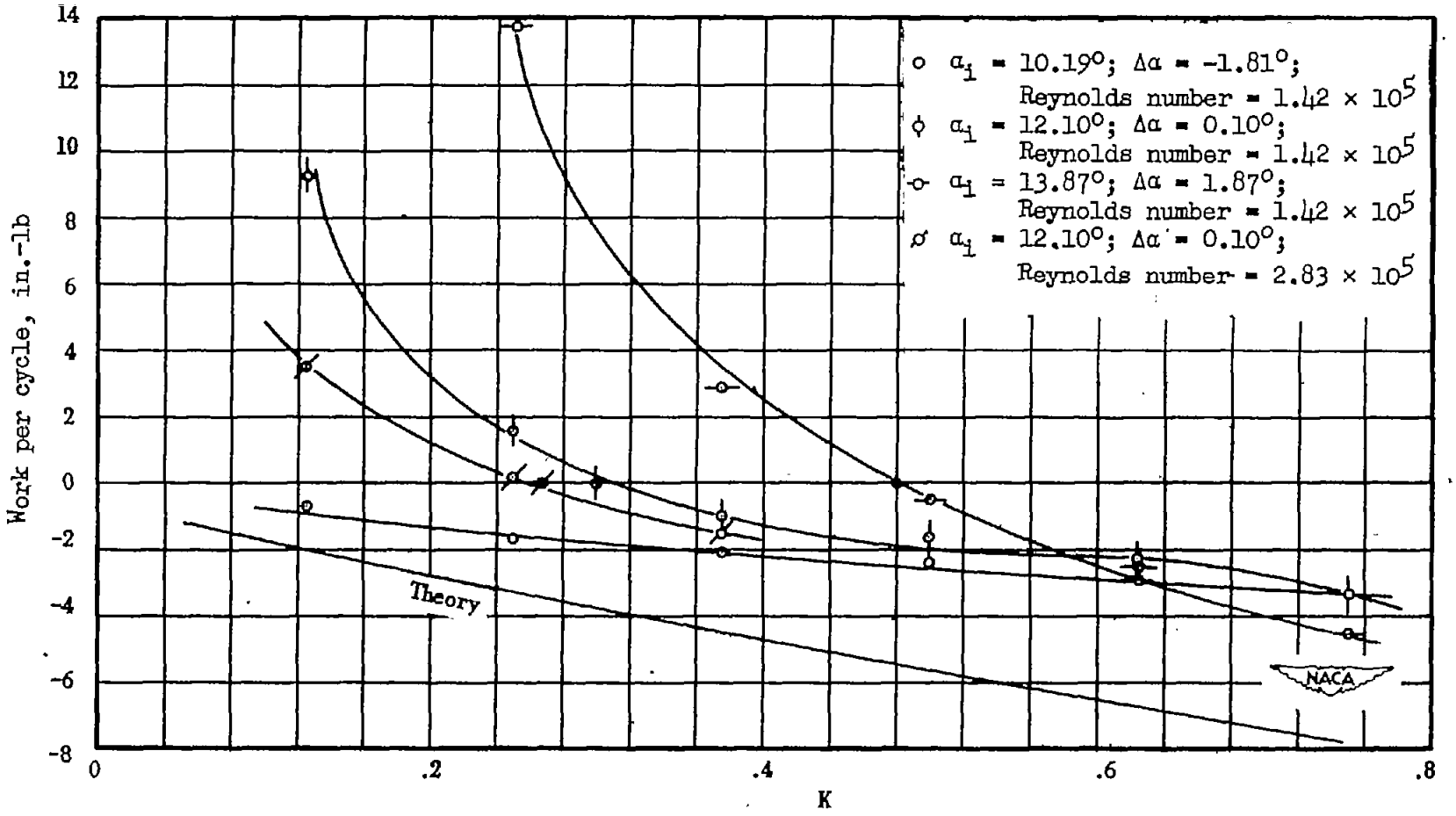

Figure 60.- Work per cycle in pure pitch. Reference 3, figure 16.
$\alpha_{\text{steady-state stall}} = 12°$; elastic axis at 33-percent chord.

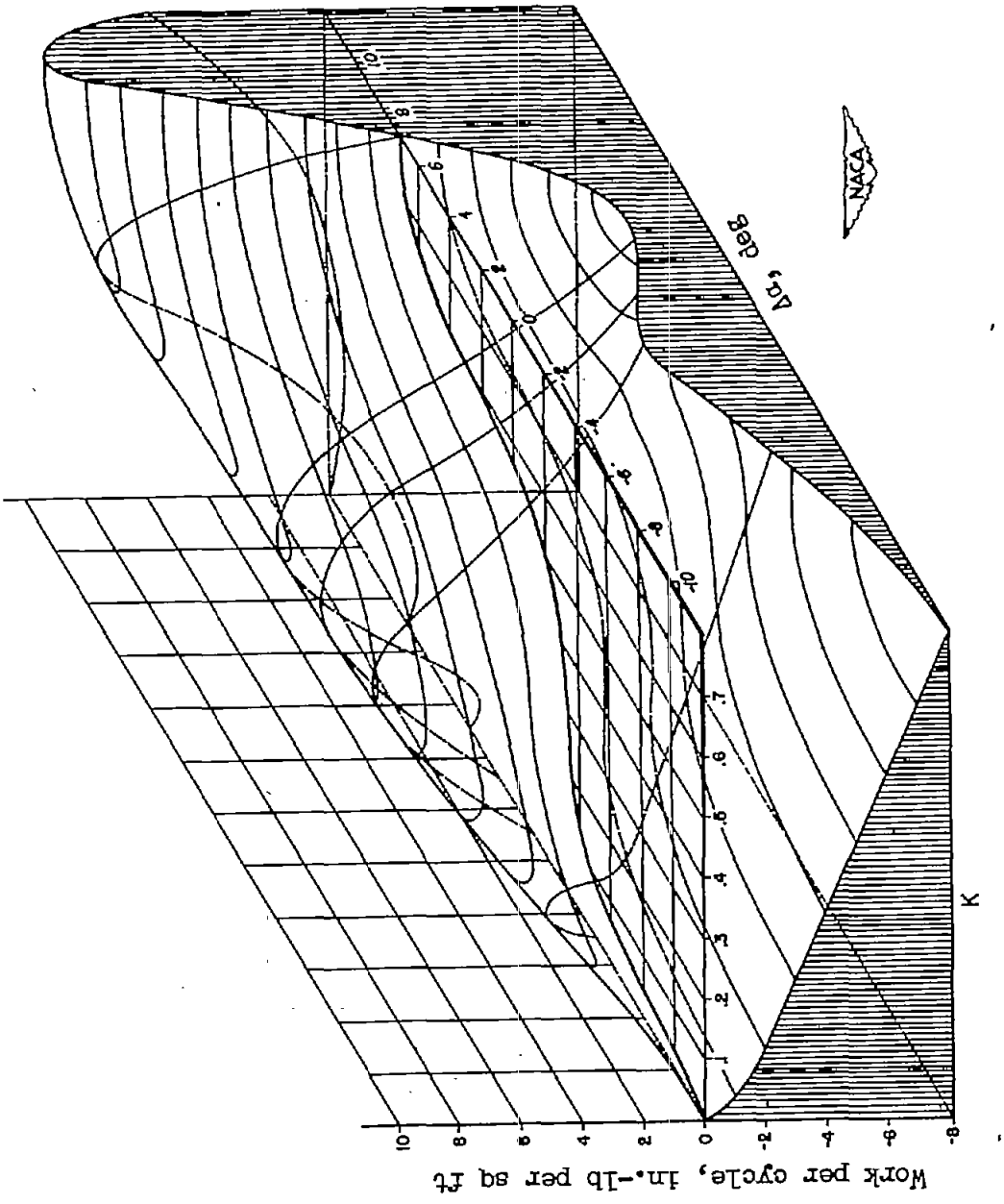

Figure 61.- Typical variation of work per cycle with K and $\Delta\alpha$.

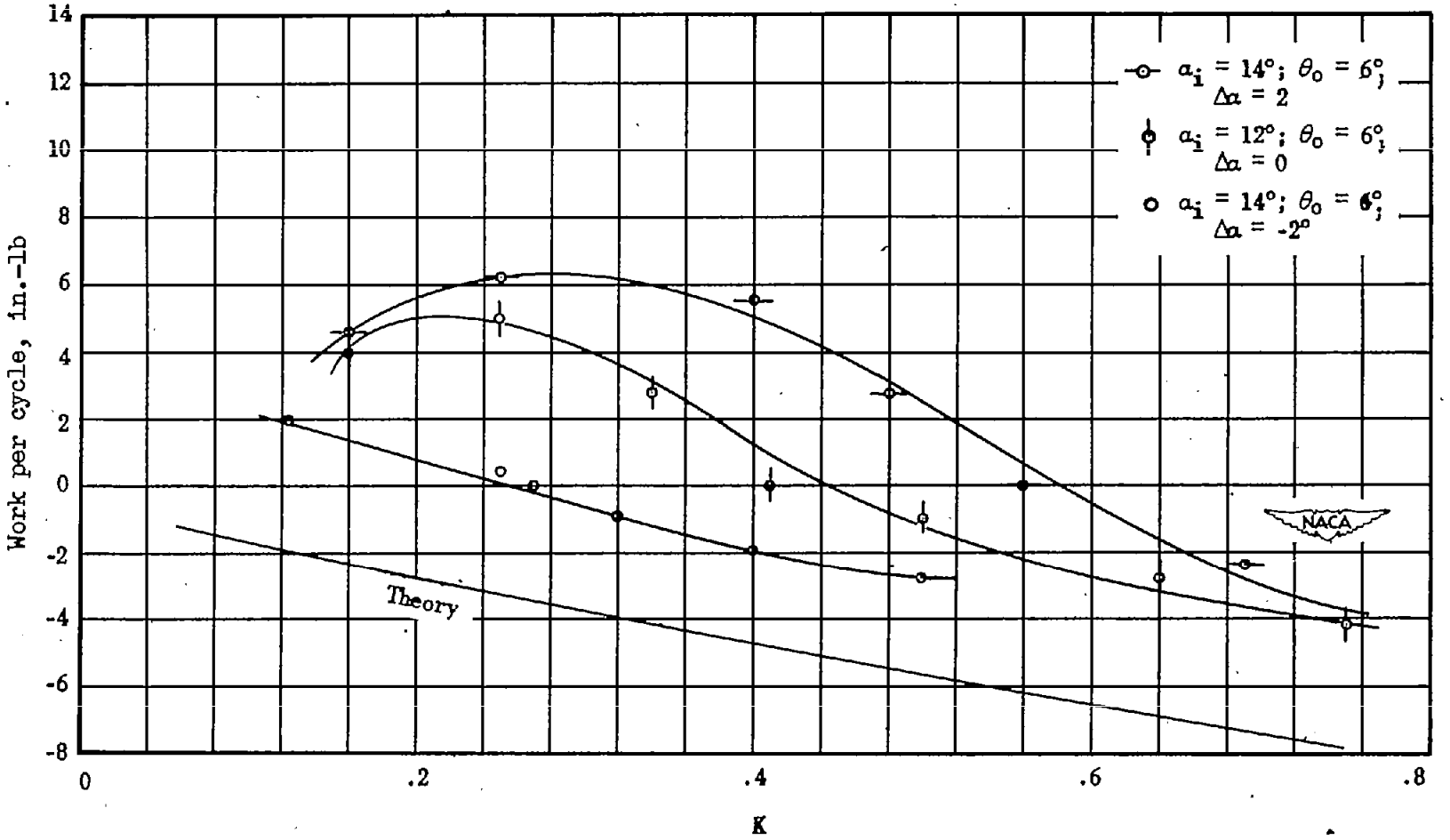

Figure 62.- Work per cycle in pure pitch. Reference 7, figure 1. $\alpha_{steady\text{-}state\ stall} = 12°$; elastic axis at 33-percent chord; Reynolds number = 1.42×10^5.

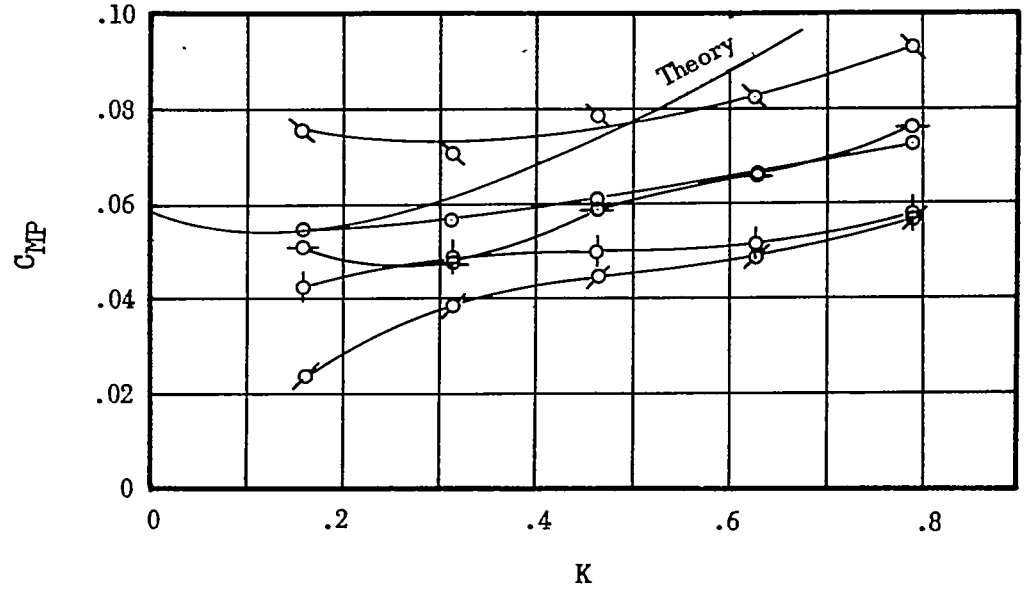

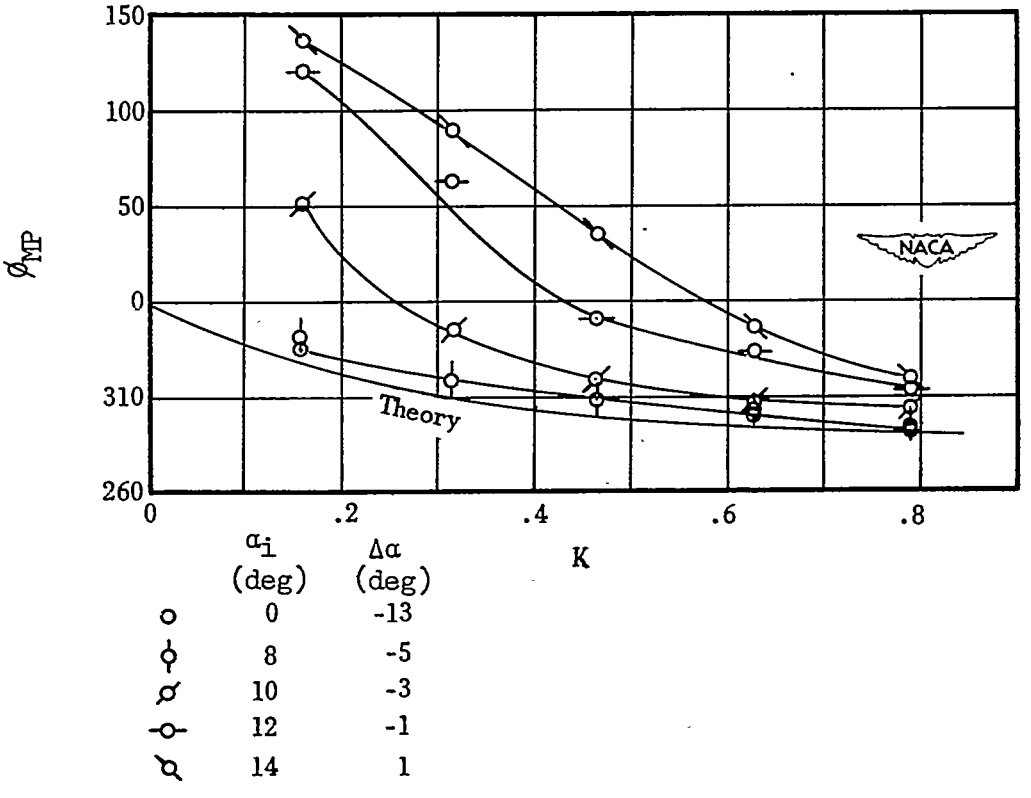

	α_i (deg)	$\Delta\alpha$ (deg)
o	0	-13
ϕ	8	-5
ϕ	10	-3
ϕ	12	-1
ϕ	14	1

Figure 63.- Moment amplitude and phase angle in pure pitch from harmonic analysis in reference 7. $\alpha_{stall} = 13^{\circ}$; $\alpha_i = 6^{\circ}$; elastic axis at 33-percent chord; Reynolds number = 1.42×10^5.

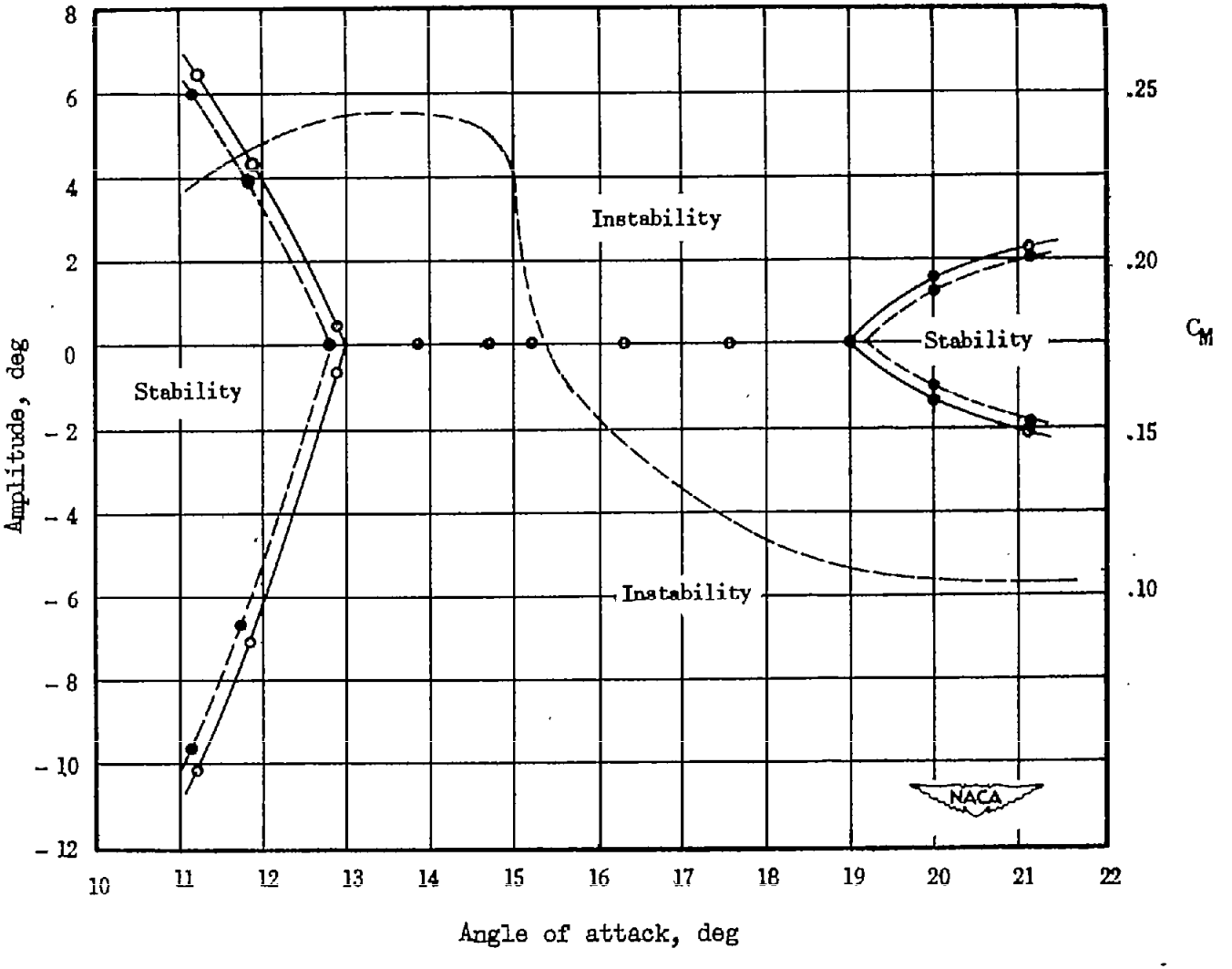

Figure 64.- Dependence of critical amplitude on initial angle of attack. Reference 11. Reynolds number = 2.83×10^5; K = 0.242.

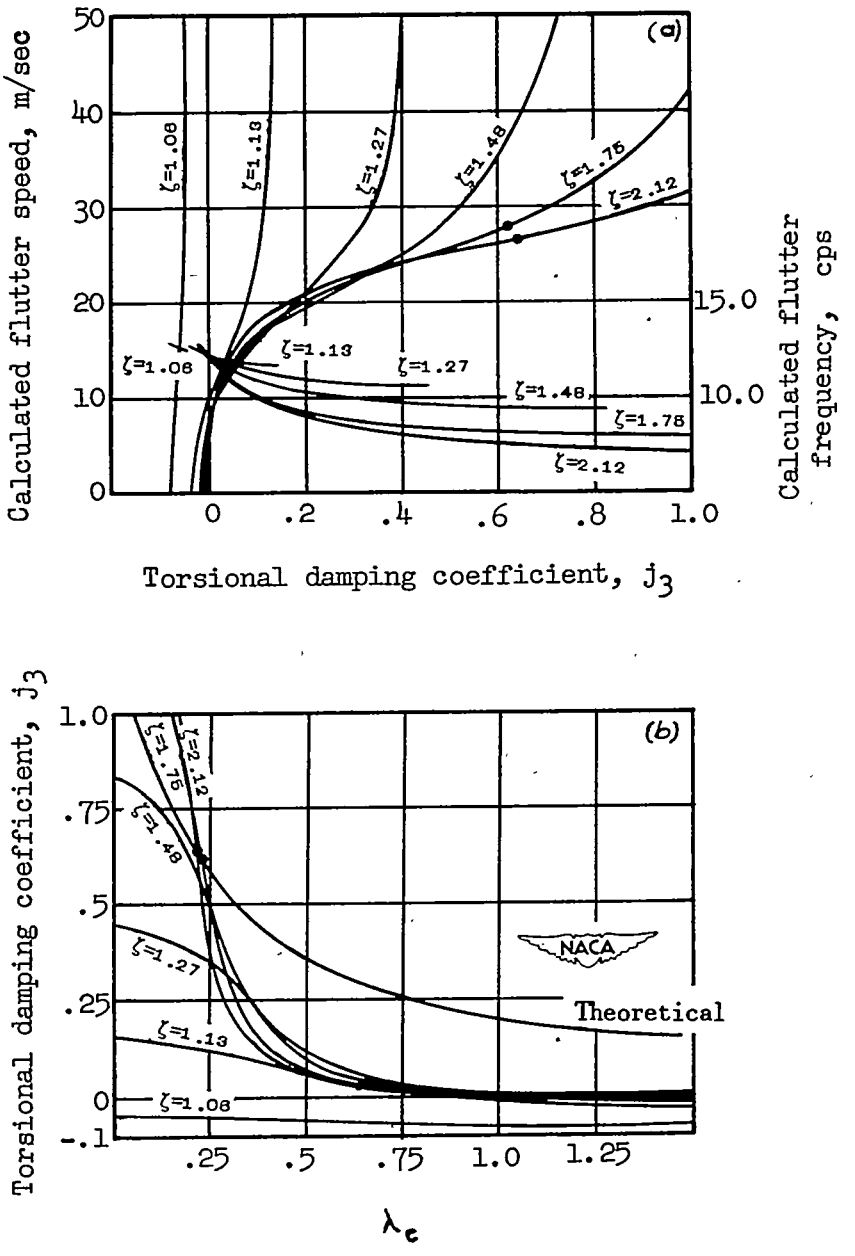

Figure 65.- Effect of torsional damping coefficient j_3 on flutter for different frequency ratios $\left(\zeta = \omega_\alpha/\omega_b\right)$. Reference 3.

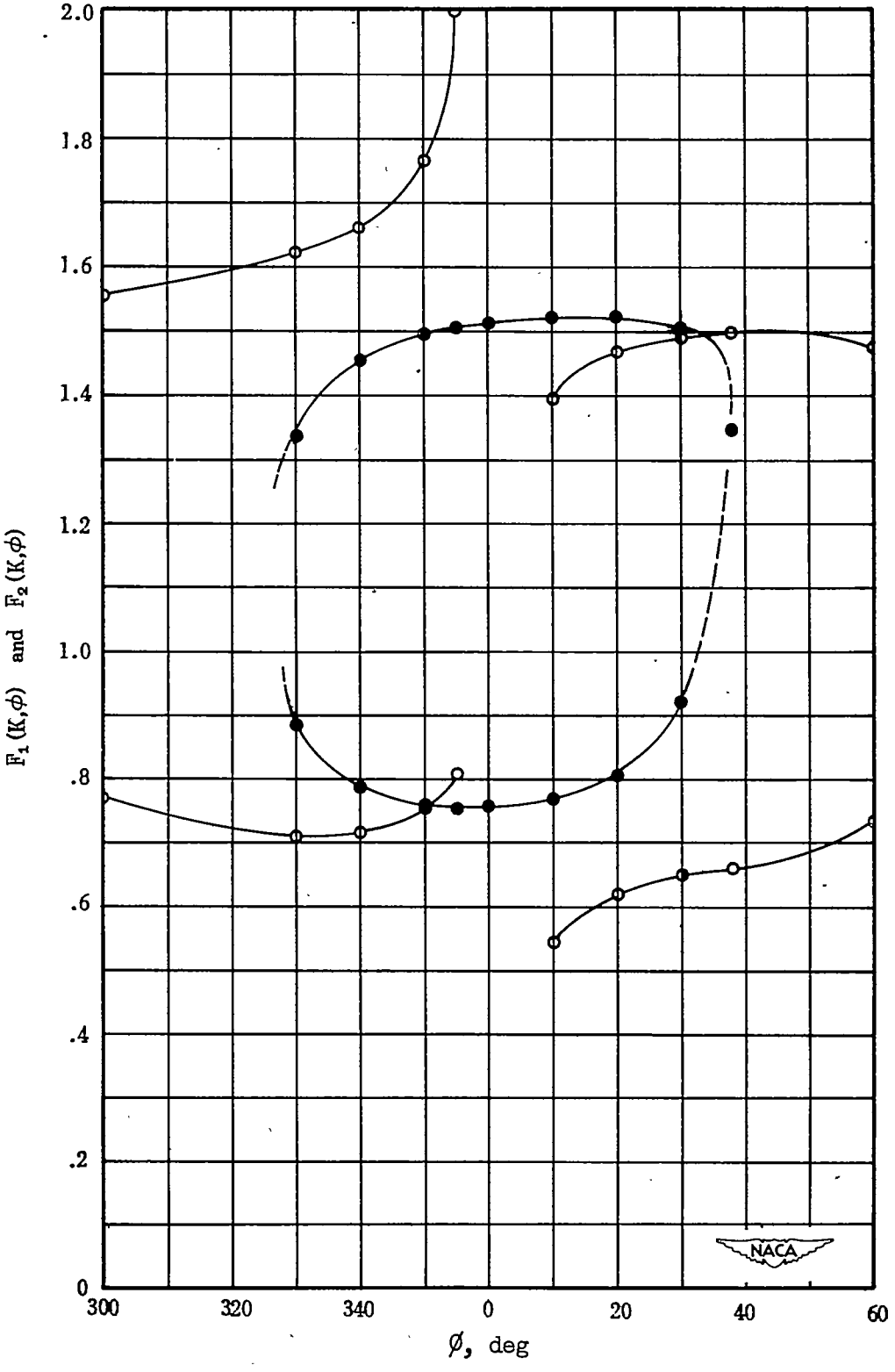

Figure 66.- Solution of Mendelson's ϕ at K = 0.30.

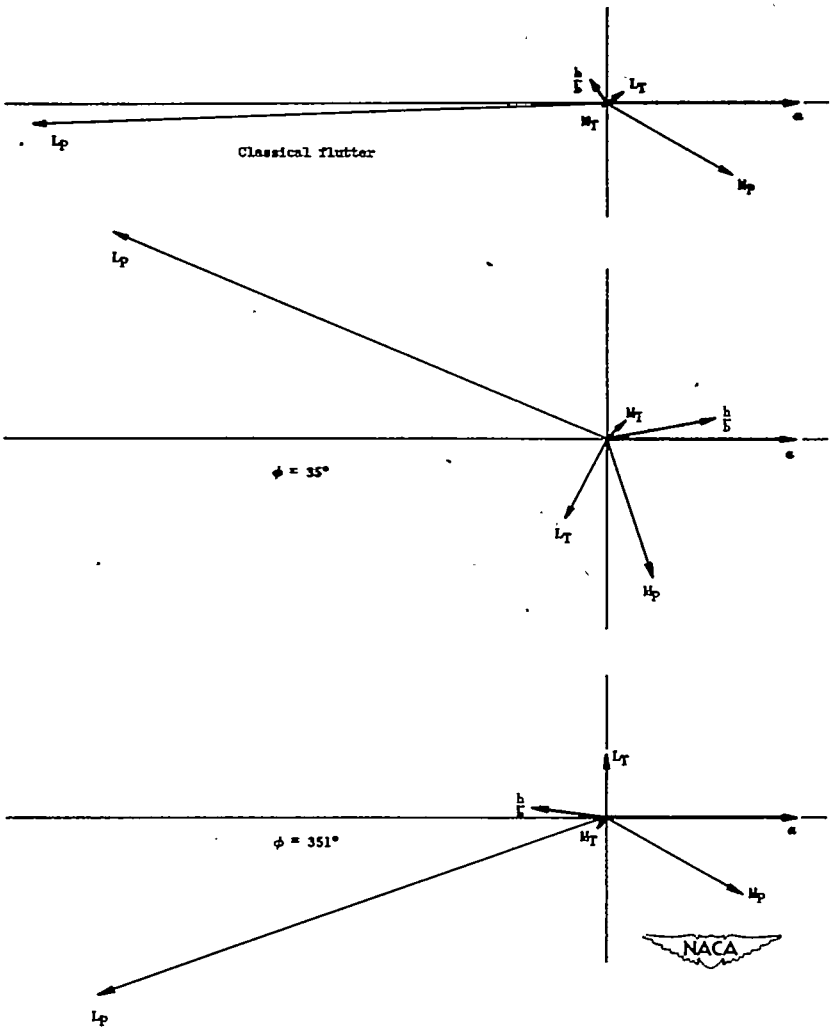

Figure 67.- Vector plots of aerodynamic derivatives at flutter.

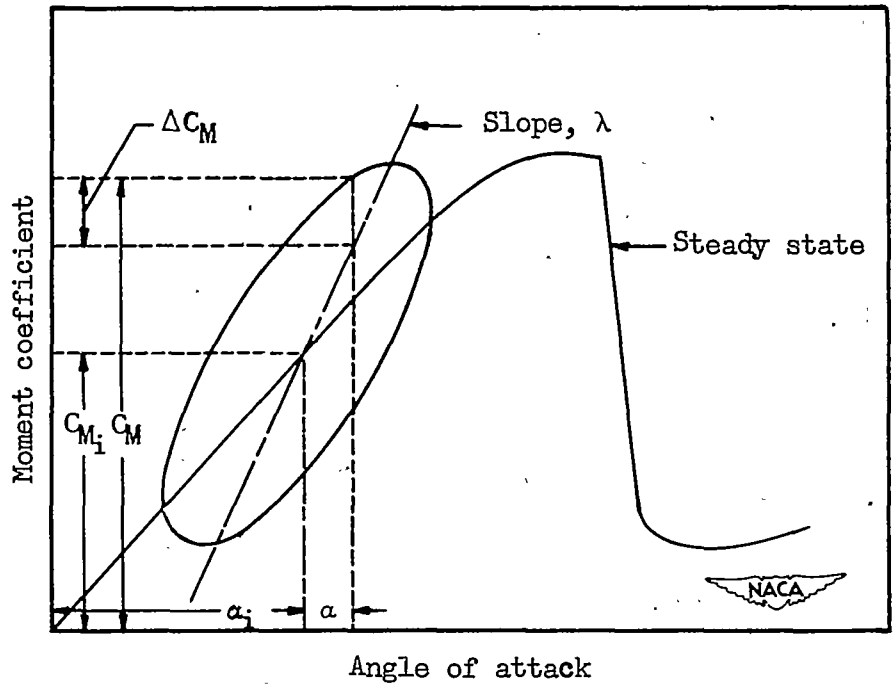

Figure 68.- Moment due to pitch at low initial angle of attack.

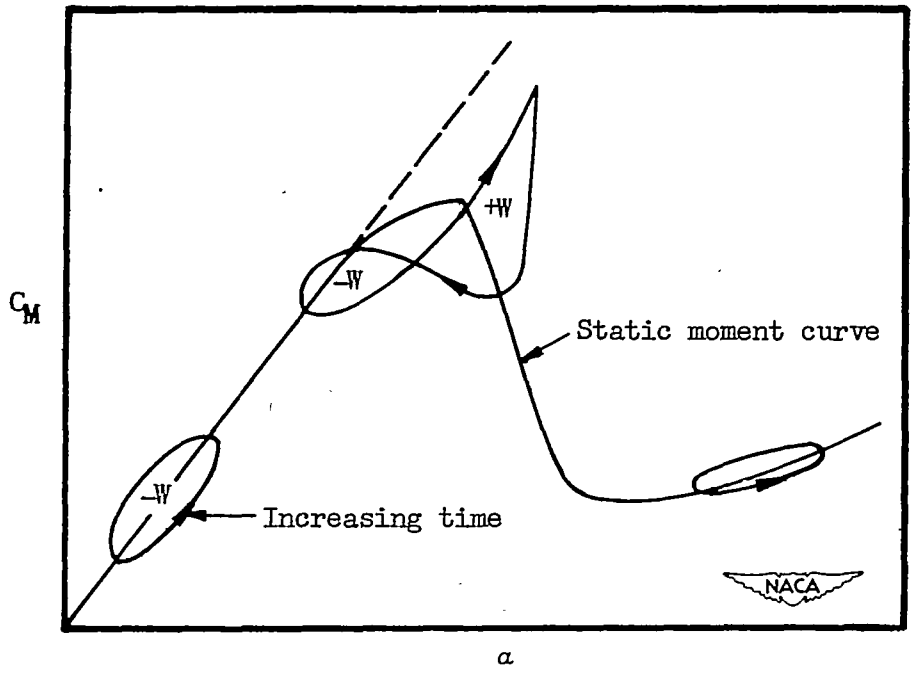

Figure 69.- Typical variations of moment due to pitch.

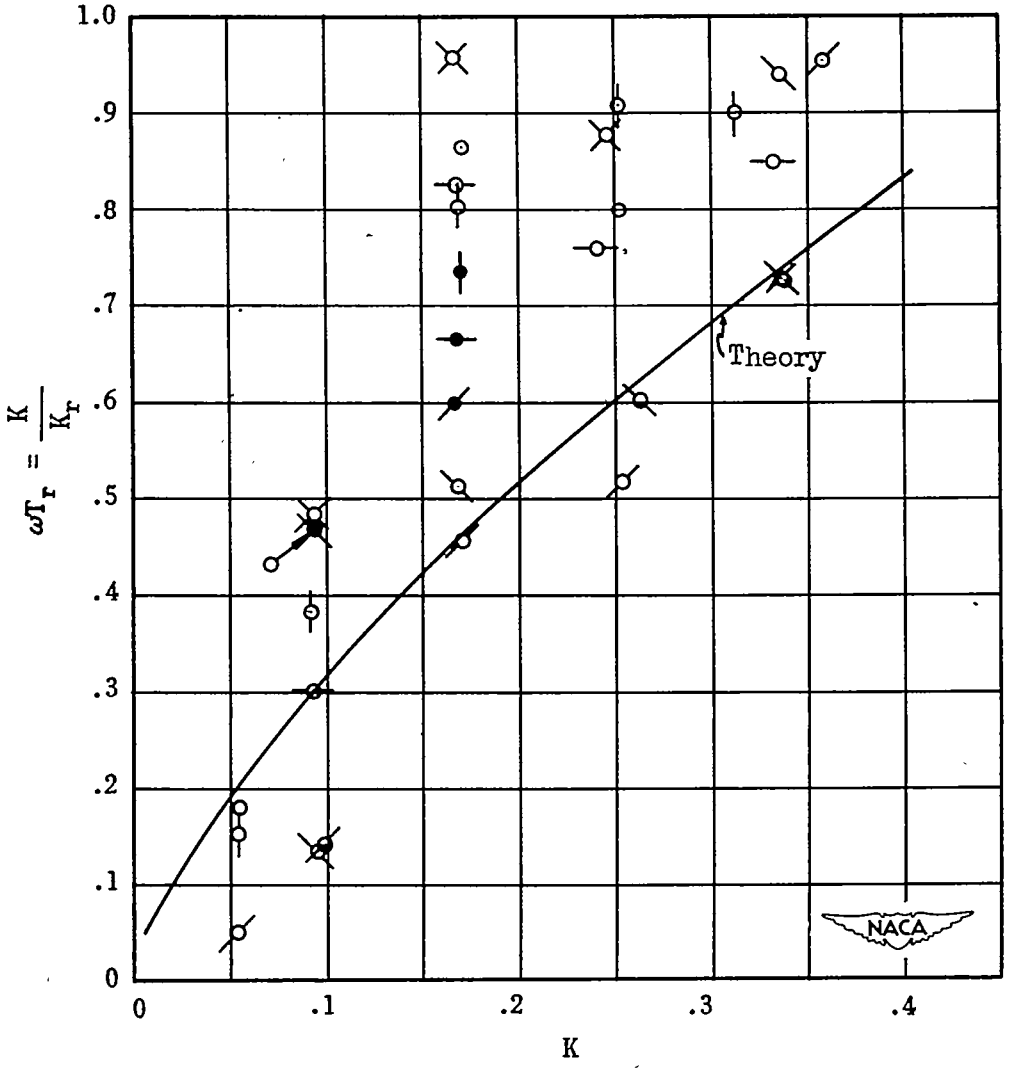

From work per cycle

α_i (deg)		
0	Blunt	
6		
0	Intermediate	
6		
0	Sharp	
6		

From average direct measurements

α_i (deg)	
0	Blunt
6	
10	Sharp
12	

Figure 70.- Plot of ωT_r against K.

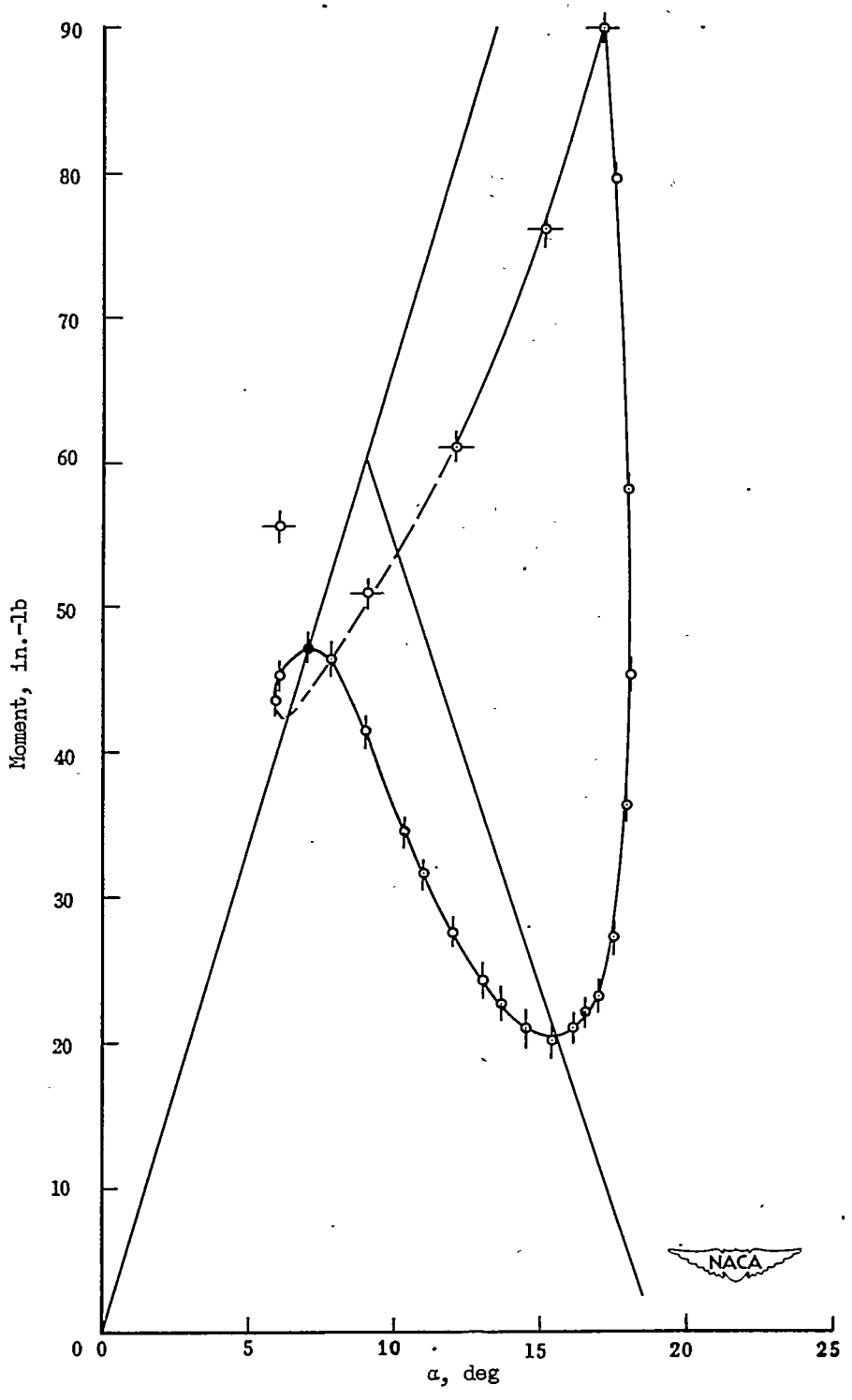

(a) $\alpha_1 = 12^\circ$; $\omega = 16.66$ cycles per second.

Figure 71.- Hysteresis loops from empirical theory. Sharp airfoil.

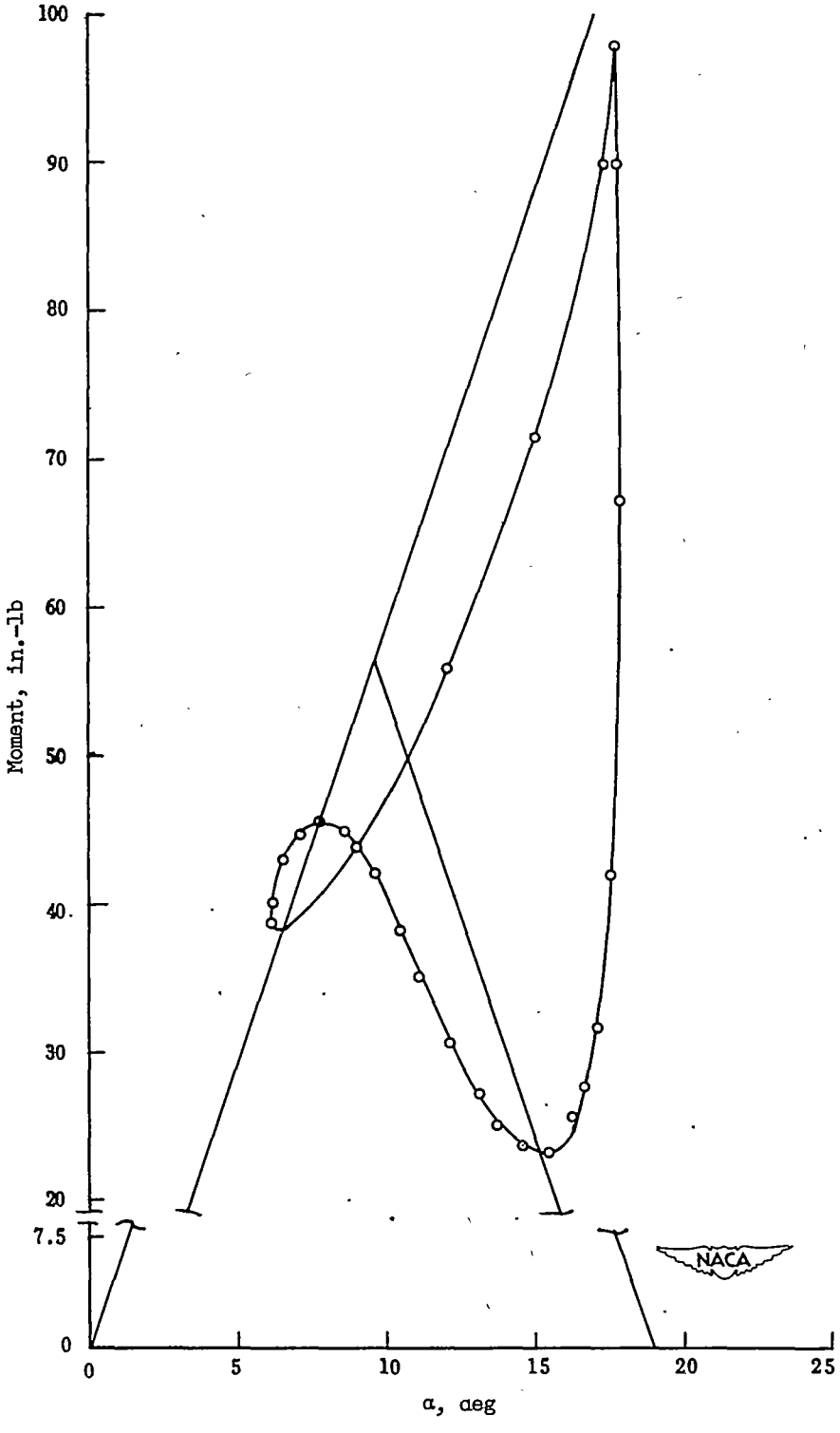

(b) $\alpha_i = 12^\circ$; 7.64 cycles per second.

Figure 71.- Concluded.

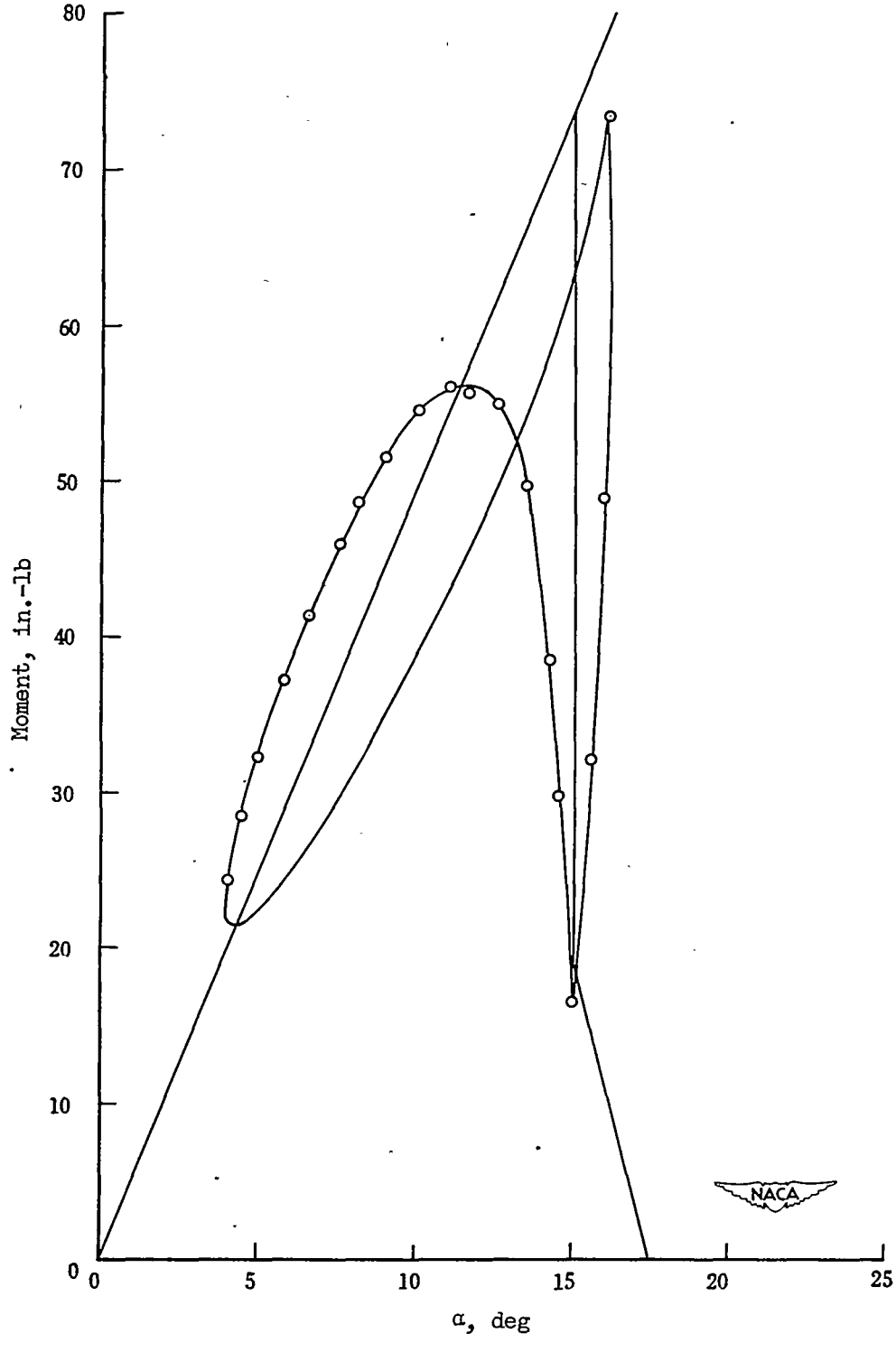

(a) $\alpha_1 = 10^\circ$; $\omega = 7.9$ cycles per second.

Figure 72.- Hysteresis loops from empirical theory. Blunt airfoil.

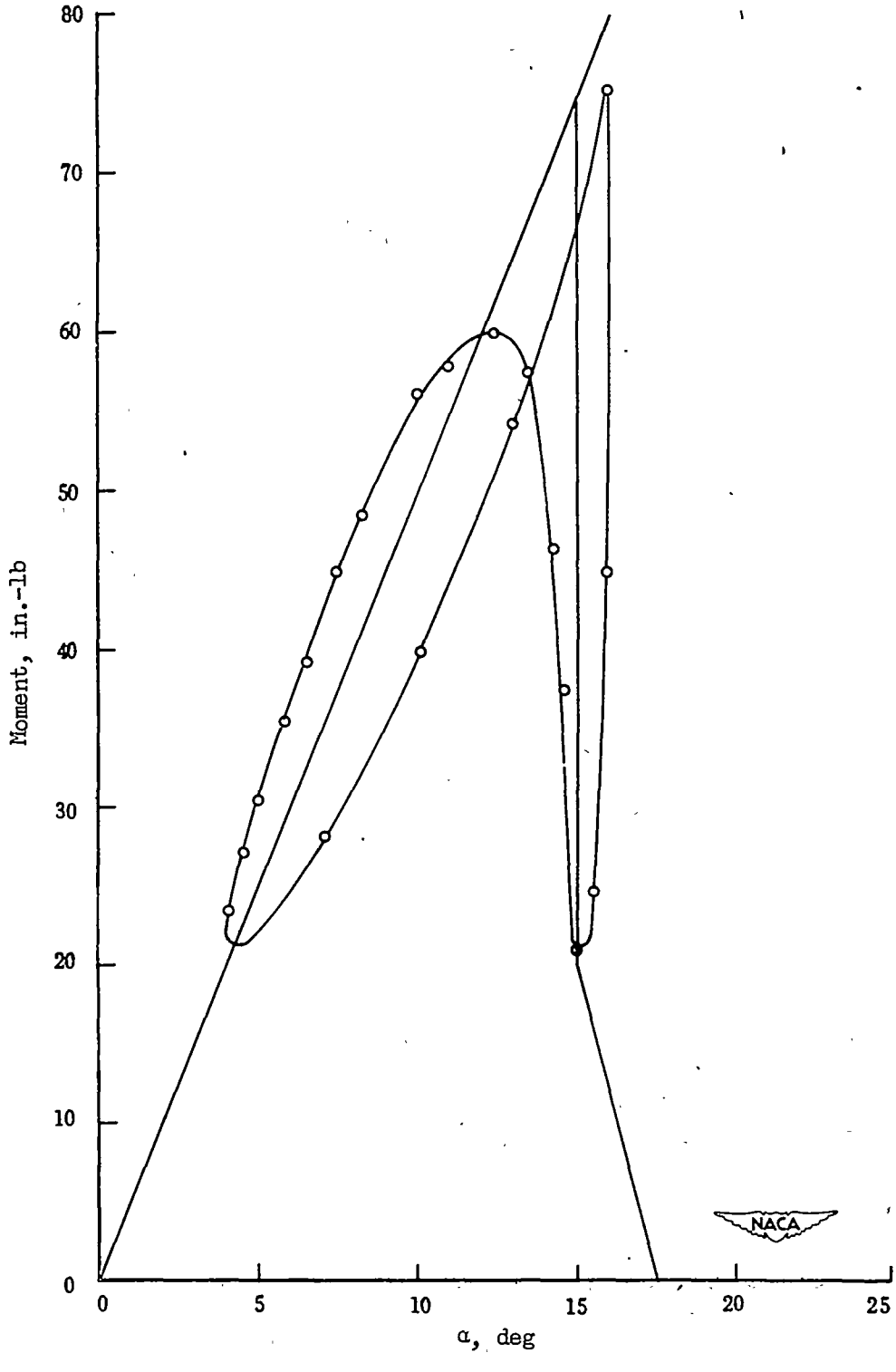

(b) $\alpha_i = 10^\circ$; $\omega = 4.25$ cycles per second.

Figure 72.- Concluded.

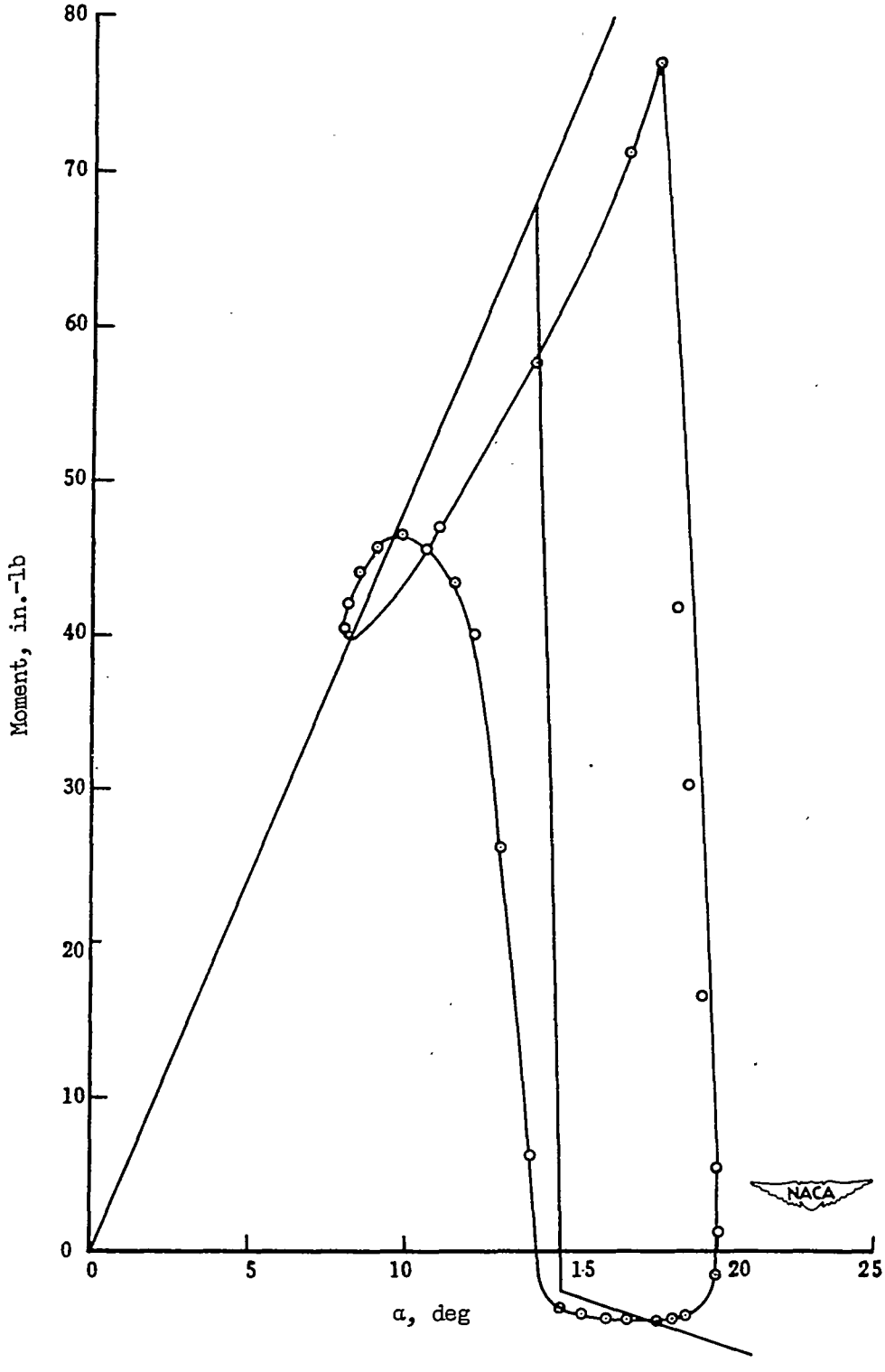

Figure 73.- Hysteresis loops from empirical theory. Intermediate airfoil. $\alpha_1 = 14^\circ$; $\omega = 7.9$ cycles per second.

NACA-Langley - 11-12-51 - 1000